Aus dem Adolf-Butenandt-Institut der Ludwig-Maximilians-Universität München
Lehrstuhl für Stoffwechselbiochemie
Vorstand: Prof. Dr. rer. nat. Dr. h.c. Christian Haass

Linking Neurodegeneration to Vascular Dysfunction

–

Loss of ALS/FTD-Associated TDP-43 Causes Angiogenic Defects

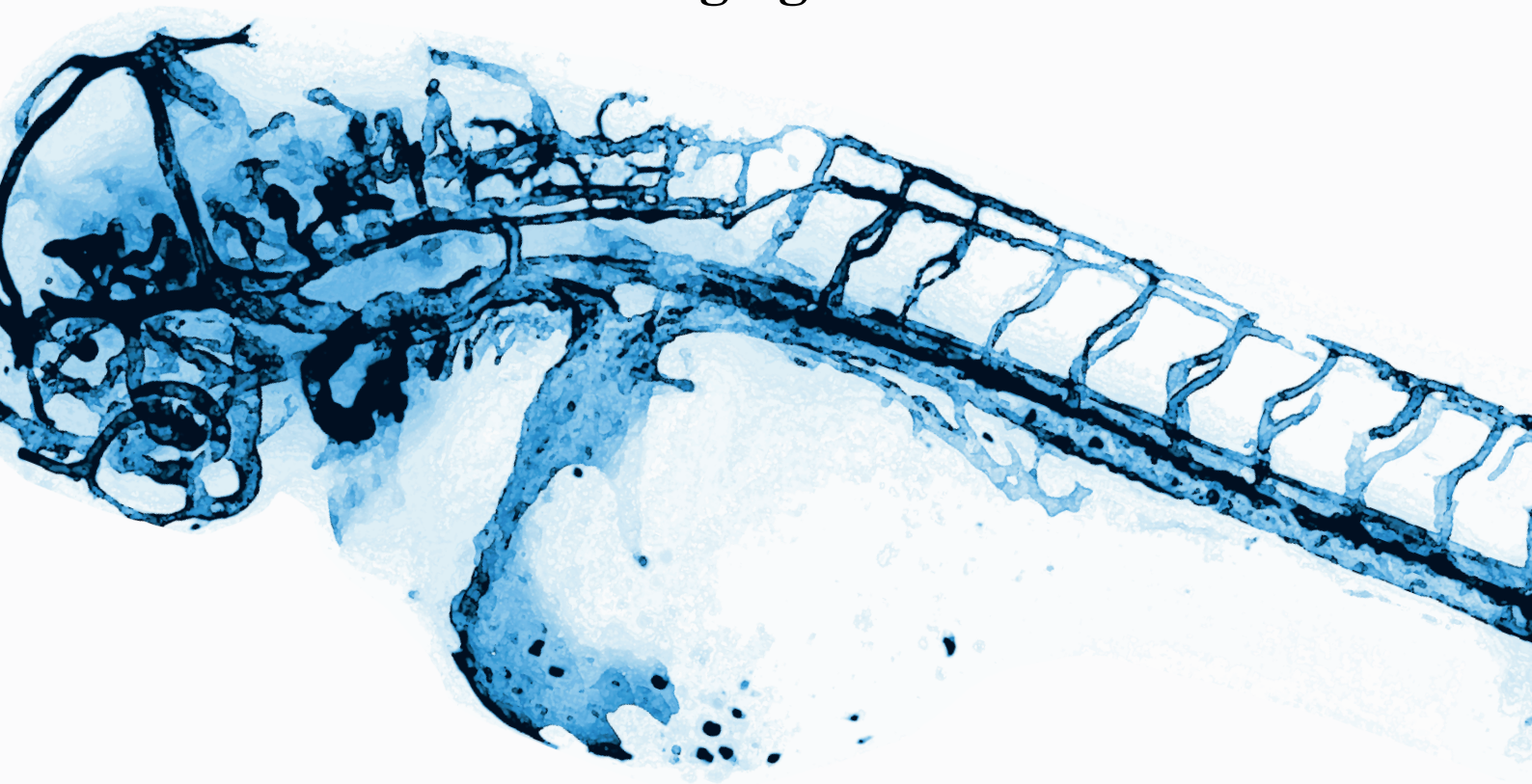

Dissertation
zum Erwerb des Doktorgrades der Naturwissenschaften (Dr. rer. nat.)
an der Medizinischen Fakultät der
Ludwig-Maximilians-Universität München

Vorgelegt von
Katrin Strecker
aus Heilbronn-Neckargartach

2015

Gedruckt mit Genehmigung der Medizinischen Fakultät
der Ludwig-Maximilians-Universität München

Betreuer:	Prof. Dr. rer. nat. Dr. h.c. Christian Haass
Zweitgutachter:	Prof. Dr. rer. nat. Regina Fluhrer
Dekan:	Prof. Dr. med. dent. Reinhard Hickel
Dissertation eingereicht am:	30.09.2015
Tag der mündlichen Prüfung:	26.01.2016

Eidesstattliche Versicherung

München, den 24.09.2015

Ich, Katrin Strecker, erkläre hiermit an Eides statt, dass ich die vorliegende Dissertation mit dem Thema

Linking Neurodegeneration to Vascular Dysfunction –
Loss of ALS/FTD-Associated TDP-43 causes angiogenic defects

selbstständig verfasst, mich aufler der angegebenen keiner weiteren Hilfsmittel bedient und alle Erkenntnisse, die aus dem Schrifttum ganz oder annähernd übernommen sind, als solche kenntlich gemacht und nach ihrer Herkunft unter Bezeichnung der Fundstelle einzeln nachgewiesen habe.

Ich erkläre des Weiteren, dass die hier vorgelegte Dissertation nicht in gleicher oder ähnlicher Form bei einer anderen Stelle zur Erlangung eines akademischen Grades eingereicht wurde.

Katrin Strecker

Summary

Aggregated Tar DNA-binding protein of 43 kDa (TDP-43) is the pathological hallmark of 97% of Amyotrophic lateral sclerosis (ALS) and 45% of Frontal temporal dementia (FTD) cases. Both are fatal neurodegenerative diseases with no cure available and unknown pathomechanism. Gain- and loss-of-function disease mechanisms are discussed, as well as a combination of both. A zebrafish mutant lacking both TDP-43 encoding orthologous genes has been generated to identify *in vivo* functions of TDP-43 and to analyze whether loss of these functions contributes to disease. The mutant dies during late embryonic stage and has shortened motor neurons, muscle degeneration, as well as severe vascular mis-patterning combined with weak or absent blood flow. In this thesis, the vascular mis-patterning phenotype is characterized and the underlying molecular mechanism identified.

In TDP-43 mutants, sprouting of endothelial cells (EC) from the dorsal aorta (DA) is increased and ectopic. EC extend ectopic lateral lamellipodia and fail to migrate along their normal path. This phenotype is cell autonomous and conserved in human umbilical vein endothelial cells (HUVEC). Pathways known to regulate sprouting angiogenesis, like vascular endothelial growth factor (VEGF) and Notch signaling, and candidate guidance cues, including PlexinD1 and Semaphorins, are not affected. Instead, expression of the extracellular matrix protein fibronectin 1 (FN1), of the vascular cell adhesion molecule 1 (VCAM1), as well as of their receptor integrin $\alpha 4\beta 1$ is elevated. Integrin $\alpha 4\beta 1$ signaling is known to regulate intrinsic random migration and directional migration of leukocytes. Importantly, partial knockdown (KD) of integrin $\alpha 4$, FN1, and VCAM1 homologues in the TDP-43 loss-of-function zebrafish rescues the angiogenic defects. This finding suggests that loss of TDP-43 function mediated up-regulation of

integrin α4β1 and its ligands leads to ectopic activation of integrin α4β1, increasing random migration and impaired integration of other guidance cues.

Future analysis of ALS and FTD autopsy material will show whether these TDP-43 regulated genes are also up-regulated in disease and whether they contribute to the disease pathomechanism. If so, an FDA-approved drug targeting integrin α4 currently used to treat Multiple sclerosis patients would be a suitable therapeutic approach.

Zusammenfassung

Die neurodegenerativen Erkrankungen Amyotrophe Lateralsklerose (ALS) und Frontotemporale Demenz (FTD) sind pathologisch durch die Präsenz von „Tar DNA-binding protein of 43 kDa“ (TDP-43) positiven Aggregaten gekennzeichnet. Die Ursachen dieser unheilbaren, tödlichen Krankheiten sind noch immer unbekannt. Es wird vermutet, dass entweder die Aggregate selbst, der Funktionsverlust des aggregierenden TDP-43, oder ein Zusammenspiel beider Prozesse zum neuronalen Zelltod führen. Um die *in vivo* Funktionen von TDP-43 und deren Beitrag zu ALS und FTD zu untersuchen, wurde eine Zebrafischmutante generiert, in der beide TDP-43 kodierenden orthologen Gene defekt sind. Die Mutante stirbt in der späten Embryonalentwicklung, hat verkürzte Motorneurone, degenerierende Muskeln und eine fehlentwickelte Vaskulatur mit stark verminderter oder fehlender Durchblutung. Diese Dissertation widmet sich der Charakterisierung der fehlentwickelten Vaskulatur und der Untersuchung der verantwortlichen molekularen Mechanismen.

In der TDP-43 Mutante migrieren Endothelzellen während der Angiogenese vermehrt sowie an ektopischen Stellen aus der dorsalen Aorta. Des Weiteren bilden sie laterale Lamellipodien aus und verlassen ihren natürlichen Migrationsweg. Dieser Phänotyp ist zellautonom und tritt ebenfalls in humanen Endothelzellen der Nabelschnur auf. Für das Auswachsen von Blutgefäßen bekannte Signalwege wie der des vaskulären Wachstumsfaktors VEGF oder des Notch-Signalwegs sind nicht verändert, ebenso wenig wie die molekularen Wegweiser PlexinD1 und Semaphorin. Stattdessen ist die Expression des extrazellulären Matrixproteins Fibronectin 1 (FN1), des vaskulären Adhäsionsmoleküls VCAM1, sowie deren Rezeptors Integrin $\alpha 4\beta 1$ erhöht. Durch lokal begrenzte intrazelluläre Signale erhöht der Integrin $\alpha 4\beta 1$-Signalweg die gerichtete Migration

von Leukozyten. Reduktion der entsprechenden homologen Proteine in der TDP-43 Zebrafischmutante führt zu einer signifikanten Verbesserung des Angiogenesedefekts. Dies deutet darauf hin, dass die durch den Verlust von TDP-43 bedingte erhöhte Expression von Integrin $\alpha 4\beta 1$ und seiner beiden Liganden zu vermehrter ektopischer Aktivität des Integrin $\alpha 4\beta 1$ Signalwegs führt, was wiederum ungerichtete Migration und beeinträchtigte Integration anderer wegweisender Signalwege verursacht.

Die zukünftige Analyse von Autopsiematerial wird zeigen, ob diese von TDP-43 regulierten Gene auch in ALS- und FTD-Patienten verstärkt exprimiert werden und ob dies zum Pathomechanismus beiträgt. Sollte dies der Fall sein, so wäre ein durch die FDA zur Behandlung von Multipler Sklerose zugelassenes Medikament verfügbar, das die Integrinrezeptoruntereinheit $\alpha 4$ blockiert und somit auch ALS- und FTD-Patienten helfen könnte.

Table of contents

1 Introduction

Neurodegenerative diseases are causing an important public health issue in our aging society, as the main risk factor for neurodegeneration is advancing age [1]. This problem is even more pressing since there is no primary therapy available to date. In most neurodegenerative diseases such as Alzheimer's disease (AD), Parkinson's disease, Huntington's disease, Prion disorders, Tauopathies, as well as ALS and FTD, subsets of neurons are particularly susceptible to degeneration [1]. Also, most of them share the presence of distinct, abnormal insoluble protein aggregates as a pathological hallmark [2, 3].

Disease-causing mutations in many different genes of patients with positive family history were identified in recent genome-wide association studies (GWAS) [4, 5]. Investigating the genes' physiological functions and the mutations' functional impact in cell culture and animal models led to identification of several cellular functions that are likely to be impaired in neurodegeneration. For example, the protein degradation machinery is one cellular function discussed to be involved in neurodegenerative disease pathomechanisms [1].

However, it becomes increasingly evident that not only mutations in single genes cause neurodegeneration, but that there are also other factors at play that can cause sporadic occurrence of neurodegeneration. Risk factor genes and environmental factors acting locally at the cellular level (e.g. cell adhesion, neurotransmission) or at the systemic level (e.g. inflammation, vascular factors, metabolism) are implicated in neurodegeneration pathomechanisms [4, 6, 7, 8, 9].

The diversity of often unknown disease-causing mechanisms and the overlap of clinical symptoms of neurodegenerative diseases is a major challenge for the development of drugs. To appropriately treat a subgroup of patients with a certain neurological disorder, the upstream pathological events that are causative for the clinical symptoms must be determined and therapeutic interventions tailored accordingly [10]. For achievement of this goal, it is necessary to understand the physiological function of each disease-causing gene on both, the cellular and systemic level.

1.1 Aim of this thesis

The aim of this thesis is to identify novel *in vivo* functions and downstream targets of TDP-43 that can be used as therapeutic drug targets in ALS and FTD or as biomarkers for evaluation of disease progression and success of medical treatment. TDP-43 is found in aggregates of the vast majority of ALS and in about half of FTD patients. Mutations in the TDP-43 encoding gene cause ALS and FTD, demonstrating its causal involvement in the diseases' pathomechanism. TDP-43 aggregates are also found if a mutation in another gene causes the diseases, suggesting that TDP-43 is part of a common downstream cascade involved in neuronal cell death in ALS and FTD. Thus, the investigation of the physiological function of TDP-43 is a promising approach to define the pathways leading to neurodegeneration. In order to achieve this on a systemic level, an animal model system is required. However, TDP-43 deficiency is embryonically lethal in mice. Therefore, my laboratory used the small vertebrate model zebrafish to generate a loss-of-function mutant for the TDP-43 encoding zebrafish orthologues. The earliest phenotype of this zebrafish mutant is a severe defect in vascular patterning, revealing a novel, crucial *in vivo* function of TDP-43. Importantly, there is increasing evidence for an involvement of the vascular system in neurodegenerative diseases. In this thesis I will characterize the vascular phenotype in detail, address whether the phenotype is cell autonomous or non-autonomous, and identify the molecular mechanism causing this phenotype induced by TDP-43 deficiency. Importantly, I will investigate the conservation of the vascular function of TDP-43 across species, specifically in a human cell culture system, to ensure translatability of my findings.

1.2 ALS and FTD

1.2.1 Clinical classification

Historically, ALS and FTD were thought to represent two distinct neurodegenerative disorders. FTD is a clinical syndrome that accounts for 5-15% of all cases of dementia. It is the second most frequent type of dementia below the age of 65, with an incidence of about 4 per 100 000 persons per year in the 45–64 year age-group [11, 12]. FTD comprises a heterogenous group of diseases that present with degeneration of the frontal and temporal lobes, leading to behavioral and personality changes and/or language deterioration symptoms. The clinical symptoms are subcategorized into behavioral variant FTD, semantic dementia, and progressive non-fluent aphasia (for review see [13]). About 25-50% of FTD cases are familial (fFTD), predominantly with a dominant pattern of inheritance [11].

ALS, also known as Lou Gehrig's disease, is an adult-onset disease characterized by progressive upper and lower motor neuron degeneration. The clinical discrimination from other motor neuron diseases is often difficult. The revised El Escorial criteria, a catalogue of guidelines, help to diagnose ALS [14]. The name of the disease refers to clinical and pathological findings: "Amyotrophic" refers to muscle atrophy, weakness and fasciculation due to loss of lower motor neurons. "Lateral sclerosis" refers to the hardness to palpation of the lateral columns of the spinal cord in autopsy tissue due to the gliosis following degeneration of the corticospinal tracts. Starting often focally and unilaterally by signs of weakness in one limb, the neuronal degeneration spreads rapidly, leading to death due to respiratory failure within one to five years [10, 12]. Being the most frequent form of motor neuron disease, ALS has an incidence of 2 to 3 per 100 000 persons per year. About 10% of ALS cases are inherited in a mostly dominant manner (familial ALS (fALS)) [15, 16].

Interestingly, more than 10% of FTD patients were reported to also present with signs of motor neuron disease [17]. Moreover, more than 15% of ALS patients fulfill the consensus criteria for probable or definite FTD [18, 10, 12]. These findings provide

clinical evidence that there is an overlap of both diseases. Indeed, pathological characterization of both diseases as well as the identification of disease-associated genes subsequently established the view of ALS and FTD to represent the clinical extremes of a broad disease spectrum that is heterogenous with respect to clinical symptoms, pathology, and genetics [19, 20, 21, 22, 11].

1.2.2 Pathological classification

FTD is a clinical syndrome that is associated with heterogenous neuropathological findings. However, a common feature is the relatively selective degeneration of the frontal and temporal lobes, providing the basis for the term Frontotemporal lobar degeneration (FTLD) that is used to describe the pathological condition underlying FTD [23]. The pathological hallmark of FTD are abnormal intracellularly deposited insoluble protein accumulations [23]. Postmortem immunohistochemistry of autopsy samples allows for further pathological subclassification, since subgroups of patients have a characteristic pathological signature. The first two pathological categories were defined based on the presence of either hyperphosphorylated tau or ubiquitin-positive neuronal inclusions. FTLD characterized by ubiquitin-positive inclusions is the predominantly occurring pathology [12]. Also in ALS, the presence of neuronal ubiquitin-positive cytoplasmic and intranuclear inclusions is a characteristic pathological feature [12].

In 2006, a major breakthrough was achieved by the discovery of TDP-43 as a major constituent of the neuronal aggregates in both, ALS and FTLD patients [24, 25]. TDP-43 is part of the ubiquitinated neuronal cytoplasmic inclusions in about 97% of ALS and 45% of FTLD cases [26]. In addition, mutations in the TDP-43 encoding gene (*TARDBP*) are causative for both diseases, further substantiating the perception of ALS and FTD as representatives of two ends of the same disease continuum [24, 25]. Based on these findings, FTLD and ALS cases with TDP-43-positive inclusions were subsequently termed FTLD-TDP and ALS-TDP, respectively [19, 27].

In ALS-TDP antibodies detect aggregated TDP-43 in neurons and glia of the primary motor cortex, brainstem motor nuclei, spinal cord, and associated white matter

tracts [27]. Besides cytosolic localization, inclusions can also be detected in the nucleus [24, 25]. In FTLD-TDP, TDP-43 antibodies stain cytoplasmic neuronal inclusions and neurites in the frontotemporal neocortex and dentate granule cells of the hippocampus. Moreover, glial pathology is found in the subcortical white matter as well as in further subcortical neuroanatomical sites [16]. A further neuropathological observation is the abnormal redistribution of TDP-43 from the nucleus to the cytosol, resulting in nuclear clearing of TDP-43 in proportions of neurons with inclusions [28]. This shift in localization appears to be an early event in ALS [29], pointing towards a loss-of-function disease mechanism. Biochemical analysis revealed a pathological molecular signature of TDP-43 including hyperphosphorylation, ubiquitination, and truncation into about 25 kDa C-terminal fragments [24, 25].

Interestingly, TDP-43-positive neuronal inclusions were not only found in ALS and FTD, but also in other neurodegenerative diseases like AD (in 25 to 50% of cases). Whether TDP-43 pathology in those diseases is a bystander or whether TDP-43 aggregation is a common downstream event of pathomechanistic relevance in several neurodegenerative diseases is currently unknown [30]. Furthermore, TDP-43 pathology is not always restricted to the central nervous system (CNS). For example, in some forms of myopathies TDP-43 inclusions are found in muscle biopsies [31, 32, 33], and accumulated TDP-43 has been reported in cells of the skin in sporadic ALS, of which the pathological relevance is currently unclear [34].

Subsequently, the identification of disease causing mutations in several different genes (see below) and the following pathological investigations led to further pathological subcategorization of ALS and FTLD: ALS-SOD is characterized by aggregated Cu/Zn superoxid-dismutase 1 (SOD1), ALS-UPS by aggregated proteins of the ubiquitin-proteasome system (UPS), ALS-FUS and FTLD-FUS display fused in sarcoma (FUS) inclusions [35, 19, 36, 16]. With regard to the clinical aspect, these pathological classes are positioned either exclusively on the ALS side of the spectrum (SOD1-positive inclusions), or can underly, to a varying degree, ALS and/or FTD symptoms (TDP-43/UPS/FUS-positive inclusions) [11, 16].

1.2.3 Genetics and pathomechanisms

The high percentage of FTD and ALS patients with a positive family history suggests that there is a genetic cause for the diseases. Indeed, several major genes with disease causing mutations could be identified that have a high penetration and are found in different populations described in different studies [37]. Besides major genes, also disease causing genes with low penetration and disease modifier genes have been identified. Patients frequently have mutations in more than one ALS or FTD linked gene. ALS and FTD are therefore discussed to be "oligogenic" diseases [37]. The function of ALS- and FTD-linked genes and their clustering in cellular pathways allows for insight into potential pathomechanisms. The major ALS and FTD genes as well as ALS- and FTD-associated genes leading to TDP-43 pathology and their possible pathomechanisms are summarized in the following. Owing to its particular relevance the gene *TARDBP* and its disease mechanisms are addressed in a separate section.

1.2.3.1 *SOD1*

The first pathological mutations causing ALS were identified in *SOD1* and account for about 12-20% of fALS cases [35, 38, 39]. Mutations in *SOD1* lead to pure ALS, with cognitive impairment only manifesting in later stages of the disease in few cases [39]. Since ALS-SOD1 patients lack the TDP-43 and FUS pathology present in nearly all other cases of ALS, the SOD1 pathomechanism is thought to be different [40, 27, 39]. Mutant SOD1 misfolds and impairs the proteasomal pathway and autophagy, the main protein degradation machineries of the cell. In addition, mutant SOD1 itself escapes degradation and accumulates as oligomers and subsequently as aggregates in the cell [38]. In ALS-SOD1 patients, these defects manifest in increased autophagosome number in motor neurons of the spinal cord and SOD1-positive inclusions [41]. In mice overexpressing mutant SOD1, mitochondrial functions as well as axonal transport functions are impaired [38]. It is unclear, however, to which extend these findings transfer to the human pathological situation [42]. Another potential pathomechanism involves the breakdown of the blood brain barrier (BBB), which is described in section 1.4.2.

1.2.3.2 *FUS*

FUS is an RNA binding protein. Mutations in *FUS* are therefore hypothesized to mediate neuronal cell death via perturbation of the neuron's RNA metabolism. Mutations in FUS account for about 4% of fALS, 1% of sALS cases, as well as for rare cases of FTLD-FUS and cluster in the PY-NLS domain at the C-terminus of the protein [43, 11]. Whereas ALS-FUS is mostly associated with mutations in FUS, FTLD-FUS cases are predominantly sporadic [11]. A further difference is the presence of two further FET protein family members (to which FUS also belongs), namely TATA-binding protein-associated factor 15 (TAF15) and Ewing's sarcoma (EWS), in the FUS-positive inclusions in FTLD, but not in ALS-FUS [44]. FUS pathology never occurs together with TDP-43 pathology [11].

ALS-associated mutations in FUS lead to disruption of the nonclassical PY nuclear localization signal, impairing transportin-mediated nuclear import [45]. This is thought to cause redistribution of FUS into the cytosol. The other FET protein family members have still a predominantly nuclear localization. In FTLD-FUS, abnormal post-translational modifications of all FET proteins causing altered transportin binding is speculated to result in cytosolic accumulation [46]. In the cytosol, FUS functions in the cellular stress response being a component of stress granules (SG) [47]. In SG, RNA is temporally stored during phases of cellular stress [48]. It is thus hypothesized that after redistribution of FUS, e.g. due to mutations and/or hampered nuclear import, cellular stress as an additional factor causes persistent accumulation of FUS (and FET proteins). Eventually, these then form the stable inclusions found as the pathological hallmark in patients ("multiple hit model") [49]. Whether the inclusions are themselves toxic to the cell, or consequently reduced functional FUS levels are disease causative, remains an unresolved and controversial topic [46]. However, since FUS functions as a transcriptional regulator and is involved in splicing regulation of many genes, a loss-of-function mechanism with perturbed RNA metabolism seems plausible.

1.2.3.3 Protein degradation pathways

The characteristic depositions of aggregated proteins are hallmarks of ALS and FTLD. It is thus not surprising that mutations in genes involved in protein degradation were found to cause ALS and FTD, supporting the hypothesis of impaired protein degradation as an involved pathomechanism. Examples are mutations in the major gene *sequestosome* (*SQSTM1*) encoding p62 protein as well as mutations in *ubiquilin 2* (*UBQLN2*) or in *valosin-containing protein* (*VCP*) [50, 51, 52, 53]. *UBQLN2* encodes UBQLN2 that delivers ubiquitinated proteins to the proteasomal degradation machinery [54]. VCP is important during endoplasmatic reticulum-associated and proteasomal protein degradation and in autophagy [55]. Besides causing ALS, mutations in this gene also lead to inclusion formation in several tissues, such as muscle and bones, causing inclusion body myopathy with early-onset Paget disease and frontotemporal dementia [56]. They all have TDP-43-positive inclusions and are hence neuropathologically classified as ALS-TDP (UBQLN2 cases) and/or FTD-TDP (SQSTM1 and VCP cases) [52, 53].

1.2.3.4 *Progranulin*

Mutations in progranulin (*GRN*) account for a large fraction of FTD cases (5-20% of fFTD and 1-5% of sFTD cases). Progranulin (PGRN) participates in several biological processes, for example it functions as a mitogenic, angiogenic and neurotrophic factor, and has pro- as well as anti-inflammatory properties [57, 58, 59]. It is largely accepted that haploinsufficiency is the underlying disease mechanism, as mutation carriers have substantially reduced PGRN plasma, serum, and cerebrospinal fluid levels [60, 61, 62]. It is still unclear, however, which of the functions of PGRN is disease-relevant. Since homozygous loss of PGRN function leads to the lysosomal storage disorder Neuronal ceroid lipofuscinosis [63], impaired lysosomal function is speculated to play an important role [64]. Neuropathologically, FTD cases with underlying *GRN* mutation present with TDP-43 pathology [24], but it is unclear how reduced PGRN levels lead to TDP-43 pathology [28].

1.2.3.5 *C9ORF72*

Recently, the most common genetic cause for ALS and FTD could be identified [11]. The mutation is an expanded hexanucleotide repeat in the noncoding region of the chromosome 9 open reading frame 72 (*C9orf72*) gene [65, 66]. 40-50% of fALS and 7-10% of sporadic ALS (sALS) cases, as well as 25% of fFTD and 6% of sFTD patients have a repeat expansion in *C9orf72*, which is transmitted as a dominant trait [42, 39]. Whereas the GGGGCC hexanucleotide is repeated two to five times and never more than 30 times in most unaffected persons, the repeat is present several hundreds or even thousand times in patients [39]. The repeat itself shows instability, as repeat number varies in different tissues of one patient as well as across families [67]. Clinically, patients present with a strong overlap of ALS and FTD symptoms, with adult-onset psychosis, Parkinsonism, and ataxia as co-occurring features [11].

The physiological function of *C9orf72* remains unknown, making it difficult to speculate about possible loss-of-function disease mechanisms. In support of this hypothesis, the extended repeat shifts relative expression of different *C9orf72* transcripts, leading to a decrease in expression of one transcript by 50% [66, 65, 68]. Alternatively, the accumulation of transcripts with the repeat sequence in nuclear RNA foci provides evidence for a toxic RNA gain-of-function pathomechanism. RNA binding proteins could be sequestered in the foci, resulting in perturbed cellular RNA metabolism [66, 69]. A further potential mechanism is provided by the discovery that the repeat is subject to repeat-associated non-ATG translation (RAN translation): All possible reading frames of the sense and anti-sense strand are found to be translated into dipeptide repeat proteins (DPR) that aggregate in patients and might be, to a different extend, toxic to neurons [70, 71, 72, 73]. Thus, besides *C9orf72* RNA foci, also DPR-positive protein deposits are found, which are p62-positive, TDP-43-negative [72]. In all cases of pathological *C9orf72* repeat expansion, TDP-43 is found in neuronal inclusions, for example in the extramotor cerebral cortex, hippocampus, basal ganglia, substantia nigra, and lower motor neurons of the brain stem and spinal cord [11].

1.2.4 *TARDBP*

TDP-43 is deposited in intracellular inclusions of 97% of all ALS and 45% of all FTLD cases [26]. The clear mechanistic relevance of TDP-43 function for ALS and FTD is strongly supported by the finding that mutations in *TARDBP* are causative for both diseases [74, 75, 76, 77, 78, 79, 80].

1.2.4.1 Physiological functions of TDP-43

TDP-43 is well-conserved between species, ubiquitously expressed, and predominantly localized in the nucleus, although it is able to shuttle between the nucleus and the cytosol [81, 82, 83]. Built up by 414 amino acids, TDP-43 contains two RNA recognition motifs, has a nuclear localization signal (NLS), a nuclear export signal (NES) [84], and a glycine-rich C-terminus. The latter is essential for protein-protein interactions and lacks secondary or tertiary structure [85, 86, 87]. TDP-43 belongs to the family of heterogenous nuclear ribonucleoproteins (hnRNPs). It is involved in many aspects of RNA metabolism, ranging from transcription regulation, splicing, mRNA stability and transport to microRNA processing [88].

Of the two RNA binding motifs (RRM1 and RRM2), particularly the first is necessary and sufficient for binding and recognition of single stranded nucleic acid sequences (RNA and DNA) that have a minimum number of six UG (or TG) repeats [89]. Binding of DNA by TDP-43 is thought to lead to transcriptional repression [81, 90, 91], which is also a function that gave the protein its name: Initially, TDP-43 was characterized as a transcriptional repressor binding TAR DNA sequence motifs of the human immunodeficiency virus type-1 (HIV-1) [81]. By binding to mRNA, TDP-43 regulates splicing and RNA stability: Thousands of mRNAs in the mouse brain are identified to be bound by TDP-43 (about 30% of the mouse transcriptome). Binding of TDP-43 regulates the splicing of hundreds of these mRNAs. Moreover, also expression levels of several hundred mRNAs are affected by loss of TDP-43 [92, 93].

Furthermore, TDP-43 regulates its own RNA levels by binding to its 3'UTR, which might play a role in pathogenesis (see below) [94, 95]. In addition, there is evidence

for TDP-43 to regulate transport of mRNA to synaptic terminals and local RNA translation at synaptic sites, which is important for synaptic plasticity [96, 97, 98, 99]. This function of TDP-43 is also reported to influence dendritic branching and synaptic formation of neurons in *Drosophila* [100, 101]. Furthermore, its RNA binding properties implicate TDP-43, like FUS, in the cellular stress response. Once localized to the cytosol and under conditions of stress, it is recruited into SG [102, 103, 104]. During repeatedly occuring stress events, SG could serve as a seed for the stable inclusions found in patients, as it is discussed for ALS-FUS and FTLD-FUS in the "multiple hit model" above [49, 105]. A further physiological aspect of TDP-43 translocation to the cytosol and subsequent SG formation might be important during neuronal damage like axotomy. In this context, TDP-43 is proposed to stabilize and transport low molecular weight neurofilament (NFL) mRNA, thereby contributing to local translation of NFL, which is required for axonal repair [106, 107, 108, 109].

Furthermore, most of the reported interactions with other proteins serve RNA related functions. For example TDP-43 is found in the Drosha and Dicer complexes and influences miRNA biogenesis [110, 111]. Moreover, it can interact with itself and with other hnRNPs like hnRNPA2, hnRNPC, and FUS [112, 113, 86, 114].

1.2.4.2 Pathogenesis of TDP-43 proteinopathies

The presence of TDP-43-positive aggregates in most ALS and many FTD cases is strongly suggestive of their disease relevance. The aggregates themselves could be neurotoxic or they could capture toxic oligomeric species thus being neuroprotective [115], both options implying a toxic gain-of-function disease mechanism. However, the nuclear clearance found in the majority of remaining neurons of patients with TDP-43 pathology led to an alternative hypothesis: A loss of nuclear TDP-43 function may mediate some of the deleterious effects of abnormal TDP-43 metabolism [28]. The two mechanisms are not mutually exclusive and might contribute both to pathogenesis. In addition to TDP-43-positive inclusions, the identification of mutations in *TARDBP* provides striking evidence for a critical involvement of TDP-43 in disease development. One would expect that characterization of the mutations' impact on physiological functions and/or

aggregation properties resolved the disease mechanism. However, the characterization of mutated proteins does currently not conclusively elucidate whether they cause gain-of-function, loss-of-function, or both.

Impact of disease-causing mutations in *TARDBP* Except for one truncation mutation, all of the 38 mutations identified in *TARDBP* are mis-sense mutations and almost exclusively cluster in the C-terminal region [28]. Thus, C-terminal functions of TDP-43 are thought to be particularly important for its pathogenesis. The glycine rich C-terminus is essential for protein-protein interactions of TDP-43 [82] and prone to aggregation due to its prion-domain like properties [116]. Disease-causing mutations promote TDP-43 misfolding. However, the consequences of TDP-43 mis-folding for cellular functions are still under debate [116, 117, 114, 118, 119, 120, 121, 88].

Mutations in the C-terminus of TDP-43 have been described to affect its behavior in SG formation. It is clear that TDP-43 has to be cytosolic in order to be recruited into SG, that the RRM1 and the C-terminal region are necessary for recruitment, and that cellular stress leads to TDP-43 incorporation into SG [105]. However, different studies reported contradicting effects of mutations on SG formation, ranging from promotion to reduction of SG formation [103, 122, 123]. In any case, SG might be the precursors of the stable inclusions found in patients and thus stress an important trigger of neurodegeneration [49]. Overexpression artifacts make it also difficult to interpret the effect of increased toxicity of cytosolic mutant TDP-43 in comparison to wild type TDP-43 [28]. Increased cytosolic TDP-43 rather seems to be a physiological response to neuronal injury [108, 109]. Nevertheless, overexpression studies show that TDP-43 levels need to be tightly regulated to prevent toxic effects [28].

Role of posttranslational modifications of TDP-43 in ALS and FTD Aggregated TDP-43 in ALS and FTLD patients is found to be fragmented, phosphorylated, and ubiquitinated. It is therefore discussed whether these posttranslational alterations are pathomechanistically important. Studies present conflicting results of their impact on TDP-43 mediated toxicity. For review see [118] and [28] (and references therein).

Loss of TDP-43 function leads to disturbance of RNA metabolism in ALS and FTD Like FUS, TDP-43 is an RNA binding protein with thousands of RNA targets [124, 125]. Upon knockdown (KD) of TDP-43 or in diseased tissue, RNA levels and splicing are misregulated [92, 93]. In addition, the RNA foci found in *C9orf72* mutation carriers, that also present with TDP-43 pathology, sequester RNA binding proteins, also perturbing RNA homeostasis [69, 126]. Moreover, mutations in further genes with functions in RNA metabolism in ALS (and/or FTD) have been identified, including *ANG* [127], also causing TDP-43 pathology, as well as *hnRNPA1* and *hnRNPA2/B1* [128]. Thus, disturbance of RNA metabolism, supporting a loss-of-function mechanism, is likely to be part of ALS and FTD pathogenesis.

Taking all so far proposed mechanisms together in order to explain TDP-43 proteinopathy in ALS- and FTLD-TDP, one could speculate about the following options: Either a mutation in *TARDBP*, in the protein degradation machinery and/or exposure to cellular and environmental stress may lead to mis-localized TDP-43. Mis-localized TDP-43 might be incorporated into SG and/or other precursors of protein aggregates, finally resulting in stable inclusion formation seen in patients. In an alternative hypothesis, the initiating event could be disturbed RNA homeostasis of the cell, caused e.g. by mutations in *TARDBP* or cellular stress. Upon additional environmental stress aggregation and inclusion formation of TDP-43 could be triggered. Which of these events in the long term leads to neuronal cell death in patients, whether an accumulation of insults at some point induce cell death, and whether this involves gain- or loss-of-function of TDP-43 or both, still remains elusive.

Lessons from TDP-43 animal models Animal models are crucial to test the biological relevance of an *in vitro* finding and to study biological processes in a complex environment that more closely resembles the situation in a human being. In order to shed light onto the intricate functions of TDP-43, and to extract the relevant pathological events in a whole organism, many animal models have been generated. Amongst those, overexpression models, however, proved not to be very helpful in elucidating disease mechanisms. One reason are contradictory results. For example, rodent models

with different or even same promoters employed for overexpression of mutant or wild type TDP-43 show different symptoms' onset and large variation in symptoms displayed, some not developing any symptoms at all. In addition, the typical pathological hallmarks of ALS/FTD-TDP are missing, because the animals do not develop overt TDP-43 pathology (reviewed in [129] and [130]). One consistent feature is the correlation of increase in severity of symptoms with expression levels [131]. However, no copy number variation of *TARDBP* has been found in ALS/FTD patients and TDP-43 mRNA levels in brain are not increased (with one exception of a patient with a mutation in the 3'UTR) [28]. Furthermore, overexpression of TDP-43 is already toxic in cell culture (see above). Thus, overexpression experiments seem to be a rather inadequate approach for addressing human disease pathogenesis. In order to investigate the consequences of expression of mutant TDP-43 in an animal model, knock-in studies of mutations in the endogenous locus, e.g. by using the Clustered regularly interspaced short palindromic repeats/CRISPR-associated (CRISPR/CAS) system, are more likely to produce reliable results. Therefore, the focus of this paragraph lies on the knockout models that have been generated so far.

Knockout of *Tardbp* in rodents, the homologue of human *TARDBP*, is embryonically lethal due to defective outgrowth of the inner cell mass [132, 133, 134], demonstrating the requirement of TDP-43 for embryonic development. It is also consistent with findings in human cell culture models, where TDP-43 deficiency is also toxic [135, 87]. Conditional knockout of *Tardbp* in adult mice leads to loss of body fat due to increased fatty acid oxidation, likely caused by down-regulation of the skeletal muscle gene *Tbc1d1*, a Rab-GTPase-activating protein, and death within approximately 9 days [136]. Since also ALS patients have been reported to have defects in energy metabolism, this is the first study with direct clinical relevance [137], although it is not clear how this relates to neurodegeneration.

Heterozygous *Tardbp* knockout mice are reported in one study to develop motor deficits, albeit without motor neuron degeneration [134]. Further, reduction of TDP-43 levels using an RNAi approach leads to motor deficits, which are accompanied by neurodegen-

eration in layer V of the cortex and the ventral horn of the spinal cord [138]. Selectively induced deletion of *Tardbp* in motor neurons also causes motor deficits in mice, with degeneration of motor neurons of the spinal cord, astrogliosis, and reduction in body weight [139, 140]. In the first published study [140], knockout is induced at E9.5 leading to reduction in motor neuron number already after ten weeks. In the second study [139], a different promoter is utilized that leads to knockout of *Tardbp* postnatally in 50% of motor neurons and becomes strongest after five weeks. After one year, those animals have atrophic motor neurons and show reduction only of larger motor neurons. In both studies knockout of *Tardbp* also causes defects in protein degradation, leading to ubiquitin-positive accumulations in one study [140]. Both studies strongly support a loss-of-function disease mechanism to be at play in ALS, since loss of TDP-43 in both studies causes ALS-like phenotypes and pathologies.

Another, very recent model to address *C9orf72* repeat expansion mediated TDP-43 pathogenesis was generated by expression of either 2 or 66 GGGGCC repeats lacking an ATG in the CNS. Strikingly, mice expressing the repeat expansion show motor deficits and behavioral abnormalities. Pathologically, they develop dipeptide containing inclusions that are ubiquitin-positive, RNA foci, and phospho-TDP-43 pathology accompanied by loss of neurons, e.g. in the motor cortex [141].

Numerous studies in invertebrate organisms like *Caenorhabditis elegans* (*C. elegans*), *Drosophila melanogaster* provided further evidence for the loss-of-function disease mechanism as they underscore dependence of cellular function on TDP-43. In *C. elegans*, the *TARDBP* orthologue *tdp-1* is not required for embryonic development and its loss even increases lifespan. However, deficiency of *tdp-1* leads to defects in fertility, growth, and locomotion. Moreover, it increases stress vulnerability due to alterations in the insulin/insulin like growth factor pathway [142, 143]. Also *Drosphila* loss-of-function models show impairment in locomotion, as well as axonal loss, reduction in synaptic bouton number (but also increase in another study [144]), and impaired synaptic transmission [145, 146, 101]. In contrast to *C. elegans*, and similar to rodent models, the *Drosphila* orthologue of TDP-43, *TBPH*, is required for embryonic development

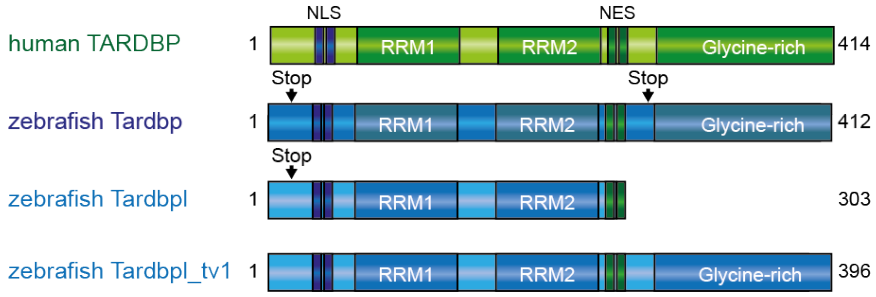

Figure 1.1: Schematic illustration of the TDP-43 domain structures of human TARDBP, and the zebrafish orthologues Tardbp and Tardbpl. *tardbpl* is alternatively spliced if *tardbp* is knocked out or knocked down, leading to expression of Tardbpl_tv1. This demonstrates the functional importance of the C-terminal glycine-rich domain of TDP-43. "Stop" indicates the location of zink finger binding used to generate knockout lines. Length in amino acids.

because only few escapers survive until adulthood. Surviving adults have a shortened life span [101]. In contrast to *C. elegans* or *Drosophila*, zebrafish is a vertebrate model organism. The embryo develops *ex utero*, making it especially attractive to investigate TDP-43 function since knockout in mice is embryonically lethal. In addition, the zebrafish embryo is optically transparent, allowing for imaging of cellular processes in the living animal. The rapid development of the embryo combined with the availability of numerous transgenic fluorescent lines make it an excellent tool to study developmental processes *in vivo*. For example, the zebrafish is used to image formation of blood vessels, with the first network being completed already after 32 hours post fertilization (hpf). The zebrafish is a traditional model to study gene function during development in forward genetic screens. Thanks to newly developed genetic tools such as zinc finger nucleases and the CRISPR/Cas9 system, zebrafish evolved as a model that is also frequently used in reverse genetic approaches. The advantages of little cost for housing due to, e.g., the small size of the animals greatly facilitate generation of single, double, or multiple knockout animals. In addition, the easy accessibility of the embryo makes it possible to inject exogenic RNA, DNA, or the modified nucleotides used for KD of genes in zebrafish, called morpholinos (MO). Moreover, a single healthy pair of adult zebrafish provides more than 200 eggs per week, making the zebrafish embryo an optimal model organism for large scale experimental approaches like screening of chemical compound libraries. Thus, several studies made use of the advantages of the zebrafish to study TDP-43 function during development.

Due to gene duplication in the teleost lineage, zebrafish have two *TARDBP* orthologues, *tardbp* and *tardbp like* (*tardbpl*), the latter lacking the glycine-rich C-terminal domain. Loss-of-function mutants homozygous for *tardbp* or *tardbpl* knockout do not show any phenotype, respectively [147]. Surprisingly, homozygous deletion of *tardbp* results in alternative splicing of *tardbpl* leading to expression of a protein containing a C-terminus highly homologous to Tardbp, called Tardbp_tv1 (Figure 1.1) [147, 148]. This protein functionally compensates for the loss of Tardbp underscoring the functional importance of the glycine-rich domain. Therefore, only the double homozygous mutants show phenotypes. Double homozygous mutants are affected by multiple organ defects, including shortened motor neuron outgrowth, disruption of muscle tissue, as well as mis-patterning and non-perfusion of blood vessels finally leading to early death at about 6 dpf [147]. Expression of human TDP-43 in the double homozygous TDP-43 mutant background rescues perfusion, demonstrating the conservation of TDP-43 function in evolution. In contrast, rescue with a *TARDBP* construct harboring an ALS patient mutation is only partially successful, indicating a subtle loss-of-function. Furthermore, quantitative proteome comparison revealed increased expression of muscle-specific Filamin Ca, which is also up-regulated in samples of frontal cortex of FTLD-TDP patients, additionally supporting the loss-of-function hypothesis. Another zebrafish TDP-43 study used MO KD of only *tardbp*, already causing motor neuron defects [149]. However, in contrast to genetic disruption of a gene, results gained by using MO KD technique are ambiguous due to possible unspecific toxic side effects of the MO used. Thus, the conflicting results are likely attributable to MO KD technology itself.

In summary, various animal models lacking functional TDP-43 or its orthologue(s) clearly demonstrate TDP-43 to be a protein whose function is necessary for normal development, particularly motor neurons, thus supporting a loss-of-function disease mechanism.

1.3 Vascular development

The cardiovascular system fulfills essential functions for the organism: transport of fluids, nutrients, circulation of cells, hormones, and gases [150]. Blood vessels are formed by two different morphogenic processes, vasculogenesis and angiogenesis. Vasculogenesis is the *de novo* formation of the first blood vessels in an embryo by the precursor cells of endothelial cells (EC), the angioblasts. In contrast, angiogenesis is the process by which new blood vessels are formed from an already existing vasculature. Understanding the molecular mechanisms of angiogenesis is of particular interest for development of drugs considering its role also in the adult body, for example during wound healing and tissue regeneration, and its pathological relevance, e.g. in tumor growth [150, 151]. In order to support an organism with oxygen and nutrients, the newly formed vessels need to form a patent lumen that allows blood flow. Therefore, many cell biological processes have to be regulated and coordinated during formation of a functional vascular network, not only on the single cell level but also on the level of cell – cell and cell – extracellular matrix (ECM) interactions. These interactions ultimately define EC fate, EC directional migration, as well as their collective migration in a sprout, and finally fusion of sprouts to a vascular network and lumen formation. VEGF and notch signaling pathways are two of the best studied pathways involved in vascular development. Therefore, the ECM and its receptors in EC are introduced first. Then, the critical players of VEGF and Notch signaling pathways will be described before the development of the zebrafish vasculature and their involvement therein will be addressed.

1.3.1 The extracellular matrix and its receptors in vascular development

Cells of a multicellular organism secrete molecules into the extracellular space that make up the ECM. Histologically, various forms of ECM have been defined, such as basement membranes, interstitial ECM, or the large structural ECM of vertebrates like bone and cartilage [152]. Thus, the ECM can vary substantially in its composition and function. Many studies established a role of the ECM in a multitude of developmental, physiological, and pathological processes. The cellular functions regulated by the

ECM include cell proliferation, differentiation, and survival, as well as cell adhesion, cytoskeletal organization, and cell migration [152]. These functions are mediated by interaction of cells with components of the ECM, such as fibronectin, laminins, vitronectin, thrombospondins, fibrinogen, and collagen. Each of these proteins can be bound by distinct cellular receptors to mediate specific cellular responses and in turn, cells can modulate the surrounding ECM by controlling matrix assembly [153].

Interactions between EC and the ECM are indispensable during vascular development and later for stabilization and maintenance of the vascular system. Especially the physical adhesion of EC to the underlying matrix is pivotal. Importantly, EC – ECM interactions also induce several signaling events, which are crucial for polarization and directed migration of EC. Among the many components of the ECM, fibronectin and its cellular heterodimeric receptors, the integrins, are of particular importance for EC function and will be described in the following sections.

1.3.1.1 Fibronectin

Fibronectin (FN) is a high molecular weight glycoprotein of 250 kDa and forms dimers. It is found in two distinct forms, plasma FN and cellular FN. Plasma FN is synthesized by hepatocytes and circulates in the blood plasma through the body where it is required for stable thrombus formation upon vascular injury. Cellular FN is secreted by fibroblasts and other cell types, like EC, and deposited as fibrils in the ECM [153].

Structurally, FN monomers are mainly made up by three types of repeating modules: twelve type I, two type II, and 15-17 type III repeats. Of functional importance is further a variable (V) sequence close to the C-terminus. FN is alternatively spliced, giving rise to up to 20 different variants in humans. Alternative exon usage leads to inclusion or exclusion of two FN domains. One domain is called extra domain A (EDA) and is located between the eleventh and twelfth type III module, and the other one is named extra domain B (EDB) situated between the seventh and eighth type III module. Additionally, the V region is alternatively spliced, resulting in five further variants with different amino acid length or a completely absent V region. Alternative splicing is

dependent on cell type, stage of development, and age. For example, isoforms including EDA and EDB are strongly expressed around developing blood vessels during development as well as during wound healing, tumor formation, and myocardial infarctions [154].

The integrin binding sites of FN mediate the cellular interactions of FN. The most important site is located in the tenth type III module, which harbors the Arg-Gly-Asp (RGD) motif, mediating binding to the integrins α3β1, α5β1, α8β1, αvβ1, αIIβ3, αvβ3, αvβ5 and αvβ6. In contrast, α4β1 and α4β7 recognize the Leu-Asp-Val (LDV) sequence in the V region. Integrins also bind to other sequences of different FN modules, for example to sites in the EDA module (α4β1 and α9β1integrins), to the fifth (α4β1 integrin) and 14th type III module (α4β1 and α4β7 integrins) [153].

The binding of integrins to FN is required for FN assembly into an insoluble fibrillar matrix. The fibril assembly process is initiated by integrin binding to FN. This induces conformational changes by generation of mechanical forces through cytoskeletal contractility. Thereby exposure of cryptic binding sites in FN is induced, allowing FN molecules to interact with each other. This leads to formation of fibrils, fibril elongation, and finally the formation of a fibrillar matrix. The most important integrin involved in this process is α5β1 integrin and its binding to the RGD motif. However, α4β1 and other integrins have been shown to be able to support FN assembly [153].

Fibronectin in vascular development FN is essential for embryonic development, as knockout of FN1 in mice leads to early embryonic lethality with defects in heart and blood vessel development [155, 156, 157]. The severity of defects varies dependent on the genetic background. Therefore, it could be shown that FN1 is required both during vasculogenesis for assembling of the DA as well as for lumen formation following assembling of the DA. Using embryoid bodies deficient for FN1 or its main receptor α5β1, Hynes *et al.* measured a severe reduction in early capillary plexus formation indicating a direct role of FN1 in vascular network formation [158]. Furthermore, numerous *in vitro* studies demonstrated the strong relevance of FN function in a multitude of aspects of EC behavior, e.g. as a ligand for integrin receptors during cell migration [151].

Fibronectin in zebrafish Unlike other vertebrates, zebrafish have two FN genes, *fn1a* and *fn1b* [159, 160]. Both encode full-length *fn* isoforms containing the RGD motif and the alternative splice sites EDA and EDB as well as the V region with the LDV adhesion site. No *fn1a* splice variants lacking the EDA, EDB or V sequences were found so far. However, another truncated isoform was identified and was shown to be conserved in mice and humans [161]. In contrast, *fn1b* splice variants lacking the EDB module and V region exist, with the EDB- V+ isoform being the predominant form expressed in the zebrafish embryo. *fn1a* is relatively highly expressed before gastrulation, whereas *fn1b* expression is low during the first hours post fertilization and increases during development [160].

The zebrafish mutant *natter* has been shown to have a premature stop mutation in the *fn1a* gene and has been used to analyze the functions of *fn1a*. *fn1a* expression by endocardial and endodermal precursor cells is responsible for deposition of FN at the midline of the embryo and regulates temporal migration of myocardial precursors. In addition, FN expressed by *fn1a* is required for polarization and formation of adherens junctions of the myocardial precursors during maturation of the myocardial epithelium. Consequently, *natter* mutants develop pericardial edema. Additionally, they are characterized by a flattened hindbrain [162].

fn1a has also been shown to regulate sprouting of EC from the DA to form the interrenal vessel (IRV). FN is deposited around the angioblasts that form the axial vessels [163] and was found to be locally increased at the perivascular region at the time of IRV sprouting. During extension of the IRV, FN is increased around the tip of the vessel [164]. Chiu *et al.* could show that *fn1a*, mainly via $\alpha 5\beta 1$, but not *fn1b* is responsible for IRV development [164]. Development of intersegmental vessels (ISV) is unaffected in *fn1a* morphants.

Both, *fn1a* and *fn1b* have been demonstrated to be required cooperatively for somite boundary formation and maintenance, as well as muscle morphogenesis [165, 166, 167]. During somitogenesis, *fn1a* is expressed in the notochord, posterior tailbud and pre-

somitic mesoderm (PSM), whereas *fn1b* is expressed throughout the whole paraxial mesoderm with weaker expression in the tailbud/PSM. However, assembly of a FN matrix is restricted to the somite boundaries due to locally confined integrin signaling. *fn1a* deficiency leads to mild somite boundary defects in the anterior somites, whereas KD of *fn1b* allows initial formation of somites but then causes tail extension defects and disruption of the regular somite morphology by the 15 - 20 somite stage. Co-injection of *fn1a* and *fn1b* MO as well as increasing MO concentrations enhance the defects in axis formation and elongation [165].

1.3.1.2 Integrins

Integrins are a family of glycoproteins that form α-β heterodimeric transmembrane receptors. Both, α and β subunits, have a large extracellular domain, a single transmembrane helix, and a short cytoplasmic domain [168]. Each of the described 24 pairings of 18 α-subunits and 8 β-subunits has distinct binding partners [154].

Integrins can influence nearly all aspects of cellular functions and cell fate ranging from migration, polarity, proliferation to survival. They transmit signals from outside to inside of the cell ("outside-in signaling") and are also subject to signaling from inside the cell to outside ("inside-out signaling"). Inside-out signaling mediates the activation of integrins by conformational change, resulting in higher affinity to their ECM ligands. Ligand binding can then induce clustering of integrins, enabling formation of more stable ECM – integrin connections [169, 170]. In addition, integrin ligand binding and clustering in turn leads to outside-in signaling. Integrins lack catalytic activity. However, they recruit adaptor molecules and signaling molecules that mediate different cellular behaviors at sites of integrin activation. The most relevant signaling events will be described in the context of cell migration below.

Integrins in vascular development Integrins are expressed by EC and have a central position in organizing the vasculature by mediating functions like adhesion, migration, proliferation, survival, and differentiation [171]. Nine of the 24 integrin receptor pairs have known functions in angiogenesis (reviewed in [154, 172, 153]): α1β1 and α2β1

(collagen receptors), α3β1, α6β4 and α6β4 (laminin receptors), α5β1 and α4β1 (FN receptors), as well as αvβ3 and αvβ5 (receptors for FN and other ligands). Among those, the FN receptors have received most attention owing to key functions in vascular morphogenesis.

α5β1 integrin is the receptor mediating most functions of FN in vascular development, which has been demonstrated by knockout studies in mice. Global knockout of *Itgβ1* leads to early lethality in mice [173, 174]. EC specific knockout is also lethal at about E10 and leads to defects in angiogenic sprouting and vascular patterning without affecting vasculogenesis [175, 176, 177]. Recent studies employing inducible integrin β1 EC knockout strategies identified postnatal angiogenetic roles of β1 in vascular junctional integrity and lumen formation [178, 179]. Knockout of α5 results in a slightly milder but an overall very similar phenotype compared to knockout of FN [180]. Vascular defects of α5 knockout mice are a less branched cranial vasculature and decreased sprouting. In addition, embryoid bodies deficient for α5 or the α5β1 ligand FN show decreased network formation [158]. Further, it has been demonstrated that most functions of α5β1 are mediated by its binding to the RGD motif of FN. However, EC specific knockout of α5 did not cause the same defects as the global knockout. Vasculogenesis and initial angiogenesis are normal in these mice [181].

The role of αv subunit-containing integrin receptors in angiogenesis is less clear because of contradicting results gained from genetic ablation and *in vitro* pharmacological inhibition experiments. *In vitro* studies suggest a role of the αv containing heterodimers αvβ3 and αvβ5 in EC migration (reviewed in [151]). Further, αvβ3 integrin is reported to bind to and potentiate the activity of VEGF receptor 2 (VEGFR2) [182]. However, single or combined knockout of β3 and β5 in mice does not impair angiogenesis or pathological angiogenesis [183]. Moreover, mouse knockout studies showed that αv itself is also not essential for vascular development [158]. However, in α5 deficient embryonic cells, αv was able to functionally replace FN1 – α5 interaction needed for FN1 matrix assembly. α5/ αv double mutants show a more severe phenotype than mice deficient for FN1 or α5 alone. It was therefore suggested that α5 and αv have overlapping functions

in FN matrix assembly, but have distinct roles during gastrulation that are mediated by interaction of αvβ1 with other ligands [184, 185]. In mice with conditional knockout of *Itgαv* developmental angiogenesis is normal. EC specific *Itgα5* and *Itgαv* double knockout leads to remodeling defects of the great blood vessels and the heart as well as to reduced FN1 assembly. However, vasculogenesis and angiogenesis are normal [181].

Further knockout experiments showed that α4β1 (also called very late antigen 4 (VLA-4) receptor) and α5β1 do not have overlapping functions. Integrin α4 is not required for early blood vessel development [185, 184]. However, α4β1 integrin has been shown to support FN fibril assembly. Furthermore, α4β1 integrin has been demonstrated to be required for *in vivo* migration of several cell types. Knockout of *Itgα4* in mice leads to impaired migration of neural crest cells [186], epicardial progenitor cells [187] and pericytes/presumptive vascular smooth muscle cells [188]. Moreover, it mediates adhesion of hematopoietic cells [189] via interaction either with FN or its other receptor VCAM1. Furthermore, α4 integrin is required for development of the placenta and maintenance of the epicardium of the heart via adhesion to VCAM1 [190]. α4 integrin can also form a heterodimeric receptor with α4β7. This integrin has important functions in lymphoid tissue [191]. For review of integrin mouse knockout studies, see [192].

As mentioned above, α4β1 not only mediates its functions by binding to FN, but also via VCAM1. VCAM1 expression is stimulated by several cytokines such as TNFα or reactive oxygen species. It mediates recruitment of leukocytes to sites of inflammation where they then attach to VCAM1 expressed on activated EC via α4β1 and α4β7 [193]. In addition, α4β1 also mediates transendothelial migration of leukocytes [194]. VCAM1 has been shown to be involved in different inflammatory processes and in embryonic development [195, 196]. In addition to its role in mediating leukocyte adhesion, it can also influence the stability of cell – cell junctions. *In vitro* crosslinking of VCAM1 leads to activation of RAC1, which then promotes dissociation of VE-cadherin mediated cellular contacts [197, 198].

FN binding integrins in zebrafish Although there is a zebrafish homologue annotated for α4 integrin and VCAM1, respectively, no functional characterization of these genes has been conducted so far. Investigation of β1 integrin is rather difficult in zebrafish, considering that there have been described six different paralogues: β1-1 and β1-2 are most closely related to human β1, β1-3 is a more distant paralogue, and additionally there exist three truncated paralogues (β1tr1-3) that are closest to β1-3 [199]. Recently, their expression pattern during embryogenesis was analyzed [200]. For instance, β1-1 (now called β1a) is expressed in the DA from 22 hpf till 48 hpf and β1-2 (now called β1b) at myotome borders at 24 hpf and in the DA at 36 hpf. Functionally, β1 integrin has been described to regulate body asymmetry together with integrin αv and suggested to be the pairing partner of α5 during somite boundary formation (see below) [165].

More is known about the function of zebrafish α5 integrin: The zebrafish mutant *before eight* (*bfe*) is a loss-of-function mutant of *itgα5* and shows defective somitogenesis of the anterior somites [165]. This finding is also described by another group who performed a mutagenesis screen identifying *fn* and *itgα5* to be the responsible genes for anterior somite formation [166]. In addition, Koshida *et al.* showed the requirement of α5 integrin and Fn for maintenance of somite boundaries during development as well as for polarization of somite boundary cells. In a third study, the mechanism by which Fn fibril assembly is restricted to the somite boundaries has been revealed: Jülich *et al.* identified Ephrin 4/Ephrin B2a signaling to be the locally restricted initiator of inside-out mediated integrin α5 clustering leading to Fn matrix formation. The clustering of integrins precedes Fn matrix assembly, is independent of binding of integrin α5 to Fn and is only initiated at the sites of boundary formation. In other areas where no Ephrin 4/Ephrin B2a signaling is present, integrins non-cell-autonomously inhibit clustering and fibril formation in adjacent cells [201].

1.3.2 Vascular endothelial growth factors and their receptors

VEGFs are secreted pro-angiogenic ligands that are crucial regulators of blood vessel formation. In mammals, five different *VEGF* family genes have been identified: *VEGFA, B, C, D*, and *placental growth factor* (*PLGF*). They bind in an overlapping pattern to

three receptor tyrosine kinases: VEGF receptor 1, also known as FLT1 (fms-related tyrosine kinase 1), VEGFR2, also named FLK1 (fetal liver kinase 1) or KDR (kinase insert domain receptor)), and VEGFR3, also named FLT4 (fms-related tyrosine kinase 4). VEGFR1 and especially VEGFR2 play essential roles during blood vessel development and function, whereas VEGFR3 mainly regulates development and function of the lymphatic system. Upon binding of ligands, VEGFRs form homo- or heterodimers, which leads to activation of receptor-kinase activity and autophosphorylation of the receptors. After interacting proteins are recruited, an array of signaling pathways is induced that execute the diverse functions of VEGFR signaling. (For review of VEGFs and VEGFRs see [202]).

In mammals, VEGFA mediated signaling via VEGFR2 is essential for vasculogenesis as VEGFR2-deficient mice fail to form the primary vasculature and die at early embryonic stage [203]. VEGFR2 signaling mediates different context dependent EC responses to VEGFA, such as survival, proliferation, migration, and vascular permeability, that are all essential for vessel formation, stabilization, and maintenance. In detail, ligand binding of VEGFA leads to homodimerization of VEGFR2 and subsequent autophosphorylation of different tyrosin residues. These serve as binding sites for different adaptor molecules or signaling molecules, that mediate distinct cellular responses. One example is the recruitment of PLCG, which activates protein kinase C (PKC) and the mitogen-activated protein kinase (MAPK)/extracellular-signal-regulated kinase-1/2 (ERK1/2) cascade, stimulating proliferation of EC [204]. Cell survival, vascular permeability, and migration can be induced via the adaptor protein Shb, which activates PI3K followed by AKT and RAC signaling [205, 206, 207]. Further downstream targets of VEGFR2 signaling are FAK and p38 MAPK, also influencing EC migration (FAK, p38) as well as vascular permeability (p38) (for review see [202]). Furthermore, signaling outputs can vary dependent on the receptor composition, as VEGFR2 can not only form homodimers, but also heterodimers (VEGFR2 - VEGFR1 or VEGFR2 - VEGFR3) [208, 209, 210].

VEGF receptors in zebrafish In contrast to mammals, zebrafish have four different VEGF receptors. According to a revised nomenclature and phylogenetic analysis [211], three of them are orthologues of the human VEGF receptors: *flt1* is the orthologue of *VEGFR1/FLT1* [212, 213], *kdr* the orthologue of *VEGFR2/FLK1/KDR*,[212, 214, 215] and *flt4* the orthologue of *VEGFR3/FLT4* [216]. In addition, a fourth VEGF receptor gene, called *kdrl* (*kdr like*) exists that was secondarily lost within the eutherian lineage [217, 211].

1.3.3 Notch signaling

Notch signaling is a well conserved mechanism of determining cell fates and behaviors [218]. In vertebrates, there are five Notch ligands (Jagged1 and Jagged2, Delta-like 1 (Dll1), Dll3 and Dll4) and four Notch paralogues (Notch 1–4). In contrast to VEGF signaling, both, the ligands and receptors are transmembrane proteins. Upon binding of a Notch ligand presented by the neighboring cell, cleavage of the Notch intracellular domain (NICD) by ADAM10 (a disintegrin and metalloprotease 10), ADAM17, and presenilins is induced. The NICD then translocates to the nucleus where it functions as a transcriptional regulator of the hairy and enhancer of split (Hes) family of basic-loop-helix proteins, which are mainly transcriptional repressors (for review see [219]).

1.3.4 Development of the zebrafish vasculature

The zebrafish is a well suited animal model to study vascular development. Their optical transparency and availability of transgenic lines allows for live imaging of the formation of the vasculature. Additionally, zebrafish embryos can survive without a vascular system or blood circulation for up to one week due to their small size allowing for circulation independent diffusion of oxygen and nutrients [220, 221].

In zebrafish, as in all vertebrates, the first blood vessels are formed by vasculogenesis. Taking advantage of live imaging in the developing embryo, especially the formation of the major vessels of the zebrafish trunk, namely the DA and the posterior

cardinal vein (PCV), is well studied. During vasculogenesis of the DA and the PCV, angioblasts migrate guided as individual cells towards the embryonic midline where they coalesce [222]. In this primary vascular cord, both precursors of the DA and the PCV can be found [223]. Arterial cell fate is then mediated by Vegfa signaling via Kdrl, leading to up-regulation of Notch, which represses the venous cell fate [224, 225, 226]. In contrast, venous cell fate requires signaling via Flt4 and is independent of Vegfa [223, 225]. As a result of Vegf and Notch mediated arterio-venous specification several markers are differentially expressed, which can be used to asses for defects in this process: For example, EC of the DA express Ephrin-B2a, whereas EC of the PCV express Ephrin 4a [227, 228].

After the first axial blood vessels have formed by vasculogenesis, the elaboration of the vasculature by angiogenesis is achieved by sprouting of blood vessels from the already existing ones. Due to their easy accessibility and highly stereotypic order, the growth of the vessels that sprout dorsally from the DA and later the PCV, the ISV, is intensively studied [229, 230, 231]: In a first wave of sprouting, the intersegmental arteries (SA) are formed. They emerge from the DA at 22 hpf and grow dorsally between the somites (which will later in development give rise to skeletal muscle, vertebrae, and dermis) along the intersomitic fissure until they reach the horizontal myoseptum. Then, they migrate to the dorsal roof of the neural tube, which the EC reach at about 30 hpf. From there, the EC extend laterally and interconnect with the EC of the neighboring SA to form the future dorsal longitudinal anastomotic vessel (DLAV) at 32 hpf. At the same time, the PCV gives rises to a second wave of sprouts, which connect either with the SA and subsequently become intersegmental veins (IV), or migrate further dorsally to the level of the horizontal myoseptum and contribute to the development of the lymphatic system.

The control of sprouting of the SA depends largely on regulation by Vegfa and Vegfc, their signaling via flt1, kdrl, and flt4, and the interplay with Notch signaling (see section 1.3.5). In contrast, less is known about regulation of the second wave of sprouting. Vegfa signaling in SV seems not to be as important as in SA, as mutants for the Vegfa downstream signaling mediator Plcγ do only show impaired SA growth whereas SV growth is unaffected [225, 232]. In contrast, Vegfc signaling via Flt4 is crucial for SV

sprouting and lymphangiogenesis [233]. Besides collagen and calcium-binding EGF domain-1 (Ccbe1), which leads to similar defects in lymphangiogenesis if missing [231], Bone morphogenic protein (Bmp) signaling has been shown to regulate sprouting from the PCV. Apart from inducing growth of dorsal sprouting from the PCV, Bmp signaling induces also ventral sprouting and thereby the formation of the caudal vein plexus [234, 235].

1.3.5 Mechanisms of sprouting during angiogenesis

During sprouting angiogenesis, a number of EC tasks have to be regulated: migration, proliferation, adhesion to other EC and the ECM. In addition, the behavior of several individual EC in the sprout has to be orchestrated in a way that the sprout as a cell collective can grow. This means that not only polarization and directional migration of the individual EC is required, but the sprout as a whole needs to acquire an overall polarized character. The leading cell senses and integrates chemotactic and haptotactic stimuli, leading to extension of one lamellipodium and several filopodia into the guided direction whereas the trailing cells maintain cell-cell contacts. Thus, formation of an entire vascular network requires directed growth and migration of sprouts at distinct sites along specific paths.

To ensure initiation of sprouting at distinct sites and sprout growth along defined paths, pro-angiogenic signaling cues have to be provided either locally restricted at the correct time, or the EC need to integrate and respond distinctively to such cues. Evidence for both mechanisms exist, and especially the VEGF and Notch signaling pathways proved to be pivotal in this process. Results obtained from using the mouse retina and the zebrafish ISV as model systems are implemented in the so called “tip cell concept”, a framework to explain regulation of sprouting angiogenesis [236]. First, the basic concepts of tip and stalk cell selection and the most important signaling events are explained that are shared by both model systems. Then, the regulation of arterial sprouting in the zebrafish is described in more detail. In the sections following afterwards, additional aspects regulating sprouting angiogenesis are introduced.

1.3.5.1 The tip cell concept

As the first step of sprouting angiogenesis, the EC that starts to sprout from an existing vessel and leads the newly forming vessel has to be selected. In the tip cell concept, the cell with the highest VEGFR2 signaling, either due to high expression of VEGFR2 or a locally high VEGF environment, is selected for this position, as VEGFR2 signaling leads to a highly motile behavior with high filopodia activity. Indeed, cells with such a phenotype are found at the tip of sprouting vessels and are thought to guide the sprout along growth factor gradients and other guidance cues. In addition to VEGFR2, tip cells are characterized by high expression of VEGFR3 and VEGFR2/3 heterodimers, which also promote sprouting.

In the sprout, tip cells are followed by EC named stalk cells. They are characterized by low filopodia extensions and stable EC-EC contacts and are thought to extend the sprouting vessel by proliferation. The stalk cell phenotype is a result of lateral inhibition by the tip cell via Notch signaling: As a consequence of high VEGFR signaling, the leading tip cell expresses high levels of the Notch ligand Dll4. Dll4 ligands bind to Notch receptors expressed on neighboring EC leading to reduced expression of VEGFR2 and 3, but increased expression of VEGFR1. VEGFR1 has higher affinity for VEGFA than VEGFR2 but has only a weak Tyr kinase activity. In addition, two isoforms of VEGFR1 exist, a membrane bound and a soluble version. The membrane bound VEGFR1 has lower signaling capacity than VEGFR2. In addition, the soluble form captures VEGFA thus leading to less VEGFA signaling via VEGFR2. Therefore, VEGFR1 functions as a decoy receptor reducing angiogenesis and sprouting. Expression of VEGFR1 in stalk cells thus not only leads to less VEGF signaling in those cells, but also laterally inhibits sprouting of neighboring EC via the soluble decoy isoform, thus contributing to regulate the number of selected tip cells.

An additional aspect of the tip cell model is its dynamic nature: Tip and stalk cells are no states of cellular differentiation but rather a result of stochastic selection due to differences in VEGF and Notch signaling. Therefore, if a stalk cell experiences reduced Notch input or is exposed to stronger VEGFR signaling, it can become a tip cell and

vice versa. Taken together, competition of EC for VEGF and the interplay between VEGF and Notch signaling ensure cooperated sprouting in angiogenesis. (For review see [237] and references therein; for a more in-depth discussion of the concept see [238].)

1.3.5.2 Regulation of sprouting of the zebrafish intersegmental artery

As in mice and humans, VEGFA signaling has a crucial function in zebrafish angiogenesis [239, 224, 215]. The zebrafish Vegfa receptors *kdrl* and *kdr* are expressed in all EC [214]. Of the two receptors, Kdrl is more important than Kdr: KD of *kdr* alone does not lead to defects in SA formation, whereas knockout of *kdrl* leads to impaired SA growth. In addition, knockout of *kdrl* more closely resembles the phenotype observed upon loss of zebrafish Vegf or Plcγ, which is required for SA formation downstream of Vegf [225, 215].

In contrast to *kdrl*, the human *VEGFR3* homologue *flt4* is expressed and required for differentiation of the PCV, but not for the DA. However, like *kdrl*, it is also needed for normal SA formation. KD of *flt4* in wildtype embryos causes partial SA formation [215, 240]. This phenotype was, however, not replicated by a recently generated *flt4* mutant [241].

In agreement with the tip cell concept, Dll4 mediated Notch signaling antagonizes VEGF signaling also in zebrafish SA. *dll4* KD embryos show increased proliferation in the sprout as well as prolonged migratory and excessive filopodia activity of EC in the SA at the level of the DLAV [242, 240]. Consistently, absence of Notch signaling increases the number of EC migrating into the sprout as well as their proliferation. Furthermore, individual EC lacking Notch activity were found to occupy the tip position of a sprout more frequently than wild type EC whereas cells with increased Notch signaling are excluded from this position. A further consequence of missing Notch signaling is that *flt4* expression is not longer restricted to the PCV and the cell at the tip of the SA sprout, but ectopically expressed also in the DA and throughout the sprout. Reducing Flt4 levels in the Notch-deficient background partially rescues EC number within SA sprouts [240], suggesting that Notch antagonizes VEGF signaling by

blocking expression of *flt4* [227, 240]. In conclusion, Notch signaling restricts angiogenic cell behavior to tip cells in developing SA by antagonizing VEGF signaling (reviewed in [243]).

Like its human homologue *VEGFR1*, zebrafish *flt1* was also found to negatively regulate angiogenesis [244]: KD of *flt1* leads to increased branching of SA that develop a patent lumen. Supporting increased VEGF signaling in *flt1* morphants, expression of Notch receptors and the Notch downstream target *efn B2a* is reduced and *flt4* is ectopically expressed in the DA. However, although the *flt1* KD phenotype shows aspects of reduced Notch signaling, it does not phenocopy the *dll4* KD phenotype: the aberrant branching patterns are different.

Although the above described aspects of SA development support a model of an organized SA formation according to the tip cell concept, there are several other findings that suggest a less strictly ordered growth. Live imaging recordings of EC with GFP labeled nuclei showed that also EC at the tip of a sprout divide [245]. According to the tip cell concept, however, due to increased Notch signaling only EC in the stalk should proliferate [242]. Furthermore, the observations that EC in the sprouting SA change their position within the sprout, and that junctional organization between EC varies between different SA, speak for a less stereotypical and more plastic behavior of EC in SA formation [245].

1.3.5.3 Guidance cues

Besides the major regulators of SA development, VEGF and Notch signaling, there are several other mechanisms that can influence angiogenesis (reviewed in [150]). Among those, guidance cues are important to ensure controlled migration of EC along certain paths, e.g. along tissue boundaries. Interestingly, many guidance cues are not only needed to direct migration of EC but have already been implicated in axonal guidance, such as Netrins and receptors, Ephrin and Ephrin-receptors, ROBO and Slit, and Semaphorins with their receptor families of Neuropilins (as co-receptors of VEGFRs) and Plexins [150].

The function of muscular semaphorin Sema3aa/ab and its endothelial receptor PlexinD1 (PlxnD1) are well described in zebrafish angiogenic sprouting [246, 247, 248]. ISV sprout from the DA and PCV at defined sites, namely the somite boundaries. In the zebrafish mutant *out of bounds* (*obd*), which has a mutation in the gene encoding the zebrafish *plxnD1*, or upon KD of *plxnD1*, additional ectopic ISV sprouts are formed. The sprouts are not restricted to somite boundaries, no longer avoid the ventral somites and interconnect with each other. This results in ISV with a ventral plexus-like organization and normal DLAV formation, which is able to form a functionally perfused vascular network. Further, remodeling of the caudal vein sinus and ventral sprouting from the PCV is abnormal [246, 247]. The number of EC in the mis-patterned vessels is not different to wild type vessels, showing that mis-guided migration rather than overt proliferation causes this phenotype. Also, the axial blood vessels, the DA and the PCV, form normally and arterial-venous differentiation is not affected [247]. In a further study, Zygmunt *et al.* showed that PlxnD1 deficiency leads to decreased relative abundance of the soluble Vegf decoy isoform of *flt1*, *sflt1*. Decreased levels of *sflt1* lead to increased Vegf availability for Vegfr signaling and consequently to increased angiogenic behavior of EC in *obd* mutants. KD of the PlxnD1 receptors expressed by somites, the SEMA3A orthologues *sema3aa* and *sema3ab*, leads to a similar phenotype than loss of PlxnD1 [247]. In summary, Sema – PlxnD1 signaling is required not only to guide the sprout along the somite boundaries but also to restrict the angiogenic potential of individual EC spatially by regulating relative abundance of *sflt1*.

1.3.5.4 EC – EC contacts in angiogenesis

Maintenance as well as rearrangements of EC – EC contacts are required for collective migration of EC in angiogenesis. Contacts are made by tight and adherens junctions. VE-cadherin is the critical component of adherens junctions. Mutant mice die at mid-gestation with defects in the vasculature pointing to defects in maintenance of vascular integrity [249]. In zebrafish, VE-cadherin KD leads to prolonged angiogenic activity of the ISV due to lack of contact formation between EC of adjacent SA leading to a dorsal hypersprouting phenotype. The lack of stable contacts between EC also causes lack of perfusion, since stable contact formation is required for lumen formation [250].

1.3.5.5 ECM – EC interactions and interplay with VEGF

Besides the above described functions of FN in vascular morphogenesis, further angiogenesis regulating mechanisms of FN and ECM involving VEGF are described (reviewed in [251]). One way is the action of the ECM as a regulator of VEGFA diffusion and gradient shaping [252, 253]. VEGFA is differentially spliced resulting in the isoforms VEGFA121, VEGFA145, VEGFA165, VEGFA189 and VEGFA206. In mice, the five different splice variants of *Vegfa* are one amino acid residue shorter. The different variants are characterized by different abilities to associate with heparan sulfate proteoglycans like FN in the ECM. VEGFA189 has two domains to interact with heparan sulfates and is tightly associated with the ECM, whereas VEGFA121 lacks those domains and is hence freely diffusible. The VEGFA165 isoform has one heparan sulfate binding domain and shows intermediate diffusive properties [251]. By expression of variable ratios of the VEGFA isoforms a concentration gradient can be generated, resulting in a patterning cue for vascular network formation [253]. If only the diffusible form VEGFA120 is expressed in mice, vascular branching complexity is reduced, whereas in mice expressing only VEGFA188, vascular branching complexity is increased [253]. In mouse retinas deficient for FN, EC migration is slightly reduced due to missing integrin $\alpha 5\beta 1$ binding to the RGD sequence of FN and branch points in the vascular plexus are increased due to missing VEGFA binding to FN [252].

Another example of ECM – VEGF interaction is the influence of the ECM on VEGFA signaling strength via VEGFR2. Further, matrix bound VEGFA can trigger $\beta 1$ integrin clustering thereby influencing integrin signaling. In addition, laminin411 was shown to activate the notch pathway via integrin signaling and control of Dll4 expression thereby indirectly influencing VEGF responsiveness of EC and hence tip cell selection [254, 255]. Further, the ECM influences branching morphogenesis by its mechanical properties. For example, cell – ECM interactions lead to generation of forces that can modulate the expressed ratio of VEGFA splice variants [256]. Also, the "stiffness" of the ECM influences protrusion and extension of filopodia and thereby regulates EC branching *in vitro* [257].

1.4 Conjunction of vascular and neuronal (dys-)functions

Over half a millennium ago, Andreas Vesalius already noted the close proximity of nerve and vessel networks in the human body. It should therefore not come as a surprise that shaping of both networks is based on similar mechanisms. Indeed, both systems have to reach and serve every part of the body, and dysfunction of each system leads to serious, often lethal diseases. During development, neuronal axons have to be guided to their target region, just like the collectively migrating EC. Originally identified in neuronal pathfinding, the guiding cues have now also been described to direct angiogenic sprouting: Netrins, Semaphorins, Slits, and Ephrins and their receptors [258]. Interestingly, also integrins and ECM composition regulate not only migration and network formation of EC, but also neurite extension during embryonic development and axon regeneration [259, 260]. Upon injury of nerve terminals in the adult peripheral nervous system (PNS), FN is alternatively spliced resembling embryonic splice variant patterns leading to increased integrin $\alpha 4$ signaling thus promoting regeneration [261, 262, 263]. Also in the CNS, FN associated with astrocytes might be critical for axonal regeneration, although this is only shown in an *in vitro* model of white matter with dorsal root ganglion neurons [264].

A further striking example of a factor that regulates crucial functions in neurons and EC is VEGF. Already having described numerous functions of VEGF and its receptors in EC in the previous chapters, its functions in neurons and the brain include increase of neurogenesis, improvement of cognitive performance and memory, effects on synaptic transmission, and promotion of neurite extension [9]. Owing to these functions, intracerebroventricular treatment of an SOD1 ALS mouse model with VEGFA 165 shows beneficial effects [265]. Taken together with other positive results of similar studies [266, 267], this led to a clinical trial of VEGF therapy in ALS patients [268]. A possible role of decreased neurotrophic support due to reduced VEGF levels in ALS is implied by another mouse model. This model lacks the regulatory sequence regulating transcription of the *VEGF* gene in response to lack of oxygen: the hypoxia-inducible

factor (HIF1) response element in the VEGF promotor sequence. The mouse model develops age-dependent, selective degeneration of motor neurons strikingly similar to ALS [269]. GWAS studies in ALS patients attempting to link a *VEGF* haplotype leading to reduced expression of VEGF could not support this hypothesis, leaving the question of relevance of this mouse model for humans open [270]. However, other links between neurodegeneration and vascular dysfunction have been discovered. These are described in the next sections.

1.4.1 Hypoperfusion in neurodegeneration

The human brain heavily depends on oxygen and nutrient supply provided by the vascular system. This is highlighted by its high share of total oxygen and glucose consumption (about 20 and 25%, respectively) [271]. Upon increased neuronal activity, the so called hemodynamic response or neurovascular coupling leads to an increase in blood flow, thus ensuring sufficient oxygen and nutrient delivery as well as removal of carbon dioxide and other metabolites. The functional unit regulating the hemodynamic response and building the anatomical, biochemical, and immunological BBB is the "neurovascular unit" (NVU), comprised of neurons, EC, pericytes, vascular smooth muscle cells, and glia (astrocytes, microglia, and oligodendroglia) [271]. Thus, defects in non-neuronal cells of the brain can lead to defective neurovascular coupling ("neurovascular uncoupling"), impairing neuronal functions like synaptic plasticity. A reduction in cerebral perfusion of greater than 80% causes neuronal death. Therefore, defects in the NVU and, as a consequence, insufficient cerebral blood flow are discussed to contribute to neurodegeneration. Indeed, as reviewed by Berislav Zlokovic in [7] and other authors in [272, 273, 274], reductions in cerebral blood flow or its dysregulation have been observed in many neurological disorders, including AD and ALS, with AD being the best studied disease in this respect. Intriguingly, neuroimaging studies of patients with AD or ALS have shown that neurovascular uncoupling precedes neurodegenerative changes [275, 276, 277, 278].

1.4.2 Defects of the blood brain barrier in neurodegeneration

As described above, the BBB, a highly specialized continuous endothelial cell membrane, is part of the NVU. It regulates entry of cells, e.g. leukocytes, from the blood into the brain and the chemical composition of the neuronal "milieu", hence guarding the functional environment required for neuronal function, angiogenesis, and neurogenesis in the adult brain [271]. The BBB forming EC are connected by tight and adherens junctions, preventing solutes to diffuse freely across the barrier. The main components of tight junctions are occludins and claudins, with ZO-1 proteins linking them to the cytoskeleton. The adherens junctions are intermingled with tight junctions.

Perturbation of BBB integrity and function is reported in many neurological disorders, such as Alzheimer's disease, Parkinson's disease, multiple sclerosis, trauma, brain tumors, stroke, and epilepsy [274]. For example, reduced expression of mRNAs encoding key tight junction proteins is described in ALS [279]. Moreover, the barrier between blood and spinal cord, the blood spinal cord barrier (BSCB) is reported to be damaged in ALS patients [280]. The deposition of hemoglobin-derived iron within the CNS, being indicative of barrier leakage, is reported in two further studies [281, 282]. However, the studies conducted in patients or with patient material do not reveal whether BBB or BSCB disruption is an early, potentially disease causative event, or a late downstream effect reflective of a more general brain damage.

Mouse models also support an involvement of defective BBB/BSCB in neurodegeneration. Age-dependent progressive pericyte loss can cause BBB disruption and microvascular degeneration, eventually leading to neuronal dysfunction and neurodegenerative symptoms [283]. Further, several studies using SOD1 rodent models overexpressing human SOD1 with disease mutations demonstrated that these mice have compromised BBB/BSCB function. BBB/BSCB impairment is accompanied by reduced capillary perfusion, even preceding neuronal degeneration [284, 285, 286, 287, 288, 289]. PGRN is also implicated in BBB function, as loss of *GRN* promotes BBB disruption in an ischemia mouse model [290]. Recently, a further piece of evidence for vascular deficiency as a contributing element in neurodegeneration was discovered: Loss of TDP-43 in

neurons leads to temporary BSCB defects in mice. In contrast to the SOD1 mouse model, expression of tight junction proteins like claudin-5, occludin, or ZO-1 in spinal cords is not altered. However, in the early symptomatic stage, EC of the BSCB have vacuoles, are swollen, and extend protrusions into the lumen of the capillaries. Tight junctions appear ultrastructurally intact. In the late symptomatic stage, when motor neurons appear smaller, the defects in the EC could no longer be detected, presumably due to compensatory mechanisms by microglia and astrocytes [291].

Taken together, defects in BBB and BSCB are related to several genes associated with ALS and FTD. Defects are also found in patients and might contribute to disease initiation and/or progression. Additionally, dysregulation of cerebral perfusion is a phenomenon found in many neurodegenerative diseases including ALS, substantiating the link between the vascular system and neurodegeneration. However, the causative contribution of vascular system-associated defects to most neurodegenerative diseases, such as ALS and FTD, remains unclear.

2 Material and Methods

2.1 Material

2.1.1 Zebrafish lines

The following zebrafish lines were used for the study:

Zebrafish line	**Origin, Reference**
wild type AB	G. Streisinger, Institute of Neuroscience, University of Oregon, Eugene, USA
wild type TLF	C. Nüsslein-Volhard, MPI for Developmental Biology, Tübingen, Germany
tardbp^{mde198}*-/-* (*tardbp -/-* in this thesis)	B. Schmid & A. Hruscha, DZNE and LMU Munich, Germany [147]
tardbp^{mde159}*-/-* (*tardbp -/-* in this thesis)	B. Schmid & A. Hruscha, DZNE and LMU Munich, Germany [147]
tardbpl^{mde222}*-/-* (*tardbpl -/-* in this thesis)	B. Schmid & A. Hruscha, DZNE and LMU Munich, Germany [147]
Tg(fli1:EGFP)^{y1}	J. Bussmann, MPI for Molecular Biomedicine, Münster, Germany, [222]
Tg(fli1:nlsEGFP)^{y7}	H.G Belting, University of Basel, Switzerland, [292]
Tg(kdrl:HRAS-mCherry)^{s896}	P. Hammerl, Helmholtz Center Munich, Germany, [293]

2.1.2 Cell lines

Cell line	Origin
HEK293T	ATCC-Nr. CRL-1573
HUVEC pooled	PromoCell, C-12203

2.1.3 Morpholinos

MO were purchased from Gene Tools. Sequences are given in 5'-3' orientation; e: exon; i: intron.

Targeted mRNA and region	Sequence
tardbp-5'UTR	CAATAAACAACTGCTCGGGTCCAGT
tardbp-ATG	CTCGAATGTACATCTCGGCCATCTT
tardbp-e3i3	TTTTACCTGCACCATGATGACTTCC
tardbpl-5'UTR	AGCACTAAGGCAACAAACGGAGCCG
tardbpl-ATG	ATAGCACTCCGTCATGATTACACCG
tardbp-e3i3	CTAACCTGCACCATGATCACCTCTC
vcam1-e1i1	CTAACAGATGAAACTTACCTGCAAC
itga4-e2i2	GTAATGGAGGGAAAACCTACCAACA
itga5-5'UTR [165]	TAACCGATVTATCAAAATCCACTGC
itgaV-ATG [294]	CGGACGAAGTGTTTGCCCATGTTTT
*fn1a*mo1 [162]	TTTTTTCACAGGTGCGATTGAACAC
*fn1b*mo1 [165]	TACTGACTCACGGGTCATTTTCACC
*fn1b*mo2 [165]	GCTTCTGGCTTTGACTGTATTTCGG

2.1.4 Whole mount *in situ* hybridization probe sequences

RNA antisense probes for whole mount *in situ* hybridization (WISH) are listed in Table 2.2 and were kindly provided by the cited laboratories. The indicated restriction

Gene	Plasmid No.	Restriction enzyme	Polymerase	Origin, Reference
ephrin B2a	I08	SalI	T7	B. Weinstein, [227]
flt4	I61	EcoRI	T7	A. Siekmann, [227]
mflt1	I64	NcoI	SP6	A. Siekmann, [212]
sflt1 (UTR)	I57	HindIII	T7	Mathias Teucke
plxnD1	I13	HindIII	T7	B. Weinstein, [247]
sema3aa	I14	XbaI	T7	S. Childs [295]
sema3ab	I15	XbaI	T7	S. Childs, [247]

Table 2.2: WISH probes

enzyme was used for linearization of the respective vector and the indicated polymerase used for generation of the respective antisense probe. The probe binding *mflt1* covers 700 nt of sequence that is shared with *sflt1* and 400 nt that are specific for *mflt1*. The expression pattern is identical to a *mflt1* binding probe published in [248] and hence termed *mflt1*.The *sflt1* probe was cloned from zebrafish cDNA by Mathias Teucke and cloned into the vector pCS2+GW-A.

2.1.5 Oligonucleotides

Oligonucleotides were synthesized by Thermo Scientific or Sigma-Aldrich. Sequences are given in 5'-3' orientation. The abbreviation and number in the oligonucleotide name refer to the Schmid laboratory oligonucleotide database. F: forward primer; R: reverse primer.

2.1.5.1 Oligonucleotides for cloning of shRNAs (target sequence in capitals)

shCtr (targeting luciferase) sense	gatccccCGTACGCGGAATACTTCGAttcaagaga TCGAAGTATTCCGCGTACGttttttggaaa
shCtr (targeting luciferase) antisense	tttccaaaaaCGTACGCGGAATACTTCGAtctcttgaa TCGAAGTATTCCGCGTACGggggatc
sh*TARDBP*#1 sense	gatccccGGAGAGGACTTGATCATTAttcaagaga TAATGATCAAGTCCTCTCCttttttggaaa

sh*TARDBP*#1 antisense	tttccaaaaaGGAGAGGACTTGATCATTAtctcttgaa TAATGATCAAGTCCTCTCCggggatc
sh*TARDBP*#2 sense	gatccccGGGTATGATGGGCATGTTAttcaagaga TAACATGCCCATCATACCCtttttggaaa
sh*TARDBP*#2 antisense	gggCCCATACTACCCGTACAATaagttctct ATTGTACGGGTAGTATGGGaaaaacctttcga

2.1.5.2 Primer for sequencing

GATC M13-F	TGTAAAACGACGGCCAGT
GATC M13-R	CAGGAAACAGCTATGACC
GATC SP6	ATTTAGGTGACACTATAGAA
GATC T7-981079	TAATACGACTCACTATAG

2.1.5.3 Primer for genotyping

oC80 Tardbp-ZFN-Ex2-F2	GAGTGCTGTGAATTTAAACATTT
oC76 Tardbp-ZFN-Ex2-R2	GCAATTGTGCATGTTTTCAGG
oC05 tardbpl start F1 ohne REZ	AATGACACAAGACGTCCTCATAAA
oD77 bpl-mod1a-R (+M13R)	caggaaacagctatgaccGGATAATTAAC CACGT ACACCAGATTGCCCCAGTC TGCTTCTGGTGCAggaagaacc
KSA41 EGFP F	AAGGGCATCGACTTCAAGGA
KSA42 EGFP R	GGCGGATCTTGAACTTCACC

2.1.5.4 Primer for KD validation of Itgα4 and Vcam1

KS A53 dr-itga4-Ex17-18 F	AGGTTTCTGCTCGTTTGGTT
KS A54 dr-itga4-3UTR R	CTTTCATGCTTGGGCACATA
KS A55 dr-vcam1-ex1-2 F	GCTTTCTTGCTGACTTTGCT

KS A56 dr-vcam1-ex1-2 R	GCATCTCAGCTCATTCCTGTC

2.1.5.5 Primer for quantitative PCR

oA03 β-actin F	TGTTTTCCCCTCCATTGTTGG
oA04 β-actin R	TTCTCCTTGATGTCACGGAC
KS A1 sema3ab_I1_F	AACGTACCCCGGCTTAAACT
KS A2 sema3ab_I1_R	GCAGAGCTGTTAGCCAATCC
KS A3 sema3aa_I1_R	TCCATCAGGAACGTGTCGTA
KS A4 sema3aa_I3_F	CTTCCAAACGCGATGAATG
KS A5 Vegfr2_I11_F	TCCTCTTCCCATTGAAAACG
KS A6 Vegfr2_I11_R	CTGTTTTCACCACCAGGGTA
KS A7 mflt_I24_F	TGGTCATATGGAGTCCTGCTC
KS A8 mflt_I24_R	AGGAGAACACATCCGAGTGC
KS A9 sflt_E10-11c_F	GTCCCACCACCTCAAATCC
KS A10 sflt_E10-11c_R	GGCCCACAACTCCACTCTC
KS A11 Rpl13a_E3-4a_F	ATTGTGGTGGTGAGGTGTGA
KS A12 Rpl13a_E3-4a_R	CATTCTCTTGCGGAGGAAAG
KS A13 elf1a2 F	AGCAGCAGCTGAGGAGTGAT
KS A14 elf1a2 R	GTGGTGGACTTTCCGGAGT
KS A43 dr-vcam1 ex9-10 F	CAAACGACCTGGGTTACGAA
KS A44 dr-vcam1-ex9-10 R	CAGCAGAACCTCCCAAGAAA
KS A45 dr-itga4-ex2-3 F	TGCAGTATGTTGAACAGCCAG
KS A46 dr-itga4-ex2-3 R	CAAACTCACACCCAGCCAC
KS A47 dr-fn1a-ex3-4 F	TGTACTTGCATTGGCTCTGC
KS A48 dr-fn1a-ex3-4 R	GTCTCTGCCATGTGTCTCCA

KS A49 dr-fn1b-ex39-40 F	CATTGCCCTTCTGAATAACCA
KS A50 dr-fn1b-ex39-40 R	ATGACTGGGCAGGCTAGGTA

2.1.6 Bacteria

Name	**Company**
DH5α *E. coli* competent cells	Hanahan
One Shot TOP10 Chemically Competent *E. coli*, C4040	Invitrogen

2.1.7 Antibodies

The following antibodies were used for whole mount immunofluoresecence stainings (IF) and immunoblot (here abbreviated as WB for Western blotting).

Antibody (Species)	**Dilution**	**Company**
α-actin, clone AC-15 (mouse)	WB: 1:1000	Sigma-Aldrich
α-tubulin, T6199 (mouse)	WB: 1:10000	Sigma-Aldrich
AKT, 9272 (rabbit)	WB: 1:1000	Cell Signaling
β-dystroglycan, NCL-b-DG	IF: 1:50	Novocastra
Calnexin, SPA-860 (rabbit)	WB: 1:10000	Stressgen
ERK1/2, 9102 (rabbit)	WB: 1:2000	Cell Signaling
FAK, 13009 (rabbit)	WB: 1:1000	Cell Signaling
Fibronectin, F3648 (rabbit)	IF: 1:100	Sigma-Aldrich
Fibronectin, HPA027066 (rabbit)	WB: 1:500	Sigma-Aldrich
GFP, 632375 (mouse)	IF: 1:500	Clontech
GFP, 632592 (rabbit)	IF: 1:500	Clontech
Integrin α4, 8440 (rabbit)	WB: 1:1000	Cell Signaling
Integrin β1, 610467 (mouse)	WB: 1:2000	BD

Ki67, NCL-Ki67p (rabbit)	IF: 1:100	Leica
Tardbp antibody 4A12-111	WB: 1:1	Helmholtz Center Munich [147]
TDP-43 N-term, SAB4200006 (rabbit)	WB: 1:10000 -1:50000	Sigma-Aldrich
p38, 9212 (rabbit)	WB: 1:1000	Cell Signaling
pAKT, 9271 (rabbit)	WB: 1:500	Cell Signaling
pERK1/2, 9101 (rabbit)	WB: 1:2000	Cell Signaling
PI3K, 4292 (rabbit)	WB: 1:1000	Cell Signaling
PLCG1, sc-426 (rabbit)	WB: 1:200	Santa Cruz
pp38, 9211 (rabbit)	WB: 1:1000	Cell Signaling
pPLCG1, SAB4300082 (rabbit)	WB: 1:500	Sigma-Aldrich
pPI3K, 4228 (rabbit)	WB: 1:1000	Cell Signaling
pVEGFR2, 2478 (rabbit)	WB: 1:1000	Cell Signaling
VCAM1, 12367 (rabbit)	WB: 1:500	Cell Signaling
VEGFR2, 9698 (rabbit)	WB: 1:1000	Cell Signaling
vinculin, V-4505(mouse)	IF: 1:200	Sigma-Aldrich

2.1.7.1 Secondary antibodies

Antibody	**Dilution**	**Company**
Alexa Fluor 405 anti-mouse, A-31553	1:500	Invitrogen
Alexa Fluor 405 anti-rabbit, A-31556	1:500	Invitrogen
Alexa Fluor 488 anti-mouse, A-11029	1:500	Invitrogen

Alexa Fluor 488 anti-rabbit, A-11034	1:500	Invitrogen
Alexa Fluor 568 anti-rabbit A-11011	1:500	Life technologies
Alexa Fluor 622 anti-rabbit A-21070	1:500	Life technologies
anti-rabbit-HRP, W401B	1:10000	Promega
anti-mouse-HRP, W402B	1:5000	Promega

2.1.8 Chemicals

2.1.9 Chemical inhibitors

Target of inhibitor	**Name of inhibitor**	**Company**
ERK1/2	SL327, Cat. S4069	Sigma
PI3K	AS605240, Cat. A0233	Sigma
VEGFR2, VEGFR3, PDGFRB	Sutent/Sutinib Malate, Cat. S1042	Selleck
VEGFR2	DMH4, Cat. 4471	Tocris

2.1.9.1 Chemicals and reagents

Acetic acid, 100063.2511	Merck
Acrylamide / bis solution, 10681.03	Serva
Agarose, 15510-027	Invitrogen
Alw26I, ER0031	Thermo Scientific
Ammonium persulfate (APS), 9592.2	Roth
Ampicillin, K029.2	Roth
Aqua Poly/Mount, 18606	Polysciences

β-Mercaptoethanol, 4227.1	Roth
Bacto agar, 214030	BD
Blocking reagent, 11096176001	Roche
Bacto trypton, 211699	BD
Boric acid, 100165.1000	Merck
Bovine serum albumin (BSA), A8022	Sigma-Aldrich
Bromophenol blue, 18030	Fluka
Calcein AM, C3100	Molecular Probes
Calcium chloride ($CaCl_2$), 102382.0500	Merck
Chloroform/isoamylalcohol, X984.1	Roth
Collagenase, C9891	Sigma-Aldrich
Copper(II) sulfate ($CuSO_4$) 102790.0250	Merck
DanKlorix	Colgate-Palmolive
Deoxynucleoside triphosphates (dATP, dCTP, dGTP, dTTP)	Thermo Scientific
Deoxynucleoside triphosphate (dNTP), 11819362001	Roche
Dextran, Cascade Blue, D-1976	Molecular Probes
Dextran, Tetramethylrhodamine, D1868	Molecular Probes
Dextran, Tetramethylrhodamine, D3307	Molecular Probes
DMEM Glutamax, 61965	Gibco
Diethylpyrocarbonate (DEPC), D5758	Sigma-Aldrich
10×DIG RNA labelling mix, 14300621	Roche
Dimethyl sulfoxide (DMSO), 317275	Merck
Disodium hydrogen phosphate (Na_2HPO_4), 106580.5000	Merck
Dithiothreitol (DTT) (100mM), Y00147	Invitrogen
6x DNA loading dye, R0611	Thermo Scientific

Dry ice	-
EDTA free Protease inhibitor cocktail tablets, 05056489001	Roche
Endothelial Cell Basal Medium, C-22010	Promocell
Ethylenediaminetetraacetic acid (EDTA), 108418.1000	Merck
80% ethanol, UN1170	CLN
Ethanol p.a., 100989.1011	Merck
Ethidium bromide, 2218.2	Roth
FastRuler high range DNA ladder, 500-10000bp, SM1123	Thermo Scientific
FastRuler middle range DNA ladder, 100-5000bp, SM1113	Thermo Scientific
FastRuler low range DNA ladder, 50-1500bp, SM1103	Thermo Scientific
Fetal bovine serum (FBS), F7524	Sigma-Aldrich
Gelatin, 104080.0100	Merck
Gelatin, from bovine skin, G9391-100G	Sigma
Geltrex, A1413202	Gibco
GeneRuler DNA ladder mix, SM0331	Thermo Scientific
GeneRuler express DNA ladder, SM1553	Thermo Scientific
Glycerol p.a., 3783.2	Roth
Glycine p.a., 04943	Biomol
5x GoTaq buffer, M791A or M792A	Promega
GoTaq DNA polymerase, M830B	Promega
Guanidine hydrochloride, G4505	Sigma-Aldrich
Hin1II,ER1831	Thermo Scientific
Immersol W 2010	Zeiss
Insect pins, 26002-10	Fine science tools
Isopropanol p.a., 109634.2511	Merck

Leibovitz's L-15 Medium no phenol red, 21083027	Gibco
Liberase TM, 05401119001	Roche
Lipofectamine 2000, 11668-019	Invitrogen
Liquid nitrogene (liq. N_2)	Linde
Loeffler's methylene blue solution, 101287	Merck
Low serum growth supplement kit, S-003-K	Life technologies
Magnesium chloride ($MgCl_2$), 105833.1000	Merck
Magnesium sulfate ($MgSO_4$), 105886.1000	Merck
Maleic acid, 80038	Merck
Medium 199, 31150-022	Life technologies
Medium 200, M-200-500	Life technologies
Mercaptoethanol, 805740	Merck
Methanol p.a., 106059.2511	Merck
Methionine [S35]-label	Hartmann Analytik
Methyl cellulose, M0387	Sigma-Aldrich
Milk powder, T145.2	Roth
Monopotassium phosphate (KH_2PO_4), 104877.1000	Merck
Neurobasal medium, 10888022	Life technologies
Newborn calf serum (NCS), N4762	Sigma-Aldrich
Non-essential amino acids (NEAA), 11140-035	Life Technologies
Nonidet P40 / NP40 / IGEPAL, 19628	USB
Normal goat serum (NGS), G9023	Sigma-Aldrich
Opti-MEM, 51985-026	Gibco
Paraformaldehyde (PFA), P6148	Sigma-Aldrich
Penicillin-Streptomycin, 15140-122	Gibco

Periodic acid	e.g. Sigma-Aldrich
Phenylthiourea (PTU), P7629	Sigma-Aldrich
Phenol/chloroform/isoamylalcohol, A156.1	Roth
PhosSTOP, 04906837001	Roche
Potassium chloride (KCl), 104936.1000	Merck
ProLong®Gold antifade reagent, P36934	Molecular Probes
Protease inhibitor (PI) mix, 05056489001	Roche
Pronase, 11459643001	Roche
Proteinase K (PK), 03115852001	Roche
Precision plus protein all blue standard, 161-0373	Bio-Rad
Random hexamere primer, S0142	Thermo Scientific
Recombinant human VEGF165, 293-VE-010	R&D Systems
Restriction endonucleases	NEB, Thermo Scientific
RiboLock RNase inhibitor (40U), EO0382	Thermo Scientific
Ribonucleic acid from torula yeast, Type VI, R6625	Sigma
RNase H, 18021071	Invitrogen
SeeBlue Plus2 pre-stained standard, LC5925	Invitrogen
SOC-Medium, 15544-034	Invitrogen
Sodium acid (NaN_3), 106688.0100	Merck
Sodium acetate (NaOAc), 6779.1	Roth
Sodium chloride (NaCl), 3975.2	Roth
Sodium dodecyl sulfate (SDS), 20765.03	Serva
SP6 polymerase, EP0131	Fermentas
Spectinomycin, 85555	Fluka
Sulforhodamin B, S1402	Sigma

Sucrose, S1888	Sigma-Aldrich
T7 polymerase, EP0111	Fermentas
Tetramethylethylenediamine (TEMED), 2367.3	Roth
5x transcription buffer, EP0111	Fermentas
Tricain, A5040	Sigma-Aldrich
Trichloracetic acid, 1.00807.1000	Merck
Tris, 08003	AppliChem
Triton X-100, 108603.1000	Merck
TRIzol, 15596	Life technologies
Tropix I-Block, T2015	Applied Biosystems
Trypsin EDTA or 2.5%, 15090046	Life technologies
Tween 20, 822184.0500	Merck
Xylene, 108681.1000	Merck
Yeast extract, 212720	BD

2.1.9.2 Solutions and buffer

All solutions and buffers were prepared with H_2O that was desalted and purified using a Milli-Q system (electric resistance 18.2MΩcm at 25°C).

1%-2% agarose	1%-2% agarose 1x TBE
Ampicillin stock	100 mg/ml dissolved in dH_2O and sterile filtered
10% APS (stock)	10% APS in dH_2O stored at -20°C
Bleaching solution	1 l tap water, 380 µl DanKlorix
10×BSA stock	0.1 g/ml
DEPC dH_2O	200 µl DEPC per 100 ml dH_2O incubate o/n at 37°C and autoclave

GuHCl-stripping buffer	6M guanidine hydrochloride 20 mM Tris 0.2% Triton X-100/NP40 adjust to pH7.5
HYB^-	125 ml 50% formamide 31.25 ml 20x SSC 2.5 ml 10%Tween-20 ad 250 ml dH_2O
HYB^+	HYB- 5 mg/ml torula (yeast) RNA 50 µg/ml heparin
I-Block	0.2% Tropix I-Block 0.1% Tween in 1xPBS
4×Lämmli sample buffer	4 ml 20% SDS 4 ml glycerol 1 ml β-mercaptoethanol 1.25 ml 1M Tris, pH7.6 1 pinch bromophenol blue
Lysis buffer	10% PK stock in TE, pH8.0
6×Loading dye orange or blue	0.5% SDS 25% glycerol 25 mM EDTA in dH_2O pinch of Orange G or Bromophenol blue
1×Maleic acid buffer	100 mM Maleic acid 150 nM NaCl in dH_2O adjust to pH7.6 with conc. NaOH
3% methyl cellulose	3% methyl cellulose in prewarmed H_2O 70°C shake o/n at 4°C and centrifuge until every bubble is gone

NCST	10% NCS stock 0.1% Tween in 1xPBS
10×PBS	80g NaCl 17.8 g $Na_2HPO_4x2H_2O$ 2.4 g KH_2PO_4 2 g KCl ad 1 l with dH_2O
PBST	0.1% Tween in 1x PBS
PBST milk	3% milk powder 0.1% Tween in 1x PBS
10×PCR buffer	100 mM Tris, pH8.3 500 mM KCl 15 mM $MgCl_2$ 0.1% (w/v) gelatin in dH_2O
PCR mix	60 µl 100mM dATP 60 µl 100mM dCTP 60 µl 100mM dGTP 60 µl 100mM dTTP 6 ml 10x PCR buffer 36.3 ml dH_2O
4% PFA	4% PFA in 1x PBS incubate approx. 5 min at 80°C until PFA is dissolved cool to 4°C prior to usage or store at -20°C
PK stock	17 mg/ml PK in dH_2O
Pronase stock	30 mg/ml pronase in dH_2O
10×PTU	0.3 mg/ml in E3

RIPA	50 mM Tris-HCl, pH 8.0 150 mM NaCl 1% NP-40 0.5% Deoxycholat 0.1% SDS
Running gel buffer	1.5 M Tris, pH8.8
10x running buffer	29 g Tris 144 g glycine ad 1 l with dH_2O and autoclave
SDS running buffer	0.1% SDS in 1x running buffer
Spectinomycin stock	30mg/ml dissolved in dH_2O and sterile filtered
20×SSC	175.3 g NaCl 88.2 g Na-citrate ad 1000 ml dH_2O adjust to pH7 and autoclave
Stacking gel buffer	1 M Tris, pH6.8
Staining buffer (NTMT)	100 mM Tris pH9.5 50 mM $MgCl_2$ 100 mM NaCl 0.1%Tween-20 1 mM Levamisol (add fresh)
Stripping buffer	62.5 mM Tris 2% SDS adjust to pH6.7 prior to use add 350 µl MercaptoEtOH per 50 ml stripping buffer

10×TBE	1080 g Tris
	550 g Boric acid
	400 ml 0.5 M EDTA, pH8.0
	ad 10 ml dH_2O
TE pH8.0	10 mM Tris
	1 mM EDTA
	adjust to pH8.0 and autoclave
10×transfer buffer	30.3 g Tris
	144 g glycine
	ad 1 l with dH_2O
	adjust to pH8.3 and autoclave
50×tricain	2g tricain
	10.5 ml 1 M Tris pH9.0
	ad 500 ml with dH_2O
	adjust to pH7.0

2.1.9.3 Media

Media used for the cultivation of bacteria were autoclaved to prevent the growth of undesired organisms. After cooling sterile filtered antibiotics in the indicated concentrations were added. HUVEC standard medium was sterile filtered.

HEK medium	DMEM Glutamax
	10% FCS
	1% penicillin/streptomycin
	1% MEM NEAA
HUVEC standard medium	50% Endothelial Cell Basal Medium
	50% Medium 199 with 20% FCS

E3	5 mM NaCl
	0.17 mM KCl
	0.33 mM $CaCl_2$
	0.33 mM $MgSO_4$
E3 Methylene blue	5 mM NaCl
	0.17 mM KCl
	0.33 mM $CaCl_2$
	0.33 mM $MgSO_4$
	0.002% Loeffler's methylene blue solution
High packaging medium	500 ml DMEM Glutamax
	5 ml penicillin/streptomycin
	5 ml NEAA
	50 ml FCS
	30 ml BSA stock (20 g BSA in 100 ml HEK Medium)
LB-Agar	1.5% Bacto Agar
	1% Bacto Trypton
	0.5% Yeast extract
	17.25 mM NaCl
	in dH_2O
	Ampicillin 100 µg/ml or Spectinomycin 100µg/ml
LB-Medium	1% Bacto Trypton
	0.5% Yeast extract
	17.25 mM NaCl
	in dH_2O
	Ampicillin 100 µg/ml or Spectinomycin 100µg/ml

2.1.10 Kits

BC Assay Protein Quantitation Kit, UP40840A	Uptima
cytoTox 96 non-radioactive cytotoxicity assay, G1780	Promega
GoTaq DNA Polymerase, M3175	Promega
iScript cDNA Synthesis Kit, 170-8891	BioRad
M-MLV Reverse Transcriptase, 28025-013	Invitrogen
MEGAClear Kit, AM1908	Ambion
mMESSAGE mMACHINE SP6 Kit, AM1340	Ambion
mMESSAGE mMACHINE T7 Kit, AM1344	Ambion
MessageMAX T7 mRNA transcription kit	Epicentre
NucleoBond Xtra Midi, 740410	Macherey-Nagel
NucleoSpin Gel and PCR Clean-up, 740609	Macherey-Nagel
NucleoSpin Plasmid, 740588	Macherey-Nagel
Pierce ECL Plus Western Blotting Substrate, 32132	Thermo Scientific
RNAqueous-Micro Kit, AM1931	Ambion
RNase-free DNase Set, 79254	Qiagen
RNeasy Mini Kit, 74104	Qiagen
SsoFast Eva Green Supermix, 172-5204	BioRad

2.1.11 Consumables

0.2 ml Strip tubes, AB-0266	Thermo Scientific
96-Well PCR Plate, AB-0600	Thermo Scientific
Blotting Paper, MN 218 B	Macherey-Nagel
Borosilicate glass capillaries, 1B120F-4	World Precision Instruments

Borosilicate glass capillaries, 1B100-4	World Precision Instruments
Centrifuge tubes 15 ml, 50 ml	Sarstedt
Combitips Plus 0.5 ml, 5ml	Eppendorf
Cover slip	Thermo Scientific
Fluorodish Cell Culture Dish - 35 mm, FD3510-100	World Precision Instruments
Hard-Shell 384-Well PCR Plates, HSP-3805	BioRad
Microcentrifuge tubes 1.5 ml, 2.0 ml	Sarstedt
Microscope slide	Thermo Scientific
Microscope slide with wells	Thermo Scientific
Microseal B Film, MSB1001	BioRad
Multi-well plates (6, 12, 24, 48, 96)	Thermo Scientific
μ-slides, 80826	Ibidi
PCR Film, AB-0558	Thermo Scientific
PES membrane filter (0.45 µm)	VWR International
Petri dishes 60 mm, 100 mm	Sarstedt
Pipette tips 10 µl, 10 µl long, 200 µl, 1000 µl	Sarstedt
Pipette tips with filter (10 µl, 10 µl long, 20 µl, 100 µl, 300 µl, 1000 µl)	Sarstedt
Phase Lock Tubes 1.5 ml	Eppendorf
PVDF Membrane, Immobilon-P, IPVH00010	Millipore
sterile serological pipetts 5 ml, 10 ml, 25 ml	Sarstedt
Superfrost Plus slides, J1800AMN3	Thermo Scientific
Transfer pipettes	Sarstedt
X-ray films Kodak, BioMax MR Film, Cat8701302	Sigma Aldrich

X-ray films Super RX, 47410 19236	Fujifilm

2.1.12 Equipment

Accu jet pro	Brand
Agarose gel documentation device	Intas
Agarose gel systems	Peqlab
Benchtop centrifuge 5415D	Eppendorf
Benchtop cool centrifuge Biofuge fresco	Heraeus
Bio-ice cooling unit, 170-3934	Bio-Rad
C1000 Thermal Cycler	Bio-Rad
Cassette for x-ray film exposure	Radiographic Products
Casting stands	Bio-Rad
Casting frames	Bio-Rad
Celltram air microinjector, 5176	Eppendorf
Centrifuge multifuge 3 S-R	Heraeus
CO_2 Incubator	Binder
Cold-light source KL 1500 LCD	Zeiss
Dumont Forceps # 5 Titanium	Fine Science Tools
DMZ-Universal (needle) Puller	Zeitz-Instrumente
Foam Pads	Bio-Rad
Freezer -20°C	Liebherr
Freezer -80°C	Heraeus
Fridge	Liebherr
Gel Releaser, 165-3320	Bio-Rad
Gel dryer, model583	Bio-Rad

Hood for cell culture	Heraeus
iCycle-MyiQ	BioRad
Incubator 28°C, 37°C, 55°C	Binder or B. Braun Biotech International
Kontes Pellet Pestle, 1.5 ml	Fisher Scientific
Kontes Pellet Pestle Cordless Motor, K749540-0000	Fisher Scientific
Micro forge, MF-900	Narishige
Microwave	Sharp
Microinjector (Femto Jet)	Eppendorf
Microinjection molds	e.g. Eppendorf
Micro scales BP2215	Sartorius
MilliQ academics	Millipore
Mini gel holder cassette, 170-3931	Bio-Rad
Mini-PROTEAN Comb, 10-well and 15-well	Bio-Rad
Mini-PROTEAN 3 cell	Bio-Rad
Mini-PROTEAN Tetra cell	Bio-Rad
Mini trans-blot central core, 170-3812	Bio-Rad
Multipipette plus	Eppendorf
Nano Photometer	IMPLEN
Needles	Kaut-Bullinger
OTF5000 Cryostat	Bright
PCR Plate Sealer	Eppendorf
PCR Thermocycler	Eppendorf, BioRad
pH Meter	WTW
Pipette 10 µl, 100 µl, 200 µl and 1000 µl	Eppendorf

Plate reader PowerWaveXS	BioTek
PowerPac Basic Power Supply, 164-5050	Bio-Rad
PowerPac HC Power Supply, 164-5052	Bio-Rad
Preserving boiler EKO 620	Petra
rotors (TLA-55, SW28)	Beckmann Coulter
Scales BP3100S	Sartorius
Schott bottles	Schott
Sonifier (Cell Disruptor B15)	Branson
Shaker Duomax 1030	Heidolph
Shaker cold room	Bachofer
Short plates, 165-3308	Bio-Rad
Spacer plates 0.75 mm, 165-3310 and 1.5 mm, 165-3312	Bio-Rad
Spring Scissors, 3 mm Blades, Straight	Fine Science Tools
Spring Scissors, 5 mm, Blades Angled to the Side	Fine Science Tools
Stereo Microscope Stemi 2000	Zeiss
Tea nets	-
Thermomixer comfort	Eppendorf
Thermomixer compact	Eppendorf
Ultracentrifuge	Beckmann Coulter
UV Detectionsystem	Intas
Vannas-Tübingen Spring Scissors, 15008-08	Fine science tools
Vortexgenie2	Scientific Industries
Waterbath	GLF

2.1.13 Microscopes

Axioskope 2 plus	Zeiss
Axiovert 135 (inverted) DIC	Zeiss
Cell Observer CSU-X1 Yokogawa Spinning Disk AxioCam MRm and Evolve 512	Zeiss
Confocal laser scanning microscope LSM 710	Zeiss
Fluorescence-Stereomicroscope MZ 16F	Leica
Fluorescence-Stereomicroscope MZ 16FA	Leica
Mikroskop Zeiss Axioplan 2 imaging AxioCam HRc	Zeiss
Light microscope (Wilovert S)	Hund Wetzlar
Phase contrast microscope (CKX41)	Olympus
Stereomicroscope Zeiss Stemi 2000-C	Zeiss

2.1.14 Hardware and software

Adobe Illustrator CS5	Adobe Systems Software
Adobe Photoshop CS5	Adobe Systems Software
Axiovision 4.0	Zeiss
Bio-Rad CFX Manager 2.0	Bio-Rad
CLC Main Workbench 6	CLC bio
Gen5	BioTek
GraphPad Prism 6	GraphPad Software
ImageJ/Fiji	NIH, USA
iMac	Apple
Microsoft Office for Mac 2011	Microsoft
Papers2	Mekentosj

Zen Black 2011	Carl Zeiss Microimaging
Zen Blue 2011	Carl Zeiss Microimaging

2.2 Methods

2.2.1 Zebrafish specific methods

2.2.1.1 Zebrafish husbandry and handling of embryos

Zebrafish husbandry, breeding, and mating was performed according to the standard methods described in [296]. Embryos and larvae were kept at 28.5°C in E3 medium. Developmental stages were determined according to Kimmel et al. [297]. For *in vivo* imaging or whole mount immunofluorescence (IF) stainings zebrafish embryos were treated with 1×PTU after gastrulation or latest at 1 dpf to prevent melanogenesis [298].

2.2.1.2 Bleaching of fertilized zebrafish eggs

To prevent contamination of the zebrafish facility, embryos were bleached at 1 dpf. The embryos were transferred to a tea net and exposed to bleaching solution for 5 min followed by a 5 min incubation in tap water. Bleaching and washing steps were repeated once. Afterwards, the embryos were flushed into a new petri dish using E3 without methylene blue and kept in a volume of 50 ml E3 without methylene blue. To allow the embryos to hatch from the denatured chorion, 10 µl of Pronase stock solution were added.

2.2.1.3 Mating of adult zebrafish

Female and male zebrafish were placed in pairs in mating boxes filled with water from the zebrafish facility in the late afternoon. If controlled mating was desired, a separator was placed between them and removed next morning. Therefore, eggs with the same developmental stage could be used for injections or all other experiments in which developmentally staged embryos were used. After mating, eggs were collected in a petri dish with 30-50 ml E3 methylene blue.

2.2.1.4 Fin biopsies from adult zebrafish

To genotype single zebrafish tail fin biopsies were taken. Adult zebrafish were anesthetized in fish facility water containing 5-10% Tricain stock solution. About 3 mm of tissue was cut from the most caudal part of the tail fin on a cutting board and fixed in 100% methanol. Each zebrafish was immediately put into a single box containing fish facility water to recover.

2.2.1.5 Staging of zebrafish embryos

tardbp-/-; tardbpl-/- and *tardbp-/-* Tardbp KD embryos as well as their respective siblings were staged prior to 24 hpf according to [297]. For later time points, embryos transgenic for *fli1:*EGFP were used in all experiments and the outgrowth of ISA was monitored and used for staging prior to fixation according to the following criteria [299]: ISA outgrowth till horizontal myoseptum: 24 hpf; ISA outgrowth completed, DLAV formed: 32 hpf.

2.2.1.6 Microinjection into zebrafish eggs

Injection needles were pulled with a needle puller using the program P(A)60. Microinjection molds were placed into a petri dish containing 1.5% agarose in E3 to generate agar plates for injections. Freshly spawned eggs were placed into the cavities generated by the molds and injected at one-cell-stage with 500 pl. For determination of the injected volume a micrometer was used to control the diameter and therefore the volume of the injected droplet. RNA and MO were injected into the yolk, DNA into the cell. After injection, the eggs were kept at 28°C in E3 with methylene blue. In the afternoon, the eggs were screened for normal development and unfertilized eggs removed.

2.2.1.7 KD of genes in zebrafish embryos using MO

Knockdown of Tardbp or Tardbpl MO targeting the ATG start codon, the 5'UTR, or exon 3 of the Tardbp and Tardbpl mRNA were ordered at Gene Tools. 1 mM stocks were prepared by solubilizing the lyophilized solid in sterile dH_2O and 3 µl aliquots stored at -20°C until injection. 1 mM, 0.75 mM, 0.5 mM, 0.33 or 0.25 mM, and

0.1 mM concentrations were injected into one-cell-stage AB embryos as described in section 2.2.1.6. The injected embryos were phenotypically analyzed, and knockdown (KD) efficiency of Tardbp and Tardbpl evaluated by immunoblot. In immunoblots, anti-Tardbpl antibody 5F5-11 was used to examine Tardbpl KD and anti-Tardbp antibody 4A12-111 for evaluation of Tardbp levels. Because injection of 1 mM MO caused unspecific toxicity and concentrations lower than 0.5 mM led to reduced KD efficiency, 0.5 mM was chosen for conduction of the following KD experiments. All three MO per gene exhibited good KD efficiencies, but only the ATG of Tardbpl targeting MO was used for establishing the KD in a mutant background. Therefore, 0.5 mM of the *Tardbpl* ATG targeting MO was injected into *tardbp-/-* embryos. The KD was validated using the anti-N-terminal TDP-43 antibody from Sigma recognizing all Tardbp and Tardbpl variants. This condition was subsequently used for all other experiments.

2.2.1.8 KD of Fn1a, Fn1b, Itgα4, Itgα5, Itgαv, and Vcam1

MO targeting *fn1a*, *fn1b*, *itgα5*, and *itgα5* are published (see section 2.1.3). For KD of Fn1b, the same combination of two different MO as described in [165] and [167] was used. Stock concentrations were as follows: *fn1a*: 3 mM; both *fn1b* MO: 6 mM, both were then mixed 1:1 to get a 3 mM concentration, respectively; *itgα5* and *itgα5* MO: 1 mM, respectively. The MO for KD of Itgα4 and Vcam1 were designed to block exon-intron boundaries of an exon with a nucleotide number that cannot be divided by three to induce a frame shift and premature stop codon. The exon exclusion or intron inclusion was verified by PCR, separation of amplicons by gel electrophoresis, excision of bands, purification of DNA followed by sequencing. The stock of both MO was 1 mM.

Establishment of KD of Fn1a and Fn1b Injection of 1.5 mM *fn1b* MO into wild type *Tg(fli1:EGFP)^{y1}* embryos (1.5 pmol or 6 ng per *fn1b* MO per embryo) reproduced the strong tail extension defect and disruption of somite boundaries described for high doses of this MO combination [165]. Also SA sprout growth was impaired at this concentration. At 0.5 mM, embryos had a weak tail extension defect, at 0.33 mM the embryos appeared phenotypically wild type. Injection of 2 mM *fn1a* MO (1 pmol or

18 ng per embryo) led to a flattened hindbrain and pericardial edema [162]. Outgrowth of SA sprouts was slightly delayed compared to uninjected siblings, likely due to an overall developmental delay caused by the injection procedure. The vascular system developed normal till at least 2 dpf (latest developmental stage evaluated). Injection of 6.75 ng per embryo (MO concentration 0.75 mM) showed normal development of ISV. As reported by [165], combined injection of *fn1a* and *fn1b* MO led to a more severe tail extension, somite boundary, and impaired SA growth phenotype as injection of the same *fn1b* MO concentration alone.

Establishment of KD of integrin α4 The *Itgα4* MO was used at a starting concentration of 1 mM (0.5 pmol or 4.25 ng per embryo). Injection into *Tg(fli1:EGFP)*^{y1} embryos resulted in somites that loose their chevron-like shape and become straight. Embryos had a shorter body axis and developed pericardial edema at 2 dpf. Growth of SA was delayed and SA sprouts were occasionally thinner or missing. At a concentration of 0.5 mM, *Itgα4* MO injection had only a very mild effect on somite boundary shape (they were slightly straighter). SA morphology was not affected.

Establishment of KD of Vcam1 1 mM MO injection (0.5 pmol or 4.22 ng per embryo) led to embryonic death during gastrulation. Using a lower concentration of 0.75 mM (3.16 ng per embryo) caused death of about 20% of injected embryos during gastrulation. The surviving *Tg(fli1:EGFP)*^{y1} embryos had a wild type morphology and vasculature.

Establishment of KD of integrins α5 and αv Injection of 0.5 mM *itgα5* MO (0.25 pmol or 2.1 ng per embryo) led to the described disruption of anterior somites [165] but did not cause vascular developmental defects. Higher doses were toxic to the embryos. To prevent a rescue of integrin α5 KD by integrin αv, *Itgα5* and *Itgαv* MO were injected together at 0.5 mM and 1 mM (2.1 ng and 4.23 ng per embryo), respectively. This combination led to a shortened tail and necrosis in about 25% of injected embryos. ISV were thinner or missing in some embryos. Injection of lower concentrations did not affect the vasculature of *Tg(fli1:EGFP)*^{y1} embryos.

Quantification of rescue capacity of Fn1a, Fn1b, integrin α4, and Vcam1 KD 0.75 mM *fn1a*, 0.33 mM *fn1b*, 0.5 mM *itgα4*, or 0.75 mM *vcam1* MO were injected into embryos derived from *tardbp-/-; tardbpl+/- Tg(fli1:EGFP)*^{y1} matings. To exclude impact of clutch to clutch variation of the *tardbp-/-; tardbpl-/-* phenotype, each clutch was split into five groups that received ctr MO, *fn1a*, *fn1b*, *itgα4*, or *vcam1* MO, respectively. When the SA sprouts reached the horizontal myoseptum, embryos were fixed and the vasculature imaged using a spinning disk microscope at 25×magnification. Afterwards, each embryo was genotyped (*tardbp-/-; tardbpl-/-* mutant or sibling). Then, sprouts of five somites of the identified *tardbp-/-; tardbpl-/-* mutants were quantified, the average number of sprouts per somite calculated and numbers subjected to statistical analysis using normality test and unpaired t test.

2.2.1.9 Generation of chimeric zebrafish embryos by transplantation

The transplantation experiments were conducted as described in [300].

Preparations prior to experiment Preparation of agarose molds for mounting of the embryos: A mold with triangular shaped wedges was placed into melted 1.5% agarose in E3 in a petri dish and removed after solidification to generate rows of triangular wells. Preparation of transplantation needles: Needles were drawn from 1B100-4 glass capillaries by a needle puller using program P(A)60. Then the tip of the taper was broken off with a forceps. The sharp edges were smoothened and a glass spike generated at the very tip by a micro forge, so that the resulting diameter of the opening was slightly larger then the blastomeres at high stage. Preparation of the tracer: To label donor derived cells, dextran tetramethylrhodamin or dextran cascade blue was used. The fluorescence of the dextran tetramethylrhodamin of 3000 MW, not fixable, was stronger and better for sorting of successfully transplanted embryos than the 10000 MW, fixable, dextran tetramethylrhodamin. For final experiments with *tardbp-/-; tardbpl-/-* embryos, dextran cascade blue was used because the recipient wild type embryos were transgenic for *kdrl*:HRAS-mCherry^{s896}. For injection into *tardbp-/-; tardbpl-/-* donor embryos, a 3% dextran stock solution was prepared, whereas for injection into *tardbp-/-* embryos a 6% stock solution was used, because the dextran was co-injected with the

tardbpl binding MO and therefore diluted 1:2 prior to injection. The stocks were filtered through a 0.22 µm filter, aliquoted, and stored at -20°C.

Injection of tracer into embryos At 1-cell-stage, ca. 500 pl of a final concentration of 3% fluorescently labeled dextran was injected into donor embryos, whereas the recipient embryos did not receive tracer. Donor embryos were homozygous for *Tg(fli1:EGFP)*^{y1}), recipient embryos did either carry no transgene or were transgenic for *kdrl*:HRAS-mCherry^{s896}. All embryos were kept at 30°C till they reached high stage.

Dechorionation and mounting of embryos The following steps were conducted using a stereomicroscope. The embryos were dechorionated using two fine forcepses in a petri dish coated with 1.5% agarose in E3 and filled with E3. The embryos were then transferred with a glass pasteur pipette with a wide opening (tip broken off and smoothed by heat) to the prepared petri dish with triangular wells containing enough E3 to cover the embryos. The donor embryos were mounted into one row of wells, the recipient embryos into the next row.

Transplantation of cells at high stage The transplantation needle was placed into the needle holder on the celltram air microinjector. Next, E3 was soaked up into the transplantation needle, till the meniscus of the E3 reached the broadening part of the needle. Then, one donor embryo was penetrated by the transplantation needle at the animal pole and about 20 cells carefully soaked into the needle. These cells were then transplanted close to the margin into the prospective mesoderm of the neighboring recipient wild type embryo of the next row of wells. This procedure was repeated for the complete rows of donor and assigned recipient embryos.

Steps after transplantation Each donor was transferred into a single well of a 48-well plate coated with 1.5% agarose in E3. The respective recipient embryo was placed in the neighboring well of the next row and labelled accordingly. Therefore, to each recipient the respective donor could be assigned later. After raising the embryos at 28°C to at least 24 hpf, recipients of surviving donor – recipient pairs were screened for donor derived green fluorescently labelled ISA. In the recipients of those pairs,

transplanted cells had differentiated into endothelial cells. Only these pairs were fixed at 32 hpf with 4% PFA o/n at 4°C. PFA was removed and samples were rinsed once with 1×PBST. Next, they were washed three times for 5 min with PBST on a shaker at room temperature (RT). Afterwards, they were imaged using a confocal microscope at 25×magnification.

2.2.1.10 Whole mount immunofluorescence stainings

For whole mount IF stainings, embryos were transferred to a microcentrifuge tube. After removal of all E3 medium, 4% PFA was added. The samples were fixed o/n at 4°C or for 4 h at RT. PFA was removed and samples were rinsed once with 1×PBST. Next, they were washed three times for 5 min with PBST on a shaker at RT. For co-staining of 24 hpf *Tg(fli1:EGFP)* embryos with antibodies specific for GFP and βdystroglycan, embryos were next treated with a methanol series of 30% methanol in PBST, 60% methanol in PBST, and 100% methanol. Each wash was conducted for 5 min at RT on a shaker. The samples were then stored o/n or longer in 100% methanol at -20°C. Prior to the staining the embryos were rehydrated by a reverse methanol series of 60% methanol in PBS and 30% methanol in PBST for 5 min on a shaker at RT, respectively. Afterwards, the samples were washed three times for 5 min in PBST at RT. To block unspecific binding of antibody, the embryos were blocked for ≥ 1 h in 10% NCST. Primary antibodies were added 1:500 (rabbit-αGFP) or 1:50 (mouse-αβDG) in NCST. Incubation with primary antibodies was conducted on a shaker at 4°C o/n. On the next day, samples were rinsed with PBST and washed four times for 30 min in PBST on a shaker at RT. Then they were blocked two times for 30 min in NCST. Secondary antibodies were used at a dilution of 1:500 in NCST (goat-αrabbit-Alexa488 and goat-αmouse-Alexa555) and incubated on a shaker at 4°C o/n. Then secondary antibodies were removed and the samples rinsed once with PBST followed by at least three washing steps for 15 min in PBST. The stained embryos were kept at 4°C in PBST or PBS until imaging with the spinning disk or confocal microscopes.

Staining of FN in 28 hpf embryos was performed with *Tg(fli1:EGFP)*^{y1} embryos fixed with 4% PFA and washed with PBST. They were then treated with 10% ProteinaseK

in PBST for 10 min and afterwards washed 3×5 min with PBST. The embryos were next incubated in 2% blocking reagent (Roche) in 1×maleic acid-NaCl for 2 h at RT. The rabbit anti-FN (Sigma F3648) was applied in a 1:100 dilution in 2% blocking reagent in 1×maleic acid-NaCl for at least 14 h at 4°C. The antibody was washed off with 1×maleic acid-NaCl in four washing steps (15 min each). Afterwards, embryos were incubated with secondary antibody (Alexa633 or Alexa568) diluted 1:200 in 2% blocking reagent in 1×maleic acid-NaCl overnight at 4°C. Next, embryos were washed 3×10 min in 1×maleic acid-NaCl followed by two washes with PBST. This protocol was kindly provided by Dörthe Jülich.

2.2.1.11 Whole mount *in situ* hybridizations

For WISH, embryos were fixed in 4% PFA o/n at 4°C, afterwards rinsed once with PBST and then washed three times for 5 min at RT on a shaker. Next, a methanol series of 60% methanol in PBS and 30% methanol in PBST for 5 min on a shaker at RT was conducted. The embryos were then stored in 100% methanol at 4°C until usage. On the first day of the WISH experiment, the samples were rehydrated stepwise by a reverse methanol series (60% methanol in PBST, 30% methanol in PBST, 5 min each) on a shaker at RT. Then, the samples were washed three times for 5 min in PBST at RT. To allow the *in situ* probes to penetrate, 21 and 31 hpf embryos were treated with 10 µg/ml PK in PBST for 10 min. After removal of PK remaining protease was inactivated by re-fixating the embryos for 20 min in 4% PFA on a shaker at RT. After removing the PFA, samples were washed for three times for 5 min in PBST. For prehybridization, 100 µl HYB+ was added and incubated at 65°C for 1 h. Next, HYP+ was replaced by new HYB+ and 50-1000 ng RNA probe added for hybridization (for generation of WISH RNA probes see section 2.2.3.11). The samples were incubated o/n at 65°C. Next day, probe was removed and stored at -20°C for further use. The embryos were then washed 2×30 min at 65°C with 50% formamide/2×SSCT (0.1% Tween) for at least 30 min, followed by a 15 min washing step in 2×SSCT at 65°C and another two with 0.2×SSCT for 30 min at 65°C. All washing solutions were prewarmed to 65°C. Next, embryos were blocked with NCST for 1 h at RT, followed by o/n incubation with secondary antibody at 4°C on an orbital shaker. Anti-DIG-Fab-AP antibody was diluted 1:4000 in NCST.

After removal of the antibody solution, samples were washed four times for 25 min with NCST at RT on an orbital shaker. Next, the embryos were washed four times 25 min in staining buffer (NTMT+0.225 mg/ml Levamisol). During the last washing step, embryos were transferred to a 24-well plate. Finally, staining buffer was replaced by BM Purple AP substrate to stain the embryos and incubated until the intensity of the staining reached a satisfying intensity. Afterwards, the embryos were washed three times 5 min in PBST at RT on a shaker and imaged using a Axioplan 2 imaging microscope.

2.2.1.12 Lysis of zebrafish samples prior to SDS-PAGE

Embryos for protein analysis were transferred to microcentrifuge tubes. The liquid was completely removed and samples were shock frozen in liquid nitrogen. The samples were stored at -80°C until usage. For determination of the protein content of a zebrafish sample, RIPA lysis was performed. Per embryo, 15 µl RIPA with 1×Proteinase and Phosphatase Inhibitor was added to the embryos. Then a tissue homogenizer was used to rupture the embryos and the embryos additionally kept on ice for 30 min for further lysis. Next, DNA was sheared by sonication and remaining debris pelleted by centrifugation of the samples for 15 min at 13000 rpm and 4°C. Supernatants were transferred to new microcentrifuge tubes and a BC assay conducted for determination of protein content (see section 2.2.3.12). Afterwards, lysates were either stored at -20°C or one third of sample volume of 4×Lämmli buffer was added, the sample boiled at 95°C for 5 min at 750 rpm, centrifuged at 13000 rpm for 5 min and loaded on a SDS-polyacrylamide gel to continue with SDS-PAGE (see section 2.2.3.13).

In case of lysis with Lämmli buffer, 10 to 15 µl Lämmli buffer per embryo were added to the frozen embryos. If single embryos were lysed, 30 µl were used instead. The embryos were ruptured with a tissue homogenizer. The samples were then either stored at -20°C or used immediately. Next or after freezing (also when remaining sample was used) samples were boiled at 95°C for 5 min at 750 rpm and afterwards centrifuged for 10 min at 13000 rpm. The equivalent volume of one embryo of the supernatant was used per lane for SDS-PAGE and remaining sample stored at -20°C.

2.2.1.13 Treatment of embryos with chemical inhibitors

Treatment with chemical inhibitors of the VEGFR2 signaling cascade Because treatment with chemical inhibitors was performed prior to outgrowth of ISA and it was hence not possible to differentiate *tardbp-/-; tardbpl-/-* embryos from their wild type siblings at this stage, *tardbp-/-*;Tardbp KD and their control MO injected *tardbp-/-* siblings were used for testing the rescue potential of the chemical inhibitors used. Thus, a defined number of embryos that is going to develop the mutant phenotype and the respective number of control embryos could be treated with inhibitors. To allow treatment of embryos when no ISA sprouts have grown yet, the embryos were kept at 21°C after gastrulation to delay development. Embryos treated with the VEGFR2 inhibitor Sutent were treated at 14-somite stage, all other inhibitors were applied at 16- to 17-somite stage. Because the chorion had a hole due to injection of the embryos, they were not dechorionated. The embryos were distributed into wells of a 24-well plate (10 embryos per well), all E3 was removed and 2 ml E3 with 1×PTU was added. Finally, DMSO as a negative control or the respective inhibitors were added to the desired final concentration. Embryos were kept at RT or 21°C till they reached the required developmental stage that was determined by status of ISA growth according to [299]. Next, they were fixed in 4% PFA o/n at 4°C. Then, PFA was removed and the embryos rinsed once with PBST before washing them three times with PBST for 5 min at RT on a shaker. Afterwards, they were stored at 4°C until imaging with confocal or spinning disk microscopes at 25×magnification.

2.2.1.14 *In vivo* imaging of zebrafish embryos and larvae

For *in vivo* imaging of living zebrafish embryos a spinning disk confocal microscope with a heated stage at 28°C was utilized. The zebrafish were anesthetized in 1×Tricain in E3 and mounted in 1% Agarose in E3 allowing growth of the embryo. A large droplet E3 containing 10×Tricain was placed on top of the mounting agarose to ensure continuous anesthetization and to prevent the agarose from drying out.

2.2.2 Cell culture methods

2.2.2.1 Cell culture initiation and maintenance

Purchased or aliquoted HUVEC or HEK 293-FT cells were thawed in a 37°C water bath and immediately transferred into 5 ml pre-warmed HUVEC standard medium or HEK 293-FT standard medium (DMEM/Glutamax medium supplemented with 10% FCS, 1% penicillin/streptomycin and 1% non-essential amino acids (NEAA)). The cells were centrifuged for 5 min at 1000 rpm, the supernatant removed and the pellet resuspended in 5 ml fresh pre-warmed standard medium. The cells were then cultured in 75 cm^2 cell culture flask, which were for HUVEC cultures pre-coated with 0.1% bovine gelatin in H_2O. Cells were kept at 37°C and 5% CO_2 until they reached the desired confluence. HUVEC cultures initiated for the first time were split first 1:3 when they reached 80% confluence and another time 1:6 when they again reached 80% confluence. Then the 80% confluent cultures were harvested with Trypsin/EDTA, centrifuged as above and resuspended per flask in 1 ml FCS with 1% DMSO. 1 ml aliquots were stored at -80°C until they were used in the respective experiments.

2.2.2.2 Virus production

For virus production, HEK 293-FT cells were used as packaging cells at low passage number and only grown to 60-70% confluence in 10 cm dishes. One day after the last passaging, cells were transfected with three different constructs, two that code for the lentiviral particles (pVSVg and pSPAX) and with the construct of interest (lentivirus packaging construct; for cloning of the constructs see section 2.2.3.10). Because the virus produced by three 10 cm dishes can be easily combined for further procedures, usually three dishes were transfected with the same construct of interest. Before transfection, medium was replaced by 5 ml pre-warmed Optimem with 10% FCS. Then, per three 10 cm dishes to be transfected, 108 µl Lipofectamin 2000 was mixed with 4500 µl Optimem (L2K) and incubated for 5 min. In the meantime, the transfection mix containing the constructs was prepared: per three 10 cm dishes 18.6 µg of the construct of interest, 11.0 µg pSPAX2, and 6.4 µg pVSVg were added to 4500 µl Optimem. This mix was combined with the L2K and incubated for 20 min at RT. Finally, 3 ml per mix

was added to one 10 cm dish. Next day, media were replaced by 10 ml high packaging media (see section 2.1.9.3). On the second day after transfection, the supernatant of three 10 cm dishes containing virus with the same sequence of interest was pooled in 50 ml tubes and centrifuged for 5 min at 2000 rpm to remove debris. The supernatant was filtered through a 0.45 µm PES membrane filter into 28SW ultracentrifuge tubes. The virus particles were then ultracentrifuged for 2.5 h at 22000 rpm. Supernatant was discarded and the virus particles resuspended over night at -4°C in 120 µl NB medium. Resuspended virus was aliquoted in 10 µL portions and stored at -80°C until transduction.

2.2.2.3 Transduction of HUVEC

When required for experiments, one HUVEC aliquot was thawed and culture initiated as stated in section 2.2.2.1. The cells were grown to 80% confluence and detached with Trypsin/EDTA. They were then seeded and transduced with virus containing either the sequence coding for shCtr, sh*TARDBP*#1, or sh*TARDBP*#2 on the following day as indicated below:

Culture plate	**Culture volume**	**Number of cells**	**Volume of virus**
10 cm	10 ml	100×10^4 cells	25 µl
6 cm	5 ml	40×10^4 cells	12.5 µl
3 cm	2 ml	16×10^4 cells	5 µl
6-well plate	2 ml	16×10^4 cells	5 µl
96-well plate	100 µl	20000 cells	2.5 µl

Medium was replaced on the following day and at least every second day till the cells were used in the respective experiments.

2.2.2.4 Stimulation of HUVEC with VEGF

6-well plates or 6 cm dishes of HUVEC were transduced with either control, sh*TARDBP*-#1, or sh*TARDBP*#2 as described in section 2.2.2.3. On the fifth day after transduction, media were replaced by starvation medium (0.1% FCS in M199) and the cells starved in

this medium for 4 h. Afterwards, the cells were starved one more hour in M199 without FCS. Depending on the experiment, a certain number of replicates per condition was then simulated with 25 ng/µl VEGF for 0/5/15/30 min at 37°C and 5% CO_2. Then, cells were quickly washed twice with ice cold PBS, PBS removed and replaced either by RIPA with 1×Proteinase and Phosphatase Inhibitor for SDS-PAGE or by TRIzol for purification of RNA.

2.2.2.5 Culture and harvesting of HUVEC for next generation sequencing

HUVEC plated in 6 cm dishes were used for next generations sequencing (NGS) experiments. Six dishes were transduced with either control, TDP-43 shRNA #1, or TDP-43 shRNA #2 as described in section 2.2.2.3. On the fifth day after transduction, three replicates per condition were stimulated with VEGF as described in section 2.2.2.4. After two washing steps with ice cold PBS, 1 ml TRIzol was added to the cells. After incubation for 5 min at RT, the cell lysates were collected in microcentrifuge tubes and stored at -80°C until they were further processed as described in section 2.2.3.2. For the next generation sequencing of mRNA and micro RNA, 20 µl of the RNA solution was sent to Stephan Bonn at the DZNE in Göttingen, further processed by Anna-Lena Schütz and the data analyzed by Vincenzo Caprese.

2.2.2.6 Lysis of cells for immunoblot

Cells for immunoblot were cultured in 6-well plates or 6 cm dishes. For lysis, 100 µl (6-well plate) or 200 µl (6 cm dish) RIPA with 1×Proteinase and Phosphatase Inhibitor were directly added to the PBS washed cells in the dishes. The dishes were kept on ice for at least 15 min before the cell lysates were collected in 1.5 ml centrifuge tubes. They were then incubated for further 10 to 30 min on ice. Next, the DNA was sheared by ultrasonication, the samples centrifuged for 15 min at 13000 rpm at 4°C to pellet debris, and the supernatant transferred to new 1.5 ml centrifuge tubes. The protein content was determined by BC assay as described in section 2.2.3.12. Afterwards, lysates were either stored at -20°C or one third of sample volume of 4×Lämmli buffer was added, the sample boiled at 95°C for 5 min at 750 rpm, centrifuged at 13000 rpm for 5 min, and loaded on a SDS-polyacrylamide gel to continue with SDS-PAGE (see section 2.2.3.13).

2.2.2.7 Immunofluorescence for the proliferation marker Ki67

Round cover slips were ethanol-sterilized. Cover slips were placed in wells of a 24-well plate and washed twice with PBS. Cover slips were then coated with 0.1% gelatin in PBS for 1 h at 4°C, gelatin removed, and cover slips washed with PBS. Next, HUVEC at day four after transduction with shCtr or sh*TARDBP*#1 were harvested and 50000 cells seeded per well in standard growth medium. Left over cells were used for immunoblot to validate KD efficiency. After 20 h, medium was carefully removed and cells fixed with 4% PFA at RT for 15 min. Afterwards, they were washed three times 15 min in PBS on a shaker. Next, cells were permeabilized using PBST with 0.1% TritonX100 for 45 min at RT. To prevent unspecific binding of antibodies, cells were then blocked with 0.5% BSA, 0.5% TritonX100 in PBS over night. The next morning, coverslips with cells were carefully placed into a staining chamber (aluminum-foil placed in a large cell culture dish) and incubated with first antibody solution. First antibody solution contained rabbit anti-Ki67 (1:500) in 0.5% BSA, 0.5% TritonX100 in PBS and was incubated at 4°C over night on a shaker. The next morning, cells were washed three times 5 min with 0.1% TritonX100 in PBS. Anti-rabbit A488 secondary antibody was diluted 1:500 in 0.5% BSA, 0.5% TritonX100 in PBS and DAPI to label nuclei was added (1:5000). Cells were washed three times 15 min with 0.1% TritonX100 in PBS and mounted on a objective slide with ProLong Gold antifade reagent (molecular probes, P36934). Images were taken at the Zeiss confocal microscope LSM710. Percentage of proliferating cells was analyzed in four fields of view per replicate, averaged, and compared using unpaired t test after having verified Gaussian distribution with a D'Agostino-Pearson omnibus normality test.

2.2.2.8 Cell viability assays

The viability assays were utilized to analyze whether KD of TDP-43 by sh*TARDBP*#1 and sh*TARDBP*#2 led to impaired viability of HUVEC compared to transduction with control shRNA. For cell viability assays, HUVEC were seeded and transduced in 6 cm dishes. The cells of one dish were detached on day four after transduction by Trypsin/EDTA. 20000 cells per well were seeded in 10 wells of a 96-well plate, respectively. The survival of the cells within each well was analyzed on the following day.

Cells not needed for the assays at four days post transduction were used for immunoblot to validate KD efficiency of TDP-43 targeting shRNAs.

CytoTox96®Non-Radioactive Cytotoxicity Assay CytoTox96®Non-Radioactive Cytotoxicity Assay from Promega was used as a measure for both, apoptosis and necrosis upon TDP-43 KD because lactate dehydrogenase (LDH) release was measured after approx. 24 h in culture, when apoptotic cells are likely to have undergone secondary necrosis due to a lacking phagocytic capacity and thus have released LDH as well [301, 302].The assay was performed as described in the manufacturer's protocol: The 100 µl standard HUVEC medium the cells were cultured in was transferred to a new 96-well plate. To rupture the cells and determine maximum LDH release, the plates with the cells were frozen at -80°C for 30 min, thawed at 37°C for 15 min and 100 µl fresh medium was added. The ruptured cells were resuspended twice and then centrifuged together with the plate containing the culture medium of the cells for 4 min at 250 g at 4°C. Next, 50 µl of the supernatants of both plates were transferred into a new 96-well plate and the LDH positive control (5 wells) as well as 50 µl of standard medium as background control (5 wells) added to the plate. Afterwards, 50 µl substrate mix were added and the plate incubated for 30 min at RT in the dark. The reaction was stopped by adding 50 µl stop solution and the emission measured at 490 nm. Percentage of cytotoxicity was calculated as experimental LDH release (LDH in the culture medium of the cells) divided by maximum LDH release (LDH release induced by rupturing the cells).

Sulforhodamine B (SRB) colorimetric assay Cell density determined by protein content of cells by SRB colorimetric assay was used as a second measurement for cell death upon TDP-43 KD in HUVEC. The method was conducted as described in [303] (starting after "cell fixation and staining"). In brief, the cell culture medium was removed, then 50 µl 10% TCA were added for fixation. Fixation was performed at 4°C for 30 min. Next, cells were washed three times with deionized water, taking care not to detach fixed cells from the wells. Plates were dried overnight at RT. Afterwards, cells were stained with 75 µl of 0.4% SRB in 1% acetic acid for 15min at RT. To completely remove unbound SRB, the cells were washed several times with 1% acetic acid. The plates were then dried overnight at RT. For detection of the staining, 200 µl of 10 mM

Tris were added per well and the SRB dye completely dissolved by shaking the plate at 300 rpm. Finally, the absorption was determined spectrophotometrically at 510 nm. For statistical analysis, the absorption of the KD samples was normalized to the absorption of control samples.

2.2.2.9 HUVEC tube formation assay

Tube formation assay was performed on an artificial extracellular matrix, called Geltrex, purchased from Gibco. First, Geltrex was slowly thawed on ice at 4°C over night. Afterwards, Geltrex was kept on ice to prevent uncontrolled polymerization. The desired number of wells of a 24-well plate was coated with 200 µl Geltrex after placing EtOH sterilized and PBS washed coverslips into them. For polymerization of the artificial matrix the plate was then incubated for 30 min at 37°C. In the meantime, 10 cm dishes with HUVEC that have been transduced with either control, sh*TARDBP*#1, or sh*TARDBP*#2 four days before were detached with Trypsin/EDTA. The Trypsin digest was stopped by adding standard HUVEC culture medium. The cells were centrifuged at 1000 rpm for 5 min, the supernatant removed, and the cells resuspended in 200RPF Medium supplemented with low serum growth kit to a final concentration of 2×10^5 cells per ml. 500 µl of this cell suspension were then transferred to the wells of the coated 24-well plate. Per condition, three to four wells were plated as biological replicates for tube formation. The plate was incubated overnight (approx. 18 h) at 37°C and 5% CO_2. Next morning, the formed tubes were stained with 4 µg/ml Calnexin for 30 min at 37°C. Cells were then fixed with 4% PFA in PBS for 10 min at RT on a shaker (350 rpm). After three washing steps in PBS (5 to 10 min), the coverslips were carefully transferred to objective slides on which they were embedded with the Geltrex-side facing the objective slide. For embedding, Aqua Poly/Mount was used. The objective slides were then immediately imaged using the Zeiss Axioskope 2 plus fluorescence microscope. Cells not needed for the assay at four days post transduction were used for immunoblot to validate KD efficiency of TDP-43 targeting shRNAs.

2.2.3 Molecular biological methods

2.2.3.1 Isolation of genomic DNA

Genomic DNA from fin biopsies was isolated for genotyping (for fin biopsies see section 2.2.1.4). The methanol was removed and remaining methanol evaporated at 55°C. Then 50 µl of lysis buffer were added and the biopsies were digested at 55°C for 1 h to o/n. Then, PK was inactivated at 95°C for 5-10 min at 750 rpm. To pellet remaining tissue debris, the samples were centrifuged at 13000 rpm for 5 min. The supernatant containing the genomic DNA was used for further analysis by PCR and, if necessary, analytical digest.

2.2.3.2 Isolation of RNA

Isolation of RNA using RNeasy Mini Kit RNA from zebrafish embryos was isolated according to the technical bulletin of the RNeasy Mini Kit including DNase treatment (RNase-free DNase Set). Usually, RNA of 20 pooled embryos was extracted. The tissue was disrupted with a tissue homogenizer in 600 µl RLT buffer containing β-mercaptoethanol. RNA was eluted in 40 µl RNase-free water. RNA integrity was evaluated by agarose gel electrophoresis and the concentration was determined using a NanoDrop device. RNA solutions were stored at -80°C.

Isolation of RNA using TRIzol Total RNA from HUVEC was isolated according to the TRIzol manufacturers protocol. This method has the advantage to recover all RNA species and allows in addition for purification of protein from the cells. In the final step of RNA purification, RNA pellets from HUVEC samples were resuspended in 43 µl DEPC H_2O. RNA integrity was confirmed by gel electrophoresis (2 μl loaded) and the concentration determined utilizing a NanoDrop device. RNA solutions were stored at -80°C.

2.2.3.3 cDNA synthesis

cDNA synthesis was performed as described in the M-MLV Reverse Transcriptase kit with the following modifications: RiboLock RNase Inhibitor was used as RNase

inhibitor. For cDNA that was used in qRT-PCRs 1 µg total RNA and Random Hexamer Primer Mix was utilized for reverse transcription. No additional dNTPs were added because the Random Hexamer Primer Mix already contains dNTPs. To optimize cDNA yield, the double volume was used for the reactions. To control for a successful cDNA synthesis, a β-*actin* PCR was performed according to section 2.2.3.4.

2.2.3.4 Polymerase chain reaction

Oligonucleotides used for Polymerase chain reactions (PCR) are listed in section 2.1.5.1. Oligonucleotides were designed to have an annealing temperature of 60°C. The following components were used per PCR reaction:

mastermix / reaction	15 µl PCR mix
	2 µl of a forward and reverse primer mix (each 10 µM)
	0.2 µl GoTaq DNA Polymerase
	2 µl DNA per sample

The following standard PCR program was used:

Cycle Step	Temperature	Time	No. of cycles
Initial Denaturation	95°C	2 min	1
Denaturation	95°C	30 s	35
Annealing	60°C	30 s	
Extension	73°C	1 min	
Final Extension	73°C	5min	1

Gradient PCR Gradient PCRs were conducted to determine the optimal annealing temperature of a primer pair, if the PCR did not yield a satisfying result with the standard PCR. Using the standard PCR reaction mix, a temperature gradient range from 50-70°C was tested as possible annealing temperatures. The extension time was adjusted to the expected size of the PCR product. PCR products were analyzed by agarose gel electrophoresis.

Quantitative PCR Primer pairs for quantitative PCR (qPCR) were designed to span exon-exon junctions with an intron larger than 1 kb and an amplicon size of 80 - 120 bp. Primer pairs were first tested in qPCR on wild type cDNA and only those chosen for further analysis, whose products had one single melting point, appeared as one band with predicted size in agarose gel electrophoresis, and could be verified by sequencing. For one reaction of the qPCR in 384-well format, 2 µl of a 50 ng/µl cDNA dilution plus 3 µl mastermix, containing 2.5 µl SsoFast Eva Green Supermix, 0.25 µl 10 µM forward primer and 0.25 µl 10 µM reverse primer were used. For standard dilutions, a starting concentration of 100 ng/µl cDNA was employed, the dilution series was done in four 1:10 dilution steps. Each reaction was conducted as technical triplicates and a no reverse transcriptase and no template control included. The PCR program run on a C1000 Thermal Cycler was the following: 30 s at 95°C, 55 cycles of 5s at 95°C and 10s at 60°C and a melting curve from 60°C to 95°C with increases of 0.5°C every 5 s. The relative expression of each gene was calculated using the ΔΔCT-method and the normalized fold expression was calculated by normalization to the reference genes *rpl13a* and *elf1a2*.

2.2.3.5 Agarose gel electrophoresis

Agarose gel electrophoresis was performed to separate PCR products by their size, for example to analyze restriction enzyme digests (e.g. for genotyping), or to control RNA quality. 1-2% agarose gels (agarose in 1xTBE buffer) containing ethidium bromide (approx. 1:50000) or GelRed (1:20000) were used, depending on the size of the DNA fragment analyzed. Loading dye was added to the samples prior to loading. A suitable DNA-Ladder was used for each gel. Electrophoresis was performed in 1×TBE buffer until bands of interest were separated. Documentation was achieved using a UV detection and documentation device.

2.2.3.6 DNA gel extraction

DNA gel extraction was performed according to the NucleoSpin Gel Clean-up protocol. Purified DNA was eluted in 30-50 µl elution buffer NE and was either analyzed by sequencing or used for cloning.

2.2.3.7 Standard bacterial transformation

First, competent *E. coli* bacteria (DH5α) were thawed on ice. Next, either 1 µl plasmid or ligation reaction were incubated with 100 µl bacteria on ice for 20 min. To induce take-up of DNA by the bacteria, the mix was heat shocked for 45 s at 42°C and quick-chilled on ice for 3 min. Then, 400 µl LB medium was added and the sample incubated for 1 h at 37°C while slowly shaking. 300 µl were afterwards plated on an agarose LB plate containing an adequate antibiotic and incubated o/n at 37°C. The remaining 100 µl were stored at 4°C and used for induction of another small bacteria culture if the plating was not successful.

2.2.3.8 Cultivation of bacteria and plasmid DNA isolation

Mini culture Mini culture and isolation of plasmids was performed if no large amount of plasmid was needed for subsequent steps. Per plasmid to be isolated, 5 ml LB Medium with the adequate antibiotic were inoculated with a single clone picked from the colonies grown on a LB agar plate and incubated o/n at 37°C shaking with 200 rpm. From this culture, plasmid DNA was subsequently isolated as described in the NucleoSpin Plasmid Kit protocol. A NanaDrop device was used to determine the concentration of plasmid DNA and the samples stored at -20°C. If required, plasmids were sequenced by GATC using appropriate primers.

Midi culture Midi cultures were used if a larger amount of a plasmid was needed for following experiments. 200 ml LB Medium with the adequate antibiotic were inoculated with a single clone picked from the colonies grown on a LB agar plate and incubated o/n at 37°C shaking with 200 rpm. On the next day, plasmid DNA was isolated according to the NucleoBond Xtra Midi protocol. A NanaDrop device was used to determine the concentration of plasmid DNA and the samples stored at -20°C. If required, plasmids were sequenced by GATC using appropriate primers.

2.2.3.9 Restriction endonuclease digest

Restriction endonuclease (restriction enzyme) digest was used for cutting out required DNA sequences from plasmids for cloning, control digest, plasmid linearization, and

genotyping. For genotyping of *tardbp* and *tardbpl*, 10 µl mastermix were added to 8 µl of the PCR product or to the whole reaction of the PCR.

Mastermix / reaction	1.5 µl buffer
	0.3 µl restriction enzyme
	8.2 µl sterile dH_2O

The digest was conducted for the time span and at the temperature recommended by the manufacturer of the restriction enzyme. The success of the digest was evaluated by agarose gel electrophoresis.

For all other digests, restriction enzymes were used as recommended by the manufacturer (https://www.neb.com/tools-and-resources/interactive-tools/double-digest-finder). Agarose gel electrophoresis was utilized to control for successful linearization of the plasmid.

2.2.3.10 Cloning of shRNAs

Annealing of Oligonucleotides Oligonucleotides for the shRNAs were designed by Dieter Edbauer, DZNE München, and were diluted to 100 µM. 1 µl of the forward and reverse oligonucleotide were used for the annealing reaction, respectively. Furthermore, 5 µl 10×NEB4 buffer and 43 µl sterile dH_2O were added. Annealing was performed by incubating the reaction first at 95°C for 4 min and letting the sample next cool down slowly to RT.

Ligation into vector backbone The vector AD422 pSUPERsub (for vector map see database of Dieter Edbauer laboratory) was linearized by digest with the restriction enzymes Bgl II and HindIII. 2 µl of the linearized vector were used for the annealing reaction. 2 µl of the annealed oligonucleotides were added together with 2 µl 10×ligase buffer, 13 µl sterile dH_2O and 1 µl ligase. The reaction was incubated for 1 h at RT. Next, 10 µl digest mix were added (2 µl NEB3 with BSA, 0.5 µl BglII, and 7.5 µl dH_2O) to cut open re-ligated vector backbone and incubated for another hour at 37°C.

Transformation, mini culture, and validation For transformation of bacteria with the ligation reaction and mini culture of ten picked clones per transformation, the

standard protocols were used (see section 2.2.3.7 and section 2.2.3.8). After purification of plasmid DNA, a control digest was performed, for which 2 µl plasmid, 13 µl sterile dH_2O, 4 µl buffer and 0.1 µl of the restriction enzymes XbaI and HindIII were used. The digest mix was incubated for 1 h at 37°C. Afterwards, samples and control backbone vector were loaded on an agarose gel and agarose gelelectrophoresis performed to determine whether the oligonucleotides were ligated into the backbone. Up to four vectors with successfully ligated oligonucleotides were sent for sequencing by GATC for validation of sequences. The final vectors were then re-transformated and a midi culture (see section 2.2.3.8) followed by sequence validation was performed. Prior to virus production, KD efficiency was tested by transfection of HEK-293T cells with 1 µg of respective constructs followed by immunoblot of TDP-43.

2.2.3.11 Generation of RNA probes for WISH

Purification and precipitation of linearized plasmids Linearized plasmids were purified prior to *in vitro* RNA probe synthesis according to the following protocol: Linearized plasmid in restriction enzyme buffer was transferred to a phase lock gel tube. Next, an equal volume of phenol/chloroform/isoamylalcohol was added and phases mixed by shaking the tubes for 3 min. The tubes were next centrifuged for 5 min at 13000 rpm and afterwards an equal volume of chloroform/isoamylalcohol was added. After shaking the tubes vigorously for 1 min, they were centrifuged again for 5 min at 13000 rpm. The supernatant was transferred to a new microcentrifuge tube. To precipitate the DNA, $\frac{1}{10}$vol% 3M NaOAc pH4.5 and $2\frac{1}{2}$vol% 100% ethanol was added and incubated for 15 min at -20°C. After centrifugation for 20 min at 4°C at 13000rpm, the supernatant was removed and 300 µl 75% ethanol were added to the samples. Again, samples were centrifuged for 10 min at 4°C at 13000 rpm, supernatant discarded and pellets dried at RT. Finally, the pellets were dissolved in 20 µl DEPC H_2O and used for WISH RNA probe synthesis (see section 2.2.3.11).

RNA probe synthesis For generation of sense and antisense probes for *in situ* hybridizations the following protocol was used:

linearized DNA template	1 µg
5x transcription buffer	4 µl
RiboLock RNase Inhibitor	1 µl
100mM DTT	1 µl
10x DIG RNA labelling mix	2 µl
SP6 or T7 Polymerase	2 µl
RNase free dH_2O	ad 20 µl

The reaction was incubated at 37°C for 2 h. Then, 2 µl DNaseI were added and the DNA was digested by incubation for 15 min at 37°C. Next, the probes were purified by precipitation. $\frac{1}{10}$vol% 8M LiCl and $2\frac{1}{2}$vol% pre-chilled 100% ethanol was added, incubated for 30 min or o/n at -20°C and centrifuged at 4°C for 20 min at 13000 rpm. Supernatant was removed and 50 µl 70% ethanol were added to wash the samples during a further centrifugation step for 5 min. The ethanol was removed and remaining liquid evaporated for 10 min at RT. Finally, the pellets were dissolved in 25 µl DEPC-dH_2O. To proof that the synthesis was successful, 2 µl were analyzed by gel electrophoresis and the WISH probes stored at -80°C until further use (for WISH see section 2.2.1.11).

2.2.3.12 Determination of protein concentration

For the determination of protein concentrations in cell culture lysates and some zebrafish lysates a BC Assay was applied as described in the protocol of the BC Assay Protein Quantitation Kit. A BSA 1:2 dilution series was used as a standard, ranging from 2 ml/mg to 0.125 ml/mg. Absorption was measured with a plate reader at 562 nm.

2.2.3.13 SDS-polyacrylamide gel electrophoresis

To separate proteins according to their molecular weight (MW), SDS-polyacrylamide gel electrophoresis (SDS-PAGE) was performed. To achieve separation of proteins of interest in different MW ranges, the percentage of the running gel was adjusted according to (http://www.thermoscientificbio.com/uploadedFiles/Resources/general-recommendations-for-sds-page.pdf). Running gel (25 ml for three 1.5 mm gels) and stacking gel (6 ml for 3 gels) was prepared according to the following table:

	7%	8%	12%	15%	St. gel
40% acrylamide	4.43 ml	5.03 ml	7.58 ml	9.45 ml	563 µl
Running buffer	12.5 ml	12.5 ml	12.5 ml	12.5 ml	-
Stacking buffer	-	-	-	-	750 µl
10% SDS	250 µl	250 µl	250 µl	250 µl	60 µl
dH_2O	7.57 ml	6.97 ml	4.42 ml	3.15 ml	4.913 ml
10% APS	250 µl	250 µl	250 µl	250 µl	60 µl
TEMED	5 µl	5 µl	5 µl	5 µl	6 µl

Samples were loaded and electrophoresis conducted at 80 V till samples were in the separation gel then at 130 V. Afterwards gels were used for Western Blotting.

2.2.3.14 Protein transfer to PVDF-membrane

Wet chamber blotting was performed for protein transfer from SDS-polyacrylamide gels to a PVDF-membranes (Western blotting). PVDF-membranes were activated in methanol, then washed first in dH_2O and then in 1×transfer buffer. Transfer of proteins was conducted in 1×transfer buffer at 400 mA for 70 min – 90 min.

2.2.3.15 Immunodetection of proteins

After Western blotting the membranes were blocked in PBST with 3% milk or 0.2% i-Block or 5% BSA for 1 h on an orbital shaker. Next, primary antibody was applied in indicated dilutions in PBST with 3% milk or 0.2% i-Block or 5% BSA o/n on an orbital shaker at 4°C. Membranes were then washed 4×15 min with PBST with 3% milk or 0.2% i-Block or 5% BSA at RT on a shaker, before they were incubated with HRP-conjugated secondary antibody diluted in PBST with 3% milk or 0.2% i-Block or 5% BSA at RT. Secondary antibody was removed by three washing steps with PBST for 15 min and six washing steps with PBST for 10 min at RT. For immunodetection, ECL plus was used following the manufacturer's instructions. After detection of the signal,

the membranes were rinsed 3× with PBST. If another immunodetection was desired, membranes were stripped by incubation with 50 ml stripping buffer containing 350 µl β-mercaptoethanol at 50°C in a horizontally shaking water bath for 2 h. Afterwards, the membranes were washed extensively with PBST and reused for another round of immunodetection. In this thesis, the combination of SDS-PAGE, Western blotting, and immunodetection is termed "immunoblot".

2.2.4 Others

2.2.4.1 Databases used for primer design and cloning strategy

Genomic and transcript sequences were downloaded from Ensembl Genome Browser (http://www.ensembl.org/index.html) or NCBI (http://www.ncbi.nlm.nih.gov/). For sequence alignements, assemblies, and analysis including restriction enzyme mapping and construction of plasmid maps CLC Main Workbench was used. For design of primers, Primer3 (http://primer3.ut.ee/) was employed and specificity of primer pairs tested by Primer-BLAST (http://www.ncbi.nlm.nih.gov/tools/primer-blast/). Other BLAST searches were performed on the Ensembl (http://www.ensembl.org/Multi/blastview) and NCBI (http://blast.ncbi.nlm.nih.gov/Blast.cgi) web pages.

2.2.4.2 Image processing and analysis

Brightness and contrast of microscope images were adjusted using ZEN blue, ZEN black, AxioVison, and ImageJ software. For further processing of images like cropping or stiching of images, ImageJ was used. For processing of films from immunoblotting, films were scanned with 600 dpi resolution, converted to greyscale and cropped using AdobePhoshop. Brightness and contrast were linearly adjusted with AdobePhotoshop.

2.2.4.3 Statistics

Statistical tests as indicated in figure legends were performed using Graph Pad Prism. This software was also used for generation of graphs shown in this thesis. In the respective graphs, the level of significance is marked with asterisks: $* p < 0.05$; $** p < 0.01$; $*** p < 0.001$. If there is no significant difference, the abbreviation n.s. is used.

3 Results

3.1 Characterization of the vascular phenotype of TDP-43 zebrafish mutants

3.1.1 *tardbp-/-; tardbpl-/-* mutants show vascular mis-patterning

As described in section 1.2.4.2 and published in [147], loss of TDP-43 in zebrafish causes several phenotypes. The defects include shortening of motor neurons, muscle degeneration, lack of perfusion, and vascular mis-patterning ultimately leading to death at embryonic stage [147]. The vascular defect is not restricted to a specific vascular bed but affects the whole embryo, as seen when visualizing the embryonic vasculature at 2 dpf (Figure 3.1). Arteries and veins of the ISV are equally mis-patterned in the trunk. Further, blood vessels often ectopically sprout ventrally over the yolk sack extension. Moreover, the head vasculature shows additional sprouting of blood vessels that grow into tissue usually devoid of EC. The vascular mis-patterning is a very early defect in development (first visible at 24 hpf), even before motor neuron defects (28 hpf) and muscle degeneration (2 dpf) become apparent ([147] and Figure 3.3). *In vivo* imaging of *tardbp-/-; tardbpl-/-* embryos showed that contacts between sprouting EC of SA are unstable and that the sprouting EC loose contact to the DA. Blood vessels of *tardbp-/-; tardbpl-/-* mutants are further characterized by very thin sections, indicating that they lack a functional lumen (Figure 3.1). Indeed, most blood vessels of the embryo are not perfused at 2 dpf [147].

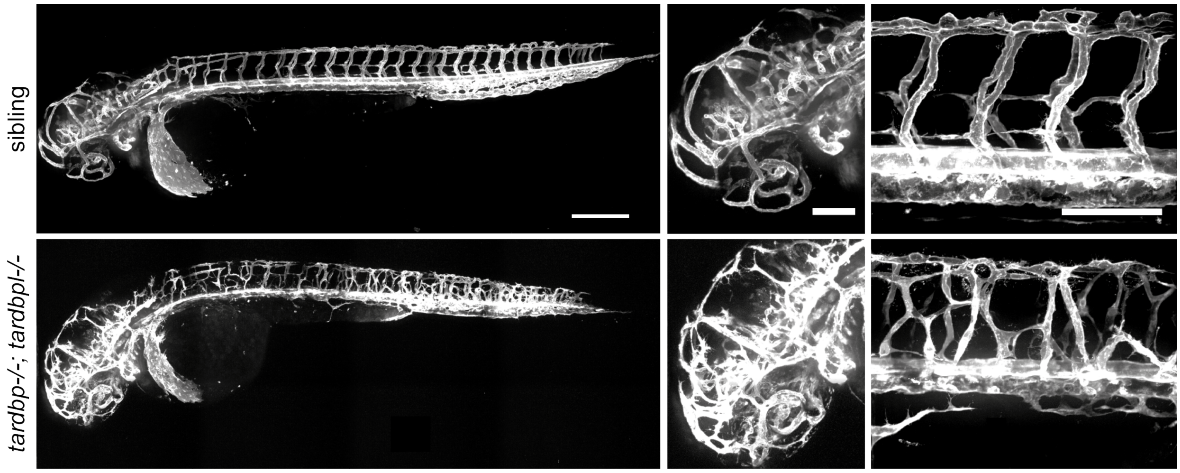

Figure 3.1: Vascular mis-patterning of *tardbp-/-; tardbpl-/-* mutants at 2 dpf. Left images show the vasculature of the whole zebrafish wild type (upper left) and *tardbp-/-; tardbpl-/-* mutant (lower left) embryos. Both embryos are transgenic for *Tg(kdrl:HsHRAS-mCherry)*^{s896}, highlighting the vasculature. Higher magnification images (right images) show the head and trunk vasculature of both embryos. Lateral view, anterior to the left. Scale bar in overview image 250 µm, in images showing head or trunk vasculature 100 µm.

3.1.2 KD of Tardbpl in *tardbp-/-* embryos phenocopies the vascular defect of *tardbp-/-; tardbpl-/-* embryos

Only double homozygous knockout mutants have the described defects that result in early death. It is thus not possible to mate *tardbp-/-; tardbpl-/-* mutants. Thus, always one *tardbp* or *tardbpl* allele must be wild type to allow development of fertile adult zebrafish. Consequently, mating of fish with one wild type TDP-43 encoding allele (TDP-43 being used here as an umbrella term for both human TDP-43 orthologues in the zebrafish, Tardbp and Tardbpl or its splice variant Tardbpl_tv1) optimally provides 25% of *tardbp-/-; tardbpl-/-* embryos per clutch. Additionally, the double homozygous mutants are morphologically indistinguishable from their siblings until they accumulate erythrocytes over the yolk at about 32 hpf. However, expression of EGFP in EC allows for separation of *tardbp-/-; tardbpl-/-* mutants from their phenotypical wild type siblings at 24 hpf, when the vascular phenotype first becomes apparent. Thus, experimental approaches aiming at influencing or characterizing earlier developmental events are extremely time consuming or even practically impossible because all embryos used in the experiments must be individually genotyped afterwards. To circumvent this restriction, KD of Tardbpl in the homozygous *tardbp* mutant background was

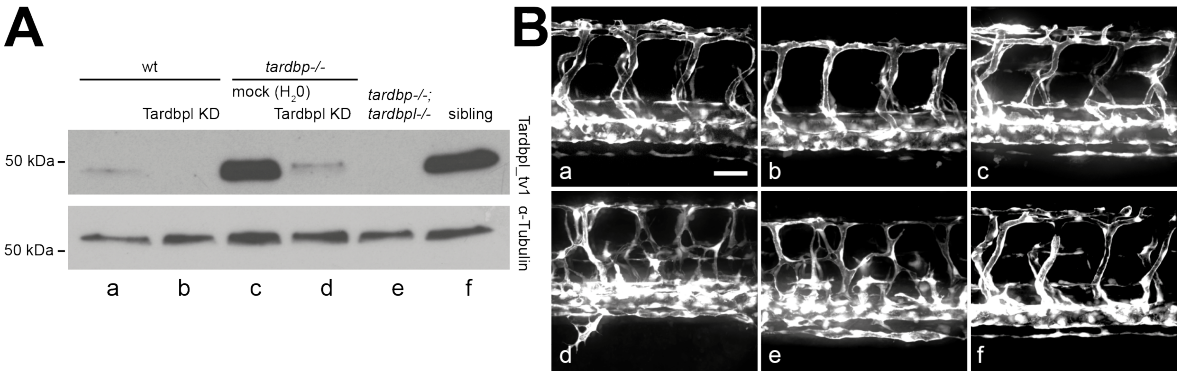

Figure 3.2: KD of Tardbpl in *tardbp-/-* embryos leads to vascular mis-patterning **(A)** Immunoblot showing expression of the Tardbp_tv1 splice variant, which can compensate for loss of *tardbp*, in single embryos. α tubulin serves as a loading control. **(B)** Whole mount *in vivo* images of single embryos subsequently used for immunoblot shown in **(A)**. In wild type embryos not injected (lane a in A and a in B) or injected with Tardbp targeting MO (lane b in A and b in B), Tardbp_tv1 levels are low. In the mock injected *tardbp-/-* embryo, Tardbp_tv1 is up-regulated and hence the vasculature is normal (lane c in A and c in B). In the *tardbp-/-*; Tardbpl KD embryo (lane d in A and d in B), Tardbpl_tv1 is knocked down, leading to phenocopy of the *tardbp-/-; tardbpl-/-* embryonic vasculature (lane e in A and e in B). A wild type sibling of the *tardbp-/-; tardbpl-/-* embryo resulting from *tardbp-/-; tardbpl+/-* incross expresses Tardbp_tv1 (lane f in A) and has a wild type vasculature (f in B). Depicted embryos are *Tg(fli1a:EGFP)*^{y1} labeling EC, the area dorsal of the yolk sack extension is shown, scale bar 50 µm, anterior to the left.

established. As shown in Figure 3.2 A, MO KD of the Tardbpl_tv1 splice variant, which is up-regulated in *tardbp-/-* embryos to compensate for *tardbp* loss, is very efficient. Importantly, KD of Tardbpl in *tardbp-/-* embryos is sufficient to cause vascular mis-patterning indistinguishable from double homozygous *tardbp-/-; tardbpl-/-* knockout (Figure 3.2 A lanes d, e and B d, e). KD of Tardbpl in wild type embryos as well as the injection procedure itself does not affect the vasculature (Figure 3.2 A lane b, c and B b, c), as the vasculature is morphologically indistinguishable from wild type embryos or siblings of double homozygous mutants (Figure 3.2 A lane a, f and B a, f). In this thesis, embryos derived from an incross of *tardbp-/-; tardbpl+/-* or *tardbp+/-; tardbpl-/-* adult zebrafish that are no *tardbp-/-; tardbpl-/-* mutants but carry at least one wild type *tardbp* or *tardbpl* allele are referred to as "sibling". These siblings are morphologically indistinguishable from wild type embryos, as shown in [147].

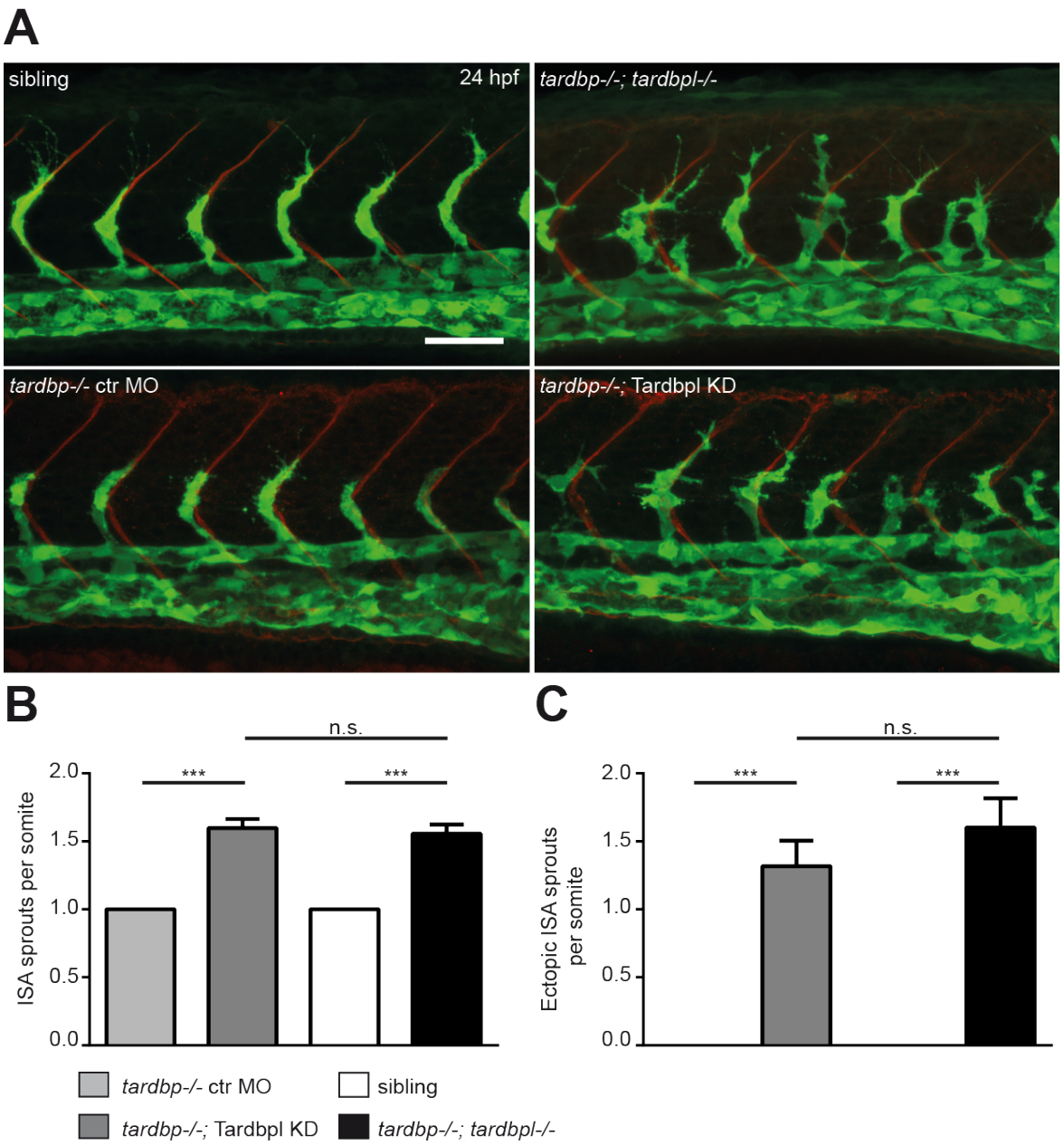

Figure 3.3: Increased and ectopic sprouting in *tardbp-/-; tardbpl-/-* and *tardbp-/-* Tardbp KD embryos. **A** Immunofluorescence of a representative sibling, a *tardbp-/-; tardbpl-/-* mutant, *tardbp-/-* ctr MO injected and *tardbp-/-* Tardbp KD embryo. All embryos are transgenic for *Tg(fli1a:EGFP)*^{y1} highlighting the vasculature, shown in green. The somite boundaries are stained with an anti-DG antibody and shown in red. Displayed are the six somites dorsal to the end of the yolk sack extension. Scale bar 50 µm, anterior to the left. **B** Average SA sprout number per somite is statistically significantly increased in *tardbp-/-; tardbpl-/-* and *tardbp-/-* Tardbp KD embryos compared to the respective controls. There is no statistically significant difference between *tardbp-/-; tardbpl-/-* and *tardbp-/-* Tardbp KD embryos. **C** Average number of ectopic SA sprouts per somite is statistically significantly increased in *tardbp-/-; tardbpl-/-* and *tardbp-/-* Tardbp KD embryos compared to the respective controls, which do have no ectopic sprouts. There is no statistically significant difference between *tardbp-/-; tardbpl-/-* and *tardbp-/-* Tardbp KD embryos. Kruskal-Wallis test and Dunn's multiple comparison post test, n≥9, sprouts between boundaries of six somites dorsal to the end of the yolk sack extension were quantified.

3.1.3 Angiogenic sprouting in TDP-43 deficient zebrafish is increased and ectopic

Quantification of the vascular mis-patterning phenotype of *tardbp-/-; tardbpl-/-* mutants was performed at 24 hpf, when the dorsally growing SA sprouts reach the horizontal myoseptum in the trunk of the fish. At this stage, all sprouts originate from the DA and in wild type embryos only one sprout per somite boundary is formed. Hence, this system allows for straightforward quantification of sprouting angiogenesis. As depicted in Figure 3.3 A, in the wild type sibling and the ctr MO injected *tardbp-/-* embryo one SA sprout per somite is formed and grows dorsally along the somite boundary. The main lamellipodium formed by migrating EC is directed dorsally towards the physiological target region of the growing sprout. In contrast, in the *tardbp-/-; tardbpl-/-* mutants and in *tardbp-/-* Tardbp KD fish, statistically significant more sprouts are formed that also sprout at ectopic positions between somite boundaries (see Figure 3.3 B and C). Additionally, the sprouts extend lateral lamellipodia perpendicular to the wild type growth direction and even interconnect with neighboring sprouts.

3.1.4 Directed migration of EC in *tardbp-/-; tardbpl-/-* mutants is impaired

The extension of lateral lamellipodia and dorsal migration of EC at ectopic positions along the DA suggests a defect in directed migration. To provide further evidence for this defect, EC that reach the dorsal roof of the neural tube to form the DLAV were quantified at 32 hpf. As shown in Figure 3.4, the number of EC in the DLAV of 5 segments dorsal to the end of the yolk sack extension is drastically reduced in *tardbp-/-; tardbpl-/-* mutants. To rule out that a decrease in EC number migrating dorsally from the DA or reduced cell proliferation leads to reduced numbers of EC reaching the dorsal roof of the neural tube, total number of EC per SA was quantified. EC number per SA is not different in *tardbp-/-; tardbpl-/-* mutants compared to wild type siblings, indicating that the pool of EC that could contribute to formation of the DLAV is the same. Consequently, the percentage of EC forming the DLAV is significantly reduced hence providing further evidence for impaired migration of EC during angiogenesis

in *tardbp-/-; tardbpl-/-* mutants. The defect in migration is not caused by a delay in migration, as the number of EC contributing to the DLAV of four segments is still statistically significantly decreased at 2.5 dpf (see Figure 3.4 E).

3.1.5 The vascular phenotype of *tardbp-/-; tardbpl-/-* mutants is cell autonomous

Increased sprouting in *tardbp-/-; tardbpl-/-* mutants developmentally precedes muscle degeneration and is spatially separated from motor neuron outgrowth. Moreover, blood vessels also form ectopic patterns in the head of *tardbp-/-; tardbpl-/-* embryos, where neither skeletal muscle nor motor neurons are present. This suggests that defects in different tissues of *tardbp-/-; tardbpl-/-* embryos occur independently from each other. To examine whether the increased and ectopic sprouting of EC is cell autonomous or cell non-autonomous, transplantation experiments were performed as illustrated in Figure 3.5. Transplantation of wild type donor cells into wild type recipients does neither alter donor derived nor recipient EC morphology, showing that the transplantation procedure per se does not affect EC morphology. Experiments with *tardbp-/-*; Tardbpl KD as well as *tardbp-/-; tardbpl-/-* donor embryos clearly demonstrate that increased sprouting at ectopic positions is caused by TDP-43 deficiency in EC in a cell autonomous fashion. In total, eight recipients with a TDP-43 deficient donor were identified to have donor-derived EC at positions in the embryo that allowed for unambiguous evaluation of cell autonomy. In all cases the donor-derived EC showed the *tardbp-/-; tardbpl-/-* mutant phenotype.

3.2 The vascular phenotype is conserved in human EC

The cell autonomy of the vascular phenotype allowed for investigation of the TDP-43 KD effect in an endothelial cell culture system. To test whether human EC function is similarly impaired upon TDP-43 deficiency, the well established HUVEC were chosen as a model system. KD of TDP-43 was achieved by using two different *TARDBP* targeting shRNAs, sh*TARDBP*#1 and #2 (Figure 3.7).

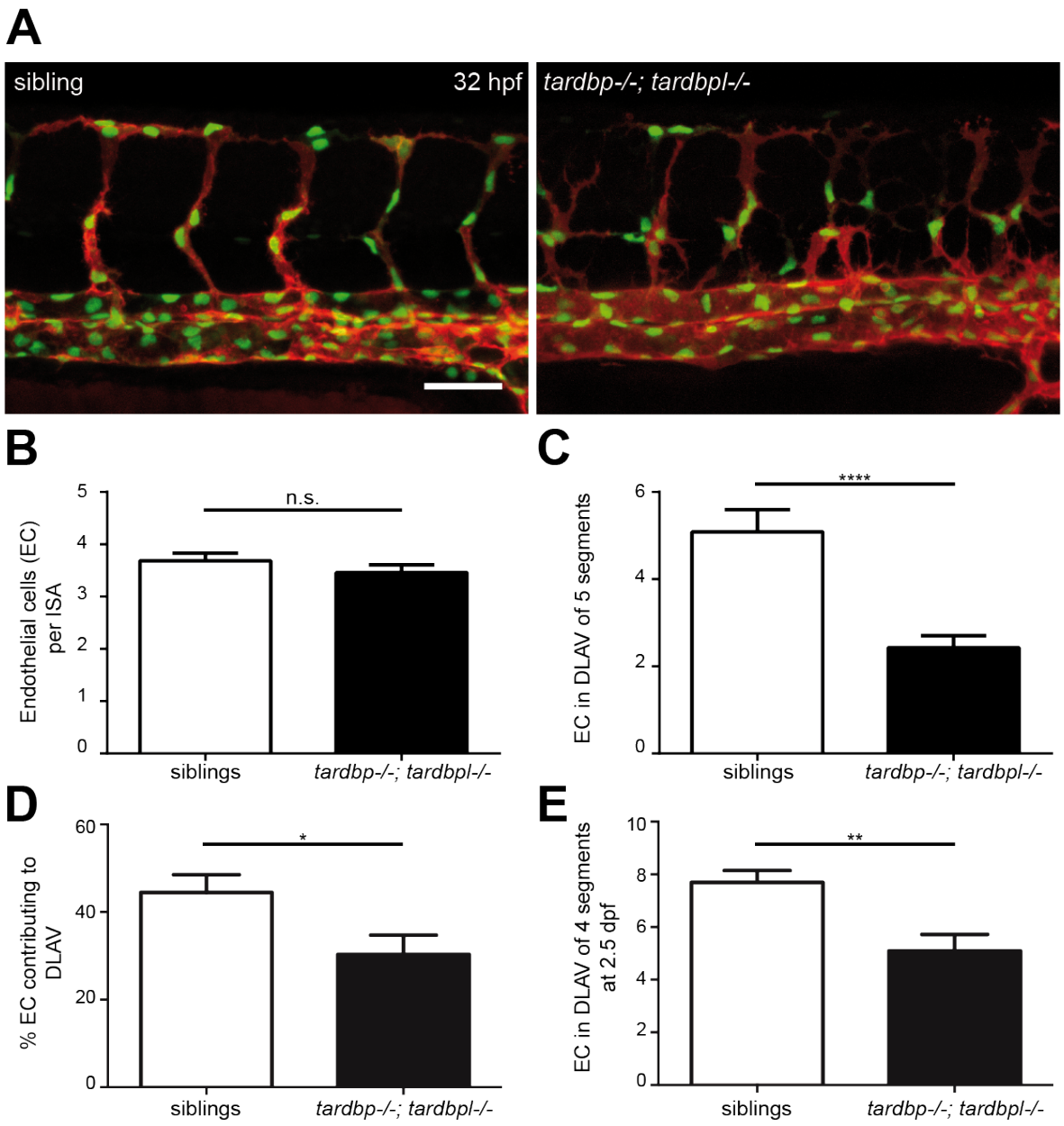

Figure 3.4: Impaired directed migration of EC in *tardbp-/-; tardbpl-/-* mutants. **A** Representative images of a sibling (left image) and a *tardbp-/-; tardbpl-/-* mutant (right image) at 32 hpf. Both embryos are transgenic for *Tg(fli1:nlsEGFP)*^{y7} leading to nuclear EGFP expression (green) and *Tg(kdrl:HsHRAS-mCherry)*^{s896}, highlighting the vasculature (red). Scale bar 50 µm, anterior to the left. Displayed is the area dorsal to the end of the yolk sack extension. **B** EC number per SA sprout is not altered in *tardbp-/-; tardbpl-/-* mutants compared to their wild type siblings at 32 hpf. **C** EC number in the DLAV of five segments is statistically significantly decreased in *tardbp-/-; tardbpl-/-* mutants compared to their wild type siblings at 32 hpf. **D** Percentage of EC contributing to DLAV of five segments at 32 hpf is statistically significantly decreased in *tardbp-/-; tardbpl-/-* mutants compared to their wild type siblings. **E** EC number in DLAV of four segments at 2.5 dpf is still statistically significantly decreased in *tardbp-/-; tardbpl-/-* mutants compared to their wild type siblings. For quantifications shown in B-D, somite boundaries were visualized by a DIC image and utilized to define the area of five (B-D) or four (E) segments in which EC were counted (DIC images not shown). D'Agostino-Pearson omnibus normality test and unpaired t test, n=10.

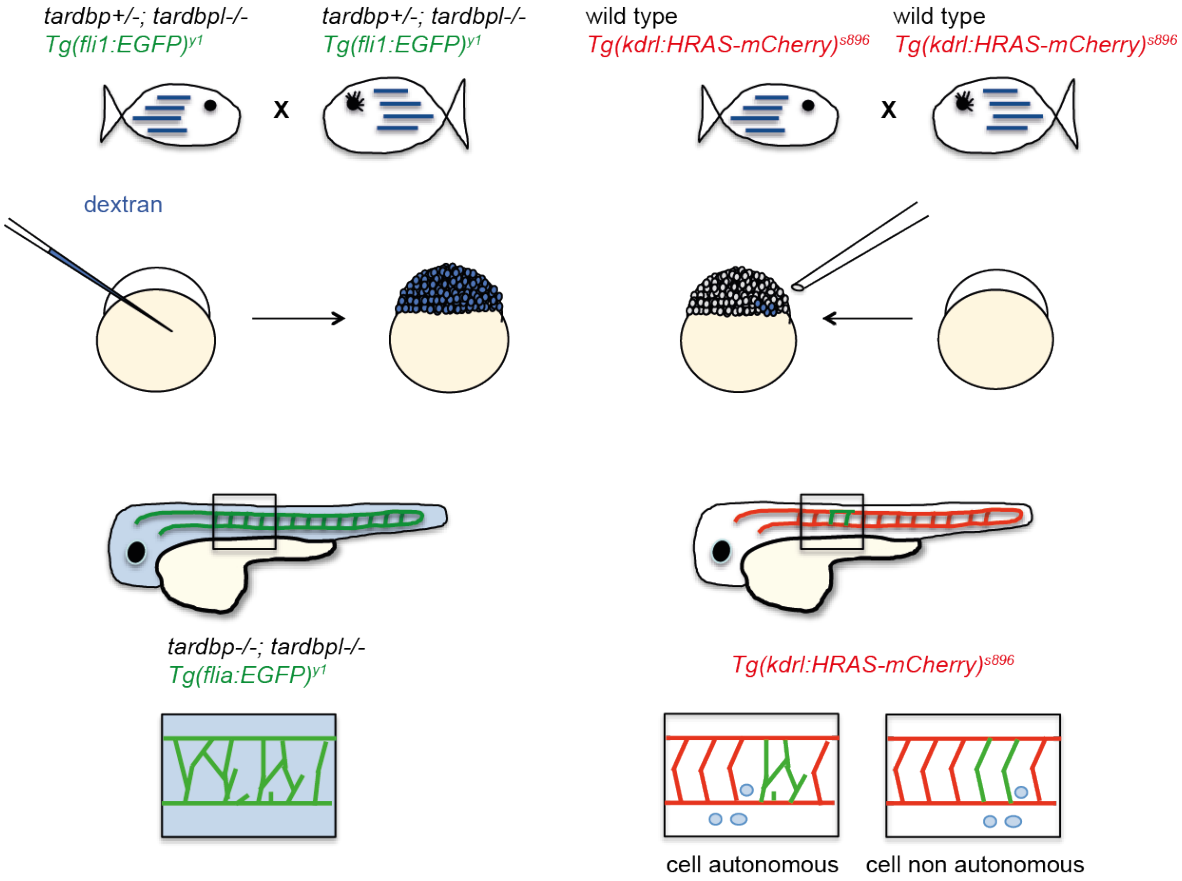

Figure 3.5: Experimental approach of transplantation experiments. Two kind of matings were set up: *tardbp-/-; tardbpl+/-* zebrafish homozygous for *Tg(fli1a:EGFP)*^{y1} (labeling EC in green) and wild type zebrafish homozygous for *Tg(kdrl:HsHRAS-mCherry)*^{s896} (labeling EC in red). In embryos derived from the former crossing, fluorescently labeled dextran was injected at the one-cell stage to label all cells in blue. These embryos served as donor embryos. The embryos derived from the wild type matings did not receive dextran. At high stage, about 20 cells were transplanted from one donor embryo to one recipient embryo. This pair of embryos was labeled as one transplantation pair. This procedure was repeated for about 100 embryos per experiment. Because transplanted cells differentiate into all different cell types and EC located anywhere in the embryo and because only 25% of donor embryos are *tardbp-/-; tardbpl-/-* mutants, only 1% of transplantation pairs had a *tardbp-/-; tardbpl-/-* mutant donor and a wild type recipient with a donor derived EC in the trunk. All other transplantation pairs served as controls. To increase the relative number of TDP-43 deficient donor embryos, in further three experiments *tardbp-/-*; Tardbpl KD instead of *tardbp-/-; tardbpl-/-* embryos were used as donors and ctr MO injected *tardbp-/-* served as controls. In this case, donors carried the *Tg(fli1a:EGFP)*^{y1} transgene whereas recipients were wild type without a transgene. In all transplantation experiments, surviving recipient embryos were screened at 28 to 32 hpf for donor derived EC, which expressed EGFP. If the donor embryo survived as well, the transplantation pair was examined with respect to vascular morphology. If the vascular phenotype of TDP-43 deficient fish is cell non-autonomous, a normal integration of EC from TDP-43 deficient donors into the wild type recipients vasculature would be expected. In case of cell autonomy, the EC derived from a TDP-43 deficient donor embryo would be expected to still show the *tardbp-/-; tardbpl-/-* mutant phenotype, even within the wild type environment.

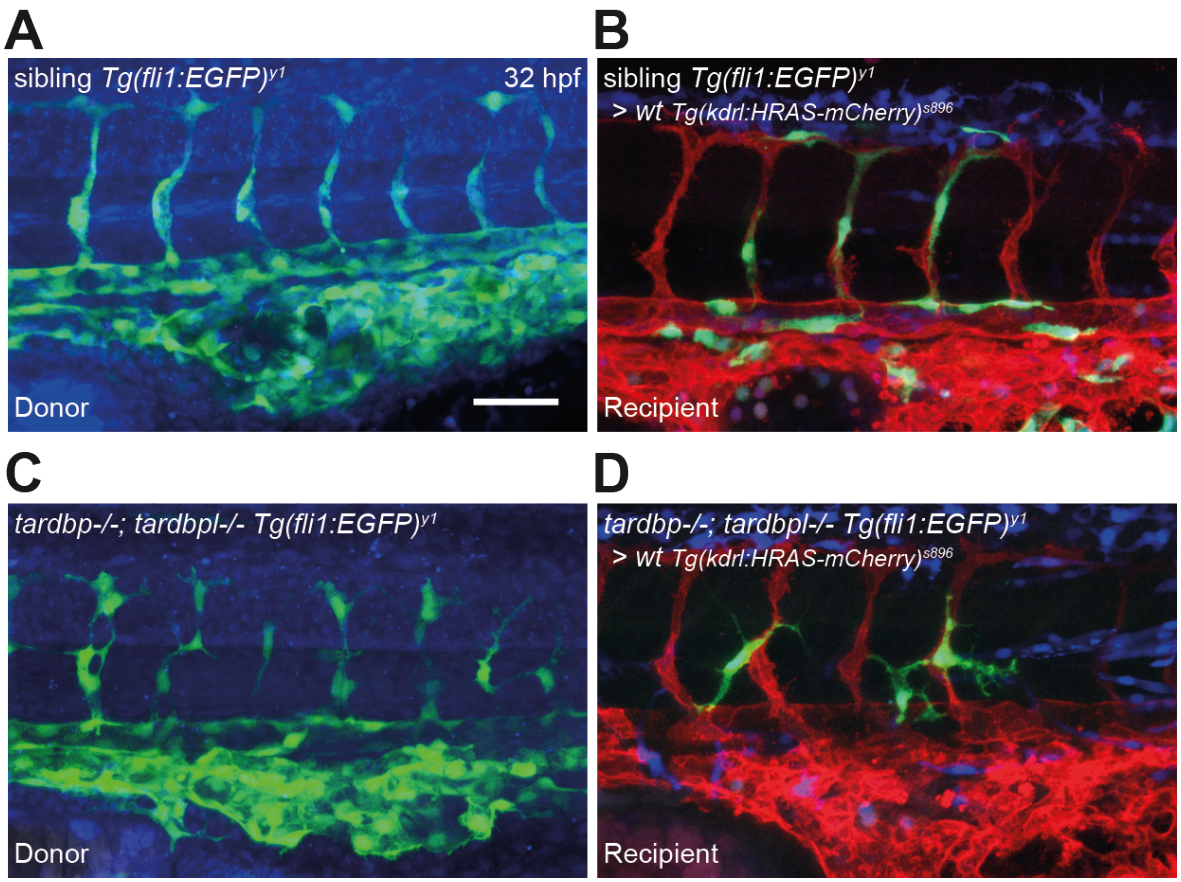

Figure 3.6: The *tardbp-/-; tardbpl-/-* mutant vascular phenotype is cell autonomous. **A** and **B**: Images of a transplantation pair; **A** Wild type sibling, transgenic for *Tg(fli1:EGFP)*^{y1}, donor (EC in green, injected tracer label in blue); **B** wild type *Tg(kdrl:HsHRAS-mCherry)*^{s896} recipient (EC in red) with donor derived EC, to be identified by *Tg(fli1:EGFP)*^{y1} expression (EC in green). Other donor derived cells in blue; **C** and **D**: Images of a transplantation pair; **C** *tardbp-/-; tardbpl-/- Tg(fli1:EGFP)*^{y1} mutant donor (EC in green, injected tracer label in blue); **D** wild type *Tg(kdrl:HsHRAS-mCherry)*^{s896} recipient with mutant donor derived EC, to be identified by *Tg(fli1:EGFP)*^{y1} expression (EC in green). Other donor derived cells in blue. The donor derived EC clearly show the TDP-43 deficient phenotype: ectopic sprouting and branching as well as formation of additional sprouts from the DA. Scale bar 50 µm, anterior the the left.

First, TDP-43 KD HUVEC proliferation and survival was examined. Figure 3.8 shows that proliferation of cells is not changed by TDP-43 KD. Proliferation was quantified based on staining of Ki67. Ki67 expression is absent from resting cells but expressed during all active phases of the cell cycle and therefore used as a marker for the so-called growth fraction, the fraction of proliferating cells [304]. As shown for other cell types, KD of TDP-43 leads to increased cell death of HUVEC as shown by decreased protein content and increased LDH release of TDP-43 KD HUVEC (Figure 3.9). Protein content was determined by SRB assay and is a measure for cell density [303]. Since

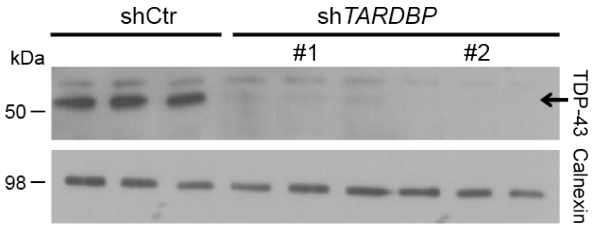

Figure 3.7: KD of TDP-43 in HUVEC with two different shRNAs, sh*TARDBP*#1 and #2 reduces TDP-43 levels. shCtr transduced HUVEC serve as control, each lane represents a biological replicate, Calnexin serves as loading control.

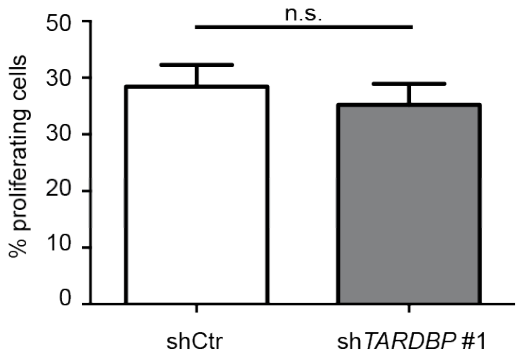

Figure 3.8: KD of TDP-43 in HUVEC does not alter proliferation as shown by quantification of percentage of Ki67 positive cells. D'Agostino-Pearson omnibus normality test and unpaired t test, n=9 in three independent experiments.

proliferation is unaffected by TDP-43 KD, reduction in cell number must be due to cell death. LDH release is a measurement for both, necrosis and apoptosis in the assay employed, thus also indicating that KD of TDP-43 in HUVEC is cytotoxic [301, 302]. Thus, cell culture assays whose results could be falsified by alteration of cell number caused by cell death were not used to investigate cellular functions.

To address angiogenic sprouting capability of HUVEC upon TDP-43 KD, a tube formation assay was performed (Figure 3.10). This assay allows to investigate an *in vitro* collective migration process on an artificial ECM [305]. The tubes formed by EC plated on an artificial ECM have been characterized in detail and the assay is routinely used as an *in vitro* angiogenesis assay [306]. Strikingly, network complexity as quantified by counting the number of connections between branch points is statistically significantly increased upon TDP-43 KD with two different shRNAs. Thus, the hypersprouting phenotype in the zebrafish *in vivo* context has a conserved *in vitro* phenotype in human

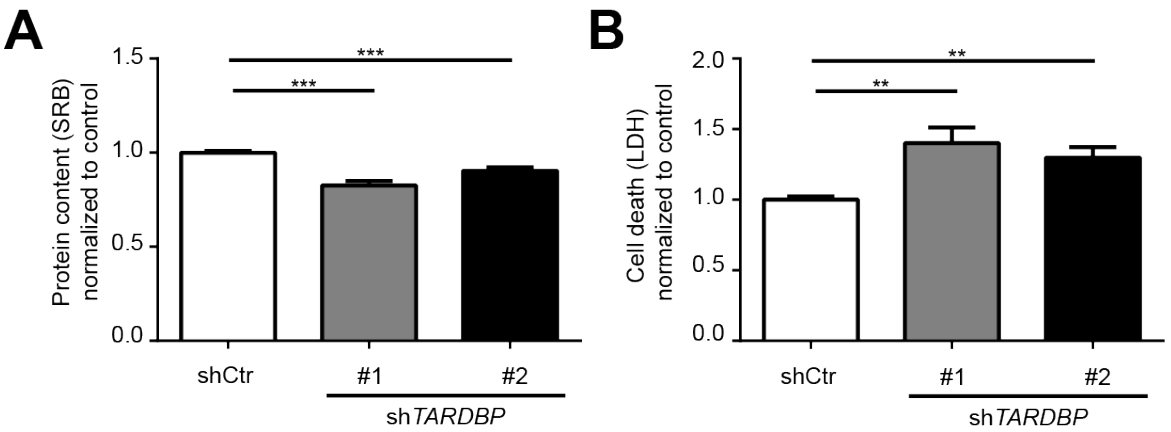

Figure 3.9: KD of TDP-43 in HUVEC reduces cell viability. **A** Protein content as a further measure of cellular survival is statistically significantly decreased upon TDP-43 KD with two TDP-43 targeting shRNAs. **B** Cell death due to apoptosis and necrosis determined by quantification of LDH release is statistically significantly increased upon TDP-43 KD with two TDP-43 targeting shRNAs. One-way ANOVA, n=30 in three independent experiments.

EC culture. This suggests that TDP-43 function is also required for normal EC function in humans.

3.3 Candidate pathways are not altered in *tardbp-/-; tardbpl-/-* mutants or TDP-43 KD HUVEC

3.3.1 PlexinD1 – Semaphorin signaling is not altered in TDP-43 deficient zebrafish

Angiogenic sprouting of SA in the zebrafish embryo is a well studied model system for angiogenesis. Numerous guidance cues and growth factors are known to regulate this complex process. Among those, PlxnD1 and its semaphorin ligands are described to restrict growth of SA to somite boundaries [246, 247, 248] (see section 1.3.5.3). The obvious similarity of the PlxnD1 loss-of-function mutant *obd* to the *tardbp-/-; tardbpl-/-* mutant phenotype suggests a possible impairment of this signaling pathway in *tardbp-/-; tardbpl-/-* EC. In *obd* mutants, the ratio of *sflt1* and *mflt1* is shifted towards increased expression of the *mflt1* splice variant, leading to an increased availability of Vegf for its pro-angiogenic receptor Kdrl [248], the zebrafish orthologue of VEGFR2. The altered ratio of *sflt1* and *mflt1* in *obd* mutants can be visualized by WISH. Therefore, *sflt1*

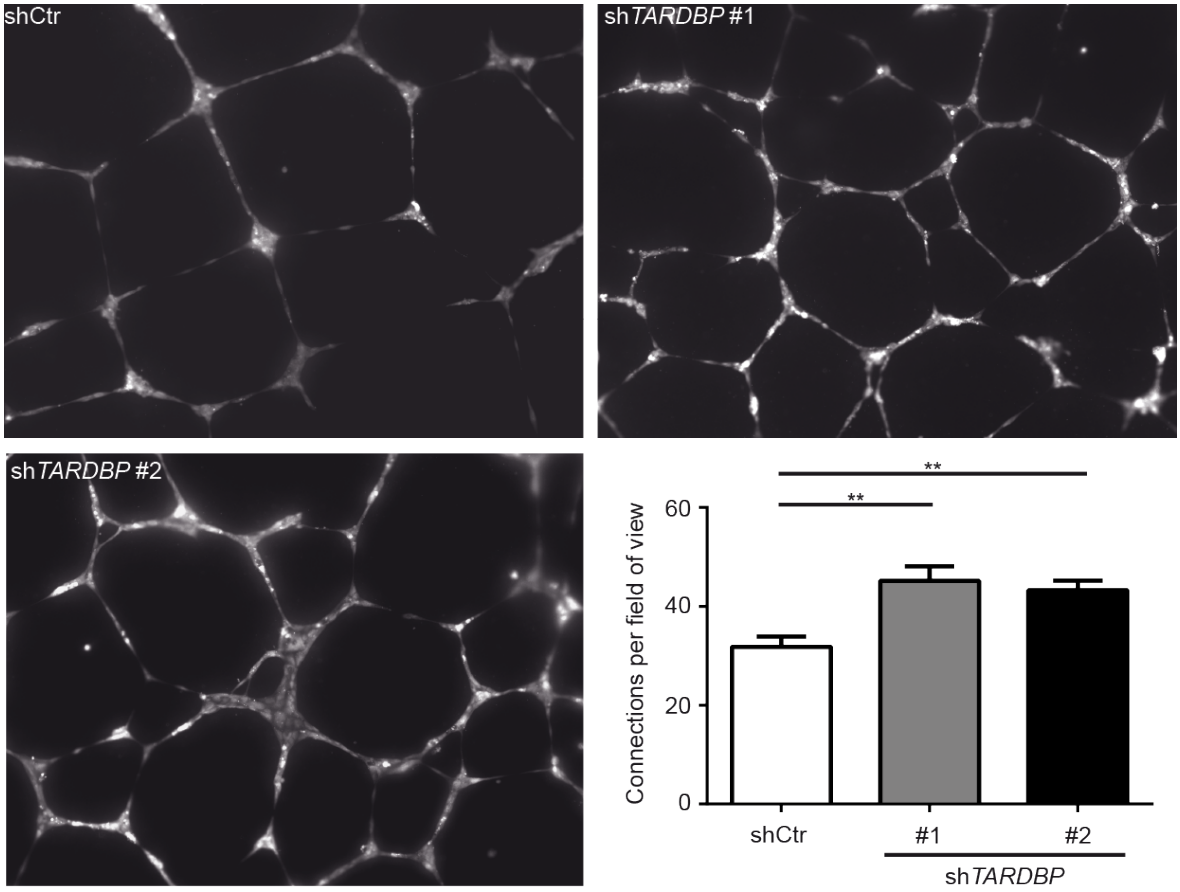

Figure 3.10: Increased *in vitro* angiogenesis upon TDP-43 KD. Images show tubular network formation (bright structures) of representative fields of view of shCtr, sh*TARDBP*#1, and sh*TARDBP*#2 transduced HUVEC (Magnification: 10 ×). Bar graph displays the quantified connections per field of view. Upon TDP-43 KD with both shRNAs, number of connections is statistically significantly increased. D'Agostino-Pearson omnibus normality test and one-way ANOVA, n≥8 in three independent experiments.

and *mflt1* expression in *tardbp-/-*; Tardbpl KD embryos was analyzed and compared to ctr MO injected *tardbp-/-* siblings. Additionally, expression patterns of *plxnD1* and its receptors *sema3aa* and *sema3ab* were examined. As shown in Figure 3.11, no difference in respective expression patterns is detectable in TDP-43 deficient embryos compared to ctr MO injected siblings. This finding was further confirmed in three clutches of *tardbp-/-; tardbpl+/-* incrosses, in which *tardbp-/-; tardbpl-/-* mutants were indistinguishable from their wild type siblings (data not shown).

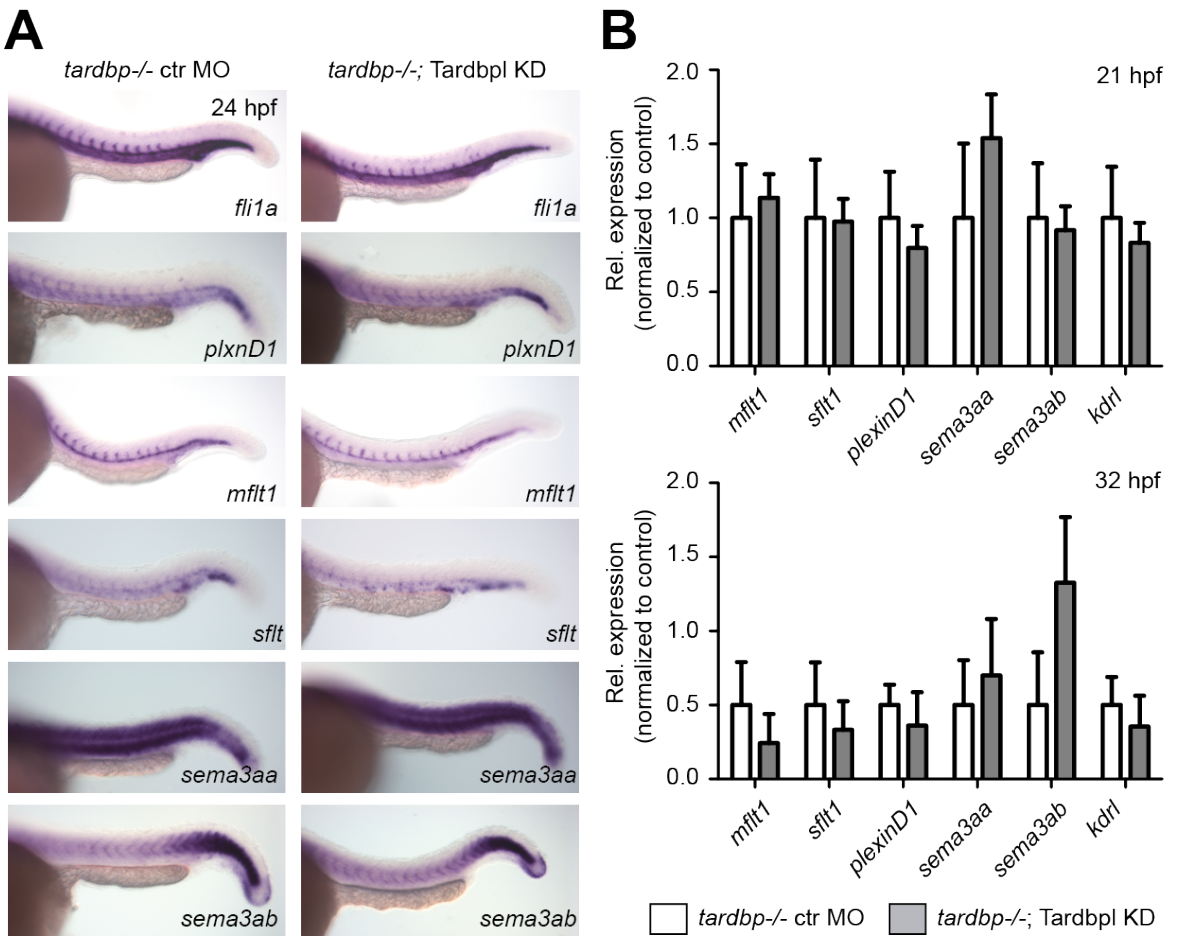

Figure 3.11: Expression patterns of candidate genes is normal in TDP-43 deficient embryos. **A** WISH with antisense probes specific for the candidate genes *fli1a*, *plxnD1*, *sflt1*, *mflt1*, *sema3aa*, and *sema3ab* in *tardbp-/-* ctr MO injected embryos and their *tardbp-/-*; Tardbpl KD siblings at 24 hpf (Magnification: 10 ×, anterior to the left). Depicted are representative images of embryos from one clutch. Experiment was performed with embryos of three independent clutches. **B** Relative mRNA expression of *mflt1*, *sflt1*, *plxnD1*, *sema3aa*, *sema3ab*, and *kdrl* in *tardbp-/-*; Tardbpl KD embryos compared to their ctr MO injected *tardbp-/-* siblings at 21 and 32 hpf. n=3 (32 hpf) or n=4 (21 hpf) pools of embryos of independent clutches, unpaired t test. Results were reproduced three times using the same cDNA.

To quantitatively compare expression levels of *sflt1*, *mflt1*, *plxnD1*, *sema3aa*, *sema3ab*, and *kdrl*, quantitative PCR was performed (Figure 3.11). However, no statistically significant differences were detected. Thus, although phenotypically similar, the *tardbp-/-; tardbpl-/-* phenotype is not caused by the same alteration of guidance cues upstream of Kdrl signaling as in *obd* mutants.

3.3.2 Notch mediated cell fate determination is not affected in TDP-43 deficient zebrafish

Notch is another regulator of angiogenic sprouting, as described in section 1.3.5.2. Reduced Notch signaling leads to prolonged sprouting of SA resulting in a denser vascular network close to the DLAV. Further, Notch is an important player in EC fate determination. Impaired Notch signaling causes ectopic expression of *flt4* in the DA, which is normally expressed in the PCV (see section 1.3.5.2). Another marker that can be used to examine arterial-venous differentiation is *ephrin-B2a*, which is normally expressed in the DA. In case of Notch deficiency, *ephrin-B2a* is expressed ectopically in the PCV.

To address arterial and venous marker expression, the expression patterns of *ephrin-B2a* (arterial expression) and *flt4* (venous expression) were visualized by WISH in *tardbp-/-*; Tardbpl KD embryos and ctr MO injected *tardbp-/-* siblings. As shown in Figure 3.12, *ephrin-B2a* and *flt4* expression patterns are normal in TDP-43 deficient embryos. Moreover, expression patterns were also unchanged in *tardbp-/-; tardbpl-/-* mutants (data not shown). In line with the lacking molecular Notch deficiency profile, there are also some major phenotypic differences between Notch and *tardbp-/-; tardbpl-/-* mutants. Besides the different location and timing of additional sprouting in Notch deficient embryos and *tardbp-/-; tardbpl-/-* mutants, the increased EC number in sprouting SA in embryos with Notch deficiency is not present in *tardbp-/-; tardbpl-/-* mutants (Figure 3.4B and [240]). Moreover, Notch determined cell fate markers are normally expressed, demonstrating that arterial-venous cell differentiation is normal. Taken together, there is no evidence for a major defect in Notch signaling in *tardbp-/-; tardbpl-/-* mutants.

3.3.3 VEGFR2 signaling is not increased in TDP-43 deficient zebrafish or HUVEC

The most important signaling pathway influencing a multitude of EC behaviors and vascular patterning in particular is VEGFR2 signaling (see section 1.3.5 and section 1.3.5.2). For example, increased signaling via the zebrafish orthologue of VEGFR2 is responsible

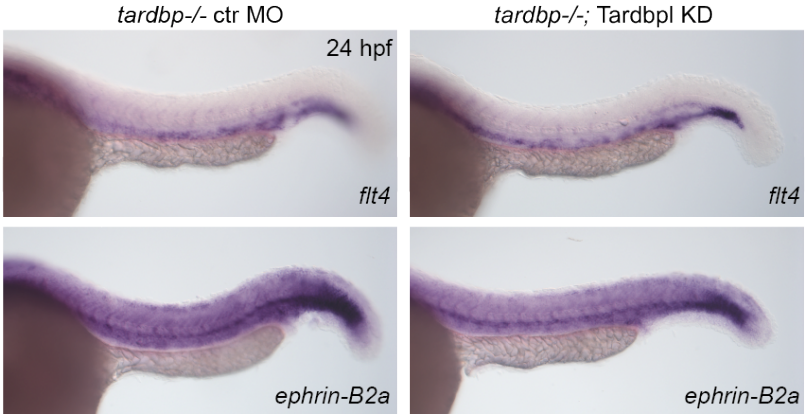

Figure 3.12: Arterial-venous differentiation is normal in TDP-43 deficient embryos. WISH with antisense probes specific for *ephrin-B2a* and *flt4* in *tardbp-/-* ctr MO injected embryos and their *tardbp-/-*; Tardbpl KD siblings at 24 hpf (Magnification: 10 ×, anterior to the left). Depicted are representative images of embryos from one clutch. Experiment was performed with embryos of three independent clutches.

for increased angiogenesis in *obd* mutant zebrafish [248]. Hence, its up-regulation could explain increased angiogenic sprouting as seen in *tardbp-/-; tardbpl-/-* mutants.

Two different VEGFR2 inhibitors were used to block VEGFR2 signaling in *tardbp-/-*; Tardbpl KD embryos to test this hypothesis. DMH4 is a selective VEGFR2 inhibitor whereas Sutent also blocks VEGFR3 and PDGFRB. Both have been used to study Vegfr2 function in zebrafish before [307, 308, 234]. Inhibitors were titrated until sprouting was strongly impaired (Sutent and DMH4) or completely absent (DMH4) in H_2O or ctr MO injected siblings. Then, the inhibitory effects of this concentration was compared between TDP-43 deficient embryos and their H_2O or ctr MO injected wild type siblings. As depicted in Figure 3.13A and B (0.1 µM and 0.5 µM DMH4 treatment), even if sprouting is severely impaired the mutant, EC still show increased and ectopic sprouting. Furthermore, titration of the DMH4 inhibitor to a concentration that is just sufficient to block SA sprouting in *tardbp-/-* ctr MO siblings is also still sufficient to block angiogenic sprouting in *tardbp-/-*; Tardbpl KD embryos (Figure 3.13B), 2.5 µM concentration).

To control for impact of inhibitor treatment in the *tardbp-/-* background, wild type embryos injected either with H_2O (mock) or *tardbpl* MO were included in the experiment

using the VEGFR2 inhibitor Sutent. As shown in Figure 3.13A, the effect of Sutent treatment of *tardbp-/-* H_2O injected embryos does not differ from that of wild type H_2O injected embryos. Furthermore, Tardbpl KD alone does also not affect responsiveness to Sutent, as SA growth in wild type Tardbpl KD embryos and mock injected wild types is similarly impaired upon VEGFR2 inhibition. Treatment with 1% DMSO (solvent) does not alter vessel morphology.

The experimental data therefore indicate that VEGFR2 signaling is not increased in *tardbp-/-*; Tardbpl KD embryos, as one would in this case expect the requirement of a higher dose to block angiogenesis completely. Additionally, partial block of VEGFR2 signaling in the lower inhibitor concentrations leads to shortened sprouts in both, *tardbp-/-*; Tardbpl KD and ctr MO injected embryos and does not ameliorate the hypersprouting phenotype.

To also examine the effect of inhibition of kinases downstream of VEGFR2, the chemical compounds AS605240 (blocking PI3K activity) and SL327 (inhibiting ERK1/2) were employed. Both inhibitors have been used to identify relevant angiogenesis pathways in zebrafish mutants before [248, 234]. As shown in Figure 3.13C, even inhibition of the two kinases at low dosage impairs overall morphology of zebrafish embryos by generating a bent axis phenotype. EC appear swollen and sprouts are shortened. However, they still show ectopic sprouts. This indicates that inhibition of the VEGFR2 downstream targets PI3K and ERK1/2 even at a slightly toxic dosage is not able to rescue SA sprouting defects.

The hitherto obtained results from TDP-43 deficient zebrafish do not support an involvement of increased VEGFR2 signaling as the mechanism that leads to vascular phenotypes in *tardbp-/-; tardbpl-/-* mutants. However, a direct analysis of levels of activation of VEGFR2 signaling components and their responsiveness to a VEGF stimulus is not possible in zebrafish due to lack of specific antibodies. Therefore, immunoblots of VEGFR2 signaling pathway components and their phosphorylation status in TDP-43 KD HUVEC in comparison to control HUVEC was performed. Baseline activation after

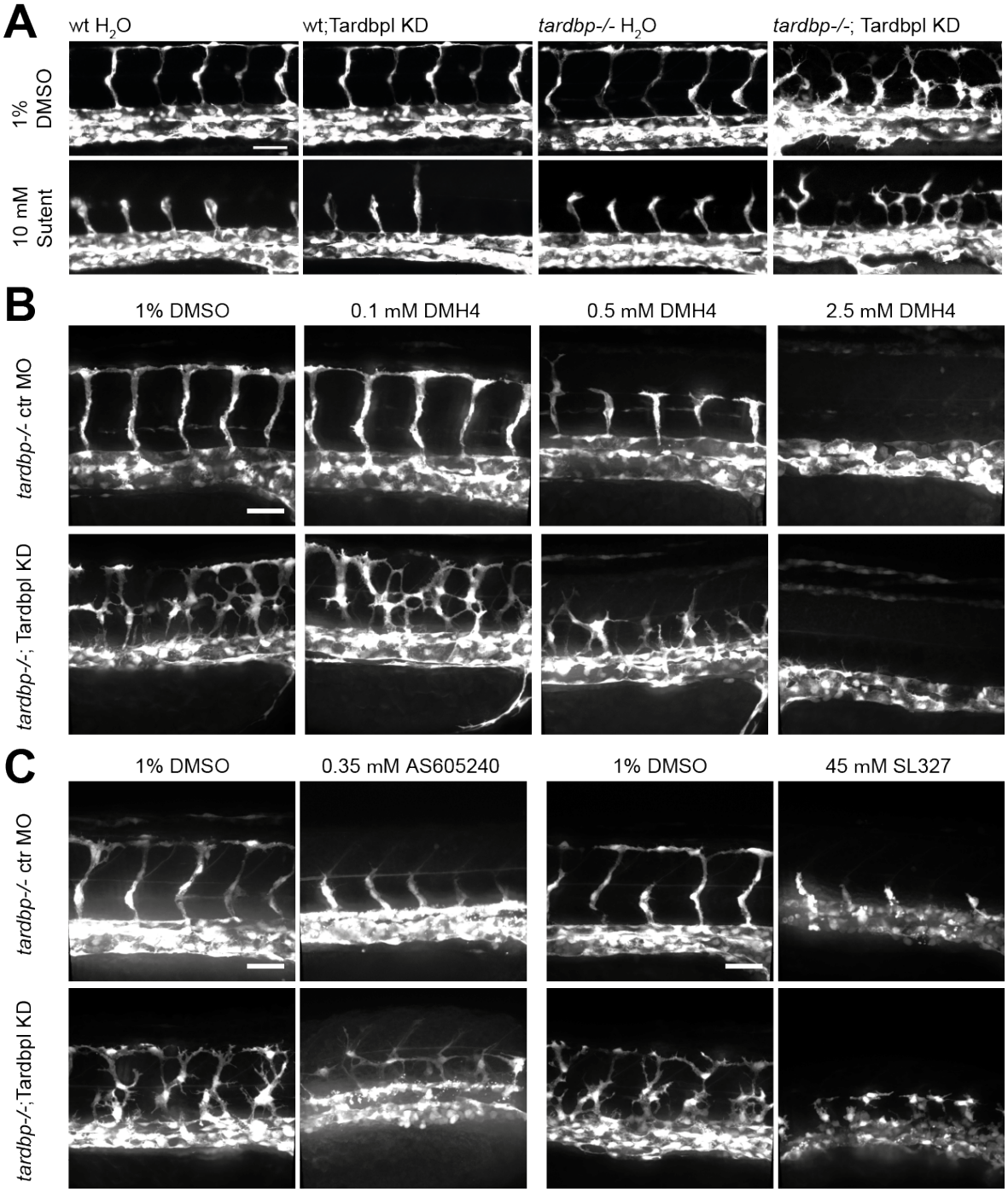

Figure 3.13: Inhibition of VEGFR2 signaling does not rescue the TDP-43 deficient phenotype. **A** Representative images of control embryos (wild type (wt) injected with H_2O, wt; Tardbpl KD, *tardbp-/-* injected with H_2O), or a TDP-43 deficient embryo (*tardbp-/-*; Tardbpl KD) with 1% DMSO (solvent) or 10 µM VEGFR2 inhibitor Sutent. Scale bar 20 µm, anterior to the left. **B** Representative images of ctr MO injected siblings and *tardbp-/-*; Tardbpl KD embryos treated with 1% DMSO (solvent) as control or 0.1 µM/0.5 µM/2.5 µM DMH4 inhibitor. Scale bar 50 µm, anterior to the left. **C** Representative images of ctr MO injected siblings and *tardbp-/-*; Tardbpl KD embryos treated with 1% DMSO (solvent) as control or 0.35 µM AS605240 or 45 µM SL327 inhibitor. Scale bar 50 µm, anterior to the left. Embryos shown in all images are *Tg(fli1:EGFP)*^{y1} and the area dorsal to the end of the yolk sack extension was imaged. Inhibitor experiments were repeated with at least three independent clutches.

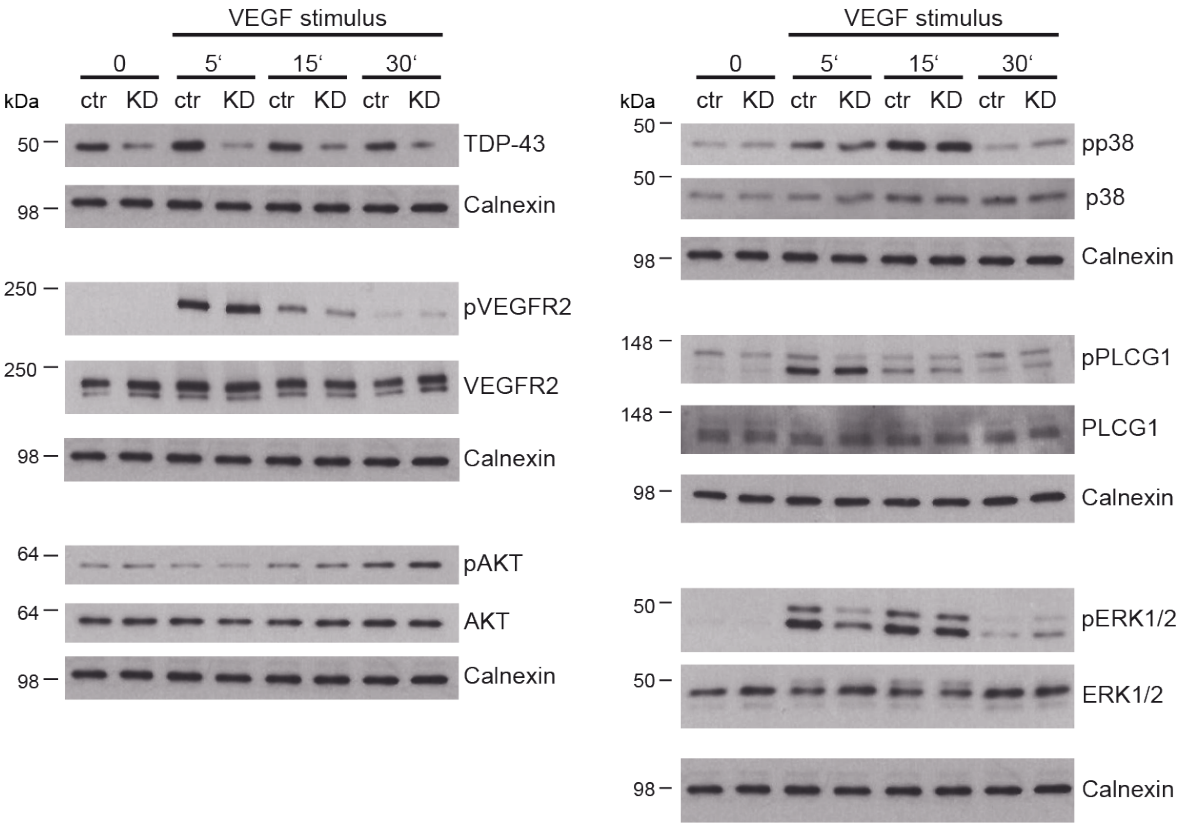

Figure 3.14: Expression as well as phosphorylation levels of VEGFR2 signaling pathway components upon VEGF stimulation is not altered upon TDP-43 KD in HUVEC. Immunoblot of TDP-43 demonstrates successful KD upon transduction with sh*TARDBP*#1 (KD) compared to shCtr transduced HUVEC (ctr). VEGFR2, AKT, p38, PLCG, and ERK1/2 levels are not altered upon TDP-43 KD or upon stimulation with VEGF after 5/15/30 min. Also, phosphorylation levels of VEGFR2, AKT, p38, PLCG, and ERK1/2 are not altered upon TDP-43 KD or upon stimulation with VEGF after 5/15/30 min (pVEGFR2, pp38, pPLCG, pERK1/2). Time point 0 represents baseline levels after deprivation of growth factors before cells were stimulated with VEGF. Calnexin served as a loading control. Depicted is one representative experiment out of three independent experiments.

deprivation of growth factors was detected as well as the time dependent increase in phosphorylation, and therefore kinase activity, upon VEGF stimulation. For analysis, VEGFR2 and its phosphorylation, as well the downstream kinases AKT, p38, and PLCG and their phosphorylation were chosen. As shown in Figure 3.14, neither expression levels of the kinases nor their activation is altered upon TDP-43 KD at any time point investigated. Thus, VEGFR2 signaling and responsiveness to VEGF as well as kinetics of activation of kinases following a VEGF stimulus are not altered upon TDP-43 KD.

Taken together, the results obtained by WISH of candidate genes involved in VEGFR2 signaling, by quantification of their expression levels, as well as by chemical inhibition of VEGFR2 signaling components indicate that VEGFR2 signaling is not increased in TDP-43 deficient zebrafish. In addition, VEGFR2 signaling upon stimulation with VEGF is not altered by TDP-43 KD in HUVEC. Thus, experimental evidence excludes increased VEGFR2 signaling as a cause for the vascular phenotype observed in *tardbp-/-; tardbpl-/-* zebrafish.

3.4 Differentially expressed genes upon TDP-43 KD in HUVEC

I excluded several candidate guidance cues and VEGFR2 signaling as underlying causes of the vascular mis-patterning in *tardbp-/-; tardbpl-/-* mutant zebrafish. Thus, an unbiased approach was chosen to identify differentially expressed genes upon TDP-43 deficiency potentially causing the vascular phenotype. TDP-43 KD HUVEC show a similar phenotype as *tardbp-/-; tardbpl-/-* zebrafish. Moreover, the vascular phenotype in zebrafish is cell autonomous, demonstrating that the defect lies within the EC lacking TDP-43 themselves. In *tardbp-/-; tardbpl-/-* zebrafish, other cell types also lacking TDP-43 might have a different set of dysregulated genes compared to EC. To only investigate differential gene expression in EC, TDP-43 KD HUVEC were used as a model system for RNA NGS. NGS was performed with HUVEC that were grown under standard conditions, and with HUVEC that had received a VEGF stimulus. By comparing the lists of differentially expressed genes under both conditions, genes affected by TDP-43 KD only if VEGF signaling is active were identified.

NGS revealed 5328 targets with differential expression of an adjusted p value smaller than 0.01 and a minimum coverage of 10 reads. A list of 73 differentially expressed genes with more than four fold change in expression was examined in more detail. 58 of them are up-regulated, 15 are down-regulated. Only five of the 73 dysregulated genes are not altered in the standard versus VEGF-stimulated condition (FAM182A, CTD-2265M8.2, INHBB, KIF19, STAB2). These genes have no known vascular function. Importantly,

Gene	Ensembl ID	Fold change	p adjusted
CXCL12	ENSG00000107562	11.64	8.89E-50
CNTN1	ENSG00000018236	10.37	7.41E-21
VCAM1	ENSG00000162692	8.79	3.54E-143
HDAC9	ENSG00000048052	8.74	2.82E-28
RP11-224O19.2	ENSG00000232480	8.65	4.70E-29
ITGA4	ENSG00000115232	8.51	1.07E-32
FAM182A	ENSG00000125804	8.31	4.62E-14
CXCL10	ENSG00000169245	7.79	7.34E-17
MIR146A	ENSG00000253522	7.65	1.37E-32
TGFB2	ENSG00000092969	6.98	1.34E-67
ACP5	ENSG00000102575	-10.28	2.80E-35
AQP1	ENSG00000240583	-7.03	3.05E-93
ACOT11	ENSG00000162390	-6.77	4.54E-27
STAB2	ENSG00000136011	-6.70	8.43E-17
KIF19	ENSG00000196169	-6.07	3.80E-13
CCL14	ENSG00000213494	-5.56	5.13E-56
MYO7A	ENSG00000137474	-5.50	1.16E-18
PTH1R	ENSG00000160801	-5.18	9.21E-09
LYVE1	ENSG00000133800	-5.12	7.61E-71
CHID1	ENSG00000177830	-4.70	5.05E-103

Table 3.1: 10 genes with the highest positive or negative fold change in TDP-43 KD HUVEC under standard conditions

VEGFA expression is reduced to a minor extend rather than increased as one would expect if it was responsible for the increase in angiogenesis in TDP-43 KD HUVEC (fold change: -1.25; p adjusted: 5.84E-03). Thus, the NGS results further substantiate that VEGF signaling is not increased upon TDP-43 KD.

Functional annotation clustering (using the open source annotation tool DAVID [309]) revealed that most differentially expressed genes fall into the categories “chemokine”, “cytokine chemotaxis”, “locomotion”, “cell migration”, and “blood vessel development”. The 10 most up- and down-regulated genes are listed in Table 3.1. Genes linked to ALS and/or FTD are only very mildly affected by TDP-43 KD in HUVEC. For example, *GRN*, *SOD1*, and *VCP* expressions are changed by less than 10%, *FUS* expression is in-

Gene	Ensembl ID	Fold change	p adjusted
FN1	ENSG00000115414	3.73	4.08E-60
VCAM1	ENSG00000162692	8.79	3.54E-143
ITGA4	ENSG00000115232	8.51	1.07E-32
ITGB1	ENSG00000150093	1.74	2.38E-06
ITGAV	ENSG00000138448	3.40	3.53E-23
ITGA5	ENSG00000161638	not changed	not available
ITGB7	ENSG00000139626	-1.21	4.71E-01

Table 3.2: Next generation RNA sequencing results of *FN1*, *VCAM1*, *ITGA4*, *ITGB1*, *ITGAV*, *ITGA5*, and *ITGB7*

creased by 25%, and C9ORF72 by 30%. *Filamin C*, previously found to be up-regulated on protein level in *tardbp-/-; tardbpl-/-* zebrafish and on RNA level in FTLD-TDP patients [147], has a fold change in expression of -1.36. Importantly, one of the top up-regulated hits, *VCAM1*, was already identified to be increasingly expressed upon TDP-43 KD and to be bound by TDP-43 in the adult mouse brain [92]. In addition, *FN1* shows a very significant change in expression and has a very high number of reads, although it does not fall under the 73 genes with the highest fold change in expression levels (fold change: 3.7). However, one of the two zebrafish orthologues of *FN1*, *fn1b*, was previously identified to be up-regulated in *tardbp-/-; tardbpl-/-* mutant zebrafish by a microarray (Alexander Hruscha, personal communication).

3.4.1 The ligands *VCAM1*, *FN1* and their receptor *ITGA4B1* are up-regulated upon TDP-43 KD

Strikingly, a ligand – receptor pair is among the top 10 up-regulated genes: the ligand *VCAM1* and its receptor subunit *ITGA4*. *ITGA4* is part of an heterodimeric integrin receptor, integrin $\alpha 4\beta 1$. Expression of *ITGB1* is also increased (1.7 fold). However, *VCAM1* is not the only ligand of $\alpha 4\beta 1$ integrin. The ECM component FN1 is another ligand for integrin $\alpha 4\beta 1$ and, as described above, its expression is also highly significantly up-regulated. Thus, there is a set of functionally interacting genes that are all

differentially expressed upon TDP-43 KD. In addition, these genes have been shown to be involved in angiogenesis and migration of cells (section 1.3.1). Therefore, the genes represent promising candidates for causing the vessel mis-patterning in *tardbp-/-; tardbpl-/-* mutants. The next generation RNA sequencing results of these genes as well as three further integrin subunits known to bind to FN1 are listed in Table 3.2.

NGS analysis also included the analysis of alternative splicing events upon TDP-43 KD. We detected 450 different alternative splicing events in HUVEC cultured under standard conditions. Although our splicing analysis was conducted in another cell type than all previously published experiments, alternative splicing of several mRNAs overlaps. Examples are CDK5RAP2, RWDD1, and POLDIP3 [93]. *ITGA4*, *ITGB1*, *FN1*, and *VCAM1* are not among the alternatively spliced mRNAs in HUVEC upon TDP-43 KD.

Next, I tested whether increased mRNA expression of *ITGA4*, *ITGB1*, *FN1*, and *VCAM1* leads to increased protein expression. Their protein expression was compared in shCtr versus sh*TARDBP*#1 or sh*TARDBP*#2 transduced HUVEC by immunoblot (Figure 3.15). Protein expression of integrin α4 and FN1 is strongly increased upon TDP-43 KD compared to controls. Integrin β1 expression is moderately increased. In the experiment shown as well as in a further experiment the precursor protein expression of integrin β1 is increased. In a third experiment, also expression of the mature protein is increased. VCAM1 expression is only detectable upon TDP-43 KD with sh*TARDBP*#1, but not detectable upon sh*TARDBP*#2 or shCtr transduction. Protein levels are thus very low and potential differences in expression upon sh*TARDBP*#2 transduction below the detection limit. Thus, protein expression of ITGA4, ITGB1, FN1, and potentially VCAM1 is increased upon TDP-43 KD in HUVEC.

3.4.2 Expression of *fn1b* is increased in *tardbp-/-; tardbpl-/-* zebrafish

Next, it was tested whether the increase in expression of *ITGA4*, *FN1*, and *VCAM1* is also present in *tardbp-/-; tardbpl-/-* mutant zebrafish. *ITGB1* levels were not quantified,

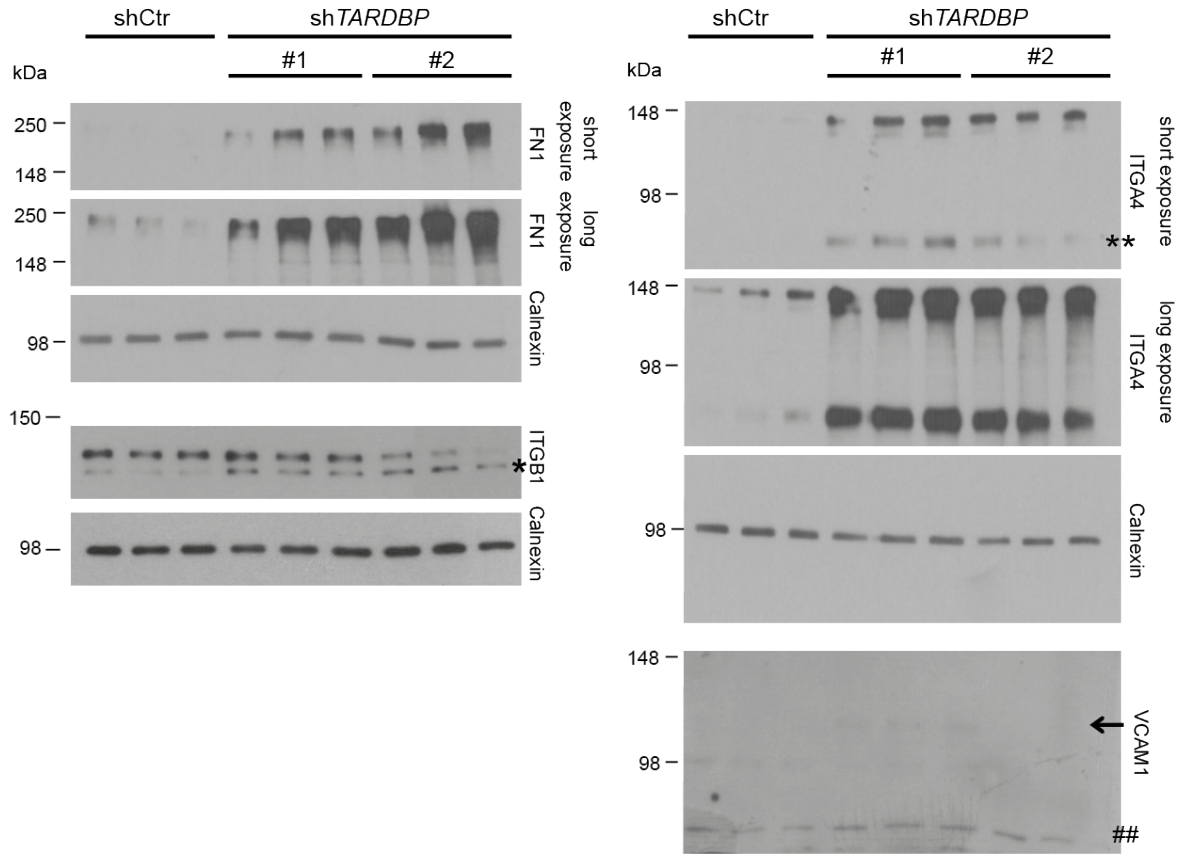

Figure 3.15: Increased expression of ITGA4, ITGB1, FN1, and VCAM1 upon TDP-43 KD in HUVEC. Immunoblots detecting the indicated proteins upon KD of TDP-43 with sh*TARDBP*#1 and sh*TARDBP*#2 in comparison to shCtr transduced cells. For ITGA4 and FN1 two different exposure times are shown. The short exposure shows unsaturated signal in the TDP-43 KD conditions but no signal under control conditions, the longer exposure oversaturated signal in the former conditions but weak signal in control cells. Each lane represents one biological replicate. * in the ITGB1 immunoblot indicates the increased ITGB1 precursor protein expression in TDP-43 KD samples. ** in the ITGA4 immunoblot mark the C-terminal fragment of ITGA4. Arrow in the VCAM1 immunoblot indicates the very weak band in the sh*TARDBP*#1 treated samples. ## marks an unspecific band (described by manufacturer of the antibody used) that allows for evaluation of equal loading amounts in this immunoblot. Shown is the strongest signal detectable. For all other immunoblots, calnexin served as a loading control.

because zebrafish express six different paralogues of the human *ITGB1* (section 1.3.1.2). Since zebrafish have two *FN1* orthologues, namely *fn1a* and *fn1b* (section 1.3.1.1), mRNA expression of both was analyzed. As depicted in Figure 3.16, only *fn1b* mRNA levels are statistically significantly increased in *tardbp-/-; tardbpl-/-* mutants compared to their wild type siblings in whole fish samples. Since *itgα4* and *vcam1* are not exclusively expressed by EC, it might be that differential expression in EC is masked

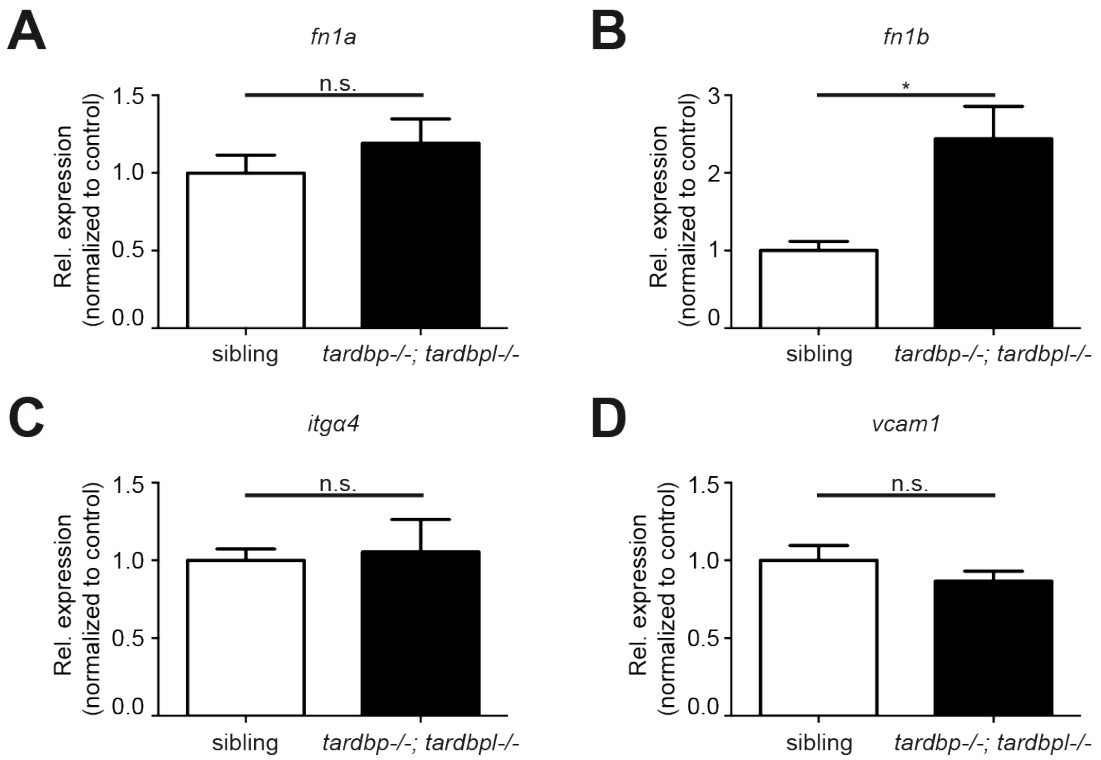

Figure 3.16: Relative mRNA expression of *fn1b* (**B**), but not *fn1a* (**A**), *itgα4* (**C**), or *vcam1* (**D**) is increased in *tardbp-/-; tardbpl-/-* mutants compared to their wild type siblings. n=6 pools of embryos of independent clutches at 24 hpf, unpaired t test. Results by qPCR were reproduced twice using the same cDNA.

by unaltered expression in other cell types. Unfortunately, no antibodies are available for zebrafish to test whether protein levels of integrin α4 and Vcam1 are increased.

3.4.3 Fn is deposited around developing SA in wild type siblings and *tardbp-/-; tardbpl-/-* mutants

An antibody against the human FN1 has been used in immunofluorescence to detect Fn1a and Fn1b in zebrafish before [162, 165], which labels for example the somite boundaries [165]. To test whether zebrafish FN1 homologues are also expressed around sprouting SA and could hence contribute to causing the vascular mis-patterning of SA in *tardbp-/-; tardbpl-/-* embryos, FN1 immunofluorescence was performed in *Tg(fli1:EGFP)*^{y1} embryos. In accordance with published results [165], zebrafish Fn is expressed along the somite boundaries and around the axial vessels in wild type siblings and *tardbp-/-; tardbpl-/-* mutants at 28 hpf (Figure 3.17).

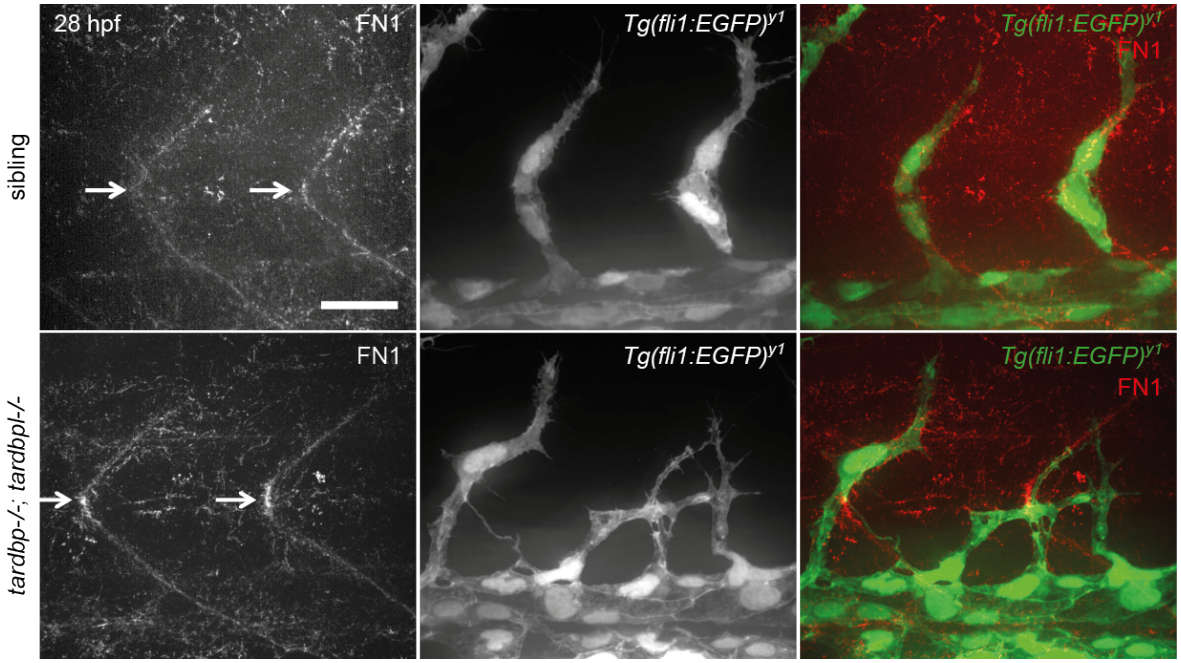

Figure 3.17: Fn is deposited at somite boundaries in wild type and *tardbp-/-; tardbpl-/- Tg(fli1:EGFP)*^{y1} zebrafish embryos. Immunofluorescence images showing two representative somites of the trunk dorsal of the yolk sack extension. Arrows point to somite boundaries, scale bar 50 µm, anterior to the left.

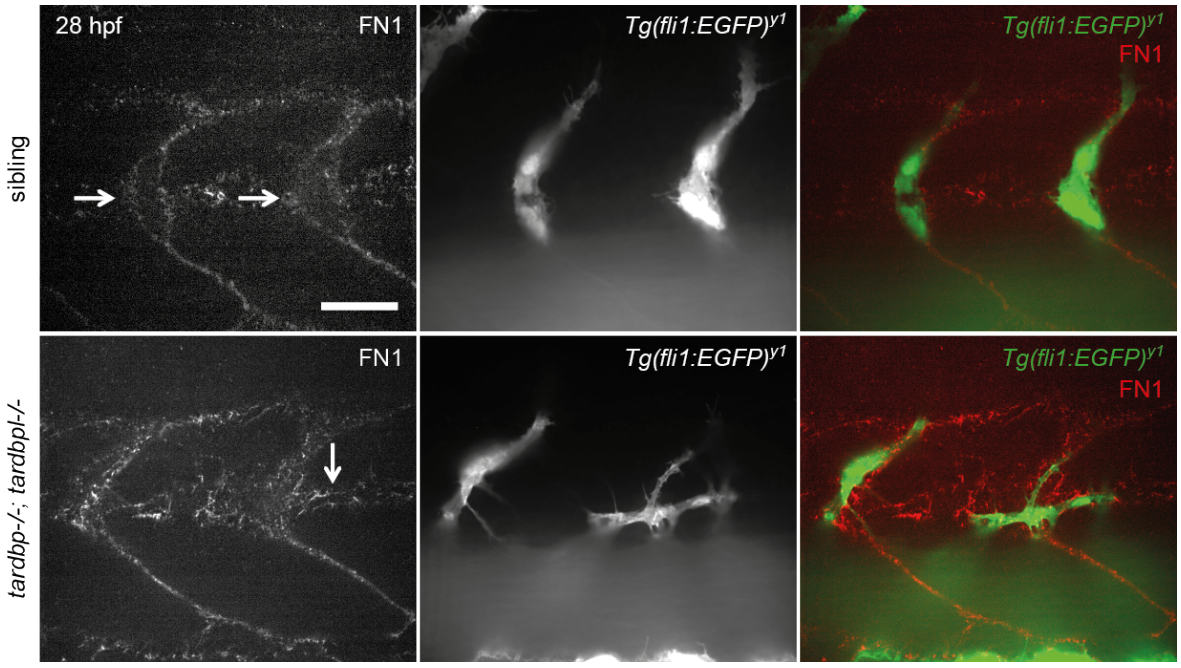

Figure 3.18: Fn is deposited around sprouting SA in wild type and *tardbp-/-; tardbpl-/- Tg(fli1:EGFP)*^{y1} zebrafish embryos. Immunofluorescence showing one section of 200 nm thickness of the same acquired stack as the z-projection shown in Figure 3.17. Arrows point to Fn deposited around SA sprouts, scale bar 50 µm, anterior to the left.

Figure 3.18 shows single planes recorded by spinning disk microscopy with a thickness of 200 nm, visualizing the thin zebrafish Fn matrix around sprouting SA. The Fn matrix is deposited both around wild type and mutant sprouts. In mutants, Fn is also present around the laterally extending lamellipodia. Therefore, a Fn matrix is deposited around developing SA of zebrafish and can thus contribute to causing the angiogenic defects in *tardbp-/-; tardbpl-/-* mutants.

3.5 Rescue of the angiogenic defect of *tardbp-/-; tardbpl-/-* zebrafish

3.5.1 KD of Fn1b, integrin α4, and Vcam1 statistically significantly rescues hypersprouting of SA in *tardbp-/-; tardbpl-/-* mutants

FN1 expression is highly significantly increased in NGS of TDP-43 KD HUVEC, FN1 protein expression is increased upon TDP-43 KD in HUVEC, and *fn1b* mRNA expression is significantly increased in *tardbp-/-; tardbpl-/-* mutant zebrafish. If this increase causes the angiogenic defect in *tardbp-/-; tardbpl-/-* embryos, reducing its expression should rescue this phenotype. Because *fn1a* RNA is not increased, KD with a *fn1a* MO is likely not able to rescue the phenotype. MO targeting *fn1a* and *fn1b* are published and validated [162, 165].

FN1 is known to bind to integrin α4β1, whose expression is also increased in HUVEC upon TDP-43 KD. In zebrafish, six paralogues of *ITGB1* exist but only one homologue of *ITGA4*. Moreover, fold change increase in *ITGA4* expression is higher than the one of *ITGB1*, which is also reflected in stronger increase in protein expression. In addition, whereas integrin β1 is part of five integrin receptors that can bind to FN, integrin α4 is a subunit of only two different integrin heterodimeric receptors, integrin α4β1 and integrin α4β7. Therefore, less side effects are expected by KD of this integrin compared to KD of integrin β1. Thus, a MO targeting *Itgα4* and not *Itgβ1* was used. If the angiogenic hypersprouting of SA in *tardbp-/-; tardbpl-/-* is caused by increased

signaling of Fn via Integrin α4β1, KD of integrin α4 should hence rescue the vascular phenotype. *VCAM1* is the gene with the third strongest increase in expression, a ligand of integrin α4β1, and already known to be bound by TDP-43 [92]. Thus, MO KD of this gene was also used for rescue experiments. The developmental stage at which SA

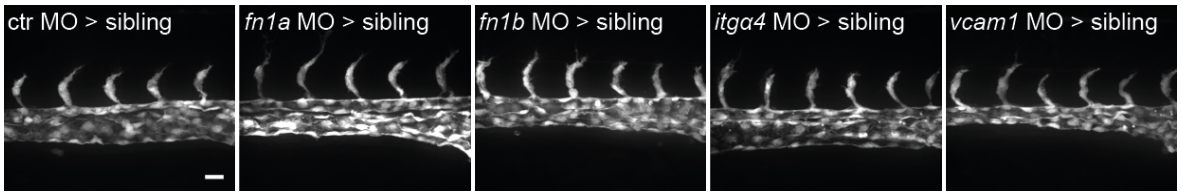

Figure 3.19: Mild KD of *fn1b*, *itgα4*, or *vcam1* does not affect SA growth in wild type embryos compared to ctr MO injected siblings. All embryos are *Tg(fli1:EGFP)*^{y1}, ISV of the trunk dorsal of the yolk sack extension are shown, scale bar 50 µm, anterior to the left.

sprouts reach the horizontal myoseptum was chosen for quantification of angiogenetic sprouting due to the rather simple vascular pattern. To exclude off-side target effects of MO in general and to reduce impact of lowered expression of targeted genes in other tissues than the vasculature, low MO concentrations were chosen that do not impact SA growth in control MO injected embryos at 24 hpf (Figure 3.19). However, as evaluated by the desired alterations in splicing patterns, successful KD of integrin α4 and Vcam1 is still detectable on RNA level (Figure 3.22).

Strikingly, KD of *fn1b*, *itgα4*, or *vcam1* rescues the hypersprouting phenotype of *tardbp-/-; tardbpl-/-* mutants (Figure 3.20A). In contrast, KD of *fn1b* does not rescue this phenotype. Figure 3.20B shows the statistical analysis of the rescue experiment: KD of *fn1b*, *itgα4*, or *vcam1* statistically significantly rescues the *tardbp-/-; tardbpl-/-* mutant phenotype. The effect is strongest for KD of *itgα4*, followed by KD of *fn1b*. Also the KD of *vcam1* reaches statistic significance, but is less pronounced compared to KD of *fn1b* or *itgα4*.

3.5.2 KD of α4 but not combined KD of α5 and αv integrins ameliorates angiogenic defects

Another important FN integrin receptor involved in angiogenesis *in vivo*, integrin α5β1, could contribute to the phenotype as well. To rule out this possibility, the rescue

potential of α5 KD was tested. Integrin αv is known to rescue the Fn fibril assembly defect of *ITGA5* knockout embryonic cells [185]. To prevent a rescue of integrin α5 KD by integrin αv, *Itgα5* and *Itgαv* MO were injected together. Both MO have been previously established [165, 294].

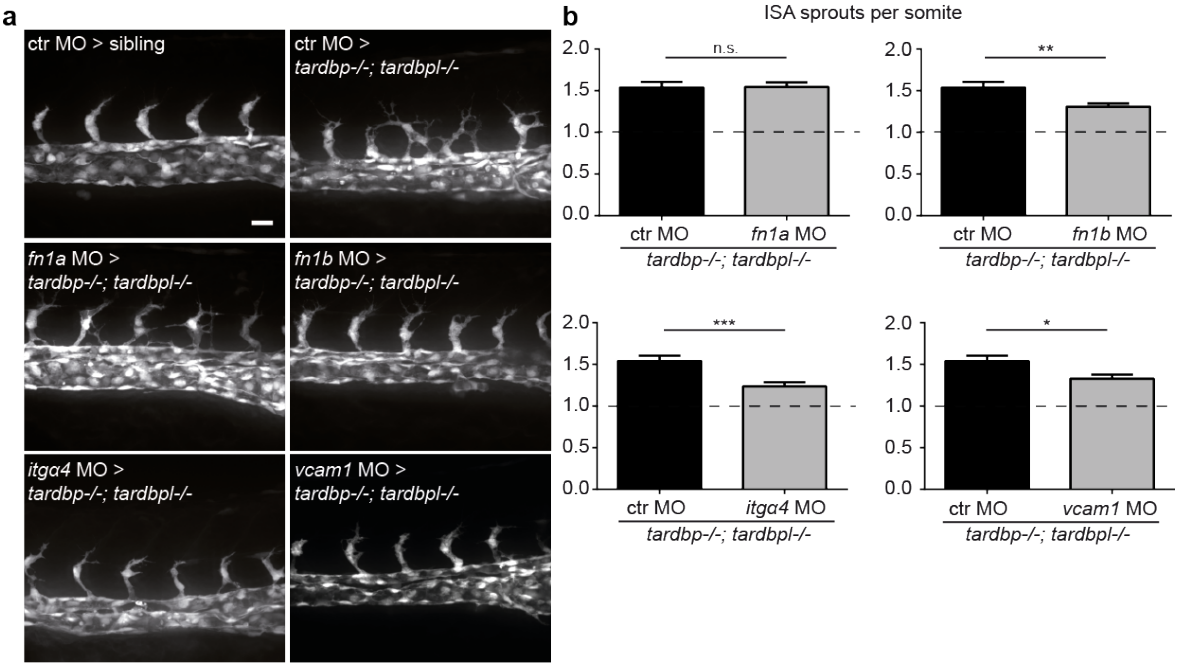

Figure 3.20: Mild KD of *fn1b*, *itgα4*, or *vcam1*, but not *fn1a* rescues increased SA sprouting in *tardbp-/-; tardbpl-/-* mutants. **A** Images showing rescue results with normal SA sprout number in *tardbp-/-; tardbpl-/-* mutants injected with 0.33 mM *fn1b*, 0.5 mM *itg.α4*, or 0.75 mM *vcam1* MO. Note the morphological difference compared to ctr MO injected *tardbp-/-; tardbpl-/-* mutants and the similarity to 0.75 mM ctr MO injected wild type sibglings. *fn1b* KD *tardbp-/-; tardbpl-/-* mutants (0.75 mM MO) are not rescued. All embryos are *Tg(fli1:EGFP)*^{y1}, ISV of the trunk dorsal of the yolk sack extension are shown, scale bar 50 µm, anterior to the left. **B** Statistical analysis demonstrating that mild KD of *fn1b*, *itgα4*, or *vcam1* can statistically significantly rescue increased sprouting of SA from the DA at 24 hpf in *tardbp-/-; tardbpl-/-* mutants compared to ctr MO injected *tardbp-/-; tardbpl-/-* mutants. The dashed lines represent the average number of sprouts per somite in wild type embryos. One of three (*fn1a*, *fn1b*, *itgα4* KD) or two (*vcam1* KD) independent experiments with two clutches per experiment are shown, normality test and unpaired t test, n≥23.

Injection of 0.5 mM *itgα5* and 1 mM *itgαv* MO leads to similar defects regarding the vasculature of wild type embryos as injection of 1 mM *itgα4* MO at 4 dpf, with more straight growing ISV and EC that occasionally lack contact with the DA or each other (Figure 3.21C and D). Having these comparable effects on wild type blood vessels, the

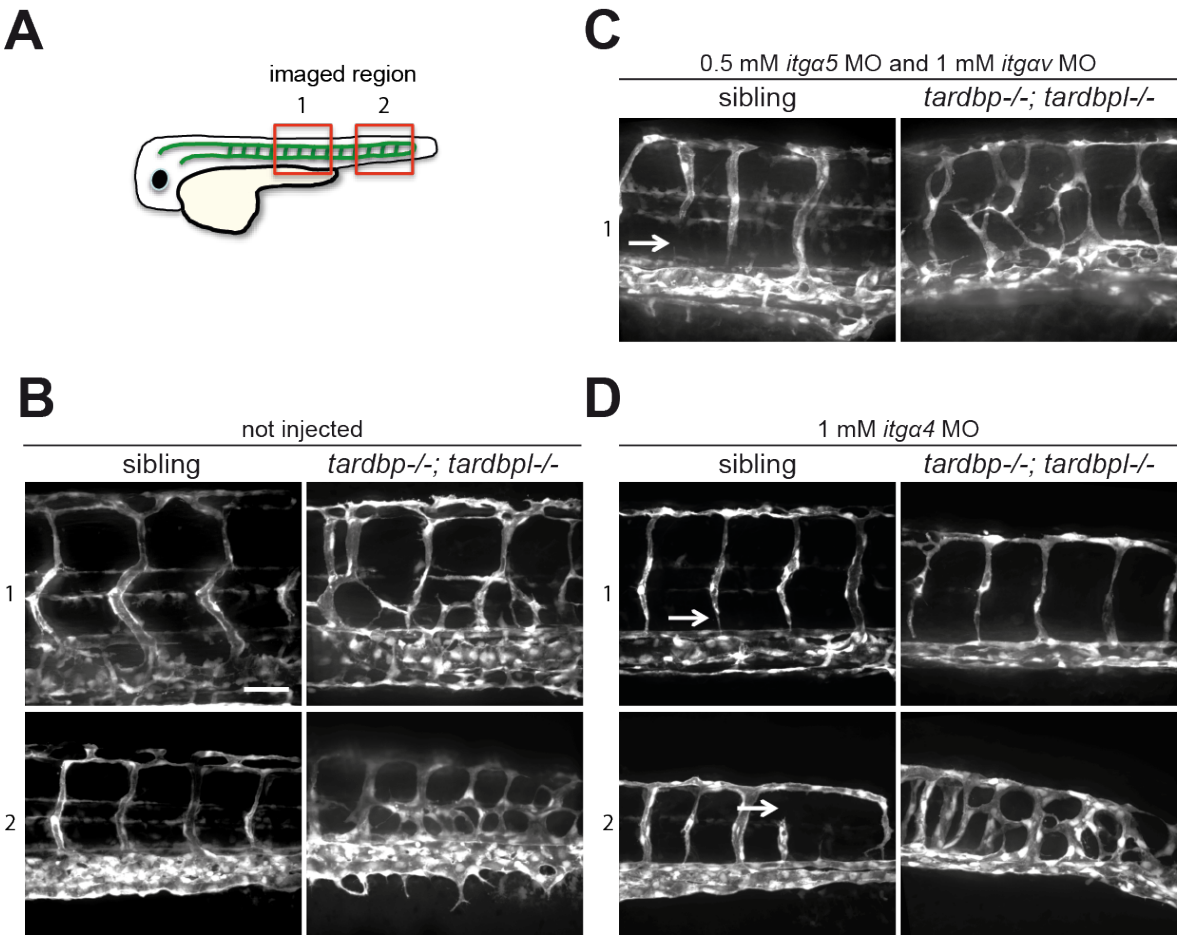

Figure 3.21: KD of Itgα4, but not combined KD of α5 and αv integrins ameliorates the vascular mis-patterning of *tardbp-/-; tardbpl-/-* embryos at 4dpf. **A** Scheme of a zebrafish embryo with the vasculature in green illustrating the position of the regions 1 and 2 that are shown in **B** - **D**. **B** Uninjected representative sibling and *tardbp-/-; tardbpl-/-* mutant. **C** Representative image of 0.5 mM *itgα5* and 1 mM *itgαv* MO injected sibling and *tardbp-/-; tardbpl-/-* mutant. **D** Representative image of 1 mM *itgα4* MO injected sibling and *tardbp-/-; tardbpl-/-* mutant. Note the normal number of ISV in region 1 of the *itgα4* MO injected *tardbp-/-; tardbpl-/-* mutant. The same embryo shows vascular mis-patterning in region 2 distal to region 1. Arrows point to ISV defects in wild type siblings injected with 1 mM *itgα4* or 0.5 mM *itgα5* and 1 mM *itgαv* MO. All embryos are *Tg(fli1:EGFP)*^{y1}, ISV of the trunk dorsal of the yolk sack extension are shown, scale bar 50 µm, anterior to the left.

potential to ameliorate the vascular mis-patterning of *tardbp-/-; tardbpl-/-* mutants is strikingly different. Whereas combined KD of *itgα5* and *itgαv* does not rescue the vascular mis-patterning in any *tardbp-/-; tardbpl-/-* mutant observed, several 1 mM *itgα4* MO injected *tardbp-/-; tardbpl-/-* mutants show a strong amelioration of the phenotype. *tardbp-/-; tardbpl-/-* embryos with integrin α4 KD have ISV with nearly wild type morphology dorsal of the yolk sack extension. These embryos can only be identified as mutants because the vascular mis-patterning is less ameliorated in distal

parts of the trunk (Figure 3.21D). Thus, in contrast to KD of integrin α4, KD of integrin α5 and integrin αv cannot ameliorate the vascular phenotype of *tardbp-/-; tardbpl-/-* mutants. This indicates that the relevant receptor of FN causing the angiogenic defect of *tardbp-/-; tardbpl-/-* mutants is an α4 subunit containing integrin.

Taken together, the signaling axis of the ECM component and ligand FN1, the ligand VCAM1, and the integrin α4 subunit of their integrin receptor α4β1 are causally involved in the vascular mis-patterning observed in *tardbp-/-; tardbpl-/-* mutant zebrafish. Their increased expression in TDP-43 KD HUVEC and the rescue of angiogenic defects of *tardbp-/-; tardbpl-/-* embryos upon their KD suggests increased FN – integrin α4 and VCAM1 – integrin α4 signaling to be the mechanistic explanation of increased initial migration and sprouting capability from the DA.

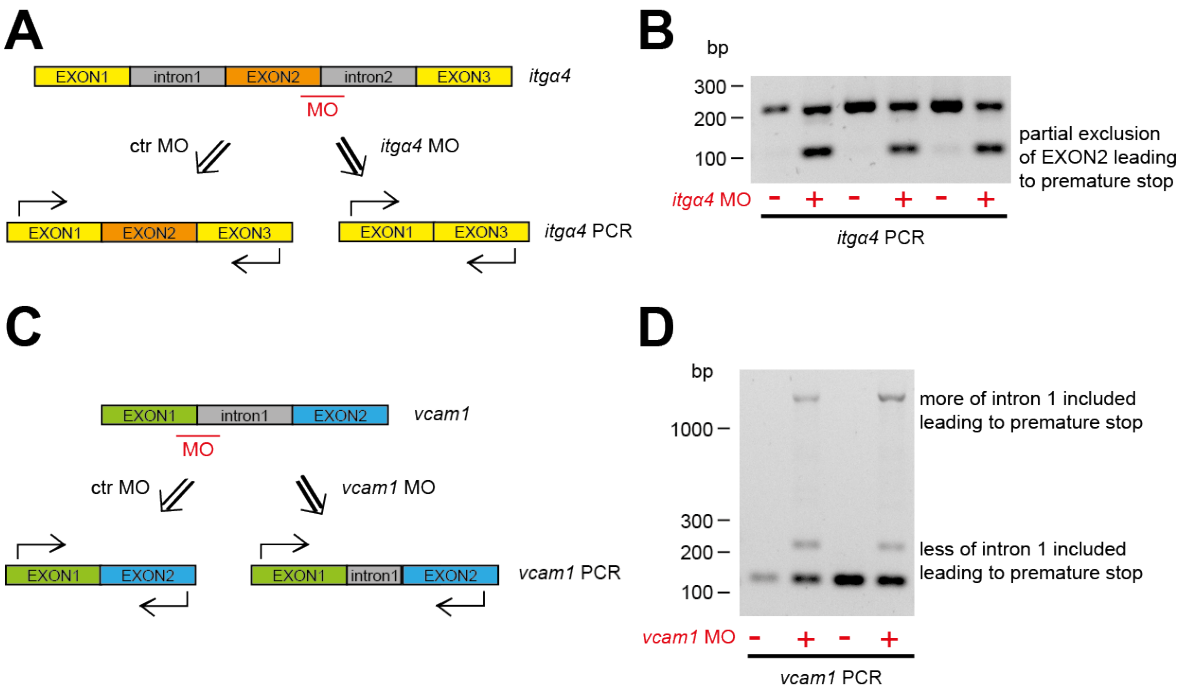

Figure 3.22: Mild KD of *itgα4* and *vcam1* causes splicing alterations leading to premature stop codons. **A** Scheme illustrating the first three exons and two introns of *itgα4*. Binding of the *itgα4* MO (indicated in red) leads to skipping of exon2, as verified by sequence analysis of the resulting lower band at about 100 bp shown in B. Primers used for amplification are indicated by black arrows. **B** PCR products of cDNA from ctr MO injected (-) or *itgα4* MO injected (+) siblings of the embryos used in the rescue experiment shown in Figure 3.20. Injection of *itgα4* MO leads to appearance of a second, lower migrating band representing *itgα4* RNA lacking exon2. The upper band represents the normally spliced *itgα4* RNA with exon1, 2, and 3. Bands were cut, DNA purified and sent for sequencing, revealing a frame shift resulting from exon skipping leading to a premature stop codon. **C** Scheme illustrating the first two exons and first intron of *vcam1*. Binding of the *vcam1* MO (indicated in red) leads to partial inclusion of intron1 resulting in two RNAs with different length (see D). This was verified by sequence analysis of the resulting higher bands appearing in *vcam1* MO injected embryos at about 200 bp and 1200 bp shown in D. Primers used for amplification are indicated by black arrows. **D** PCR products of cDNA from ctr MO injected (-) or *vcam1* MO injected (+) siblings of the embryos used in the rescue experiment shown in Figure 3.20. Injection of *vcam1* MO leads to appearance of a second and third, higher migrating band representing *vcam1* RNA with partial intron1 inclusion. The lowest band represents the normally spliced *vcam1* RNA with exon1 and 2. Bands were cut, DNA purified and sent for sequencing, revealing a frame shift resulting from partial exon inclusion leading to a premature stop codon.

4 Discussion

TDP-43 pathology is present in more than 97% of ALS, 45% of FTD, and about 30% of Alzheimer cases [26, 30]. Mutations in *TARDBP* itself and in several other ALS- and FTD-associated genes lead to TDP-43-positive aggregate formation [16]. Furthermore, the presence of TDP-43-positive inclusions correlates with neuronal degeneration [310]. Therefore, TDP-43 pathology is considered a common downstream event in neurodegeneration that is likely to cause neuronal cell death. However, the disease mechanism is still unknown. In cells with TDP-43-positive inclusions, the nucleus is often devoid of TDP-43, suggesting a loss-of-function disease mechanism. On the other hand, the inclusions could mediate cell death by perturbance of several cellular functions, indicating a gain-of-function effect. A combination of both events ultimately leading to neurodegeneration is also possible.

To address the loss-of-function hypothesis it is necessary to investigate the *in vivo* functions of TDP-43. Knowledge of the physiological function might then allow to analyze why neurons die upon a potential TDP-43 loss-of-function in patients. To this end, animal models that lack TDP-43 have been generated. They demonstrate the requirement of TDP-43 function for the whole organism, as global TDP-43 knockout in flies, zebrafish, and mice leads to early death [101, 147, 132, 133, 134]. Also conditional knockout of TDP-43 in adult mice is incompatible with life, as the mice die nine days after TDP-43 inactivation [136]. Moreover, TDP-43 knockout in motor neurons causes ALS-like phenotypes [139, 140]. Thus, animal models conclusively demonstrate the requirement of TDP-43 for normal cell function and survival. Various approaches have further shown that TDP-43 is involved in many steps of RNA metabolism by, e.g., binding to thousands of different mRNAs [26, 311, 93]. It is therefore not surprising

that the lack of TDP-43 mediated regulation of RNA metabolism leads to perturbance of cell homeostasis, which might affect vulnerable neurons more than other cell types. Taken together, all these findings strongly support a loss-of-function disease mechanism.

However, the requirement of tightly controlled TDP-43 levels for normal cell function makes it difficult to target TDP-43 itself. Therefore, the development of a drug that normalizes TDP-43 function in patients with TDP-43 pathology has not been successful yet. Thus, to intervene successfully, drug targets downstream of TDP-43 need to be identified. Moreover, such downstream targets could be used as biomarkers for monitoring of disease progression and treatment success. Although numerous TDP-43 targets have been identified, their role in the disease pathomechanism is mostly unclear and none is used therapeutically. Therefore, I used the TDP-43 loss-of-function zebrafish mutant generated in my laboratory to identify new targets of TDP-43 that are needed for normal cell function and might be used for therapeutic approaches.

4.1 Vascular phenotype of TDP-43 deficient model organisms

Loss of TDP-43 function in zebrafish leads to vascular mis-patterning. This mis-patterning is characterized by increased, ectopic sprouting of blood vessels that grow into tissue usually devoid of vessels. Most blood vessels do not form a functional lumen. In addition, the proportion of EC reaching the dorsal roof of the neural tube to form the DLAV is decreased, suggesting impaired directional migration of EC. In contrast, the DA and PCV formed by vasculogenesis are located at correct sites of the embryo but also often lack perfusion. The defects in angiogenesis are not restricted to specific vascular beds: blood vessels in the head and in the trunk, as well as arteries and veins are affected. The phenotype is cell autonomous, which is further supported by increased angiogenesis in a human EC culture model upon TDP-43 KD. Moreover, this finding demonstrates the conserved EC requirement for TDP-43 function. In collaboration with Prof. Dr. Ulrich Pohl and Dr. Eloi Montanez (both Walter Brendl-Institute, LMU Munich), we generated a conditional knockout mouse lacking TDP-43 in EC.

Strikingly, first characterization of the vascular network of the retina revealed that loss of TDP-43 leads to the same increase in angiogenesis as well as impaired EC migration in mice as observed in zebrafish: EC density at the angiogenic front is strongly increased and radial expansion of the network is decreased. These findings underscore the cell autonomous requirement of TDP-43 in EC during angiogenesis across vertebrate species and highlights the fact that invertebrates are not suitable for analysis of endothelial TDP-43 function, since they lack the closed endothelium lined vascular system of vertebrates [312].

4.2 Candidate guidance cues do not affect angiogenesis in TDP-43 KO fish

The *tardbp-/-; tardbpl-/-* phenotype of ectopic angiogenic sprouting suggests a defect in vascular patterning caused by loss of guidance cues. The similarity to the defects of the *obd* mutant, lacking functional PlxnD1, suggests a role for defects in PlxnD1 - Semaphorin signaling and/or increased VEGFR2 signaling in *tardbp-/-; tardbpl-/-* mutants [247, 248]. However, several findings speak against this hypothesis. First, the phenotypes of *obd* and *tardbp-/-; tardbpl-/-* mutants are not identical. Vessels in *obd* mutants are perfused, whereas most vessels in *tardbp-/-; tardbpl-/-* mutants are not. Second, alternative splicing alterations found to be causative of the *obd* phenotype are not present in TDP-43 deficient embryos: Expression levels of *sflt1* and *mflt1* as well as their expression patterns are not altered. Third, neither *plxnD1* itself is dysregulated, nor its ligands *sema3aa* and *sema3ab*. Fourth, altered sFlt1/mFlt1 expression in *obd* mutants leads to increased signaling via Kdrl (the zebrafish VEGFR2 homologue). However, as discussed in the next section, there is no evidence for increased VEGFR2 signaling in *tardbp-/-; tardbpl-/-* mutants or TDP-43 KD HUVEC. Taken together, I could demonstrate that the *tardbp-/-; tardbpl-/-* phenotype is not caused by alteration of candidate guidance cue expression levels or expression patterns.

4.3 VEGF and Notch do not cause the TDP-43 KO vascular phenotypes

4.3.1 VEGFR2 signaling is not altered in TDP-43 deficient zebrafish or HUVEC

VEGFR2 is the main pro-angiogenic signaling pathway (section 1.3.2). Therefore, increased VEGFA signaling via VEGFR2 could explain increased angiogenic sprouting of *tardbp-/-; tardbpl-/-* mutants. However, *kdrl* expression is not increased in TDP-43 deficient embryos. If increased VEGFR2 signaling led to increased sprouting, sufficient signaling for sprouting would be expected in the TDP-43 deficient EC upon titration of a selective VEGFR2 inhibitor (DMH4) to a concentration just blocking sprouting in control embryos. However, this concentration also blocks sprouting in TDP-43 deficient zebrafish. Moreover, treatment with further chemical inhibitors reducing VEGFR2 signaling also downstream of VEGFR2 is not able to ameliorate increased and ectopic sprouting. Importantly, treatment with VEGFR2 inhibitors to reduce VEGFR2 signaling and thereby block or impair sprouting of ISV was successfully used in zebrafish embryos before [248, 234].

Furthermore, VEGFR2 expression and activation as evaluated by its phosphorylation status is not altered in TDP-43 KD HUVEC. In addition, the downstream signaling components AKT, p38, PLCG1, and ERK1/2 are expressed at the same levels and their activation is not increased, neither after starvation nor after induction of VEGFR2 signaling by VEGF stimulation. Kinetics of activation are not altered either. Moreover, NGS revealed 73 genes with strongly dysregulated RNA expression (more than four-fold change in expression) and several hundred alternatively spliced RNAs upon TDP-43 KD in HUVEC. However, VEGFR2, VEGFR1, VEGFR3, as well as their ligands VEGFA, VEGFB, VEGFC, and VEGFD are not among these genes and none of them is dysregulated more than 1.25 fold (VEGFA, down-regulated). In summary, experimental evidence does not support a causative role of VEGF signaling for TDP-43 deficient phenotypes.

4.3.2 Notch signaling is not affected in TDP-43 deficient zebrafish

Notch signaling is an important regulator of arterial-venous differentiation and sprouting angiogenesis (section 1.3.4 and section 1.3.5.2). Reduction of Notch signaling leads to increased migration of EC into SA and increased proliferation of EC in SA [240]. Furthermore, KD of Dll4 prolongs sprouting activity after formation of the DLAV [242]. To test for correct arterial-venous specification, *ephrin-B2a* (arterial expression) and *flt4* (venous expression) expression patterns were examined. Both markers are expressed normally and at normal levels in TDP-43 deficient embryos, excluding defects in differentiation of the DA and PCV. Furthermore, EC number is unchanged in *tardbp-/-; tardbpl-/-* mutants. Moreover, sprouting activity is increased already from the very beginning of angiogenic activity and not only at the later stage as observed upon reduced Notch signaling. In conclusion, Notch signaling is not impaired in *tardbp-/-; tardbpl-/-* mutants. Furthermore, this result again speaks against a defect in VEGFR signaling. KD of the VEGFR1 homologue Flt1 leads to ectopic expression of *flt4* in the DA and reduced *ephrin-B2a* expression [244]. However, expression of both markers is normal upon loss of TDP-43, contradicting an involvement of reduced Flt1 expression in the vascular mis-patterning mechanism.

4.3.3 Impact of TDP-43 function on tip cell/stalk cell selection

The tip cell concept is based on the observation that EC migrate in a collective manner during angiogenesis. Further, it uses the cell contact dependent differential expression of receptors (e.g. VEGFR2, VEGFR1, Dll4, Notch) and the resulting varying signaling events to explain the different morphological characteristics and functions of EC in the same sprout. In the mouse retina, stalk cells proliferate and maintain cellular contacts, whereas tip cells extend numerous filopodia to integrate environmental cues and guide the sprouts. In the zebrafish trunk ISV, also EC leading the sprout proliferate and EC of the same sprout change positions. Therefore, the tasks of individual EC may not be as defined as predicted by the tip cell concept in zebrafish ISV. In the ISV of *tardbp-/-; tardbpl-/-* mutants, numerous EC are not able to maintain cell-cell contacts during the sprouting process. In addition, individual EC extend not only one lamellipodium

towards the dorsal side of the embryo as in wild types, but instead extend additional lamellipodia in all directions. Based on these morphological characteristics, an increased proportion of EC might be tip cells in the ISV of *tardbp-/-; tardbpl-/-* mutants. However, the prerequisite for collective migration of EC, namely maintenance of stable cellular contacts, is not given in the mutants. As a consequence, cell contact dependent signaling events like Notch signaling are limited. The tip cell concept with its regulation of tip versus stalk cell selection based on varying VEGF/Notch signaling may thus not apply to the migration process of EC in *tardbp-/-; tardbpl-/-* mutants. Instead, dysregulation of ECM – integrin signaling may alter the morphological appearance and functions of TDP-43 deficient EC independently of VEGF/Notch signaling, resulting in a tip cell like behavior. In-depth analysis of the TDP-43 KO EC in the retina of the above mentioned conditional knockout mice could be performed to elucidate tip/stalk cell characteristics of TDP-43 KO EC.

4.4 Identification of dysregulated candidate genes by next generation sequencing

I could exclude alterations in candidate gene expression and function as being responsible for the vascular mis-patterning of *tardbp-/-; tardbpl-/-* mutants. Therefore, an unbiased approach was used to identify differential expression of genes involved in angiogenesis upon TDP-43 KD. NGS revealed 73 genes with more than a four-fold change in differential expression upon TDP-43 KD in HUVEC. 5328 genes show a differential expression with an adjusted p value smaller than 0.01. In addition, 450 alternative splicing events were detected. Among these RNAs, there are already published TDP-43 targets, for example CDK5RAP2, RWDD1, and SKAR [93]. The number of genes with altered expression, as well as the number of alternative splicing events upon TDP-43 KD, is comparable to numbers published in other systems (reviewed in [26]). TDP-43 dependent regulation of specific mRNAs seems to vary in different tissues and organisms. In HUVEC, TDP-43 KD leads to increase of *FUS* by 25%, whereas *GRN* expression is not altered. In mouse brain, *Fus* expression was found to be decreased to 40% and *Grn* increased 3-6 fold [92]. HUVEC are therefore no ideal system to investigate interaction

of TDP-43 with these ALS- or FTD-linked genes if transfer of results to a neuronal system is intended. Similarly, Filamin C, previously identified to be up-regulated as protein in whole lysate of *tardbp-/-; tardbpl-/-* mutants and as RNA in frontal cortex of FTLD-TDP patients, is down-regulated in TDP-43 KD HUVEC. However, Filamin C is highly expressed in skeletal muscle tissue where it is required for its integrity [313, 314]. Since *tardbp-/-; tardbpl-/-* mutants have degenerating muscles, the increase in Filamin C expression in total lysate from *tardbp-/-; tardbpl-/-* mutants is likely to originate from Filamin C expression alterations in muscle tissue.

Regarding differential expression of genes that may be responsible for vascular mis-patterning in *tardbp-/-; tardbpl-/-* mutants, the two ligands FN1 and VCAM1 as well as their receptor integrin $\alpha 4\beta 1$ were promising candidates. FN1 is needed for heart and blood vessel development in mice [155, 156, 157], VCAM1 regulates cellular contacts [190, 197, 198], and integrin $\alpha 4\beta 1$ can mediate FN fibril assembly and is required for directed migration of various cell types [186, 187, 188]. mRNA levels of all four genes are significantly and strongly up-regulated upon TDP-43 KD. No splicing alteration events were detected in mRNAs of these genes, indicating regulation of transcription itself, RNA stability, or RNA degradation by TDP-43. Except for VCAM1, expression of all candidates is strongly increased also on the protein level. VCAM1 expression is under the detection limit in the immunoblots performed, except for a very faint band visible in the TDP-43 KD HUVEC transduced with sh*TARDBP*#1. This indicates that also VCAM1 is increasingly expressed on protein level upon TDP-43 KD, albeit still at low levels. Thus, increased expression of these genes could be responsible for the *tardbp-/-; tardbpl-/-* mutant hypersprouting phenotype.

4.5 Increased FN1/VCAM1 - ITGA4 interaction causes the vascular phenotype of *tardbp-/-; tardbpl-/-* mutants

FN1, integrin α4β1, and VCAM1 are increasingly expressed in TDP-43 KD HUVEC and are involved in angiogenesis or in cellular processes relevant for angiogenesis. Unfortunately, antibodies to test for their up-regulation in zebrafish are not available. Therefore, quantitative PCR was performed to compare mRNA expression of these candidates in *tardbp-/-; tardbpl-/-* mutants versus wild type siblings. *Itgβ1* was excluded from the analysis due to the presence of six paralogues in zebrafish, its lower fold change in NGS, and lower increase on protein level compared to *itgα4*. One of the two *FN1* homologues in zebrafish, *fn1b*, is up-regulated statistically significantly, whereas *itgα4* and *vcam1* are not altered. Unchanged expression of *itgα4* and *vcam1* might be attributable to the source of mRNA: NGS was performed exclusively with endothelial mRNA, whereas the mRNA of zebrafish used for quantitative PCR was a mixture of all tissues present in the embryo. Therefore, EC specific dysregulation in the absence of TDP-43 might be masked by unchanged expression in other tissues. Moreover, unaltered mRNA expression does not exclude increased expression of integrin α4β1 and VCAM1 on protein level. Since TDP-43 is known to regulate RNA stability and degradation, a possible mechanism in the zebrafish might be increased translation due to increased RNA stability upon TDP-43 deficiency. Alternatively, loss of TDP-43 could indirectly affect protein expression of these proteins. This indirect impact on protein levels might be regulated differently in human EC and zebrafish. Regardless of the mechanism, if increased expression of candidates causes the vascular phenotype, KD mediated reduction of expression should ameliorate the defects in angiogenesis. Therefore, partial KD of all candidates was performed to re-establish wild type protein levels.

4.5.1 KD of Fn1a, integrin α4, and Vcam1 rescues vascular mis-patterning of *tardbp-/-; tardbpl-/-* mutants

To quantify the rescue effect of Fn1b, Fn1a, integrin α4, and Vcam1 KD in *tardbp-/-; tardbpl-/-* mutants, the average number of sprouts per somite was quantified when SA sprouts reach the horizontal myoseptum at about 24 hpf. MO concentrations that do not affect overall morphology and SA formation in wild type embryos were used to minimize off-site target effects of MO. Strikingly, KD of Fn1b as well as of integrin α4 highly significantly rescues the hypersprouting from the DA in *tardbp-/-; tardbpl-/-* mutants. KD of Vcam1 also rescues this phenotype statistically significantly, although to a lesser extend than KD of Fn1b or integrin α4. In contrast, reduction of Fn1a does not ameliorate the hypersprouting phenotype.

This finding implies distinct functions of Fn1a and Fn1b in angiogenesis of the zebrafish trunk vasculature. Fn1b shares 62% of its amino acid sequence with Fn1a and both zebrafish fibronectins have all functional domains present in other species [160]. Both are needed for somitogenesis. However, Fn1a is more important for somitogenesis of the anterior somites, and KD of Fn1b leads to tail extension defects whereas KD of Fn1a does not [165, 166]. Moreover, Fn1a is reported to be required for sprouting from the DA to form the interrenal vessel, whereas Fn1b is not [164]. In addition, mRNA expression patterns of the two fibronectins are different [165, 166]. Also their temporal expression varies: Fn1a is expressed strongly in stages before gastrulation, whereas Fn1b expression increases during development [160]. The two zebrafish fibronectins are therefore thought to have separate roles during zebrafish development [165, 160], which is in line with the concept of split functions of paralogue pairs [315, 316]. Thus, Fn1b but not Fn1a expression regulates ISV formation in *tardbp-/-; tardbpl-/-* mutants.

Conclusively, these data suggest that signaling of Fn1b, and to a lesser extend also of Vcam1, via an α4 subunit containing integrin receptor causes vascular mis-patterning in *tardbp-/-; tardbpl-/-* mutants.

4.5.2 FN1 – ITGA4 and not FN1 – ITGA5 or FN1 – ITGAV interactions are relevant for the vascular mis-patterning phenotype

KD of Fn1b leads to profound amelioration of vascular defects in *tardbp-/-; tardbpl-/-* mutants. Fn1b and Fn1a are required for somite boundary formation and maintenance via binding to integrin α5β1 in zebrafish. Moreover, global knockout studies of *Fn1*, *Itgα4*, *Itgα5*, and *Itgαv* in mice support integrin α5β1 as the main FN receptor required for normal vascular development *in vivo* [155, 156, 157, 185, 184, 180, 158]. However, EC specific knockout of *Itgα5* does not impair angiogenesis, indicating a cell non-autonomous requirement of integrin α5 during vascular development [181]. Moreover, *ITGA5* is not differentially expressed in TDP-43 KD HUVEC. To exclude contribution of integrin α5 to the vascular mis-patterning upon TDP-43 deficiency, the rescue capacity of reduced integrin α5 was tested. Since integrin αv can compensate for impaired FN fibrillogenesis and focal contact formation upon *α5* knockout [185], combined KD of integrin α5 and αv in *tardbp-/-; tardbpl-/-* mutants was performed. The MO concentration injected affects ISV of wild type embryos, indicating that a sufficient MO dose was used. To compare the effect of integrin α5 and integrin αv KD to the rescue capacity of integrin α4 KD, a dose of *itgα4* MO similarly affecting wild type ISV was injected.

KD of integrin α4 strongly ameliorates the vascular mis-patterning phenotype of *tardbp-/-; tardbpl-/-* mutants at 4 dpf, when SA and SV are formed. Especially the region dorsal to the yolk is patterned normally upon KD of integrin α4. Ectopic sprouting is completely absent and no ectopic lateral connections are present. In the distal part of the tail, the rescue is less efficient, indicating an increasing proximal to distal expression gradient or varying dependence on integrin α4 function. Different requirement of integrin function in anterior versus posterior parts of the embryo has been reported for integrin α5: *itgα5* knockouts have somite boundary defects only in the anterior somites, whereas the distal somites are normal [165, 166]. Alternatively, the KD could be less efficient in the distal part, since the MO could already be partially degraded in the tail due to the later development of this part of the embryo. In contrast

to reduction of integrin α4 levels, combined KD of integrin α5 and αv does not reduce vascular mis-patterning at 4 dpf. Taken together, these data support an α4 subunit containing integrin receptor to cause the vascular mis-patterning in *tardbp-/-; tardbpl-/-* mutants.

4.5.3 Increased FN1 and Vcam1 binding to the ITGA4B1 receptor causes vascular mis-patterning

KD of Fn1b, integrin α4, and Vcam1 rescues the hypersprouting phenotype statistically significantly. VCAM1 binds two integrin receptors, integrin α4β1 and integrin α4β7. However, only integrin β1 expression is increased upon TDP-43 KD, whereas integrin β7 expression is even slightly reduced. Moreover, FN1 binds to α4β1 integrins, but not to α4β7 integrins and Fn1b KD rescues the vascular phenotype. KD of other integrins known to be important receptors for FN1 during angiogenesis, α5 and αv, does not ameliorate vascular mis-patterning. In conclusion, experimental evidence strongly suggests integrin α4β1 to be the relevant receptor of Vcam1 and Fn1b during aberrant ISV formation in *tardbp-/-; tardbpl-/-* mutants.

4.6 How does increased FN1/VCAM1 – integrin α4β1 signaling cause angiogenic defects?

Fn1 knockout embryoid bodies have decreased vascular network complexity of the capillary plexus, indicating that FN1 is needed for formation of branched vessels [158]. Moreover, FN1 is increasingly expressed at sites of cleft formation in salivary gland development. There, it mediates conversion of cell-cell adhesions to cell-matrix adhesions, thus enabling cleft formation and thereby epithelial branching [317]. Thus, FN1 is required for branching of both tubular organ systems. Increased FN1 expression around sprouting EC in zebrafish or of tube forming HUVEC might therefore also cause increased vascular sprouting, lateral branching, or increased network complexity. However, the main receptor required for capillary plexus formation in embryoid bodies is integrin α5β1 [158], which is not involved in the mechanism causing vascular

mis-patterning in *tardbp-/-; tardbpl-/-* mutants. Therefore, increased FN1 is likely to impair angiogenesis in zebrafish via an alternative mechanism.

In the developing mouse retina, EC migrate along a FN1 matrix scaffold produced by astrocytes [252]. Further, it is known that different splice variants of VEGFA are retained to different degree by the ECM. Thus, an VEGFA gradient is formed that is required for normal EC migration and vascular network formation [253]. If FN1 in astrocytes is knocked out, migration of EC is reduced and vascular density at the sprouting front increased [252], similarly to the preliminary phenotype of endothelial TDP-43 KO retinas. Importantly, the astrocytic FN1 KO defect is not mediated by the integrin α5 binding RGD domain of FN1. Instead, reduction of VEGFA binding to FN1 potentially impairing the VEGFA gradient reduces VEGFR2 signaling, and hence migration of EC in the retina [252]. However, also EC in the mouse retina express FN1. One could therefore hypothesize that increased production of FN1 by the EC themselves causes the EC to override the pre-defined "FN1 matrix path" and the cues provided within. As a result, the phenotype of increased endothelial FN1 production would resemble the phenotype of reduced astrocytic FN1 production or VEGF gradient disruption. However, the vascular mis-patterning in *tardbp-/-; tardbpl-/-* mutants can be rescued not only by KD of Fn1b, but also by reduction of integrin α4 levels. This implies that FN1 binding to integrin α4 is required to cause ectopic and increased sprouting. Therefore, although failure to follow astrocyte derived cues by EC might contribute to the observed phenotype, another endothelial intrinsic mechanism involving integrin α4 must be involved.

Investigation of the EC in SA of *tardbp-/-; tardbpl-/-* mutants reveals increased capacity of EC to sprout from the aorta. After leaving the cell collective of the DA, they extend lateral lamellipodia and often loose cell – cell contact to other EC. Increased sprouting can be caused by increased responsiveness to a gradient of soluble chemokines (increased chemotaxis), in case of the sprouting segmental arteries this chemokine is VEGF. However, as discussed above, several lines of evidence contradict an involvement of increased VEGF signaling in the mechanism leading to hypersprouting of TDP-43

deficient EC. An alternative explanation could be increased adhesiveness to the ECM (increased haptotaxis). Increased EC – ECM interactions and decreased EC – EC contacts could promote migration of individual EC independently of chemotactic stimuli and therefore migration on ectopic paths. However, adhesion to the ECM is mostly mediated by integrin α5β1 in focal adhesions. Since KD of integrin α5 cannot rescue the migration defect, this possibility is ruled out.

In order to migrate efficiently, cells need to polarize with defined leading and trailing edges. They then undergo multiple cycles of protrusion at the leading edge, adhesion formation, stabilization of adhesions followed by cell body translocation, release of adhesions, and detachment at the rear of the cell [318]. Whereas most integrins like α5β1 promote focal adhesion formation in lamellipodia, are localized in those focal adhesions and thereby modulate intracellular signaling and adhesion during migration, α4β1 integrin is not found in focal adhesions at the leading edge of the cell. A different mechanism of directional migration regulation and induction of cell polarization has been defined for α4β1 integrin in leukocytes: It promotes intrinsic polarity as well as directional migration toward haptotactic or chemotactic stimuli by spatially confining lamellipodia formation to the leading edge of the cell [319, 320, 321].

Mechanistically, adhesion dependent local phosphorylation and clustering of the α4 subunit restricts RAC and CDC42 activity and thus lamellipodia and filopodia formation to the leading edge. In contrast, at the lateral sites of the cell, α4 is not phosphorylated. Unphosphorylated α4 is directly bound by the adaptor molecule paxillin, resulting in inhibition of RAC activity [322, 320, 323]. In addition to its direct interaction with paxillin, α4 can form a ternary complex with paxillin and the regulator protein 14-3-3 ζ. This complex inhibits activation of CDC42, thus restricting CDC42 activity, like RAC1 activity, to the leading edge. Therefore, protrusion formation is inhibited at the lateral sites.

By transferring this mechanism of α4 mediated regulation of intrinsic polarity and directed migration in leukocytes to EC, the following model for explaining the vascular

mis-patterning in *tardbp-/-; tardbpl-/-* mutants emerges: In EC expressing more α4β1 integrin and more of its ECM ligand FN1, integrin α4 might be adhesion dependently phosphorylated also at the lateral sites or the rear of the cell. Ectopic phosphorylation of α4β1 integrin also at lateral sites of EC might lead to local RAC and CDC42 activity, resulting in formation of additional filopodia and lamellipodia. The direction of lamellipodia direct the migration of a cell [324]. Therefore, even if other growth directing stimuli are present and distributed normally, the overt input via α4β1 integrin signaling and subsequent lamellipodia formation at lateral sites ultimately defines an altered direction of migration. Thus, ectopic α4β1 integrin signaling might lead to decreased intrinsic polarity resulting in random, undirected migration. Alternatively, overt α4β1 integrin signaling at lateral sites of the cell might reduce the capability to integrate other migration directing cues adequately. Both mechanisms or their combination can explain the migration of TDP-43 deficient EC into tissue usually devoid of EC. This is phenotypically reflected by sprouting of EC from the DA (and the PCV) at ectopic positions, by lateral migration away from their normal path along somite boundaries, as well as by the reduced number of EC reaching the site of DLAV formation. Decreased intrinsic polarity might also explain lack of lumen formation in *tardbp-/-; tardbpl-/-* mutants since EC polarity is a prerequisite of vascular lumen formation [325, 326, 178]. Besides FN1, VCAM1 is a further ligand of α4β1 integrin. VCAM1 signaling in EC has been reported to promote dissociation of VE-cadherin mediated cellular contacts [197, 198]. Therefore, VCAM1 – α4β1 integrin signaling might contribute to the phenotype by reducing stability of EC – EC contacts.

Additionally, activation and/or avidity of α4β1 integrins might be additionally increased by CXCL12 [327], which is the top up-regulated hit in NGS of TDP-43 KD HUVEC. CXCL12 is a chemokine binding to its receptor CXCR4. Knockout of either gene is lethal in mice due to defects in vascularization of the gastrointestinal tract, in hematopoiesis, and neuronal migration [328, 329, 330]. CXCL12 function as a chemoattractant has been studied in detail during migration of primordial germ cells during embryonic development of mouse, *Drosophila*, and zebrafish [331]. CXCL12 also has been shown to guide angiogenesis during formation of the coronary vasculature and

fin regeneration in zebrafish via CXCR4 [332, 333]. Further, it has been described to be bound by FN, thereby inducing directed migration probably by re-localization of CXCR4 to the leading edge of migrating cells [334]. Since CXCR4 expression is not changed in TDP-43 KD HUVEC, a possible effect on angiogenesis is likely to be mediated independently of CXCR4. CXCL12 could be increasingly secreted by EC and then be bound and accumulated by the surrounding FN matrix. Increased CXCL12 presentation by FN could then additionally induce α4β1 integrin signaling.

A scheme illustrating this hypothetical mechanism to explain vascular mis-patterning in *tardbp-/-; tardbpl-/-* mutants is shown in Figure 4.1.

Rescue of the ectopic sprouting by KD of Fn1b, integrin α4, or Vcam1 can be explained with the same model: Reduction of Fn1b might lead to less adhesion dependent activation of integrin α4. Consequently, activation at lateral sites of migrating EC is reduced, therefore less lamellipodia perpendicular to the wild type direction of migration are formed and thus direction of migration along the somite boundaries maintained. In addition, relative signaling input by other guidance cues becomes stronger, also ensuring migration along somite boundaries. KD of integrin α4 might have the same consequence, being even more efficient because it is the subunit defining the specific integrin receptor (α4β1 integrin) of Fn1b for this phenotype. In contrast, FN1 also binds to other integrin receptors, provoking more off-site target effects thus allowing only for a mild KD without affecting further structures of the embryo. Reduction of Vcam1 levels is limited due to its requirement during gastrulation. However, at 24 hpf its KD leads to a measurable rescue of hypersprouting. This might be a result of increased strength of EC – EC contacts, thus limiting the migration of individual cells from the DA at random positions.

To further test the described model, endothelial α4β1 integrin localization and activation in TDP-43 deficient EC compared to control EC could be investigated. Due to lack of antibodies available for zebrafish, this experiment could be performed in HUVEC plated on FN coated culture dishes. Then, immunofluorescence stainings for total and phosphorylated (Ser988) α4 can be performed. Increased phosphorylated

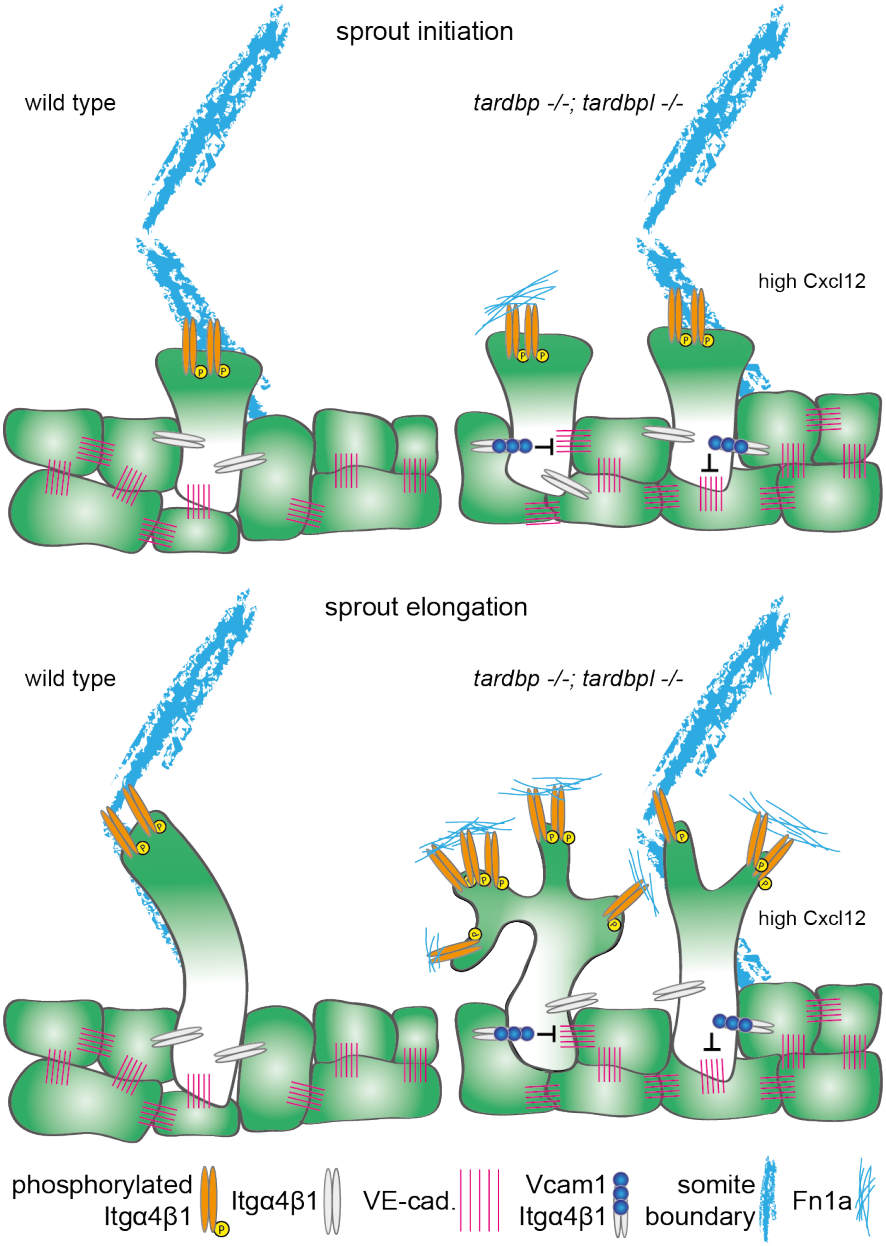

Figure 4.1: Scheme illustrating the hypothetical mechanism to explain vascular mis-patterning in *tardbp-/-; tardbpl-/-* mutants. For explanation see text.

α4 integrin at lateral sites or a change in integrin α4 localization would support the model. In addition, to quantify an increase in total RAC activity expected downstream of increased α4 phosphorylation, immunoblots to detect activated and total RAC in lysates of these cells could be performed and quantified. Moreover, human α4 integrin or phospho-mimicking α4 integrin encoding constructs could be overexpressed in wild type zebrafish to test whether increased α4 integrin expression or phosphorylated α4 integrin is sufficient to cause vascular mis-patterning. Furthermore, the role of CXCL12

could be investigated by conducting partial KD experiments in zebrafish similar to those performed with *fn1b*, *itgα4*, and *vcam1* MO.

A further phenotype of an integrin knockout has to be considered when discussing the vascular phenotype of *tardbp-/-; tardbpl-/-* mutants and the first results obtained from conditional endothelial knockout of TDP-43 in mice. Conditional endothelial knockout of *Itgβ1* in mice leads to similar vascular defects of the postnatal developing retina as knockout of TDP-43, albeit some differences exist [179]. Similar phenotypes are reduced radial outgrowth of the vasculature, increased vascular density at the angiogenic front, and increased number of filopodia at the front. However, the distal edge of the vascular plexus appears to be blunt upon *Itgβ1* KO, whereas it is not upon loss of TDP-43. Increased density at the angiogenic front in *Itgβ1* KO retinas is caused by hyperproliferation, which is not present in *tardbp-/-; tardbpl-/-* zebrafish and which remains to be determined in TDP-43 KO retinas. However, whereas loss of TDP-43 leads to hypersprouting of arterial and venous vessels, loss of integrin β1 only affects veins. Integrin β1 is furthermore required for maintenance of EC – EC contacts, which is not investigated for TDP-43 function in the retina yet. Notwithstanding ongoing experiments, one can thus already speculate about the question how endothelial loss of integrin β1 and its increased expression upon loss of TDP-43 can result in some similar phenotypes. The increase of integrin α4 is relatively larger than the one of integrin β1. This implies an increased proportion of integrin β1 to be part of α4β1 integrin and a net reduction of integrin β1 contributing to α5β1 integrin receptors. Integrin β1 has important functions during angiogenesis as part of α5β1 integrins. Therefore, loss of TDP-43 might cause a partial loss of α5β1 integrin function due to relative higher presence of α4β1 integrin receptors. However, whether and to which extend this is the case and whether the phenotypes of *Itgβ1* and *Tardbp* are indeed as similar as it appears at first glance remains to be determined. Moreover, if the *tardbp-/-; tardbpl-/-* mutant angiogenic phenotype would be a partial α5β1 integrin loss-of-function phenotype, KD of integrin α5 should worsen the phenotype. However, integrin α5 and integrin αv KD does not obviously alter the vascular mis-patterning in *tardbp-/-; tardbpl-/-* mutants.

4.7 Implications for TDP-43 proteinopathies

FN1, VCAM1, and integrin α4β1 are up-regulated in human EC upon loss of TDP-43. Furthermore, their increased expression is causative for increased random migration of TDP-43 deficient EC is zebrafish. Thus, the *in vivo* consequence of four mis-regulated genes in EC with TDP-43 loss-of-function has been identified. A loss-of-function disease mechanism in ALS and FTD is supported by first, analysis of previous loss-of-function animal models, second, the involvement of TDP-43 in regulation of hundreds of RNAs, and third, the nuclear clearance of TDP-43 in cells with TDP-43-positive inclusions in patients (see section 1.2.4.2). Thus, mis-regulation of these genes might also contribute to disease causing and/or modifying mechanisms. In the following, possible effects of dysregulated FN1 – integrin α4β1 interaction in human brain EC, neurons, and glial cells are discussed in the context of neurodegeneration.

4.7.1 Possible effects of dysregulated α4β1 integrin signaling in EC of ALS/FTD patients

To transfer the observations made in EC of zebrafish TDP-43 loss-of-function mutants to blood vessels of human ALS and FTD patients, patients would have to have TDP-43-positive inclusions in EC. Then, EC might have similar phenotypes as the TDP-43 deficient EC in fish and in human EC culture. Although the sprouting phenotype in the zebrafish mutants is developmental, EC in the human brain have to maintain polarity and cell – cell contacts for normal function, similar to EC during collective sprouting in the developing vasculature. If cellular contacts are disrupted, BBB breakdown and vascular leakage followed by neuronal damage are the consequences. Therefore, loss of TDP-43 function in EC of patients could contribute to pathology by damaging the BBB. However, no TDP-43 inclusions in EC have been reported so far making this hypothesis unlikely.

Alternatively, loss of TDP-43 function in other cell types with known TDP-43 pathology could lead to secretion of cytokines and chemokines non-cell autonomously activating EC. Consequently, integrin expression and affinity of EC might be altered. In this

thesis CXCL12, among other chemokines, was found to be drastically up-regulated in TDP-43 KD EC. CXCL12, also known as stromal cell-derived factor 1 (Sdf1), is a chemokine known to increase affinity and/or avidity of integrin α4β1 [327]. Importantly, conditional neuronal TDP-43 knockout mice have transient defects of the BSCB. EC are described to form protrusions that extend into the lumen of vessels at an early symptomatic stage [291]. The ectopic formation of protrusions is also one of the main characteristics of TDP-43 deficient EC due to ectopic integrin α4β1 signaling. One could therefore hypothesize that neurons or activated microglia in the patient's brain secrete chemokines and cytokines, for example CXCL12, that lead to ectopic activation of integrins in EC causing EC to loose their polarity and cell-cell contacts ultimately resulting in BBB/BSCB damage. In addition, mutant SOD1 expressing mouse models support an involvement of impaired BSCB/BBB in ALS, since these mice also show impaired barrier function [284, 285, 286, 287, 288, 289]. Moreover, in the neurodegenerative disease multiple sclerosis, increased immune response leads to endothelial abnormalities and BBB/BSCB damage that has been suggested to contribute to disease progression [335, 271], supporting the possibility of such a mechanism. To block epithelial transmigration of leukocytes into the brain of multiple sclerosis patients, an integrin α4 blocking antibody, natalizumab, is used as second-line treatment [336]. Besides harming the BBB/BSCB, another severe consequence of EC with lost polarity could be the collapse of the lumen of the capillaries in the brain. A recent study of capillaries of the BSCB in sALS patients showed that there is indeed a significant increase in the number of capillaries with a small diameter in sALS patients compared to controls [337]. A reduction in lumen diameter could result in defective neuro-vascular uncoupling and hypoperfusion. Both have the potential to cause neuronal loss and are observed in ALS and other neurodegenerative diseases [278, 7] (see also section 1.4).

4.7.2 Possible effects of dysregulated FN - α4β1 integrin signaling in neurons or glial cells of ALS/FTD patients

FN1 – α4β1 integrin interactions are required for migration of neural crest derived cells and for the development of the peripheral nervous system [259]. Different splice variants

of FN1 are expressed in development and adult tissue, with splice variants containing the variable region for α4β1 integrin binding being expressed in embryonic stages. However, injury leads to re-expression of embryonic FN1 splice variants binding to integrin α4 also in the adult and promotes regeneration of peripheral sensory neurons [261]. In dorsal root ganglion neuron cell bodies and growth cones, α4β1 integrin expression is increased during sciatic nerve regeneration. Interaction of α4β1 integrin with the alternatively spliced FN1 variants harboring the binding site for α4 integrins enhances neurite outgrowth [262]. Importantly, the α4 cytosolic tail interacts also in dorsal root ganglion neurons with paxillin, promoting neurite outgrowth. In PC12 cells (a cell culture model for neural crest cells) α4 was, however, not found to be phosphorylated [263]. Thus, α4 integrin not only regulates migration of cells, but also neurite outgrowth by overlapping but not identical mechanisms. Although reported for FN1 [264], α4 integrin is usually not expressed by neurons of the CNS upon injury [338, 262]. However, if ectopically expressed by neurons in the CNS of ALS/FTD patients upon loss of TDP-43 function, neuronal polarity might be lost causing functional deficits. In TDP-43 KD mouse brain, the α4β1 integrin ligand *Vcam1* was found to be up-regulated. This finding indicates that VCAM1 – α4β1 integrin signaling could be indeed up-regulated upon TDP-43 KD also in cell types other than EC and thus contribute to disease progression [92].

Similarly, if loss of TDP-43 in glial cells leads to impaired intrinsic polarity and directional migration defects, essential neuronal survival supporting functions could be affected. Moreover, TDP-43 KD in HUVEC results in up-regulation of genes that cluster functionally in the categories “cytokine” and “chemokine”. In ALS patients, microglia and astrocyte activation as well as chemokine secretion are increased and have been shown in an SOD1 mouse model to affect disease progression (reviewed in [339]). Therefore, loss of TDP-43 function in microglia and astrocytes could lead to a change in gene expression leading to their activation and secretion of chemokines. Alteration in microglia and astroglia activation and function could accelerate disease progression by affecting neuronal survival directly or by affecting the integrity of the BBB and neurovascular coupling, eventually leading to neuronal loss.

4.8 Conclusion and outlook

TDP-43 regulates angiogenic sprouting *in vivo* in the developing zebrafish and *in vitro* in human EC in a cell autonomous manner. The direct or indirect mediators of this function are FN1, integrin α4β1, and VCAM1. In case of loss of endothelial TDP-43 function, the expression of these proteins is increased, resulting in decreased intrinsic polarity, extension of ectopic lamellipodia, and undirected migration. As a further model system, the vascular network of the mouse retina confirms the defects resulting from endothelial specific TDP-43 deletion. Thus, a novel, conserved *in vivo* function of TDP-43 in EC as well as the underlying mechanism is revealed by this study. In addition, a so far unknown impact of increased integrin α4 expression on angiogenesis is defined. To deepen the mechanistic understanding, the experiments discussed in section 4.6 could be conducted. To find out whether TDP-43 binds directly to *FN1*, *ITGA4*, *ITGB1*, and *VCAM1* mRNA, an iCLIP experiment is currently under way (in collaboration with M. Modic and Dr. M. Decker, Helmholtz Zentrum Munich). To examine whether dysregulated FN1 or VCAM1 – α4β1 integrin signaling is involved in the disease mechanism of ALS/FTLD-TDP, the following questions need to be addressed: First, is EC function similarly affected in ALS/FTD patients? Second, are the identified TDP-43 targets also up-regulated or differently localized upon TDP-43 KD in cell types with known TDP-43 pathology? Third, do ALS/FTLD-TDP patients have increased expression of the identified TDP-43 targets in cells with TDP-43 pathology? Preliminary results from a collaboration with Dr. M. Ward suggest that FTD patients with a mutation in *GRN* have less complex perfused vascular networks in the retina (Dr. M. Ward, personal communication). This data indicate impaired EC function in patients with TDP-43 pathology. The second question is currently addressed in collaboration with Dr. B. Schwenk and Dr. S. Tahirovic (both DZNE Munich). They examine integrin α4 expression levels and polarity of TDP-43 KD neurons. Further, we obtained RNA sequencing data from spinal cord tissue of sALS patients showing significantly increased expression of *FN1* and *ITGB1*. Moreover, increased expression levels of *VCAM1* correlate with earlier disease onset (Dr. S. Lewandowski, personal communication). In collaboration with Prof. Dr. T. Arzberger (Zentrum für

Neuropathologie und Prionenforschung Munich) and L. Hasenkamp (DZNE Munich), immunohistochemical stainings in ALS-TDP patient tissue are currently underway to further analyze expression of FN1, integrin α4β1, and VCAM1. Thus, these experiments will reveal a potential involvement of integrin α4β1 and its ligands in ALS and FTD disease pathomechanisms. This finding may provide the basis for the far reaching goal of developing a drug for these devastating diseases. Importantly, a clinically approved drug targeting integrin α4, natalizumab, would be available for treatment.

References

[1] Smita Saxena and Pico Caroni. Selective neuronal vulnerability in neurodegenerative diseases: from stressor thresholds to degeneration. *Neuron*, 71(1):35–48, Jul 2011.

[2] Adriano Aguzzi and Christian Haass. Games played by rogue proteins in prion disorders and alzheimer's disease. *Science*, 302(5646):814–8, Oct 2003.

[3] Christian Haass and Dennis J Selkoe. Soluble protein oligomers in neurodegeneration: lessons from the alzheimer's amyloid beta-peptide. *Nat Rev Mol Cell Biol*, 8(2):101–12, Feb 2007.

[4] Vijay K Ramanan and Andrew J Saykin. Pathways to neurodegeneration: mechanistic insights from gwas in alzheimer's disease, parkinson's disease, and related disorders. *Am J Neurodegener Dis*, 2(3):145–75, 2013.

[5] Sonia Gandhi and Nicholas W Wood. Genome-wide association studies: the key to unlocking neurodegeneration? *Nat Neurosci*, 13(7):789–94, Jul 2010.

[6] Séverine Boillée, Christine Vande Velde, and Don W Cleveland. Als: a disease of motor neurons and their nonneuronal neighbors. *Neuron*, 52(1):39–59, Oct 2006.

[7] Berislav V Zlokovic. Neurovascular pathways to neurodegeneration in Alzheimer's disease and other disorders. *Nature reviews Neuroscience*, 12(12):723–738, December 2011.

[8] Nicholas J Maragakis and Jeffrey D Rothstein. Mechanisms of disease: astrocytes in neurodegenerative disease. *Nat Clin Pract Neurol*, 2(12):679–89, Dec 2006.

[9] Serena Zacchigna, Diether Lambrechts, and Peter Carmeliet. Neurovascular signalling defects in neurodegeneration. *Nat Rev Neurosci*, 9(3):169–81, Mar 2008.

[10] Martin R Turner, Orla Hardiman, Michael Benatar, Benjamin R Brooks, Adriano Chio, Mamede de Carvalho, Paul G Ince, Cindy Lin, Robert G Miller, Hiroshi Mitsumoto, Garth Nicholson, John Ravits, Pamela J Shaw, Michael Swash, Kevin Talbot, Bryan J Traynor, Leonard H Van den Berg, Jan H Veldink, Steve Vucic, and Matthew C Kiernan. Controversies and priorities in amyotrophic lateral sclerosis. *Lancet Neurol*, 12(3):310–22, Mar 2013.

[11] Rosa Rademakers, Manuela Neumann, and Ian R Mackenzie. Advances in understanding the molecular basis of frontotemporal dementia. *Nature Reviews Neurology*, pages 1–12, June 2012.

[12] Tim Van Langenhove, Julie van der Zee, and Christine Van Broeckhoven. The molecular basis of the frontotemporal lobar degeneration-amyotrophic lateral sclerosis spectrum. *Ann Med*, 44(8):817–28, Dec 2012.

[13] Murray Grossman. Frontotemporal dementia: a review. *J Int Neuropsychol Soc*, 8(4):566–83, May 2002.

[14] B R Brooks, R G Miller, M Swash, T L Munsat, and World Federation of Neurology Research Group on Motor Neuron Diseases. El escorial revisited: revised criteria for the diagnosis of amyotrophic lateral sclerosis. *Amyotroph Lateral Scler Other Motor Neuron Disord*, 1(5):293–9, Dec 2000.

[15] Matthew C Kiernan, Steve Vucic, Benjamin C Cheah, Martin R Turner, Andrew Eisen, Orla Hardiman, James R Burrell, and Margaret C Zoing. Amyotrophic lateral sclerosis. *Lancet*, 377(9769):942–55, Mar 2011.

[16] Ian RA Mackenzie, Rosa Rademakers, and Manuela Neumann. Tdp-43 and fus in amyotrophic lateral sclerosis and frontotemporal dementia. *Lancet Neurol*, 9(10):995–1007, Oct 2010.

[17] James R Burrell, Matthew C Kiernan, Steve Vucic, and John R Hodges. Motor neuron dysfunction in frontotemporal dementia. *Brain*, 134(Pt 9):2582–94, Sep 2011.

[18] G M Ringholz, S H Appel, M Bradshaw, N A Cooke, D M Mosnik, and P E Schulz. Prevalence and patterns of cognitive impairment in sporadic als. *Neurology*, 65(4):586–90, Aug 2005.

[19] Ian R A Mackenzie, Manuela Neumann, Eileen H Bigio, Nigel J Cairns, Irina Alafuzoff, Jillian Kril, Gabor G Kovacs, Bernardino Ghetti, Glenda Halliday, Ida E Holm, Paul G Ince, Wouter Kamphorst, Tamas Revesz, Annemieke J M Rozemuller, Samir Kumar-Singh, Haruhiko Akiyama, Atik Baborie, Salvatore Spina, Dennis W Dickson, John Q Trojanowski, and David M A Mann. Nomenclature and nosology for neuropathologic subtypes of frontotemporal lobar degeneration: an update. *Acta Neuropathol*, 119(1):1–4, Jan 2010.

[20] Jennifer M Murphy, Roland G Henry, Susan Langmore, Joel H Kramer, Bruce L Miller, and Catherine Lomen-Hoerth. Continuum of frontal lobe impairment in amyotrophic lateral sclerosis. *Arch Neurol*, 64(4):530–4, Apr 2007.

[21] Catherine Lomen-Hoerth, Thomas Anderson, and Bruce Miller. The overlap of amyotrophic lateral sclerosis and frontotemporal dementia. *Neurology*, 59(7):1077–9, Oct 2002.

[22] Ian R A Mackenzie and Howard H Feldman. Ubiquitin immunohistochemistry suggests classic motor neuron disease, motor neuron disease with dementia, and frontotemporal dementia of the motor neuron disease type represent a clinicopathologic spectrum. *J Neuropathol Exp Neurol*, 64(8):730–9, Aug 2005.

[23] Manuela Neumann, Markus Tolnay, and Ian R A Mackenzie. The molecular basis of frontotemporal dementia. *Expert Rev Mol Med*, 11:e23, 2009.

[24] Manuela Neumann, Deepak M Sampathu, Linda K Kwong, Adam C Truax, Matthew C Micsenyi, Thomas T Chou, Jennifer Bruce, Theresa Schuck, Murray Grossman, Christopher M Clark, Leo F McCluskey, Bruce L Miller, Eliezer Masliah, Ian R Mackenzie, Howard Feldman, Wolfgang Feiden, Hans A Kretzschmar, John Q Trojanowski, and Virginia M-Y Lee. Ubiquitinated tdp-43 in frontotemporal lobar degeneration and amyotrophic lateral sclerosis. *Science*, 314(5796):130–3, Oct 2006.

[25] Tetsuaki Arai, Masato Hasegawa, Haruhiko Akiyama, Kenji Ikeda, Takashi Nonaka, Hiroshi Mori, David Mann, Kuniaki Tsuchiya, Mari Yoshida, Yoshio Hashizume, and Tatsuro Oda. Tdp-43 is a component of ubiquitin-positive tau-negative inclusions in frontotemporal lobar degeneration and amyotrophic lateral sclerosis. *Biochem Biophys Res Commun*, 351(3):602–11, Dec 2006.

[26] Shuo-Chien Ling, Magdalini Polymenidou, and Don W Cleveland. Converging Mechanisms in ALS and FTD: Disrupted RNA and Protein Homeostasis. *Neuron*, 79(3):416–438, August 2013.

[27] Ian R A Mackenzie, Eileen H Bigio, Paul G Ince, Felix Geser, Manuela Neumann, Nigel J Cairns, Linda K Kwong, Mark S Forman, John Ravits, Heather Stewart, Andrew Eisen, Leo McClusky, Hans A Kretzschmar, Camelia M Monoranu, J Robin Highley, Janine Kirby, Teepu Siddique, Pamela J Shaw, Virginia M-Y Lee, and John Q Trojanowski. Pathological tdp-43 distinguishes sporadic amyotrophic lateral sclerosis from amyotrophic lateral sclerosis with sod1 mutations. *Ann Neurol*, 61(5):427–34, May 2007.

[28] C Lagier-Tourenne, M Polymenidou, and D. W Cleveland. Tdp-43 and fus/tls: emerging roles in rna processing and neurodegeneration. *Hum Mol Genet*, 19(R1):R46–R64, Apr 2010.

[29] Maria Teresa Giordana, Marco Piccinini, Silvia Grifoni, Giovanni De Marco, Marco Vercellino, Michela Magistrello, Alessia Pellerino, Barbara Buccinnà, Elisa Lupino, and Maria Teresa Rinaudo. Tdp-43 redistribution is an early event in sporadic amyotrophic lateral sclerosis. *Brain Pathol*, 20(2):351–60, Mar 2010.

[30] Andrea C Wilson, Brittany N Dugger, Dennis W Dickson, and Deng-Shun Wang. Tdp-43 in aging and alzheimer's disease - a review. *Int J Clin Exp Pathol*, 4(2):147–55, Jan 2011.

[31] Mohammad Salajegheh, Jack L Pinkus, J Paul Taylor, Anthony A Amato, Remedios Nazareno, Robert H Baloh, and Steven A Greenberg. Sarcoplasmic redistribution of nuclear tdp-43 in inclusion body myositis. *Muscle Nerve*, 40(1):19–31, Jul 2009.

[32] Montse Olivé, Anna Janué, Dolores Moreno, Josep Gámez, Benjamín Torrejón-Escribano, and Isidre Ferrer. Tar dna-binding protein 43 accumulation in protein aggregate myopathies. *J Neuropathol Exp Neurol*, 68(3):262–73, Mar 2009.

[33] Benno Küsters, Bas J A van Hoeve, Helenius Jurgen Schelhaas, Henk Ter Laak, Baziel G M van Engelen, and Martin Lammens. Tdp-43 accumulation is common in myopathies with rimmed vacuoles. *Acta Neuropathol*, 117(2):209–11, Feb 2009.

[34] M Suzuki, H Mikami, T Watanabe, T Yamano, T Yamazaki, M Nomura, K Yasui, H Ishikawa, and S Ono. Increased expression of tdp-43 in the skin of amyotrophic lateral sclerosis. *Acta Neurol Scand*, 122(5):367–72, Nov 2010.

[35] D R Rosen, T Siddique, D Patterson, D A Figlewicz, P Sapp, A Hentati, D Donaldson, J Goto, J P O'Regan, and H X Deng. Mutations in cu/zn superoxide dismutase gene are associated with familial amyotrophic lateral sclerosis. *Nature*, 362(6415):59–62, Mar 1993.

[36] Hazel Urwin, Keith A Josephs, Jonathan D Rohrer, Ian R Mackenzie, Manuela Neumann, Astrid Authier, Harro Seelaar, John C Van Swieten, Jeremy M Brown, Peter Johannsen, Jorgen E Nielsen, Ida E Holm, FReJA Consortium, Dennis W Dickson, Rosa Rademakers, Neill R Graff-Radford, Joseph E Parisi, Ronald C Petersen, Kimmo J Hatanpaa, Charles L White, Myron F Weiner, Felix Geser, Vivianna M Van Deerlin, John Q Trojanowski, Bruce L Miller, William W Seeley, Julie van der Zee, Samir Kumar-Singh, Sebastiaan Engelborghs, Peter P De Deyn, Christine Van Broeckhoven, Eileen H Bigio, Han-Xiang Deng, Glenda M Halliday, Jillian J Kril, David G Munoz, David M Mann, Stuart M Pickering-Brown, Valerie Doodeman, Gary Adamson, Shabnam Ghazi-Noori, Elizabeth M C Fisher, Janice L Holton, Tamas Revesz, Martin N Rossor, John Collinge, Simon Mead, and Adrian M Isaacs. Fus pathology defines the majority of tau- and tdp-43-negative frontotemporal lobar degeneration. *Acta Neuropathol*, 120(1):33–41, Jul 2010.

[37] Serena Lattante, Sorana Ciura, Guy A Rouleau, and Edor Kabashi. Defining the genetic connection linking amyotrophic lateral sclerosis (als) with frontotemporal dementia (ftd). *Trends Genet*, 31(5):263–273, May 2015.

[38] Wim Robberecht and Thomas Philips. The changing scene of amyotrophic lateral sclerosis. *Nature reviews Neuroscience*, 14(4):248–264, March 2013.

[39] Alan E Renton, Adriano Chiò, and Bryan J Traynor. State of play in amyotrophic lateral sclerosis genetics. *Nature Neuroscience*, 17(1):17–23, December 2013.

[40] Chun-Feng Tan, Hiroto Eguchi, Asako Tagawa, Osamu Onodera, Takuya Iwasaki, Akira Tsujino, Masatoyo Nishizawa, Akiyoshi Kakita, and Hitoshi Takahashi. Tdp-43 immunoreactivity in neuronal inclusions in familial amyotrophic lateral sclerosis with or without sod1 gene mutation. *Acta Neuropathol*, 113(5):535–42, May 2007.

[41] Shoichi Sasaki. Autophagy in spinal cord motor neurons in sporadic amyotrophic lateral sclerosis. *J Neuropathol Exp Neurol*, 70(5):349–59, May 2011.

[42] Owen M Peters, Mehdi Ghasemi, and Robert H Brown, Jr. Emerging mechanisms of molecular pathology in als. *J Clin Invest*, 125(5):1767–79, May 2015.

[43] Hao Deng, Kai Gao, and Joseph Jankovic. The role of fus gene variants in neurodegenerative diseases. *Nat Rev Neurol*, 10(6):337–48, Jun 2014.

[44] Manuela Neumann, Eva Bentmann, Dorothee Dormann, Ali Jawaid, Mariely DeJesus-Hernandez, Olaf Ansorge, Sigrun Roeber, Hans A Kretzschmar, David G Munoz, Hirofumi Kusaka, Osamu Yokota, Lee-Cyn Ang, Juan Bilbao, Rosa Rademakers, Christian Haass, and Ian R A Mackenzie. Fet proteins taf15 and ews are selective markers that distinguish ftld with fus pathology from amyotrophic lateral sclerosis with fus mutations. *Brain*, 134(Pt 9):2595–609, Sep 2011.

[45] Dorothee Dormann, Ramona Rodde, Dieter Edbauer, Eva Bentmann, Ingeborg Fischer, Alexander Hruscha, Manuel E Than, Ian R A Mackenzie, Anja Capell, Bettina Schmid, Manuela Neumann, and Christian Haass. Als-associated fused in sarcoma (fus) mutations disrupt transportin-mediated nuclear import. *EMBO J*, 29(16):2841–57, Aug 2010.

[46] Dorothee Dormann and Christian Haass. Fused in sarcoma (fus): an oncogene goes awry in neurodegeneration. *Mol Cell Neurosci*, 56:475–86, Sep 2013.

[47] Daryl A Bosco, Nathan Lemay, Hae Kyung Ko, Hongru Zhou, Chris Burke, Thomas J Kwiatkowski, Jr, Peter Sapp, Diane McKenna-Yasek, Robert H Brown, Jr, and Lawrence J Hayward. Mutant fus proteins that cause amyotrophic lateral sclerosis incorporate into stress granules. *Hum Mol Genet*, 19(21):4160–75, Nov 2010.

[48] Paul Anderson and Nancy Kedersha. Stress granules: the Tao of RNA triage. *Trends in biochemical sciences*, 33(3):141–150, March 2008.

[49] Dorothee Dormann and Christian Haass. Tdp-43 and fus: a nuclear affair. *Trends Neurosci*, 34(7):339–48, Jul 2011.

[50] Faisal Fecto, Jianhua Yan, S Pavan Vemula, Erdong Liu, Yi Yang, Wenjie Chen, Jian Guo Zheng, Yong Shi, Nailah Siddique, Hasan Arrat, Sandra Donkervoort, Senda Ajroud-Driss, Robert L Sufit, Scott L Heller, Han-Xiang Deng, and Teepu Siddique. Sqstm1 mutations in familial and sporadic amyotrophic lateral sclerosis. *Arch Neurol*, 68(11):1440–6, Nov 2011.

[51] Julie van der Zee, Tim Van Langenhove, Gabor G Kovacs, Lubina Dillen, William Deschamps, Sebastiaan Engelborghs, Radoslav Matěj, Mathieu Vandenbulcke, Anne Sieben, Bart Dermaut, Katrien Smets, Philip Van Damme, Céline Merlin, Annelies Laureys, Marleen Van Den Broeck, Maria Mattheijssens, Karin Peeters, Luisa Benussi, Giuliano Binetti, Roberta Ghidoni, Barbara Borroni, Alessandro Padovani, Silvana Archetti, Pau Pastor, Cristina Razquin, Sara Ortega-Cubero, Isabel Hernández, Mercè Boada, Agustín Ruiz, Alexandre de Mendonça, Gabriel Miltenberger-Miltényi, Frederico Simões do Couto, Sandro Sorbi, Benedetta Nacmias, Silvia Bagnoli, Caroline Graff, Huei-Hsin Chiang, Håkan Thonberg, Robert Perneczky, Janine Diehl-Schmid, Panagiotis Alexopoulos, Giovanni B Frisoni, Christian Bonvicini, Matthis Synofzik, Walter Maetzler, Jennifer Müller vom Hagen, Ludger Schöls, Tobias B Haack, Tim M Strom, Holger Prokisch, Oriol Dols-Icardo, Jordi Clarimón, Alberto Lleó, Isabel

Santana, Maria Rosário Almeida, Beatriz Santiago, Michael T Heneka, Frank Jessen, Alfredo Ramirez, Raquel Sanchez-Valle, Albert Llado, Ellen Gelpi, Stayko Sarafov, Ivailo Tournev, Albena Jordanova, Eva Parobkova, Gian Maria Fabrizi, Silvia Testi, Eric Salmon, Thomas Ströbel, Patrick Santens, Wim Robberecht, Peter De Jonghe, Jean-Jacques Martin, Patrick Cras, Rik Vandenberghe, Peter Paul De Deyn, Marc Cruts, Kristel Sleegers, and Christine Van Broeckhoven. Rare mutations in sqstm1 modify susceptibility to frontotemporal lobar degeneration. *Acta Neuropathol*, 128(3):397–410, Sep 2014.

[52] Han-Xiang Deng, Wenjie Chen, Seong-Tshool Hong, Kym M Boycott, George H Gorrie, Nailah Siddique, Yi Yang, Faisal Fecto, Yong Shi, Hong Zhai, Hujun Jiang, Makito Hirano, Evadnie Rampersaud, Gerard H Jansen, Sandra Donkervoort, Eileen H Bigio, Benjamin R Brooks, Kaouther Ajroud, Robert L Sufit, Jonathan L Haines, Enrico Mugnaini, Margaret A Pericak-Vance, and Teepu Siddique. Mutations in ubqln2 cause dominant x-linked juvenile and adult-onset als and als/dementia. *Nature*, 477(7363):211–5, Sep 2011.

[53] Janel O Johnson, Jessica Mandrioli, Michael Benatar, Yevgeniya Abramzon, Vivianna M Van Deerlin, John Q Trojanowski, J Raphael Gibbs, Maura Brunetti, Susan Gronka, Joanne Wuu, Jinhui Ding, Leo McCluskey, Maria Martinez-Lage, Dana Falcone, Dena G Hernandez, Sampath Arepalli, Sean Chong, Jennifer C Schymick, Jeffrey Rothstein, Francesco Landi, Yong-Dong Wang, Andrea Calvo, Gabriele Mora, Mario Sabatelli, Maria Rosaria Monsurrò, Stefania Battistini, Fabrizio Salvi, Rossella Spataro, Patrizia Sola, Giuseppe Borghero, ITALSGEN Consortium, Giuliana Galassi, Sonja W Scholz, J Paul Taylor, Gabriella Restagno, Adriano Chiò, and Bryan J Traynor. Exome sequencing reveals vcp mutations as a cause of familial als. *Neuron*, 68(5):857–64, Dec 2010.

[54] Han Seok Ko, Takashi Uehara, Kazuhiro Tsuruma, and Yasuyuki Nomura. Ubiquilin interacts with ubiquitylated proteins and proteasome through its ubiquitin-associated and ubiquitin-like domains. *FEBS Lett*, 566(1-3):110–4, May 2004.

[55] Hemmo Meyer, Monika Bug, and Sebastian Bremer. Emerging functions of the vcp/p97 aaa-atpase in the ubiquitin system. *Nat Cell Biol*, 14(2):117–23, Feb 2012.

[56] Giles D J Watts, Jill Wymer, Margaret J Kovach, Sarju G Mehta, Steven Mumm, Daniel Darvish, Alan Pestronk, Michael P Whyte, and Virginia E Kimonis. Inclusion body myopathy associated with paget disease of bone and frontotemporal dementia is caused by mutant valosin-containing protein. *Nat Genet*, 36(4):377–81, Apr 2004.

[57] Zhiheng He, Colin H P Ong, Jaroslava Halper, and Andrew Bateman. Progranulin is a mediator of the wound response. *Nat Med*, 9(2):225–9, Feb 2003.

[58] A Bateman, D Belcourt, H Bennett, C Lazure, and S Solomon. Granulins, a novel class of peptide from leukocytes. *Biochem Biophys Res Commun*, 173(3):1161–8, Dec 1990.

[59] T Zanocco-Marani, A Bateman, G Romano, B Valentinis, Z H He, and R Baserga. Biological activities and signaling pathways of the granulin/epithelin precursor. *Cancer Res*, 59(20):5331–40, Oct 1999.

[60] Marc Cruts, Samir Kumar-Singh, and Christine Van Broeckhoven. Progranulin mutations in ubiquitin-positive frontotemporal dementia linked to chromosome 17q21. *Curr Alzheimer Res*, 3(5):485–91, Dec 2006.

[61] Matt Baker, Ian R Mackenzie, Stuart M Pickering-Brown, Jennifer Gass, Rosa Rademakers, Caroline Lindholm, Julie Snowden, Jennifer Adamson, A Dessa Sadovnick, Sara Rollinson, Ashley Cannon, Emily Dwosh, David Neary, Stacey Melquist, Anna Richardson, Dennis Dickson, Zdenek Berger, Jason Eriksen, Todd Robinson, Cynthia Zehr, Chad A Dickey, Richard Crook, Eileen McGowan, David Mann, Bradley Boeve, Howard Feldman, and Mike Hutton. Mutations in progranulin cause tau-negative frontotemporal dementia linked to chromosome 17. *Nature*, 442(7105):916–9, Aug 2006.

[62] Sunita S Shankaran, Anja Capell, Alexander T Hruscha, Katrin Fellerer, Manuela Neumann, Bettina Schmid, and Christian Haass. Missense mutations in the progranulin gene linked to frontotemporal lobar degeneration with ubiquitin-immunoreactive inclusions reduce progranulin production and secretion. *J Biol Chem*, 283(3):1744–53, Jan 2008.

[63] Katherine R Smith, John Damiano, Silvana Franceschetti, Stirling Carpenter, Laura Canafoglia, Michela Morbin, Giacomina Rossi, Davide Pareyson, Sara E Mole, John F Staropoli, Katherine B Sims, Jada Lewis, Wen-Lang Lin, Dennis W Dickson, Hans-Henrik Dahl, Melanie Bahlo, and Samuel F Berkovic. Strikingly different clinicopathological phenotypes determined by progranulin-mutation dosage. *Am J Hum Genet*, 90(6):1102–7, Jun 2012.

[64] Julia K Götzl, Kohji Mori, Markus Damme, Katrin Fellerer, Sabina Tahirovic, Gernot Kleinberger, Jonathan Janssens, Julie van der Zee, Christina M Lang, Elisabeth Kremmer, Jean-Jacques Martin, Sebastiaan Engelborghs, Hans A Kretzschmar, Thomas Arzberger, Christine Van Broeckhoven, Christian Haass, and Anja Capell. Common pathobiochemical hallmarks of progranulin-associated frontotemporal lobar degeneration and neuronal ceroid lipofuscinosis. *Acta Neuropathol*, 127(6):845–60, Jun 2014.

[65] Alan E Renton, Elisa Majounie, Adrian Waite, Javier Simón-Sánchez, Sara Rollinson, J Raphael Gibbs, Jennifer C Schymick, Hannu Laaksovirta, John C van Swieten, Liisa Myllykangas, Hannu Kalimo, Anders Paetau, Yevgeniya Abramzon, Anne M Remes, Alice Kaganovich, Sonja W Scholz, Jamie Duckworth, Jinhui Ding, Daniel W Harmer, Dena G Hernandez, Janel O Johnson, Kin Mok, Mina Ryten, Danyah Trabzuni, Rita J Guerreiro, Richard W Orrell, James Neal, Alex Murray, Justin Pearson, Iris E Jansen, David Sondervan, Harro Seelaar, Derek Blake, Kate Young, Nicola Halliwell, Janis Bennion Callister, Greg Toulson, Anna Richardson, Alex Gerhard, Julie Snowden, David Mann, David Neary, Michael A Nalls, Terhi Peuralinna, Lilja Jansson, Veli-Matti Isoviita, Anna-Lotta Kaivorinne, Maarit Hölttä-Vuori, Elina Ikonen, Raimo Sulkava, Michael Benatar, Joanne Wuu, Adriano Chiò, Gabriella Restagno, Giuseppe Borghero, Mario Sabatelli, ITALSGEN Consortium, David Heckerman, Ekaterina Rogaeva, Lorne Zinman, Jeffrey D Rothstein, Michael Sendtner, Carsten Drepper, Evan E Eichler, Can Alkan, Ziedulla Abdullaev, Svetlana D Pack, Amalia Dutra, Evgenia Pak, John Hardy, Andrew Singleton, Nigel M Williams, Peter Heutink, Stuart Pickering-Brown, Huw R Morris, Pentti J Tienari, and Bryan J Traynor. A hexanucleotide repeat expansion in c9orf72 is the cause of chromosome 9p21-linked als-ftd. *Neuron*, 72(2):257–68, Oct 2011.

[66] Mariely DeJesus-Hernandez, Ian R Mackenzie, Bradley F Boeve, Adam L Boxer, Matt Baker, Nicola J Rutherford, Alexandra M Nicholson, NiCole A Finch, Heather Flynn, Jennifer Adamson, Naomi Kouri, Aleksandra Wojtas, Pheth Sengdy, Ging-Yuek R Hsiung, Anna Karydas, William W Seeley, Keith A Josephs, Giovanni Coppola, Daniel H Geschwind, Zbigniew K Wszolek, Howard Feldman, David S Knopman, Ronald C Petersen, Bruce L Miller, Dennis W Dickson, Kevin B Boylan, Neill R Graff-Radford, and Rosa Rademakers. Expanded ggggcc hexanucleotide repeat in noncoding region of c9orf72 causes chromosome 9p-linked ftd and als. *Neuron*, 72(2):245–56, Oct 2011.

[67] Jon Beck, Mark Poulter, Davina Hensman, Jonathan D Rohrer, Colin J Mahoney, Gary Adamson, Tracy Campbell, James Uphill, Aaron Borg, Pietro Fratta, Richard W Orrell, Andrea Malaspina, James Rowe, Jeremy Brown, John Hodges, Katie Sidle, James M Polke, Henry Houlden, Jonathan M Schott, Nick C Fox, Martin N Rossor, Sarah J Tabrizi, Adrian M Isaacs, John Hardy, Jason D Warren, John Collinge, and Simon Mead. Large c9orf72 hexanucleotide repeat expansions are seen in multiple neurodegenerative syndromes and are more frequent than expected in the uk population. *Am J Hum Genet*, 92(3):345–53, Mar 2013.

[68] Ilse Gijselinck, Tim Van Langenhove, Julie van der Zee, Kristel Sleegers, Stéphanie Philtjens, Gernot Kleinberger, Jonathan Janssens, Karolien Bettens, Caroline Van Cauwenberghe, Sandra Pereson, Sebastiaan Engelborghs,

Anne Sieben, Peter De Jonghe, Rik Vandenberghe, Patrick Santens, Jan De Bleecker, Githa Maes, Veerle Bäumer, Lubina Dillen, Geert Joris, Ivy Cuijt, Ellen Corsmit, Ellen Elinck, Jasper Van Dongen, Steven Vermeulen, Marleen Van den Broeck, Carolien Vaerenberg, Maria Mattheijssens, Karin Peeters, Wim Robberecht, Patrick Cras, Jean-Jacques Martin, Peter P De Deyn, Marc Cruts, and Christine Van Broeckhoven. A c9orf72 promoter repeat expansion in a flanders-belgian cohort with disorders of the frontotemporal lobar degeneration-amyotrophic lateral sclerosis spectrum: a gene identification study. *Lancet Neurol*, 11(1):54–65, Jan 2012.

[69] Youn-Bok Lee, Han-Jou Chen, João N Peres, Jorge Gomez-Deza, Jan Attig, Maja Stalekar, Claire Troakes, Agnes L Nishimura, Emma L Scotter, Caroline Vance, Yoshitsugu Adachi, Valentina Sardone, Jack W Miller, Bradley N Smith, Jean-Marc Gallo, Jernej Ule, Frank Hirth, Boris Rogelj, Corinne Houart, and Christopher E Shaw. Hexanucleotide repeats in als/ftd form length-dependent rna foci, sequester rna binding proteins, and are neurotoxic. *Cell Rep*, 5(5):1178–86, Dec 2013.

[70] Peter E A Ash, Kevin F Bieniek, Tania F Gendron, Thomas Caulfield, Wen-Lang Lin, Mariely Dejesus-Hernandez, Marka M van Blitterswijk, Karen Jansen-West, Joseph W Paul, 3rd, Rosa Rademakers, Kevin B Boylan, Dennis W Dickson, and Leonard Petrucelli. Unconventional translation of c9orf72 ggggcc expansion generates insoluble polypeptides specific to c9als/als. *Neuron*, 77(4):639–46, Feb 2013.

[71] Kohji Mori, Shih-Ming Weng, Thomas Arzberger, Stephanie May, Kristin Rentzsch, Elisabeth Kremmer, Bettina Schmid, Hans A Kretzschmar, Marc Cruts, Christine Van Broeckhoven, Christian Haass, and Dieter Edbauer. The c9orf72 ggggcc repeat is translated into aggregating dipeptide-repeat proteins in ftld/als. *Science*, 339(6125):1335–8, Mar 2013.

[72] Kohji Mori, Thomas Arzberger, Friedrich A Grässer, Ilse Gijselinck, Stephanie May, Kristin Rentzsch, Shih-Ming Weng, Martin H Schludi, Julie van der Zee, Marc Cruts, Christine Van Broeckhoven, Elisabeth Kremmer, Hans A Kretzschmar, Christian Haass, and Dieter Edbauer. Bidirectional transcripts of the expanded c9orf72 hexanucleotide repeat are translated into aggregating dipeptide repeat proteins. *Acta Neuropathol*, 126(6):881–93, Dec 2013.

[73] Stephanie May, Daniel Hornburg, Martin H Schludi, Thomas Arzberger, Kristin Rentzsch, Benjamin M Schwenk, Friedrich A Grässer, Kohji Mori, Elisabeth Kremmer, Julia Banzhaf-Strathmann, Matthias Mann, Felix Meissner, and Dieter Edbauer. C9orf72 ftld/als-associated gly-ala dipeptide repeat proteins cause neuronal toxicity and unc119 sequestration. *Acta Neuropathol*, 128(4):485–503, Oct 2014.

[74] Jemeen Sreedharan, Ian P Blair, Vineeta B Tripathi, Xun Hu, Caroline Vance, Boris Rogelj, Steven Ackerley, Jennifer C Durnall, Kelly L Williams, Emanuele Buratti, Francisco Baralle, Jacqueline de Belleroche, J Douglas Mitchell, P Nigel Leigh, Ammar Al-Chalabi, Christopher C Miller, Garth Nicholson, and Christopher E Shaw. Tdp-43 mutations in familial and sporadic amyotrophic lateral sclerosis. *Science*, 319(5870):1668–72, Mar 2008.

[75] Vivianna M Van Deerlin, James B Leverenz, Lynn M Bekris, Thomas D Bird, Wuxing Yuan, Lauren B Elman, Dana Clay, Elisabeth McCarty Wood, Alice S Chen-Plotkin, Maria Martinez-Lage, Ellen Steinbart, Leo McCluskey, Murray Grossman, Manuela Neumann, I-Lin Wu, Wei-Shiung Yang, Robert Kalb, Douglas R Galasko, Thomas J Montine, John Q Trojanowski, Virginia M-Y Lee, Gerard D Schellenberg, and Chang-En Yu. Tardbp mutations in amyotrophic lateral sclerosis with tdp-43 neuropathology: a genetic and histopathological analysis. *Lancet Neurol*, 7(5):409–16, May 2008.

[76] Nicola J Rutherford, Yong-Jie Zhang, Matt Baker, Jennifer M Gass, Nicole A Finch, Ya-Fei Xu, Heather Stewart, Brendan J Kelley, Karen Kuntz, Richard J P Crook, Jemeen Sreedharan, Caroline Vance, Eric Sorenson, Carol Lippa, Eileen H Bigio, Daniel H Geschwind, David S Knopman, Hiroshi Mitsumoto, Ronald C Petersen, Neil R Cashman, Mike Hutton, Christopher E Shaw, Kevin B Boylan, Bradley Boeve, Neill R Graff-Radford, Zbigniew K

Wszolek, Richard J Caselli, Dennis W Dickson, Ian R Mackenzie, Leonard Petrucelli, and Rosa Rademakers. Novel mutations in tardbp (tdp-43) in patients with familial amyotrophic lateral sclerosis. *PLoS Genet*, 4(9):e1000193, 2008.

[77] Edor Kabashi, Paul N Valdmanis, Patrick Dion, Dan Spiegelman, Brendan J McConkey, Christine Vande Velde, Jean-Pierre Bouchard, Lucette Lacomblez, Ksenia Pochigaeva, Francois Salachas, Pierre-Francois Pradat, William Camu, Vincent Meininger, Nicolas Dupre, and Guy A Rouleau. Tardbp mutations in individuals with sporadic and familial amyotrophic lateral sclerosis. *Nat Genet*, 40(5):572–4, May 2008.

[78] B Borroni, C Bonvicini, A Alberici, E Buratti, C Agosti, S Archetti, A Papetti, C Stuani, M Di Luca, M Gennarelli, and A Padovani. Mutation within tardbp leads to frontotemporal dementia without motor neuron disease. *Hum Mutat*, 30(11):E974–83, Nov 2009.

[79] Lina Benajiba, Isabelle Le Ber, Agnès Camuzat, Mathieu Lacoste, Catherine Thomas-Anterion, Philippe Couratier, Solenn Legallic, François Salachas, Didier Hannequin, Marielle Decousus, Lucette Lacomblez, Eric Guedj, Véronique Golfier, William Camu, Bruno Dubois, Dominique Campion, Vincent Meininger, Alexis Brice, and French Clinical and Genetic Research Network on Frontotemporal Lobar Degeneration/Frontotemporal Lobar Degeneration with Motoneuron Disease. Tardbp mutations in motoneuron disease with frontotemporal lobar degeneration. *Ann Neurol*, 65(4):470–3, Apr 2009.

[80] Gabor G Kovacs, Jill R Murrell, Sandor Horvath, Laszlo Haraszti, Katalin Majtenyi, Maria J Molnar, Herbert Budka, Bernardino Ghetti, and Salvatore Spina. Tardbp variation associated with frontotemporal dementia, supranuclear gaze palsy, and chorea. *Mov Disord*, 24(12):1843–7, Sep 2009.

[81] S H Ou, F Wu, D Harrich, L F García-Martínez, and R B Gaynor. Cloning and characterization of a novel cellular protein, tdp-43, that binds to human immunodeficiency virus type 1 tar dna sequence motifs. *J Virol*, 69(6):3584–96, Jun 1995.

[82] E Buratti, T Dörk, E Zuccato, F Pagani, M Romano, and F E Baralle. Nuclear factor TDP-43 and SR proteins promote in vitro and in vivo CFTR exon 9 skipping. *The EMBO journal*, 20(7):1774–1784, April 2001.

[83] Hurng-Yi Wang, I-Fan Wang, Jayaramakrishnan Bose, and C-K James Shen. Structural diversity and functional implications of the eukaryotic TDP gene family. *Genomics*, 83(1):130–139, January 2004.

[84] Matthew J Winton, Lionel M Igaz, Margaret M Wong, Linda K Kwong, John Q Trojanowski, and Virginia M-Y Lee. Disturbance of nuclear and cytoplasmic tar dna-binding protein (tdp-43) induces disease-like redistribution, sequestration, and aggregate formation. *J Biol Chem*, 283(19):13302–9, May 2008.

[85] Michaeline L Hebron, Irina Lonskaya, Kaydee Sharpe, Puwakdandawe P K Weerasinghe, Norah K Algarzae, Ashot R Shekoyan, and Charbel E-H Moussa. Parkin ubiquitinates tar-dna binding protein-43 (tdp-43) and promotes its cytosolic accumulation via interaction with histone deacetylase 6 (hdac6). *J Biol Chem*, 288(6):4103–15, Feb 2013.

[86] Emanuele Buratti, Antonia Brindisi, Maurizio Giombi, Sergio Tisminetzky, Youhna M Ayala, and Francisco E Baralle. Tdp-43 binds heterogeneous nuclear ribonucleoprotein a/b through its c-terminal tail: an important region for the inhibition of cystic fibrosis transmembrane conductance regulator exon 9 splicing. *J Biol Chem*, 280(45):37572–84, Nov 2005.

[87] Y. M Ayala, P Zago, A D'ambrogio, Y.-F Xu, L Petrucelli, E Buratti, and F. E Baralle. Structural determinants of the cellular localization and shuttling of tdp-43. *Journal of Cell Science*, 121(22):3778–3785, Nov 2008.

[88] Marco Baralle, Emanuele Buratti, and Francisco E Baralle. The role of tdp-43 in the pathogenesis of als and ftld. *Biochem Soc Trans*, 41(6):1536–40, Dec 2013.

[89] E Buratti. Characterization and functional implications of the rna binding properties of nuclear factor tdp-43, a novel splicing regulator of cftr exon 9. *Journal of Biological Chemistry*, 276(39):36337–36343, Sep 2001.

[90] Kshitish K Acharya, Chhabi K Govind, Amy N Shore, Mark H Stoler, and Prabhakara P Reddi. cis-Requirement for the maintenance of round spermatid-specific transcription. *Developmental Biology*, 295(2):781–790, July 2006.

[91] Mayuresh M Abhyankar, Craig Urekar, and Prabhakara P Reddi. A novel cpg-free vertebrate insulator silences the testis-specific sp-10 gene in somatic tissues: role for tdp-43 in insulator function. *J Biol Chem*, 282(50):36143–54, Dec 2007.

[92] Magdalini Polymenidou, Clotilde Lagier-Tourenne, Kasey R Hutt, Stephanie C Huelga, Jacqueline Moran, Tiffany Y Liang, Shuo-Chien Ling, Eveline Sun, Edward Wancewicz, Curt Mazur, Holly Kordasiewicz, Yalda Sedaghat, John Paul Donohue, Lily Shiue, C Frank Bennett, Gene W Yeo, and Don W Cleveland. Long pre-mrna depletion and rna missplicing contribute to neuronal vulnerability from loss of tdp-43. *Nat Neurosci*, 14(4):459–468, Apr 2011.

[93] James R Tollervey, Tomaž Curk, Boris Rogelj, Michael Briese, Matteo Cereda, Melis Kayikci, Julian König, Tibor Hortobágyi, Agnes L Nishimura, Vera Zupunski, Rickie Patani, Siddharthan Chandran, Gregor Rot, Blaž Zupan, Christopher E Shaw, and Jernej Ule. Characterizing the RNA targets and position-dependent splicing regulation by TDP-43. *Nature Neuroscience*, 14(4):452–458, April 2011.

[94] Youhna M Ayala, Laura De Conti, S Eréndira AvendaÑO-VÁZquez, Ashish Dhir, Maurizio Romano, Andrea D&Apos;Ambrogio, James Tollervey, Jernej Ule, Marco Baralle, Emanuele Buratti, and Francisco E Baralle. Tdp-43 regulates its mrna levels through a negative feedback loop. *The EMBO Journal*, 30(2):277–288, Mar 2010.

[95] S E Avendano-Vazquez, A Dhir, S Bembich, E Buratti, N Proudfoot, and F E Baralle. Autoregulation of TDP-43 mRNA levels involves interplay between transcription, splicing, and alternative polyA site selection. *Genes & development*, 26(15):1679–1684, August 2012.

[96] George Elvira, Sylwia Wasiak, Vanessa Blandford, Xin-Kang Tong, Alexandre Serrano, Xiaotang Fan, Maria del Rayo Sánchez-Carbente, Florence Servant, Alexander W Bell, Daniel Boismenu, Jean-Claude Lacaille, Peter S McPherson, Luc DesGroseillers, and Wayne S Sossin. Characterization of an rna granule from developing brain. *Mol Cell Proteomics*, 5(4):635–51, Apr 2006.

[97] L Liu-Yesucevitz, G. J Bassell, A. D Gitler, A. C Hart, E Klann, J. D Richter, S. T Warren, and B Wolozin. Local rna translation at the synapse and in disease. *Journal of Neuroscience*, 31(45):16086–16093, Nov 2011.

[98] I-Fan Wang, Lien-Szn Wu, Hsiang-Yu Chang, and C-K James Shen. Tdp-43, the signature protein of ftld-u, is a neuronal activity-responsive factor. *J Neurochem*, 105(3):797–806, May 2008.

[99] Yoshimitsu Kanai, Naoshi Dohmae, and Nobutaka Hirokawa. Kinesin transports RNA: isolation and characterization of an RNA-transporting granule. *Neuron*, 43(4):513–525, August 2004.

[100] Yubing Lu, Jacob Ferris, and Fen-Biao Gao. Frontotemporal dementia and amyotrophic lateral sclerosis-associated disease protein tdp-43 promotes dendritic branching. *Mol Brain*, 2(1):30, Jan 2009.

[101] Fabian Feiguin, Vinay K Godena, Giulia Romano, Andrea D'ambrogio, Raffaella Klima, and Francisco E Baralle. Depletion of tdp-43 affects drosophila motoneurons terminal synapsis and locomotive behavior. *FEBS Letters*, 583(10):1586–1592, Feb 2009.

[102] Claudia Colombrita, Eleonora Zennaro, Claudia Fallini, Markus Weber, Andreas Sommacal, Emanuele Buratti, Vincenzo Silani, and Antonia Ratti. Tdp-43 is recruited to stress granules in conditions of oxidative insult. *Journal of Neurochemistry*, 111(4):1051–1061, Nov 2009.

[103] Liqun Liu-Yesucevitz, Aylin Bilgutay, Yong-Jie Zhang, Tara Vanderwyde, Allison Citro, Tapan Mehta, Nava Zaarur, Ann Mckee, Robert Bowser, Michael Sherman, Leonard Petrucelli, and Benjamin Wolozin. Tar dna binding protein-43 (tdp-43) associates with stress granules: Analysis of cultured cells and pathological brain tissue. *PLoS ONE*, 5(10):e13250, Oct 2010.

[104] Eva Bentmann, Manuela Neumann, Sabina Tahirovic, Ramona Rodde, Dorothee Dormann, and Christian Haass. Requirements for stress granule recruitment of fused in sarcoma (fus) and tar dna-binding protein of 43 kda (tdp-43). *J Biol Chem*, 287(27):23079–94, Jun 2012.

[105] Eva Bentmann, Christian Haass, and Dorothee Dormann. Stress granules in neurodegeneration–lessons learnt from tar dna binding protein of 43 kda and fused in sarcoma. *FEBS J*, 280(18):4348–70, Sep 2013.

[106] Michael J Strong, Kathryn Volkening, Robert Hammond, Wencheng Yang, Wendy Strong, Cheryl Leystra-Lantz, and Christen Shoesmith. TDP43 is a human low molecular weight neurofilament (hNFL) mRNA-binding protein. *Molecular and Cellular Neuroscience*, 35(2):320–327, June 2007.

[107] Katie Moisse, Jennifer Mepham, Kathryn Volkening, Ian Welch, Tracy Hill, and Michael J Strong. Cytosolic tdp-43 expression following axotomy is associated with caspase 3 activation in nfl,àí/,àí mice: Support for a role for tdp-43 in the physiological response to neuronal injury. *Brain Research*, 1296(C):176–186, Apr 2102.

[108] Katie Moisse, Kathryn Volkening, Cheryl Leystra-Lantz, Ian Welch, Tracy Hill, and Michael J Strong. Divergent patterns of cytosolic tdp-43 and neuronal progranulin expression following axotomy: implications for tdp-43 in the physiological response to neuronal injury. *Brain Res*, 1249:202–11, Jan 2009.

[109] T Sato, S Takeuchi, A Saito, W Ding, H Bamba, H Matsuura, Y Hisa, I Tooyama, and M Urushitani. Axonal ligation induces transient redistribution of tdp-43 in brainstem motor neurons. *Neuroscience*, 164(4):1565–78, Dec 2009.

[110] Emanuele Buratti and Francisco E Baralle. The multiple roles of tdp-43 in pre-mrna processing and gene expression regulation. *RNA biology*, 7(4), Jul 2010.

[111] Yukio Kawahara and Ai Mieda-Sato. TDP-43 promotes microRNA biogenesis as a component of the Drosha and Dicer complexes. *Proceedings of the National Academy of Sciences of the United States of America*, 109(9):3347–3352, February 2012.

[112] Andrea D'Ambrogio, Emanuele Buratti, Cristiana Stuani, Corrado Guarnaccia, Maurizio Romano, Youhna M Ayala, and Francisco E Baralle. Functional mapping of the interaction between TDP-43 and hnRNP A2 in vivo. *Nucleic Acids Research*, 37(12):4116–4126, July 2009.

[113] Emanuele Buratti and Francisco E Baralle. Tdp-43: gumming up neurons through protein-protein and protein-rna interactions. *Trends Biochem Sci*, 37(6):237–47, Jun 2012.

[114] Brian S Johnson, David Snead, Jonathan J Lee, J Michael McCaffery, James Shorter, and Aaron D Gitler. Tdp-43 is intrinsically aggregation-prone, and amyotrophic lateral sclerosis-linked mutations accelerate aggregation and increase toxicity. *J Biol Chem*, 284(30):20329–39, Jul 2009.

[115] Byron Caughey and Peter T Lansbury. Protofibrils, pores, fibrils, and neurodegeneration: separating the responsible protein aggregates from the innocent bystanders. *Annu Rev Neurosci*, 26:267–98, 2003.

[116] Rodrigo A Fuentealba, Maria Udan, Shaughn Bell, Iga Wegorzewska, Jieya Shao, Marc I Diamond, Conrad C Weihl, and Robert H Baloh. Interaction with polyglutamine aggregates reveals a q/n-rich domain in tdp-43. *J Biol Chem*, 285(34):26304–14, Aug 2010.

[117] Mauricio Budini, Valentina Romano, S Eréndira Avendaño-Vázquez, Sara Bembich, Emanuele Buratti, and Francisco E Baralle. Role of selected mutations in the q/n rich region of tdp-43 in egfp-12xq/n-induced aggregate formation. *Brain Res*, 1462:139–50, Jun 2012.

[118] Emma L Scotter, Han-Jou Chen, and Christopher E Shaw. Tdp-43 proteinopathy and als: Insights into disease mechanisms and therapeutic targets. *Neurotherapeutics*, 12(2):352–63, Apr 2015.

[119] Liqun Liu-Yesucevitz, Amy Y Lin, Atsushi Ebata, Joon Y Boon, Whitney Reid, Ya-Fei Xu, Kendra Kobrin, George J Murphy, Leonard Petrucelli, and Benjamin Wolozin. Als-linked mutations enlarge tdp-43-enriched neuronal rna granules in the dendritic arbor. *J Neurosci*, 34(12):4167–74, Mar 2014.

[120] Nael H Alami, Rebecca B Smith, Monica A Carrasco, Luis A Williams, Christina S Winborn, Steve S W Han, Evangelos Kiskinis, Brett Winborn, Brian D Freibaum, Anderson Kanagaraj, Alison J Clare, Nisha M Badders, Bilada Bilican, Edward Chaum, Siddharthan Chandran, Christopher E Shaw, Kevin C Eggan, Tom Maniatis, and J Paul Taylor. Axonal transport of tdp-43 mrna granules is impaired by als-causing mutations. *Neuron*, 81(3):536–43, Feb 2014.

[121] Chunxing Yang, Weijia Tan, Catheryne Whittle, Linghua Qiu, Lucheng Cao, Schahram Akbarian, and Zuoshang Xu. The c-terminal tdp-43 fragments have a high aggregation propensity and harm neurons by a dominant-negative mechanism. *PLoS One*, 5(12):e15878, 2010.

[122] C. M Dewey, B Cenik, C. F Sephton, D. R Dries, P Mayer, S. K Good, B. A Johnson, J Herz, and G Yu. Tdp-43 is directed to stress granules by sorbitol, a novel physiological osmotic and oxidative stressor. *Molecular and Cellular Biology*, pages 1–48, Dec 2010.

[123] Karli K McDonald, Anaïs Aulas, Laurie Destroismaisons, Sarah Pickles, Evghenia Beleac, William Camu, Guy A Rouleau, and Christine Vande Velde. Tar dna-binding protein 43 (tdp-43) regulates stress granule dynamics via differential regulation of g3bp and tia-1. *Human Molecular Genetics*, Jan 2011.

[124] Clotilde Lagier-Tourenne, Magdalini Polymenidou, Kasey R Hutt, Anthony Q Vu, Michael Baughn, Stephanie C Huelga, Kevin M Clutario, Shuo-Chien Ling, Tiffany Y Liang, Curt Mazur, Edward Wancewicz, Aneeza S Kim, Andy Watt, Sue Freier, Geoffrey G Hicks, John Paul Donohue, Lily Shiue, C Frank Bennett, John Ravits, Don W Cleveland, and Gene W Yeo. Divergent roles of als-linked proteins fus/tls and tdp-43 intersect in processing long pre-mrnas. *Nat Neurosci*, 15(11):1488–97, Nov 2012.

[125] Daiyu Honda, Shinsuke Ishigaki, Yohei Iguchi, Yusuke Fujioka, Tsuyoshi Udagawa, Akio Masuda, Kinji Ohno, Masahisa Katsuno, and Gen Sobue. The als/ftld-related rna-binding proteins tdp-43 and fus have common downstream rna targets in cortical neurons. *FEBS Open Bio*, 4:1–10, 2013.

[126] Johnathan Cooper-Knock, Matthew J Walsh, Adrian Higginbottom, J Robin Highley, Mark J Dickman, Dieter Edbauer, Paul G Ince, Stephen B Wharton, Stuart A Wilson, Janine Kirby, Guillaume M Hautbergue, and Pamela J Shaw. Sequestration of multiple rna recognition motif-containing proteins by c9orf72 repeat expansions. *Brain*, 137(Pt 7):2040–51, Jul 2014.

[127] Matthew J Greenway, Peter M Andersen, Carsten Russ, Sean Ennis, Susan Cashman, Colette Donaghy, Victor Patterson, Robert Swingler, Dairin Kieran, Jochen Prehn, Karen E Morrison, Andrew Green, K Ravi Acharya, Robert H Brown, Jr, and Orla Hardiman. Ang mutations segregate with familial and 'sporadic' amyotrophic lateral sclerosis. *Nat Genet*, 38(4):411–3, Apr 2006.

[128] Hong Joo Kim, Nam Chul Kim, Yong-Dong Wang, Emily A Scarborough, Jennifer Moore, Zamia Diaz, Kyle S MacLea, Brian Freibaum, Songqing Li, Amandine Molliex, Anderson P Kanagaraj, Robert Carter, Kevin B Boylan, Aleksandra M Wojtas, Rosa Rademakers, Jack L Pinkus, Steven A Greenberg, John Q Trojanowski, Bryan J Traynor, Bradley N Smith, Simon Topp, Athina-Soragia Gkazi, Jack Miller, Christopher E Shaw, Michael Kottlors, Janbernd Kirschner, Alan Pestronk, Yun R Li, Alice Flynn Ford, Aaron D Gitler, Michael Benatar, Oliver D King, Virginia E Kimonis, Eric D Ross, Conrad C Weihl, James Shorter, and J Paul Taylor. Mutations in prion-like domains in hnrnpa2b1 and hnrnpa1 cause multisystem proteinopathy and als. *Nature*, 495(7442):467–73, Mar 2013.

[129] Iga Wegorzewska and Robert H Baloh. Tdp-43-based animal models of neurodegeneration: new insights into als pathology and pathophysiology. *Neurodegener Dis*, 8(4):262–74, 2011.

[130] Yu-Chih Liu, Po-Min Chiang, and Kuen-Jer Tsai. Disease animal models of tdp-43 proteinopathy and their pre-clinical applications. *Int J Mol Sci*, 14(10):20079–111, 2013.

[131] Tania F Gendron and Leonard Petrucelli. Rodent models of tdp-43 proteinopathy: investigating the mechanisms of tdp-43-mediated neurodegeneration. *J Mol Neurosci*, 45(3):486–99, Nov 2011.

[132] Lien-Szu Wu, Wei-Cheng Cheng, Shin-Chen Hou, Yu-Ting Yan, Si-Tse Jiang, and C-K James Shen. Tdp-43, a neuro-pathosignature factor, is essential for early mouse embryogenesis. *Genesis*, 48(1):56–62, Jan 2010.

[133] Chantelle F Sephton, Shannon K Good, Stan Atkin, Colleen M Dewey, Paul Mayer, Joachim Herz, and Gang Yu. Tdp-43 is a developmentally regulated protein essential for early embryonic development. *J Biol Chem*, 285(9):6826–34, Feb 2010.

[134] Brian C Kraemer, Theresa Schuck, Jeanna M Wheeler, Linda C Robinson, John Q Trojanowski, Virginia M Y Lee, and Gerard D Schellenberg. Loss of murine tdp-43 disrupts motor function and plays an essential role in embryogenesis. *Acta Neuropathol*, 119(4):409–19, Apr 2010.

[135] Yohei Iguchi, Masahisa Katsuno, Jun-ichi Niwa, Shin-ichi Yamada, Jun Sone, Masahiro Waza, Hiroaki Adachi, Fumiaki Tanaka, Koh-ichi Nagata, Nariko Arimura, Takashi Watanabe, Kozo Kaibuchi, and Gen Sobue. Tdp-43 depletion induces neuronal cell damage through dysregulation of rho family gtpases. *J Biol Chem*, 284(33):22059–66, Aug 2009.

[136] Po-Min Chiang, Jonathan Ling, Yun Ha Jeong, Donald L Price, Susan M Aja, and Philip C Wong. Deletion of tdp-43 down-regulates tbc1d1, a gene linked to obesity, and alters body fat metabolism. *Proc Natl Acad Sci USA*, 107(37):16320–4, Sep 2010.

[137] Luc Dupuis, Hugues Oudart, Frédérique René, Jose-Luis Gonzalez de Aguilar, and Jean-Philippe Loeffler. Evidence for defective energy homeostasis in amyotrophic lateral sclerosis: benefit of a high-energy diet in a transgenic mouse model. *Proc Natl Acad Sci U S A*, 101(30):11159–64, Jul 2004.

[138] C Yang, H Wang, T Qiao, B Yang, L Aliaga, L Qiu, W Tan, J Salameh, D M McKenna-Yasek, T Smith, L Peng, M J Moore, R H Brown, H Cai, and Z Xu. Partial loss of TDP-43 function causes phenotypes of amyotrophic lateral sclerosis. *Proceedings of the National Academy of Sciences of the United States of America*, 111(12):E1121–E1129, March 2014.

[139] Yohei Iguchi, Masahisa Katsuno, Jun-ichi Niwa, Shinnosuke Takagi, Shinsuke Ishigaki, Kensuke Ikenaka, Kaori Kawai, Hirohisa Watanabe, Koji Yamanaka, Ryosuke Takahashi, Hidemi Misawa, Shoichi Sasaki, Fumiaki Tanaka, and Gen Sobue. Loss of tdp-43 causes age-dependent progressive motor neuron degeneration. *Brain*, 136(Pt 5):1371–82, May 2013.

[140] Lien-Szu Wu, Wei-Cheng Cheng, and C-K James Shen. Targeted depletion of tdp-43 expression in the spinal cord motor neurons leads to the development of amyotrophic lateral sclerosis-like phenotypes in mice. *J Biol Chem*, 287(33):27335–44, Aug 2012.

[141] Jeannie Chew, Tania F Gendron, Mercedes Prudencio, Hiroki Sasaguri, Yong-Jie Zhang, Monica Castanedes-Casey, Chris W Lee, Karen Jansen-West, Aishe Kurti, Melissa E Murray, Kevin F Bieniek, Peter O Bauer, Ena C Whitelaw, Linda Rousseau, Jeannette N Stankowski, Caroline Stetler, Lillian M Daughrity, Emilie A Perkerson, Pamela Desaro, Amelia Johnston, Karen Overstreet, Dieter Edbauer, Rosa Rademakers, Kevin B Boylan, Dennis W Dickson, John D Fryer, and Leonard Petrucelli. C9orf72 repeat expansions in mice cause tdp-43 pathology, neuronal loss, and behavioral deficits. *Science*, May 2015.

[142] T Zhang, H.-Y Hwang, H Hao, C Talbot, and J Wang. Caenorhabditis elegans rna-processing protein tdp-1 regulates protein homeostasis and lifespan. *Journal of Biological Chemistry*, pages 1–21, Jan 2012.

[143] Alexandra Vaccaro, Arnaud Tauffenberger, Peter E A Ash, Yari Carlomagno, Leonard Petrucelli, and J Alex Parker. Tdp-1/tdp-43 regulates stress signaling and age-dependent proteotoxicity in caenorhabditis elegans. *PLoS Genet*, 8(7):e1002806, Jul 2012.

[144] Meng-Jau Lin, Ching-Wei Cheng, and C-K James Shen. Neuronal function and dysfunction of drosophila dtdp. *PLoS One*, 6(6):e20371, 2011.

[145] Danielle C Diaper, Yoshitsugu Adachi, Ben Sutcliffe, Dickon M Humphrey, Christopher J H Elliott, Alan Stepto, Zoe N Ludlow, Lies Vanden Broeck, Patrick Callaerts, Bart Dermaut, Ammar Al-Chalabi, Christopher E Shaw, Iain M Robinson, and Frank Hirth. Loss and gain of drosophila tdp-43 impair synaptic efficacy and motor control leading to age-related neurodegeneration by loss-of-function phenotypes. *Hum Mol Genet*, 22(8):1539–57, Apr 2013.

[146] Ji-Wu Wang, Jonathan R Brent, Andrew Tomlinson, Neil A Shneider, and Brian D McCabe. The als-associated proteins fus and tdp-43 function together to affect drosophila locomotion and life span. *J Clin Invest*, 121(10):4118–26, Oct 2011.

[147] Bettina Schmid, Alexander Hruscha, Sebastian Hogl, Julia Banzhaf-Strathmann, Katrin Strecker, Julie van der Zee, Mathias Teucke, Stefan Eimer, Jan Hegermann, Maike Kittelmann, Elisabeth Kremmer, Marc Cruts, Barbara Solchenberger, Laura Hasenkamp, Frauke van Bebber, Christine Van Broeckhoven, Dieter Edbauer, Stefan F Lichtenthaler, and Christian Haass. Loss of ALS-associated TDP-43 in zebrafish causes muscle degeneration, vascular dysfunction, and reduced motor neuron axon outgrowth. *Proceedings of the National Academy of Sciences of the United States of America*, 110(13):4986–4991, March 2013.

[148] Channa A A Hewamadduma, Andrew J Grierson, Taylur P Ma, Luyuan Pan, Cecilia B Moens, Philip W Ingham, Tennore Ramesh, and Pamela J Shaw. Tardbpl splicing rescues motor neuron and axonal development in a mutant tardbp zebrafish. *Hum Mol Genet*, 22(12):2376–86, Jun 2013.

[149] Edor Kabashi, Li Lin, Miranda L Tradewell, Patrick A Dion, Valérie Bercier, Patrick Bourgouin, Daniel Rochefort, Samar Bel Hadj, Heather D Durham, Christine Vande Velde, Guy A Rouleau, and Pierre Drapeau. Gain and loss of function of als-related mutations of tardbp (tdp-43) cause motor deficits in vivo. *Human Molecular Genetics*, 19(4):671–83, Feb 2010.

[150] Shane P Herbert and Didier Y. R Stainier. Molecular control of endothelial cell behaviour during blood vessel morphogenesis. *Nat Rev Mol Cell Biol*, 12(9):551–564, Aug 2011.

[151] U Ruth Michaelis. Mechanisms of endothelial cell migration. *Cell Mol Life Sci*, 71(21):4131–48, Nov 2014.

[152] Richard O Hynes. Stretching the boundaries of extracellular matrix research. *Nat Rev Mol Cell Biol*, 15(12):761–3, Dec 2014.

[153] Jielin Xu and Deane Mosher. Fibronectin and Other Adhesive Glycoproteins. In *The extracellular matrix : an overview*, pages 41–75. Springer Berlin Heidelberg, Berlin, Heidelberg, December 2010.

[154] R O Hynes. Cell-matrix adhesion in vascular development. *Journal of thrombosis and haemostasis : JTH*, 5 Suppl 1:32–40, July 2007.

[155] E L George, E N Georges-Labouesse, R S Patel-King, H Rayburn, and R O Hynes. Defects in mesoderm, neural tube and vascular development in mouse embryos lacking fibronectin. *Development*, 119(4):1079–1091, December 1993.

[156] E N Georges-Labouesse, E L George, H Rayburn, and R O Hynes. Mesodermal development in mouse embryos mutant for fibronectin. *Developmental dynamics : an official publication of the American Association of Anatomists*, 207(2):145–156, October 1996.

[157] E L George, H S Baldwin, and R O Hynes. Fibronectins are essential for heart and blood vessel morphogenesis but are dispensable for initial specification of precursor cells. *Blood*, 90(8):3073–3081, October 1997.

[158] Sheila E Francis, Keow Lin Goh, Kairbaan Hodivala-Dilke, Bernhard L Bader, Margaret Stark, Duncan Davidson, and Richard O Hynes. Central roles of alpha5beta1 integrin and fibronectin in vascular development in mouse embryos and embryoid bodies. *Arterioscler Thromb Vasc Biol*, 22(6):927–33, Jun 2002.

[159] Q Zhao. Identification and Characterization of a Novel Fibronectin in Zebrafish. *Experimental Cell Research*, 268(2):211–219, August 2001.

[160] Lu Sun, Zhiying Zou, Paul Collodi, Fang Xu, Xiaofeng Xu, and Qingshun Zhao. Identification and characterization of a second fibronectin gene in zebrafish. *Matrix Biology*, 24(1):69–77, February 2005.

[161] Xiangyu Liu, Qingshun Zhao, and Paul Collodi. A truncated form of fibronectin is expressed in fish and mammals. *Matrix Biology*, 22(5):393–396, September 2003.

[162] L A Trinh and Didier Y R Stainier. Fibronectin regulates epithelial organization during myocardial migration in zebrafish. *Dev Cell*, 6(3):371–82, Mar 2004.

[163] Suk-Won Jin, Dimitris Beis, Tracy Mitchell, Jau-Nian Chen, and Didier Y R Stainier. Cellular and molecular analyses of vascular tube and lumen formation in zebrafish. *Development*, 132(23):5199–5209, December 2005.

[164] Chih-Hao Chiu, Chih-Wei Chou, Shinji Takada, and Yi-Wen Liu. Development and Fibronectin Signaling Requirements of the Zebrafish Interrenal Vessel. *PLoS ONE*, 7(8):e43040, August 2012.

[165] Dörthe Julich, Robert Geisler, and Scott A Holley. Integrinα5 and Delta/Notch Signaling Have Complementary Spatiotemporal Requirements during Zebrafish Somitogenesis. *Developmental Cell*, 8(4):575–586, April 2005.

[166] Sumito Koshida, Yasuyuki Kishimoto, Hideko Ustumi, Toshihiro Shimizu, Makoto Furutani-Seiki, Hisato Kondoh, and Shinji Takada. Integrinα5-Dependent Fibronectin Accumulation for Maintenance of Somite Boundaries in Zebrafish Embryos. *Developmental Cell*, 8(4):587–598, April 2005.

[167] Chelsi J Snow, Matthew T Peterson, Andre Khalil, and Clarissa A Henry. Muscle development is disrupted in zebrafish embryos deficient for fibronectin. *Developmental dynamics : an official publication of the American Association of Anatomists*, 237(9):2542–2553, September 2008.

[168] Hynes. Integrins: Bidirectional,Review Allosteric Signaling Machines. *Cell*, Cell, Vol. 110, 673–687:1–15, September 2002.

[169] Ping Hu and Bing-Hao Luo. Integrin bi-directional signaling across the plasma membrane. *J Cell Physiol*, 228(2):306–12, Feb 2013.

[170] B Geiger, A Bershadsky, R Pankov, and K M Yamada. Transmembrane crosstalk between the extracellular matrix–cytoskeleton crosstalk. *Nature reviews Molecular cell biology*, 2(11):793–805, November 2001.

[171] R O Hynes, B L Bader, and K Hodivala-Dilke. Integrins in vascular development. *Braz J Med Biol Res*, 32(5):501–10, May 1999.

[172] Sophie Astrof and Richard O Hynes. Fibronectins in vascular morphogenesis. *Angiogenesis*, 12(2):165–175, February 2009.

[173] R Fässler and M Meyer. Consequences of lack of beta 1 integrin gene expression in mice. *Genes Dev*, 9(15):1896–908, Aug 1995.

[174] L E Stephens, A E Sutherland, I V Klimanskaya, A Andrieux, J Meneses, R A Pedersen, and C H Damsky. Deletion of beta 1 integrins in mice results in inner cell mass failure and peri-implantation lethality. *Genes Dev*, 9(15):1883–95, Aug 1995.

[175] Li Lei, Dinggang Liu, Yan Huang, Ion Jovin, Shaw-Yung Shai, Themis Kyriakides, Robert S Ross, and Frank J Giordano. Endothelial expression of beta1 integrin is required for embryonic vascular patterning and postnatal vascular remodeling. *Mol Cell Biol*, 28(2):794–802, Jan 2008.

[176] Timothy R Carlson, Huiqing Hu, Rickmer Braren, Yung Hae Kim, and Rong A Wang. Cell-autonomous requirement for beta1 integrin in endothelial cell adhesion, migration and survival during angiogenesis in mice. *Development*, 135(12):2193–202, Jun 2008.

[177] Harikrishna Tanjore, Elisabeth M Zeisberg, Behzad Gerami-Naini, and Raghu Kalluri. Beta1 integrin expression on endothelial cells is required for angiogenesis but not for vasculogenesis. *Dev Dyn*, 237(1):75–82, Jan 2008.

[178] Ann C Zovein, Alfonso Luque, Kirsten A Turlo, Jennifer J Hofmann, Kathleen M Yee, Michael S Becker, Reinhard Fassler, Ira Mellman, Timothy F Lane, and M Luisa Iruela-Arispe. Beta1 integrin establishes endothelial cell polarity and arteriolar lumen formation via a par3-dependent mechanism. *Dev Cell*, 18(1):39–51, Jan 2010.

[179] Hiroyuki Yamamoto, Manuel Ehling, Katsuhiro Kato, Kenichi Kanai, Max van Lessen, Maike Frye, Dagmar Zeuschner, Masanori Nakayama, Dietmar Vestweber, and Ralf H Adams. Integrin β1 controls ve-cadherin localization and blood vessel stability. *Nat Commun*, 6:6429, 2015.

[180] J T Yang, H Rayburn, and R O Hynes. Embryonic mesodermal defects in alpha 5 integrin-deficient mice. *Development*, 119(4):1093–1105, December 1993.

[181] Arjan van der Flier, Kwabena Badu-Nkansah, Charles A Whittaker, Denise Crowley, Roderick T Bronson, Adam Lacy-Hulbert, and Richard O Hynes. Endothelial alpha5 and alphav integrins cooperate in remodeling of the vasculature during development. *Development*, 137(14):2439–49, Jul 2010.

[182] R Soldi, S Mitola, M Strasly, P Defilippi, G Tarone, and F Bussolino. Role of alphavbeta3 integrin in the activation of vascular endothelial growth factor receptor-2. *EMBO J*, 18(4):882–92, Feb 1999.

[183] Louise E Reynolds, Lorenza Wyder, Julie C Lively, Daniela Taverna, Stephen D Robinson, Xiaozhu Huang, Dean Sheppard, Richard O Hynes, and Kairbaan M Hodivala-Dilke. Enhanced pathological angiogenesis in mice lacking beta3 integrin or beta3 and beta5 integrins. *Nat Med*, 8(1):27–34, Jan 2002.

[184] J T Yang, B L Bader, J A Kreidberg, M Ullman-Culleré, J E Trevithick, and R O Hynes. Overlapping and independent functions of fibronectin receptor integrins in early mesodermal development. *Developmental Biology*, 215(2):264–277, November 1999.

[185] J T Yang and R O Hynes. Fibronectin receptor functions in embryonic cells deficient in alpha 5 beta 1 integrin can be replaced by alpha V integrins. *Molecular Biology of the Cell*, 7(11):1737–1748, November 1996.

[186] S H Kil, C E Krull, G Cann, D Clegg, and M Bronner-Fraser. The alpha4 subunit of integrin is important for neural crest cell migration. *Developmental Biology*, 202(1):29–42, October 1998.

[187] Jennifer K Sengbusch, Wei He, Karen A Pinco, and Joy T Yang. Dual functions of [alpha]4[beta]1 integrin in epicardial development: initial migration and long-term attachment. *J Cell Biol*, 157(5):873–82, May 2002.

[188] Alison Grazioli, Christina S Alves, Konstantinos Konstantopoulos, and Joy T Yang. Defective blood vessel development and pericyte/pvsmc distribution in alpha 4 integrin-deficient mouse embryos. *Dev Biol*, 293(1):165–77, May 2006.

[189] R O Hynes. Integrins: versatility, modulation, and signaling in cell adhesion. *Cell*, 69(1):11–25, Apr 1992.

[190] J T Yang, H Rayburn, and R O Hynes. Cell adhesion events mediated by alpha 4 integrins are essential in placental and cardiac development. *Development*, 121(2):549–560, February 1995.

[191] N Wagner, J Löhler, E J Kunkel, K Ley, E Leung, G Krissansen, K Rajewsky, and W Müller. Critical role for beta7 integrins in formation of the gut-associated lymphoid tissue. *Nature*, 382(6589):366–70, Jul 1996.

[192] D Bouvard, C Brakebusch, E Gustafsson, A Aszódi, T Bengtsson, A Berna, and R Fässler. Functional consequences of integrin gene mutations in mice. *Circ Res*, 89(3):211–23, Aug 2001.

[193] R R Lobb and M E Hemler. The pathophysiologic role of alpha 4 integrins in vivo. *J Clin Invest*, 94(5):1722–8, Nov 1994.

[194] H E Chuluyan and A C Issekutz. Vla-4 integrin can mediate cd11/cd18-independent transendothelial migration of human monocytes. *J Clin Invest*, 92(6):2768–77, Dec 1993.

[195] Joan M Cook-Mills, Michelle E Marchese, and Hiam Abdala-Valencia. Vascular cell adhesion molecule-1 expression and signaling during disease: regulation by reactive oxygen species and antioxidants. *Antioxid Redox Signal*, 15(6):1607–38, Sep 2011.

[196] L Kwee, H S Baldwin, H M Shen, C L Stewart, C Buck, C A Buck, and M A Labow. Defective development of the embryonic and extraembryonic circulatory systems in vascular cell adhesion molecule (vcam-1) deficient mice. *Development*, 121(2):489–503, Feb 1995.

[197] Sandra van Wetering, Nadia van den Berk, Jaap D van Buul, Frederik P J Mul, Ingrid Lommerse, Rogier Mous, Jean-Paul ten Klooster, Jaap-Jan Zwaginga, and Peter L Hordijk. Vcam-1-mediated rac signaling controls endothelial cell-cell contacts and leukocyte transmigration. *Am J Physiol Cell Physiol*, 285(2):C343–52, Aug 2003.

[198] Matthias Vockel and Dietmar Vestweber. How t cells trigger the dissociation of the endothelial receptor phosphatase ve-ptp from ve-cadherin. *Blood*, 122(14):2512–22, Oct 2013.

[199] A Paul Mould, Jennifer A McLeish, Julie Huxley-Jones, Alexander C Goonesinghe, Adam F L Hurlstone, Raymond P Boot-Handford, and Martin J Humphries. Identification of multiple integrin β1 homologs in zebrafish (danio rerio). *BMC Cell Biol*, 7:24, 2006.

[200] Xin Wang, Liping Li, and Dong Liu. Expression analysis of integrin β1 isoforms during zebrafish embryonic development. *Gene Expr Patterns*, 16(2):86–92, Nov 2014.

[201] D Julich, A P Mould, E Koper, and S A Holley. Control of extracellular matrix assembly along tissue boundaries via Integrin and Eph/Ephrin signaling. *Development*, 136(17):2913–2921, August 2009.

[202] Anna-Karin Olsson, Anna Dimberg, Johan Kreuger, and Lena Claesson-Welsh. VEGF receptor signalling — in control of vascular function. *Nature Publishing Group*, 7(5):359–371, May 2006.

[203] F Shalaby, J Rossant, T P Yamaguchi, M Gertsenstein, X F Wu, M L Breitman, and A C Schuh. Failure of blood-island formation and vasculogenesis in flk-1-deficient mice. *Nature*, 376(6535):62–6, Jul 1995.

[204] T Takahashi, S Yamaguchi, K Chida, and M Shibuya. A single autophosphorylation site on kdr/flk-1 is essential for vegf-a-dependent activation of plc-gamma and dna synthesis in vascular endothelial cells. *EMBO J*, 20(11):2768–78, Jun 2001.

[205] Kristina Holmqvist, Michael J Cross, Charlotte Rolny, Robert Hägerkvist, Nader Rahimi, Taro Matsumoto, Lena Claesson-Welsh, and Michael Welsh. The adaptor protein shb binds to tyrosine 1175 in vascular endothelial growth factor (vegf) receptor-2 and regulates vegf-dependent cellular migration. *J Biol Chem*, 279(21):22267–75, May 2004.

[206] Y Fujio and K Walsh. Akt mediates cytoprotection of endothelial cells by vascular endothelial growth factor in an anchorage-dependent manner. *J Biol Chem*, 274(23):16349–54, Jun 1999.

[207] D Fulton, J P Gratton, T J McCabe, J Fontana, Y Fujio, K Walsh, T F Franke, A Papapetropoulos, and W C Sessa. Regulation of endothelium-derived nitric oxide production by the protein kinase akt. *Nature*, 399(6736):597–601, Jun 1999.

[208] Monica Autiero, Johannes Waltenberger, Didier Communi, Andrea Kranz, Lieve Moons, Diether Lambrechts, Jens Kroll, Stephane Plaisance, Maria De Mol, Françoise Bono, Stefanie Kliche, Guido Fellbrich, Kurt Ballmer-Hofer, Domenico Maglione, Ulrike Mayr-Beyrle, Mieke Dewerchin, Saskia Dombrowski, Danica Stanimirovic, Paul Van Hummelen, Christoph Dehio, Daniel J Hicklin, Graziella Persico, Jean-Marc Herbert, David Communi, Masabumi Shibuya, Désiré Collen, Edward M Conway, and Peter Carmeliet. Role of plgf in the intra- and intermolecular cross talk between the vegf receptors flt1 and flk1. *Nat Med*, 9(7):936–43, Jul 2003.

[209] N Rahimi, V Dayanir, and K Lashkari. Receptor chimeras indicate that the vascular endothelial growth factor receptor-1 (vegfr-1) modulates mitogenic activity of vegfr-2 in endothelial cells. *J Biol Chem*, 275(22):16986–92, Jun 2000.

[210] Johan Dixelius, Taija Makinen, Maria Wirzenius, Marika J Karkkainen, Christer Wernstedt, Kari Alitalo, and Lena Claesson-Welsh. Ligand-induced vascular endothelial growth factor receptor-3 (vegfr-3) heterodimerization with vegfr-2 in primary lymphatic endothelial cells regulates tyrosine phosphorylation sites. *J Biol Chem*, 278(42):40973–9, Oct 2003.

[211] Jeroen Bussmann, Nathan Lawson, Leonard Zon, Stefan Schulte-Merker, and Zebrafish Committee. Zebrafish vegf receptors: a guideline to nomenclature. *PLoS Genet*, 4(5):e1000064, May 2008.

[212] Jeroen Bussmann, Jeroen Bakkers, and Stefan Schulte-Merker. Early endocardial morphogenesis requires Scl/Tal1. *PLoS Genetics*, 3(8):e140, August 2007.

[213] Wolfgang Rottbauer, Steffen Just, Georgia Wessels, Nicole Trano, Patrick Most, Hugo A Katus, and Mark C Fishman. VEGF-PLCgamma1 pathway controls cardiac contractility in the embryonic heart. *Genes & development*, 19(13):1624–1634, July 2005.

[214] Nathan Bahary, Katsutoshi Goishi, Carsten Stuckenholz, Gerhard Weber, Jocelyn Leblanc, Christopher A Schafer, Sarah S Berman, Michael Klagsbrun, and Leonard I Zon. Duplicate vegfa genes and orthologues of the kdr receptor tyrosine kinase family mediate vascular development in the zebrafish. *Blood*, 110(10):3627–36, Nov 2007.

[215] L D Covassin, J A Villefranc, M C Kacergis, B M Weinstein, and N D Lawson. Distinct genetic interactions between multiple Vegf receptors are required for development of different blood vessel types in zebrafish. *Proceedings of the National Academy of Sciences of the United States of America*, 103(17):6554–6559, April 2006.

[216] M A Thompson, D G Ransom, S J Pratt, H MacLennan, M W Kieran, H W Detrich, 3rd, B Vail, T L Huber, B Paw, A J Brownlie, A C Oates, A Fritz, M A Gates, A Amores, N Bahary, W S Talbot, H Her, D R Beier, J H Postlethwait, and L I Zon. The cloche and spadetail genes differentially affect hematopoiesis and vasculogenesis. *Dev Biol*, 197(2):248–69, May 1998.

[217] Hinrich Habeck, Jörg Odenthal, Brigitte Walderich, Hans Maischein, Stefan Schulte-Merker, and Tübingen 2000 screen consortium. Analysis of a zebrafish VEGF receptor mutant reveals specific disruption of angiogenesis. *Current biology : CB*, 12(16):1405–1412, August 2002.

[218] S Artavanis-Tsakonas, M D Rand, and R J Lake. Notch signaling: cell fate control and signal integration in development. *Science*, 284(5415):770–6, Apr 1999.

[219] Kazuya Hori, Anindya Sen, and Spyros Artavanis-Tsakonas. Notch signaling at a glance. *J Cell Sci*, 126(Pt 10):2135–40, May 2013.

[220] D Y Stainier, B Fouquet, J N Chen, K S Warren, B M Weinstein, S E Meiler, M A Mohideen, S C Neuhauss, L Solnica-Krezel, A F Schier, F Zwartkruis, D L Stemple, J Malicki, W Driever, and M C Fishman. Mutations affecting the formation and function of the cardiovascular system in the zebrafish embryo. *Development*, 123:285–292, December 1996.

[221] Amy J Sehnert, Anja Huq, Brant M Weinstein, Charline Walker, Mark Fishman, and Didier Y R Stainier. Cardiac troponin t is essential in sarcomere assembly and cardiac contractility. *Nat Genet*, 31(1):106–10, May 2002.

[222] N Lawson. In vivo imaging of embryonic vascular development using transgenic zebrafish. *Developmental Biology*, 248(2):307–318, Aug 2002.

[223] S. P Herbert, J Huisken, T. N Kim, M. E Feldman, B. T Houseman, R. A Wang, K. M Shokat, and D. Y. R Stainier. Arterial-venous segregation by selective cell sprouting: An alternative mode of blood vessel formation. *Science*, 326(5950):294–298, Oct 2009.

[224] Nathan D Lawson, Andreas M Vogel, and Brant M Weinstein. sonic hedgehog and vascular endothelial growth factor act upstream of the notch pathway during arterial endothelial differentiation. *Dev Cell*, 3(1):127–36, Jul 2002.

[225] Nathan D Lawson, Joshua W Mugford, Brigid A Diamond, and Brant M Weinstein. phospholipase C gamma-1 is required downstream of vascular endothelial growth factor during arterial development. *Genes & development*, 17(11):1346–1351, June 2003.

[226] N D Lawson, N Scheer, V N Pham, C H Kim, A B Chitnis, J A Campos-Ortega, and B M Weinstein. Notch signaling is required for arterial-venous differentiation during embryonic vascular development. *Development*, 128(19):3675–83, Oct 2001.

[227] N D Lawson, N Scheer, V N Pham, C H Kim, A B Chitnis, J A Campos-Ortega, and B M Weinstein. Notch signaling is required for arterial-venous differentiation during embryonic vascular development. *Development*, 128(19):3675–3683, October 2001.

[228] R H Adams, G A Wilkinson, C Weiss, F Diella, N W Gale, U Deutsch, W Risau, and R Klein. Roles of ephrinb ligands and ephb receptors in cardiovascular development: demarcation of arterial/venous domains, vascular morphogenesis, and sprouting angiogenesis. *Genes Dev*, 13(3):295–306, Feb 1999.

[229] Sumio Isogai, Nathan D Lawson, Saioa Torrealday, Masaharu Horiguchi, and Brant M Weinstein. Angiogenic network formation in the developing vertebrate trunk. *Development*, 130(21):5281–5290, November 2003.

[230] Karina Yaniv, Sumio Isogai, Daniel Castranova, Louis Dye, Jiro Hitomi, and Brant M Weinstein. Live imaging of lymphatic development in the zebrafish. *Nat Med*, 12(6):711–6, Jun 2006.

[231] Benjamin M Hogan, Frank L Bos, Jeroen Bussmann, Merlijn Witte, Neil C Chi, Henricus J Duckers, and Stefan Schulte-Merker. Ccbe1 is required for embryonic lymphangiogenesis and venous sprouting. *Nat Genet*, 41(4):396–8, Apr 2009.

[232] Laurence Covassin, Julio D Amigo, Kana Suzuki, Viktor Teplyuk, Juerg Straubhaar, and Nathan D Lawson. Global analysis of hematopoietic and vascular endothelial gene expression by tissue specific microarray profiling in zebrafish. *Developmental Biology*, 299(2):551–562, November 2006.

[233] Axel M Küchler, Evisa Gjini, Josi Peterson-Maduro, Belinda Cancilla, Hartwig Wolburg, and Stefan Schulte-Merker. Development of the zebrafish lymphatic system requires vegfc signaling. *Curr Biol*, 16(12):1244–8, Jun 2006.

[234] David M Wiley, Jun-Dae Kim, Jijun Hao, Charles C Hong, Victoria L Bautch, and Suk-Won Jin. Distinct signalling pathways regulate sprouting angiogenesis from the dorsal aorta and the axial vein. *Nat Cell Biol*, 13(6):687–693, Jun 2011.

[235] J E Cannon, P D Upton, J C Smith, and N W Morrell. Intersegmental vessel formation in zebrafish: requirement for vegf but not bmp signalling revealed by selective and non-selective bmp antagonists. *Br J Pharmacol*, 161(1):140–9, Sep 2010.

[236] Holger Gerhardt, Matthew Golding, Marcus Fruttiger, Christiana Ruhrberg, Andrea Lundkvist, Alexandra Abramsson, Michael Jeltsch, Christopher Mitchell, Kari Alitalo, David Shima, and Christer Betsholtz. VEGF guides angiogenic sprouting utilizing endothelial tip cell filopodia. *The Journal of Cell Biology*, 161(6):1163–1177, June 2003.

[237] Raquel Blanco and Holger Gerhardt. VEGF and Notch in tip and stalk cell selection. *Cold Spring Harbor perspectives in medicine*, 3(1):a006569, January 2013.

[238] Arndt F Siekmann, Markus Affolter, and Heinz-Georg Belting. The Tip Cell Concept Ten Years After New players tune in for a common theme. *Experimental Cell Research*, pages 1–27, February 2013.

[239] D Liang, J R Chang, A J Chin, A Smith, C Kelly, E S Weinberg, and R Ge. The role of vascular endothelial growth factor (vegf) in vasculogenesis, angiogenesis, and hematopoiesis in zebrafish development. *Mech Dev*, 108(1-2):29–43, Oct 2001.

[240] Arndt F Siekmann and Nathan D Lawson. Notch signalling limits angiogenic cell behaviour in developing zebrafish arteries. *Nature*, 445(7129):781–784, February 2007.

[241] Fatma O Kok, Masahiro Shin, Chih-Wen Ni, Ankit Gupta, Ann S Grosse, Andreas van Impel, Bettina C Kirchmaier, Josi Peterson-Maduro, George Kourkoulis, Ira Male, Dana F DeSantis, Sarah Sheppard-Tindell, Lwaki Ebarasi, Christer Betsholtz, Stefan Schulte-Merker, Scot A Wolfe, and Nathan D Lawson. Reverse genetic screening reveals poor correlation between morpholino-induced and mutant phenotypes in zebrafish. *Dev Cell*, 32(1):97–108, Jan 2015.

[242] Jonathan D Leslie, Linda Ariza-McNaughton, Adam L Bermange, Ryan McAdow, Stephen L Johnson, and Julian Lewis. Endothelial signalling by the notch ligand delta-like 4 restricts angiogenesis. *Development*, 134(5):839–44, Mar 2007.

[243] Arndt F Siekmann, Laurence Covassin, and Nathan D Lawson. Modulation of VEGF signalling output by the Notch pathway. *BioEssays : news and reviews in molecular, cellular and developmental biology*, 30(4):303–313, April 2008.

[244] J Krueger, D Liu, K Scholz, A Zimmer, Y Shi, C Klein, A Siekmann, S Schulte-Merker, M Cudmore, A Ahmed, and F Le Noble. Flt1 acts as a negative regulator of tip cell formation and branching morphogenesis in the zebrafish embryo. *Development*, 138(10):2111–2120, May 2011.

[245] Yannick Blum, Heinz-Georg Belting, Elín Ellertsdóttir, Lukas Herwig, Florian Lüders, and Markus Affolter. Complex cell rearrangements during intersegmental vessel sprouting and vessel fusion in the zebrafish embryo. *Developmental Biology*, 316(2):312–322, April 2008.

[246] Sarah Childs, Jau-Nian Chen, Deborah M Garrity, and Mark C Fishman. Patterning of angiogenesis in the zebrafish embryo. *Development*, 129(4):973–82, Feb 2002.

[247] Jesús Torres-Vázquez, Aaron D Gitler, Sherri D Fraser, Jason D Berk, Van N Pham, Mark C Fishman, Sarah Childs, Jonathan A Epstein, and Brant M Weinstein. Semaphorin-Plexin Signaling Guides Patterning of the Developing Vasculature. *Developmental Cell*, 7(1):117–123, July 2004.

[248] Tomasz Zygmunt, Carl Michael Gay, Jordan Blondelle, Manvendra K Singh, Kathleen Mccrone Flaherty, Paula Casey Means, Lukas Herwig, Alice Krudewig, Heinz-Georg Belting, Markus Affolter, Jonathan A Epstein, and Jesús Torres-Vázquez. Semaphorin-plexind1 signaling limits angiogenic potential via the vegf decoy receptor sflt1. *Developmental Cell*, 21(2):301–314, Aug 2011.

[249] P Carmeliet, M G Lampugnani, L Moons, F Breviario, V Compernolle, F Bono, G Balconi, R Spagnuolo, B Oosthuyse, M Dewerchin, A Zanetti, A Angellilo, V Mattot, D Nuyens, E Lutgens, F Clotman, M C de Ruiter, A Gittenberger-de Groot, R Poelmann, F Lupu, J M Herbert, D Collen, and E Dejana. Targeted deficiency or cytosolic truncation of the ve-cadherin gene in mice impairs vegf-mediated endothelial survival and angiogenesis. *Cell*, 98(2):147–57, Jul 1999.

[250] Mercedes Montero-Balaguer, Kendra Swirsding, Fabrizio Orsenigo, Franco Cotelli, Marina Mione, and Elisabetta Dejana. Stable Vascular Connections and Remodeling Require Full Expression of VE-Cadherin in Zebrafish Embryos. *PLoS ONE*, 4(6):e5772, June 2009.

[251] Amel Mettouchi. The role of extracellular matrix in vascular branching morphogenesis. *Cell Adhesion & Migration*, 6(6):528–534, November 2012.

[252] D Stenzel, A Lundkvist, D Sauvaget, M Busse, M Graupera, A van der Flier, E S Wijelath, J Murray, M Sobel, M Costell, S Takahashi, R Fassler, Y Yamaguchi, D H Gutmann, R O Hynes, and H Gerhardt. Integrin-dependent and -independent functions of astrocytic fibronectin in retinal angiogenesis. *Development*, 138(20):4451–4463, September 2011.

[253] Christiana Ruhrberg, Holger Gerhardt, Matthew Golding, Rose Watson, Sofia Ioannidou, Hajime Fujisawa, Christer Betsholtz, and David T Shima. Spatially restricted patterning cues provided by heparin-binding VEGF-A control blood vessel branching morphogenesis. *Genes & development*, 16(20):2684–2698, October 2002.

[254] Denise Stenzel, Claudio A Franco, Soline Estrach, Amel Mettouchi, Dominique Sauvaget, Ian Rosewell, Andreas Schertel, Hannah Armer, Anna Domogatskaya, Sergey Rodin, Karl Tryggvason, Lucy Collinson, Lydia Sorokin, and Holger Gerhardt. Endothelial basement membrane limits tip cell formation by inducing dll4/notch signalling in vivo. *EMBO Rep*, 12(11):1135–43, Nov 2011.

[255] S Estrach, L Cailleteau, C A Franco, H Gerhardt, C Stefani, E Lemichez, L Gagnoux-Palacios, G Meneguzzi, and A Mettouchi. Laminin-Binding Integrins Induce Dll4 Expression and Notch Signaling in Endothelial Cells. *Circulation research*, 109(2):172–182, July 2011.

[256] Nicolas C Rivron, Erik J Vrij, Jeroen Rouwkema, Severine Le Gac, Albert van den Berg, Roman K Truckenmüller, and Clemens A van Blitterswijk. Tissue deformation spatially modulates vegf signaling and angiogenesis. *Proc Natl Acad Sci U S A*, 109(18):6886–91, May 2012.

[257] Robert S Fischer, Margaret Gardel, Xuefei Ma, Robert S Adelstein, and Clare M Waterman. Local cortical tension by myosin ii guides 3d endothelial cell branching. *Curr Biol*, 19(3):260–5, Feb 2009.

[258] Peter Carmeliet and Marc Tessier-Lavigne. Common mechanisms of nerve and blood vessel wiring. *Nature*, 436(7048):193–200, Jul 2005.

[259] Natalie J Gardiner. Integrins and the extracellular matrix: key mediators of development and regeneration of the sensory nervous system. *Dev Neurobiol*, 71(11):1054–72, Nov 2011.

[260] Michele L Lemons and Maureen L Condic. Integrin signaling is integral to regeneration. *Exp Neurol*, 209(2):343–52, Feb 2008.

[261] M G Vogelezang, S S Scherer, J W Fawcett, and C ffrench Constant. Regulation of fibronectin alternative splicing during peripheral nerve repair. *J Neurosci Res*, 56(4):323–33, May 1999.

[262] M G Vogelezang, Z Liu, J B Relvas, G Raivich, S S Scherer, and C ffrench Constant. Alpha4 integrin is expressed during peripheral nerve regeneration and enhances neurite outgrowth. *J Neurosci*, 21(17):6732–44, Sep 2001.

[263] Mariette Vogelezang, Ulrike B Forster, Jaewon Han, Mark H Ginsberg, and Charles ffrench Constant. Neurite outgrowth on a fibronectin isoform expressed during peripheral nerve regeneration is mediated by the interaction of paxillin with alpha4beta1 integrins. *BMC Neurosci*, 8:44, 2007.

[264] Veronica J Tom, Catherine M Doller, Alfred T Malouf, and Jerry Silver. Astrocyte-associated fibronectin is critical for axonal regeneration in adult white matter. *J Neurosci*, 24(42):9282–90, Oct 2004.

[265] Erik Storkebaum, Diether Lambrechts, Mieke Dewerchin, Maria-Paz Moreno-Murciano, Saskia Appelmans, Hideyasu Oh, Philip Van Damme, Bart Rutten, Wing Yan Man, Maria De Mol, Sabine Wyns, David Manka, Kristel Vermeulen, Ludo Van Den Bosch, Nico Mertens, Christoph Schmitz, Wim Robberecht, Edward M Conway, Désiré Collen, Lieve Moons, and Peter Carmeliet. Treatment of motoneuron degeneration by intracerebroventricular delivery of vegf in a rat model of als. *Nat Neurosci*, 8(1):85–92, Jan 2005.

[266] Mimoun Azzouz, G Scott Ralph, Erik Storkebaum, Lucy E Walmsley, Kyriacos A Mitrophanous, Susan M Kingsman, Peter Carmeliet, and Nicholas D Mazarakis. Vegf delivery with retrogradely transported lentivector prolongs survival in a mouse als model. *Nature*, 429(6990):413–7, May 2004.

[267] Chengyun Zheng, Inger Nennesmo, Bengt Fadeel, and Jan-Inge Henter. Vascular endothelial growth factor prolongs survival in a transgenic mouse model of als. *Ann Neurol*, 56(4):564–7, Oct 2004.

[268] Orion P Keifer, Jr, Deirdre M O'Connor, and Nicholas M Boulis. Gene and protein therapies utilizing VEGF for ALS. *Pharmacology & Therapeutics*, pages 1–11, October 2013.

[269] B Oosthuyse, L Moons, E Storkebaum, H Beck, D Nuyens, K Brusselmans, J Van Dorpe, P Hellings, M Gorselink, S Heymans, G Theilmeier, M Dewerchin, V Laudenbach, P Vermylen, H Raat, T Acker, V Vleminckx, L Van Den Bosch, N Cashman, H Fujisawa, M R Drost, R Sciot, F Bruyninckx, D J Hicklin, C Ince, P Gressens, F Lupu, K H Plate, W Robberecht, J M Herbert, D Collen, and P Carmeliet. Deletion of the hypoxia-response element in the vascular endothelial growth factor promoter causes motor neuron degeneration. *Nat Genet*, 28(2):131–8, Jun 2001.

[270] Sivakumar Sathasivam. VEGF and ALS. *Neuroscience Research*, 62(2):71–77, October 2008.

[271] Berislav V Zlokovic. The blood-brain barrier in health and chronic neurodegenerative disorders. *Neuron*, 57(2):178–201, Jan 2008.

[272] Costantino Iadecola. Neurovascular regulation in the normal brain and in alzheimer's disease. *Nat Rev Neurosci*, 5(5):347–60, May 2004.

[273] Annelies Quaegebeur, Christian Lange, and Peter Carmeliet. The neurovascular link in health and disease: Molecular mechanisms and therapeutic implications. *Neuron*, 71(3):406–424, Aug 2011.

[274] Edward A Neuwelt, Björn Bauer, Christoph Fahlke, Gert Fricker, Constantino Iadecola, Damir Janigro, Luc Leybaert, Zoltán Molnár, Martha E O'Donnell, John T Povlishock, Norman R Saunders, Frank Sharp, Danica Stanimirovic, Ryan J Watts, and Lester R Drewes. Engaging neuroscience to advance translational research in brain barrier biology. *Nat Rev Neurosci*, 12(3):169–82, Mar 2011.

[275] C D Smith, A H Andersen, R J Kryscio, F A Schmitt, M S Kindy, L X Blonder, and M J Avison. Altered brain activation in cognitively intact individuals at high risk for alzheimer's disease. *Neurology*, 53(7):1391–6, Oct 1999.

[276] Annemieke Ruitenberg, Tom den Heijer, Stef L M Bakker, John C van Swieten, Peter J Koudstaal, Albert Hofman, and Monique M B Breteler. Cerebral hypoperfusion and clinical onset of dementia: the rotterdam study. *Ann Neurol*, 57(6):789–94, Jun 2005.

[277] S Y Bookheimer, M H Strojwas, M S Cohen, A M Saunders, M A Pericak-Vance, J C Mazziotta, and G W Small. Patterns of brain activation in people at risk for alzheimer's disease. *N Engl J Med*, 343(7):450–6, Aug 2000.

[278] R. R Rule, N Schuff, R. G Miller, and M. W Weiner. Gray matter perfusion correlates with disease severity in als. *Neurology*, 74(10):821–827, Mar 2010.

[279] J. S Henkel, D. R Beers, S Wen, R Bowser, and S. H Appel. Decreased mrna expression of tight junction proteins in lumbar spinal cords of patients with als. *Neurology*, 72(18):1614–1616, May 2009.

[280] Ethan A Winkler, Jesse D Sengillo, John S Sullivan, Jenny S Henkel, Stanley H Appel, and Berislav V Zlokovic. Blood–spinal cord barrier breakdown and pericyte reductions in amyotrophic lateral sclerosis. *Acta neuropathologica*, September 2012.

[281] H Oba, T Araki, K Ohtomo, S Monzawa, G Uchiyama, K Koizumi, Y Nogata, K Kachi, Z Shiozawa, and M Kobayashi. Amyotrophic lateral sclerosis: T2 shortening in motor cortex at mr imaging. *Radiology*, 189(3):843–6, Dec 1993.

[282] Justin Y Kwan, Suh Young Jeong, Peter Van Gelderen, Han-Xiang Deng, Martha M Quezado, Laura E Danielian, John A Butman, Lingye Chen, Elham Bayat, James Russell, Teepu Siddique, Jeff H Duyn, Tracey A Rouault, and Mary Kay Floeter. Iron accumulation in deep cortical layers accounts for mri signal abnormalities in als: correlating 7 tesla mri and pathology. *PLoS One*, 7(4):e35241, 2012.

[283] Robert D Bell, Ethan A Winkler, Abhay P Sagare, Itender Singh, Barb Larue, Rashid Deane, and Berislav V Zlokovic. Pericytes control key neurovascular functions and neuronal phenotype in the adult brain and during brain aging. *Neuron*, 68(3):409–427, November 2010.

[284] Svitlana Garbuzova-Davis, Samuel Saporta, Edward Haller, Irina Kolomey, Steven P Bennett, Huntington Potter, and Paul R Sanberg. Evidence of compromised blood-spinal cord barrier in early and late symptomatic sod1 mice modeling als. *PLoS One*, 2(11):e1205, 2007.

[285] Svitlana Garbuzova-Davis, Edward Haller, Samuel Saporta, Irina Kolomey, Santo V Nicosia, and Paul R Sanberg. Ultrastructure of blood-brain barrier and blood-spinal cord barrier in sod1 mice modeling als. *Brain Res*, 1157:126–37, Jul 2007.

[286] Zhihui Zhong, Rashid Deane, Zarina Ali, Margaret Parisi, Yuriy Shapovalov, M Kerry O'Banion, Konstantin Stojanovic, Abhay Sagare, Severine Boillee, Don W Cleveland, and Berislav V Zlokovic. Als-causing sod1 mutants generate vascular changes prior to motor neuron degeneration. *Nat Neurosci*, 11(4):420–2, Apr 2008.

[287] Charles Nicaise, Dinko Mitrecic, Pieter Demetter, Robert De Decker, Michèle Authelet, Alain Boom, and Roland Pochet. Impaired blood-brain and blood-spinal cord barriers in mutant sod1-linked als rat. *Brain Res*, 1301:152–62, Dec 2009.

[288] Kazunori Miyazaki, Kazuto Masamoto, Nobutoshi Morimoto, Tomoko Kurata, Takahumi Mimoto, Takayuki Obata, Iwao Kanno, and Koji Abe. Early and progressive impairment of spinal blood flow-glucose metabolism coupling in motor neuron degeneration of als model mice. *J Cereb Blood Flow Metab*, 32(3):456–67, Mar 2012.

[289] E A Winkler, J D Sengillo, A P Sagare, Z Zhao, Q Ma, E Zuniga, Y Wang, Z Zhong, J S Sullivan, J H Griffin, D W Cleveland, and B V Zlokovic. Blood-spinal cord barrier disruption contributes to early motor-neuron degeneration in ALS-model mice. *Proceedings of the National Academy of Sciences of the United States of America*, 111(11):E1035–E1042, March 2014.

[290] K Jackman, T Kahles, D Lane, L Garcia-Bonilla, T Abe, C Capone, K Hochrainer, H Voss, P Zhou, A Ding, J Anrather, and C Iadecola. Progranulin Deficiency Promotes Post-Ischemic Blood-Brain Barrier Disruption. *The Journal of neuroscience : the official journal of the Society for Neuroscience*, 33(50):19579–19589, December 2013.

[291] Shoichi Sasaki, Yohei Iguchi, Masahisa Katsuno, and Gen Sobue. Alterations in the blood-spinal cord barrier in tdp-43 conditional knockout mice. *Neurosci Lett*, 598:1–5, May 2015.

[292] Beth L Roman, Van N Pham, Nathan D Lawson, Magdalena Kulik, Sarah Childs, Arne C Lekven, Deborah M Garrity, Randall T Moon, Mark C Fishman, Robert J Lechleider, and Brant M Weinstein. Disruption of acvrl1 increases endothelial cell number in zebrafish cranial vessels. *Development*, 129(12):3009–19, Jun 2002.

[293] N C Chi, R M Shaw, S De Val, G Kang, L Y Jan, B L Black, and D Y R Stainier. Foxn4 directly regulates tbx2b expression and atrioventricular canal formation. *Genes & development*, 22(6):734–739, March 2008.

[294] Jing Liu, Lei Zeng, Regan M Kennedy, Nicole M Gruenig, and Sarah J Childs. βpix plays a dual role in cerebral vascular stability and angiogenesis, and interacts with integrin αvβ8. *Dev Biol*, 363(1):95–105, Mar 2012.

[295] C S Yee, A Chandrasekhar, M C Halloran, W Shoji, J T Warren, and J Y Kuwada. Molecular cloning, expression, and activity of zebrafish semaphorin Z1a. *Brain research bulletin*, 48(6):581–593, April 1999.

[296] Mary C. Mullins, Matthias Hammerschmidt, Pascal Haffter, and Christiane Nüsslein-Volhard. Large-scale mutagenesis in the zebrafish: in search of genes controlling development in a vertebrate. *Current Biology*, 4(3):189–202, Mar 1994.

[297] C B Kimmel, W W Ballard, S R Kimmel, B Ullmann, and T F Schilling. Stages of embryonic development of the zebrafish. *Dev Dyn*, 203(3):253–310, Jul 1995.

[298] Johnny Karlsson, Jonas von Hofsten, and Per-Erik Olsson. Generating transparent zebrafish: A refined method to improve detection of gene expression during embryonic development. *Marine Biotechnology*, 3(6):522–527, Nov 2001.

[299] S Isogai. Angiogenic network formation in the developing vertebrate trunk. *Development*, 130(21):5281–5290, Aug 2003.

[300] Hilary A Kemp, Amanda Carmany-Rampey, and Cecilia Moens. Generating chimeric zebrafish embryos by transplantation. *Journal of Visualized Experiments : JoVE*, 29:1394, 2009.

[301] DmitriV. Krysko, Katharina D'Herde, and Peter Vandenabeele. Clearance of apoptotic and necrotic cells and its immunological consequences. *Apoptosis*, 11(10):1709–1726, 2006.

[302] T Vanden Berghe, N Vanlangenakker, E Parthoens, W Deckers, M Devos, N Festjens, C J Guerin, U T Brunk, W Declercq, and P Vandenabeele. Necroptosis, necrosis and secondary necrosis converge on similar cellular disintegration features. *Cell Death Differ*, 17(6):922–930, 06 2010.

[303] Vanicha Vichai and Kanyawim Kirtikara. Sulforhodamine b colorimetric assay for cytotoxicity screening. *Nat Protoc*, 1(3):1112–6, 2006.

[304] T Scholzen and J Gerdes. The ki-67 protein: from the known and the unknown. *J Cell Physiol*, 182(3):311–22, Mar 2000.

[305] Peter Friedl and Darren Gilmour. Collective cell migration in morphogenesis, regeneration and cancer. *Nat Rev Mol Cell Biol*, 10(7):445–57, Jul 2009.

[306] Eloi Montañez, Ricardo P Casaroli-Marano, Senén Vilaró, and Roser Pagan. Comparative study of tube assembly in three-dimensional collagen matrix and on matrigel coats. *Angiogenesis*, 5(3):167–72, 2002.

[307] E Van Rooijen, E. E Voest, I Logister, J Bussmann, J Korving, F. J Van Eeden, R. H Giles, and S Schulte-Merker. von hippel-lindau tumor suppressor mutants faithfully model pathological hypoxia-driven angiogenesis and vascular retinopathies in zebrafish. *Disease Models & Mechanisms*, 3(5-6):343–353, May 2010.

[308] Jijun Hao, Joshua N Ho, Jana A Lewis, Kaleh A Karim, R Nathan Daniels, Patrick R Gentry, Corey R Hopkins, Craig W Lindsley, and Charles C Hong. In vivo structure-activity relationship study of dorsomorphin analogues identifies selective vegf and bmp inhibitors. *ACS Chem Biol*, 5(2):245–53, Feb 2010.

[309] Glynn Dennis, Jr, Brad T Sherman, Douglas A Hosack, Jun Yang, Wei Gao, H Clifford Lane, and Richard A Lempicki. David: Database for annotation, visualization, and integrated discovery. *Genome Biol*, 4(5):P3, 2003.

[310] Ian R Mackenzie, Thomas Arzberger, Elisabeth Kremmer, Dirk Troost, Stefan Lorenzl, Kohji Mori, Shih-Ming Weng, Christian Haass, Hans A Kretzschmar, Dieter Edbauer, and Manuela Neumann. Dipeptide repeat protein pathology in c9orf72 mutation cases: clinico-pathological correlations. *Acta Neuropathol*, 126(6):859–79, Dec 2013.

[311] Chantelle F Sephton, Can Cenik, Alper Kucukural, Eric B Dammer, Basar Cenik, Yuhong Han, Colleen M Dewey, Frederick P Roth, Joachim Herz, Junmin Peng, Melissa J Moore, and Gang Yu. Identification of neuronal rna targets of tdp-43-containing ribonucleoprotein complexes. *J Biol Chem*, 286(2):1204–15, Jan 2011.

[312] Eckhard Lammert and Jennifer Axnick. Vascular lumen formation. *Cold Spring Harb Perspect Med*, 2(4):a006619, Apr 2012.

[313] Avnika A Ruparelia, Mo Zhao, Peter D Currie, and Robert J Bryson-Richardson. Characterization and investigation of zebrafish models of filamin-related myofibrillar myopathy. *Hum Mol Genet*, 21(18):4073–83, Sep 2012.

[314] Misato Fujita, Hiroaki Mitsuhashi, Sumio Isogai, Takahiro Nakata, Atsushi Kawakami, Ikuya Nonaka, Satoru Noguchi, Yukiko K Hayashi, Ichizo Nishino, and Akira Kudo. Filamin c plays an essential role in the maintenance of the structural integrity of cardiac and skeletal muscles, revealed by the medaka mutant zacro. *Dev Biol*, 361(1):79–89, Jan 2012.

[315] Ross N W Kettleborough, Elisabeth M Busch-Nentwich, Steven A Harvey, Christopher M Dooley, Ewart de Bruijn, Freek van Eeden, Ian Sealy, Richard J White, Colin Herd, Isaac J Nijman, Fruzsina Fényes, Selina Mehroke, Catherine Scahill, Richard Gibbons, Neha Wali, Samantha Carruthers, Amanda Hall, Jennifer Yen, Edwin Cuppen, and Derek L Stemple. A systematic genome-wide analysis of zebrafish protein-coding gene function. *Nature*, 496(7446):494–7, Apr 2013.

[316] Kerstin Howe, Matthew D Clark, Carlos F Torroja, James Torrance, Camille Berthelot, Matthieu Muffato, John E Collins, Sean Humphray, Karen McLaren, Lucy Matthews, Stuart McLaren, Ian Sealy, Mario Caccamo, Carol Churcher, Carol Scott, Jeffrey C Barrett, Romke Koch, Gerd-Jörg Rauch, Simon White, William Chow, Britt Kilian, Leonor T Quintais, José A Guerra-Assunção, Yi Zhou, Yong Gu, Jennifer Yen, Jan-Hinnerk Vogel, Tina Eyre, Seth Redmond, Ruby Banerjee, Jianxiang Chi, Beiyuan Fu, Elizabeth Langley, Sean F Maguire, Gavin K Laird, David Lloyd, Emma Kenyon, Sarah Donaldson, Harminder Sehra, Jeff Almeida-King, Jane Loveland, Stephen Trevanion, Matt Jones, Mike Quail, Dave Willey, Adrienne Hunt, John Burton, Sarah Sims, Kirsten McLay, Bob

Plumb, Joy Davis, Chris Clee, Karen Oliver, Richard Clark, Clare Riddle, David Elliot, David Eliott, Glen Threadgold, Glenn Harden, Darren Ware, Sharmin Begum, Beverley Mortimore, Beverly Mortimer, Giselle Kerry, Paul Heath, Benjamin Phillimore, Alan Tracey, Nicole Corby, Matthew Dunn, Christopher Johnson, Jonathan Wood, Susan Clark, Sarah Pelan, Guy Griffiths, Michelle Smith, Rebecca Glithero, Philip Howden, Nicholas Barker, Christine Lloyd, Christopher Stevens, Joanna Harley, Karen Holt, Georgios Panagiotidis, Jamieson Lovell, Helen Beasley, Carl Henderson, Daria Gordon, Katherine Auger, Deborah Wright, Joanna Collins, Claire Raisen, Lauren Dyer, Kenric Leung, Lauren Robertson, Kirsty Ambridge, Daniel Leongamornlert, Sarah McGuire, Ruth Gilderthorp, Coline Griffiths, Deepa Manthravadi, Sarah Nichol, Gary Barker, Siobhan Whitehead, Michael Kay, Jacqueline Brown, Clare Murnane, Emma Gray, Matthew Humphries, Neil Sycamore, Darren Barker, David Saunders, Justene Wallis, Anne Babbage, Sian Hammond, Maryam Mashreghi-Mohammadi, Lucy Barr, Sancha Martin, Paul Wray, Andrew Ellington, Nicholas Matthews, Matthew Ellwood, Rebecca Woodmansey, Graham Clark, James D Cooper, James Cooper, Anthony Tromans, Darren Grafham, Carl Skuce, Richard Pandian, Robert Andrews, Elliot Harrison, Andrew Kimberley, Jane Garnett, Nigel Fosker, Rebekah Hall, Patrick Garner, Daniel Kelly, Christine Bird, Sophie Palmer, Ines Gehring, Andrea Berger, Christopher M Dooley, Zübeyde Ersan-Ürün, Cigdem Eser, Horst Geiger, Maria Geisler, Lena Karotki, Anette Kirn, Judith Konantz, Martina Konantz, Martina Oberländer, Silke Rudolph-Geiger, Mathias Teucke, Christa Lanz, Günter Raddatz, Kazutoyo Osoegawa, Baoli Zhu, Amanda Rapp, Sara Widaa, Cordelia Langford, Fengtang Yang, Stephan C Schuster, Nigel P Carter, Jennifer Harrow, Zemin Ning, Javier Herrero, Steve M J Searle, Anton Enright, Robert Geisler, Ronald H A Plasterk, Charles Lee, Monte Westerfield, Pieter J de Jong, Leonard I Zon, John H Postlethwait, Christiane Nüsslein-Volhard, Tim J P Hubbard, Hugues Roest Crollius, Jane Rogers, and Derek L Stemple. The zebrafish reference genome sequence and its relationship to the human genome. *Nature*, 496(7446):498–503, Apr 2013.

[317] Takayoshi Sakai, Melinda Larsen, and Kenneth M Yamada. Fibronectin requirement in branching morphogenesis. *Nature*, 423(6942):876–81, Jun 2003.

[318] Anna Huttenlocher and Alan Rick Horwitz. Integrins in cell migration. *Cold Spring Harb Perspect Biol*, 3(9):a005074, Sep 2011.

[319] P D Kassner, R Alon, T A Springer, and M E Hemler. Specialized functional properties of the integrin alpha 4 cytoplasmic domain. *Mol Biol Cell*, 6(6):661–74, Jun 1995.

[320] Karen A Pinco, Wei He, and Joy T Yang. alpha4beta1 integrin regulates lamellipodia protrusion via a focal complex/focal adhesion-independent mechanism. *Mol Biol Cell*, 13(9):3203–17, Sep 2002.

[321] Nicholas O Deakin, Mark D Bass, Stacey Warwood, Julia Schoelermann, Zohreh Mostafavi-Pour, David Knight, Christoph Ballestrem, and Martin J Humphries. An integrin-alpha4-14-3-3zeta-paxillin ternary complex mediates localised cdc42 activity and accelerates cell migration. *J Cell Sci*, 122(Pt 10):1654–64, May 2009.

[322] Lawrence E Goldfinger, Jaewon Han, William B Kiosses, Alan K Howe, and Mark H Ginsberg. Spatial restriction of alpha4 integrin phosphorylation regulates lamellipodial stability and alpha4beta1-dependent cell migration. *J Cell Biol*, 162(4):731–41, Aug 2003.

[323] Naoyuki Nishiya, William B Kiosses, Jaewon Han, and Mark H Ginsberg. An alpha4 integrin-paxillin-arf-gap complex restricts rac activation to the leading edge of migrating cells. *Nat Cell Biol*, 7(4):343–52, Apr 2005.

[324] Ryan J Petrie, Andrew D Doyle, and Kenneth M Yamada. Random versus directionally persistent cell migration. *Nat Rev Mol Cell Biol*, 10(8):538–49, Aug 2009.

[325] Wonshill Koh, Rachel D Mahan, and George E Davis. Cdc42- and rac1-mediated endothelial lumen formation requires pak2, pak4 and par3, and pkc-dependent signaling. *J Cell Sci*, 121(Pt 7):989–1001, Apr 2008.

[326] Wonshill Koh, Kamakshi Sachidanandam, Amber N Stratman, Anastasia Sacharidou, Anne M Mayo, Eric A Murphy, David A Cheresh, and George E Davis. Formation of endothelial lumens requires a coordinated pkcepsilon-, src-, pak- and raf-kinase-dependent signaling cascade downstream of cdc42 activation. *J Cell Sci*, 122(Pt 11):1812–22, Jun 2009.

[327] A Peled, V Grabovsky, L Habler, J Sandbank, F Arenzana-Seisdedos, I Petit, H Ben-Hur, T Lapidot, and R Alon. The chemokine sdf-1 stimulates integrin-mediated arrest of cd34(+) cells on vascular endothelium under shear flow. *J Clin Invest*, 104(9):1199–211, Nov 1999.

[328] Y R Zou, A H Kottmann, M Kuroda, I Taniuchi, and D R Littman. Function of the chemokine receptor cxcr4 in haematopoiesis and in cerebellar development. *Nature*, 393(6685):595–9, Jun 1998.

[329] Q Ma, D Jones, P R Borghesani, R A Segal, T Nagasawa, T Kishimoto, R T Bronson, and T A Springer. Impaired B-lymphopoiesis, myelopoiesis, and derailed cerebellar neuron migration in CXCR4- and SDF-1-deficient mice. *Proc Natl Acad Sci U S A*, 95(16):9448–53, Aug 1998.

[330] K Tachibana, S Hirota, H Iizasa, H Yoshida, K Kawabata, Y Kataoka, Y Kitamura, K Matsushima, N Yoshida, S Nishikawa, T Kishimoto, and T Nagasawa. The chemokine receptor cxcr4 is essential for vascularization of the gastrointestinal tract. *Nature*, 393(6685):591–4, Jun 1998.

[331] Andy Aman and Tatjana Piotrowski. Cell migration during morphogenesis. *Dev Biol*, 341(1):20–33, May 2010.

[332] Cong Xu, Sana S Hasan, Inga Schmidt, Susana F Rocha, Mara E Pitulescu, Jeroen Bussmann, Dana Meyen, Erez Raz, Ralf H Adams, and Arndt F Siekmann. Arteries are formed by vein-derived endothelial tip cells. *Nat Commun*, 5:5758, 2014.

[333] Michael R M Harrison, Jeroen Bussmann, Ying Huang, Long Zhao, Arthela Osorio, C Geoffrey Burns, Caroline E Burns, Henry M Sucov, Arndt F Siekmann, and Ching-Ling Lien. Chemokine-guided angiogenesis directs coronary vasculature formation in zebrafish. *Dev Cell*, 33(4):442–54, May 2015.

[334] A J Pelletier, L J van der Laan, P Hildbrand, M A Siani, D A Thompson, P E Dawson, B E Torbett, and D R Salomon. Presentation of chemokine sdf-1 alpha by fibronectin mediates directed migration of t cells. *Blood*, 96(8):2682–90, Oct 2000.

[335] S Leech, J Kirk, J Plumb, and S McQuaid. Persistent endothelial abnormalities and blood-brain barrier leak in primary and secondary progressive multiple sclerosis. *Neuropathol Appl Neurobiol*, 33(1):86–98, Feb 2007.

[336] Alberto Gajofatto and Maria Donata Benedetti. Treatment strategies for multiple sclerosis: When to start, when to change, when to stop? *World J Clin Cases*, 3(7):545–55, Jul 2015.

[337] Shoichi Sasaki. Alterations of the blood-spinal cord barrier in sporadic amyotrophic lateral sclerosis. *Neuropathology*, Aug 2015.

[338] C U Kloss, A Werner, M A Klein, J Shen, K Menuz, J C Probst, G W Kreutzberg, and G Raivich. Integrin family of cell adhesion molecules in the injured brain: regulation and cellular localization in the normal and regenerating mouse facial motor nucleus. *J Comp Neurol*, 411(1):162–78, Aug 1999.

[339] Thomas Philips and Wim Robberecht. Neuroinflammation in amyotrophic lateral sclerosis: role of glial activation in motor neuron disease. *Lancet Neurol*, 10(3):253–63, Mar 2011.

List of figures

List of abbreviations

+/+	wild type
+/-	heterozygous
-/-	homozygous
aa	amino acid
ACOT11	acyl-CoA thioesterase 11
ACP5	acid phosphatase 5
AD	Alzheimer's disease
ADAM	a disintegrin and metalloprotease
AKT	AKT8 virus oncogene cellular homolog or protein kinase B
ALS	Amyotrophic lateral sclerosis
ALS-FTLD	clinical presentation with similarly strong signs of ALS and FTLD
ALS-FUS	ALS with FUS-positive inclusions
ALS-SOD	ALS with SOD1-positive inclusions
ALS-TDP	ALS with TDP-43-positive inclusions
APS	ammonium persulfate
AQP1	aquaporin 1
BBB	blood brain barrier
be	*before eight*
Bmp	bone morphogenic protein
bp	base pair
BSA	bovine serum albumin
BSCB	blood spinal cord barrier
C. elegans	*Caenorhabditis elegans*
$CaCl_2$	calcium chloride
Cas9	CRISPR-associated 9
Ccbe1	collagen and calcium-binding endothelial growth factor domain-1
CCL14	chemokine (C-C motif) ligand 14
cDNA	complementary DNA
CDK5	cyclin-dependent kinase 5

CDK5RAP2	CDK5 regulatory subunit associated protein 2
DHID1	chitinase domain containing 1
CDC42	cell division cycle 42
CLIP	cross-linking and immunoprecipitation technology
CNS	central nervous system
CNTN1	contactin 1
CO_2	carbon dioxide
CRISPR	clustered regularly interspaced short palindromic repeats
CXCL	chemokine (C-X-C motif) ligand
$CuSO_4$	copper sulfate
DA	dorsal aorta
DAB	3,3'-diaminobenzidine
dATP	deoxyadenosine triphosphate
dCTP	deoxycytosine triphosphate
DEPC	diethylpyrocarbonate
dGTP	deoxyguanosine triphosphate
DIC	differential interference contrast
DLAV	dorsal longitudinal anastomotic vessels
Dll	delta-like
DMEM	Dulbecco's Modified Eagel's Medium
DMSO	dimethyl sulfoxide
DNA	deoxyribonucleic acid
dNTP	deoxynucleoside triphosphates
DTT	dithiothreitol
dTTP	deoxytyrosine triphosphate
dpf	days post fertilization
DPR	dipeptide-repeat
DZNE	German center for neurodegnerative diseases
EC	endothelial cells
EDA	extra domain A
EDB	extra domain B
EDTA	ethylenediaminetetraacetic acid
EGFP	enhanced GFP
Eif2α	eukaryotic translation initiation factor 2α
ENU	N-ethyl-N-nitrosouresa
ERK	extracellular regulated kinase
EST	expressed sequence tag
EWS	Ewing's sarcoma

fALS	familial ALS
FAM182A	family with sequence similarity 182, member A
FBS	fetal bovine serum
FDA	US Food and Drug Administration
FET	FUS/EWS/TAF15
Fli1	friend leukemia integration 1
FLK1	fetal liver kinase 1
FLT1	fms-related tyrosine kinase 1
FLT4	fms-related tyrosine kinase 4
FN	fibronectin
FN1	human or mouse fibronectin 1
Fn1a	zebrafish fibronectin
Fn1b	zebrafish fibronectin
FTD	Frontotemporal dementia
FTLD	Frontotemporal lobar degeneration
FTLD-FUS	FTLD with FUS-positive inclusions
FTLD-TDP	FTLD with TDP-43-positive inclusions
FUS	human fused in sarcoma gene
FUS	human fused in sarcoma protein
Gal4	yeast transcription activator protein Gal4
GFP	green fluorescent protein
GRN	progranulin (gene name)
gRNA	guide RNA
GuHCl	guanidine hydrochloride
GWAS	genome-wide association studies
H_2O_2	hydrogen peroxide
H_2O	water
HDAC9	histone deacetylase 9
HEK	human embryonic kidney
He's	hairy and enhancer of split
HIV-1	human immunodeficiency virus type-1
hnRNP	heterogeneous nuclear ribonucleoprotein
hpf	hours post fertilization
HRP	horseradish peroxidase
HSP	heat shock protein
HUVEC	human umbilical vein endothelial cells
IF	immunofluorescence
IHC	Immunohistochemistry

INHBB	inhibin beta B
IRV	interrenal vessel
ISH	*in situ* hybridization
ISV	intersegmental vessels
ITG	integrin
KIF19	kinesin 19
KCl	potassium chloride
kDa	kilo-Dalton
KD	knockdown
KH_2PO_4	monopotassium phosphate
liq. N_2	liquid nitrogene
LDH	lactate dehydrogenase
Luc	luciferase
LYVE1	lymphatic vessel endothelial hyaluronan receptor 1
MAPK	mitogen-activated protein kinase
Met	methionine
mFlt	membrane bound Flt1
$MgCl_2$	magnesium chloride
$MgSO_4$	magnesium sulfate
MIR146A	micro RNA 146 A
miRNA	micro RNA
MO	morpholino
MPI	Max Planck Institute
mRNA	messenger RNA
MW	molecular weight
MYO7A	myosin 7 A
NaCl	sodium chloride
Na_2HPO_4	disodium hydrogen phosphate
NaN_3	sodium acid
NaOAc	sodium acetate
NCS	newborn calf serum
NEAA	non-essential amino acids
NES	nuclear export signal
NFL	low molecular weight neurofilament
NGS	next generation sequencing
NICD	Notch intracellular domain
NLS	nuclear localization signal
NVU	neurovascular unit

obd	*out of bounds*
o/n	overnight
ORF	open reading frame
OVA	ovalbumin
PAGE	polyacrylamide gel electrophoresis
PB	phosphate buffer
PBS	phosphate buffered saline
PCR	polymerase chain reactions
PCV	posterior cardinal vein
PFA	paraformaldehyde
PGRN	progranulin (protein name)
PI3K	phosphatidyl inositol-3 kinase
PLGF	placental growth factor
PLXND1	plexinD1
PK	proteinase K
PKC	protein kinase C
PLCG	phospholipase C γ
POLDIP3	polymerase (DNA-directed), delta interacting protein 3
PSM	presomitic mesoderm
PTH1R	parathyroid hormone 1 receptor
PTU	phenylthiourea
qPCR	quantitative PCR
RAC	Ras-related C3 botulinum toxin substrate 1
RAN	repeat-associated non-ATG
RE	restriction endonucleases
RIPA	radioimmunoprecipitation assay buffer
RNA	ribonucleic acid
RNAi	RNA interference
ROS	reactive oxygen species
RRM	RNA recognition motif
RT	room temperature
RWDD1	RWD domain containing 1
SA	intersegmental arteries
sALS	sporadic ALS
SDS	sodium dodecyl sulfate
S.E.M.	standard error of the mean
Sema	semaphorin
sFlt1	soluble Flt1

SG	stress granules
sh	short hairpin
SOD1	Cu/Zn superoxid-dysmutase 1
SQSTM1	sequestosome 1
SRB	sulforhodamine B
STAB2	stabilin 2
SV	intersegmental veins
TAF15	TATA-binding protein-associated factor 15
TALE	transcription activator-like effector
TALEN	transcription activator-like effector nuclease
TAR	trans-active response
TARDBP	TAR DNA-binding protein (human gene name)
Tardbp	TAR DNA-binding protein (zebrafish orthologue)
Tardbpl	TAR DNA-binding protein like (zebrafish orthologue)
TBPH	TAR DNA-binding protein 43 homologue
tdp-1	*c. elegans* orthologue of TDP-43
TDP-43	TAR DNA-binding protein of 43kDa (protein name used here for human and zebrafish proteins)
TEMED	tetramethylethylenediamine
TGFB2	transforming growth factor 2
TFEB	transcription factor EB
TILLING	targeted induced local lesions in genomes
UBQLN2	ubiquilin 2
UAS	upstream activation sequence
UPS	ubiquitin/proteasome system
UTR	untranslated region
VCAM1	human vascular cell adhesion molecule 1
VCP	valosin-containing protein-1
VE-cadherin	vascular epithelium-cadherin
VEGF	vascular endothelial growth factor
VEGFR	vascular endothelial growth factor receptor
V sequence	variable sequence of FN
WISH	whole mount *in situ* hybridization
wt	wild type
ZO-1	zonula occludens-1 or tight junction protein 1

The herein listed abbreviations of genes and proteins are modified throughout the thesis according to the nomenclature guidelines of the respective species (http://www.genenames.org, http://www.informatics.jax.org, http://www.zfin.org)

Danksagung

Allen voran möchte ich meinem Doktorvater Prof. Christian Haass und meiner direkten Betreuerin Dr. Bettina Schmid für die tolle Unterstützung und den Freiraum für meine Forschung danken! Es war ein Privileg, an diesem super ausgestatteten Lehrstuhl forschen zu dürfen. Besonders die Vernetzung verschiedener Gruppen mit Expertise im Umgang mit verschiedenen Modellorganismen sowie molekularbiologischem und biochemischem Methodenwissen hat es sehr erleichtert, an einem solch vielfältigen Projekt zu arbeiten. Danke Tina für das Vertrauen in meine Fähigkeiten, die ermunternden Worte zwischendurch und die vielen hilfreichen Kommentare zu dieser Arbeit.

Ohne die finanzielle Unterstützung durch die Hans- und Ilse-Breuer-Stiftung sowie dem Reisegeld und den Workshops von IMPRS-LS wäre meine Doktorarbeit sicher um einiges schwieriger geworden. Nicht nur hat mich die Hans- und Ilse-Breuer-Stiftung direkt für drei Jahre finanziert, sondern auch ermöglicht, zu vielen internationalen Konferenzen zu fahren. Die wissenschaftlichen Diskussionen auf diesen Tagungen haben mich motiviert und mir neuen Schub und Ideen für weitere Experimente geliefert.

Vielen Dank auch für die gute Zusammenarbeit an Bettina Pitter, Eloi Montanez und Prof. Ulrich Pohl. Außerdem möchte ich Prof. Thomas Misgeld für seine offenen Kommentare in meinen TAC Meetings danken. Danke auch an weitere Kooperationspartner und Unterstützer am Lehrstuhl: Eva für die Zellkultur-Starthilfe, Denise für die Hilfe bei der Virenproduktion und Stephie für Hilfe bei den Viability Assays.

Natürlich möchte ich mich auch bei allen derzeitigen und ehemaligen Mitgliedern der Fischgruppe bedanken. Ich empfand die Atmospäre immer als angenehm und

freundschaftlich und es hat auch dank euch Spaß gemacht, ins Labor zu kommen. Danke für Finclips, die Arbeit mit den Fischen, wissenschaftlichen Austausch und Ratschläge. Danke Laura, dass du mir am Anfang so viel mit neuen Methoden geholfen hast, obwohl du selbst noch ganz neu warst. Nicht zu vergessen die vielen privaten schönen Momente und dass ich dank euch die Wiesn zu schätzen gelernt habe! Wenn wir beim Thema Feiern angelangt sind, darf ich natürlich auch die anderen ehemaligen 7. Stock Bewohner nicht vergessen, allen voran die Eddies (plus Möchtegern-Eddies), aber danke auch an Maria für nette Mittagspausen. Alles in allem war es also eine schöne Zeit, durch die ich nicht nur wissenschaftliche Ergebnisse, sondern auch Freunde gewonnen habe.

Den allerwichtigsten Menschen möchte ich zum Schluss danken, die mir immer die nötige Kraft gegeben haben, durchzuhalten. Das sind Freunde in näherer und weiterer Ferne, die meist ähnliche Phasen durchlaufen haben und mit Rat und Trost zur Seite standen. Vor allem aber möchte ich mich bei Arthur und meiner Familie bedanken. Ohne euch wäre ich nicht, wer ich bin und ich bin froh, dass ich euch habe!